Lecture Notes in Computational Vision and Biomechanics 10

L. K. Cheng
A. J. Pullan
G. Farrugia *Editors*

New Advances in Gastrointestinal Motility Research

Springer

Lecture Notes in Computational Vision and Biomechanics

Volume 10

Series Editors

João Manuel R. S. Tavares, Porto, Portugal
R. M. Natal Jorge, Porto, Portugal

Editorial Advisory Board

Alejandro Frangi, Sheffield, UK
Chandrajit Bajaj, Austin, USA
Eugenio Oñate, Barcelona, Spain
Francisco Perales, Palma de Mallorca, Spain
Gerhard A. Holzapfel, Stockholm, Sweden
J. Paulo Vilas-Boas, Porto, Portugal
Jeffrey A. Weiss, Salt Lake City, USA
John Middleton, Cardiff, UK
Jose M. García Aznar, Zaragoza, Spain
Perumal Nithiarasu, Swansea, UK
Kumar K. Tamma, Minneapolis, USA
Laurent Cohen, Paris, France
Manuel Doblaré, Zaragoza, Spain
Patrick J. Prendergast, Dublin, Ireland
Rainald Löhner, Fairfax, USA
Roger Kamm, Cambridge, USA
Thomas J. R. Hughes, Austin, USA
Yongjie Zhang, Pittsburgh, USA
Yubo Fan, Beijing, China

For further volumes:
http://www.springer.com/series/8910

The research related to the analysis of living structures (Biomechanics) has been a source of recent research in several distinct areas of science, for example, Mathematics, Mechanical Engineering, Physics, Informatics, Medicine and Sport. However, for its successful achievement, numerous research topics should be considered, such as image processing and analysis, geometric and numerical modelling, biomechanics, experimental analysis, mechanobiology and enhanced visualization, and their application to real cases must be developed and more investigation is needed. Additionally, enhanced hardware solutions and less invasive devices are demanded.

On the other hand, Image Analysis (Computational Vision) is used for the extraction of high level information from static images or dynamic image sequences. Examples of applications involving image analysis can be the study of motion of structures from image sequences, shape reconstruction from images and medical diagnosis. As a multidisciplinary area, Computational Vision considers techniques and methods from other disciplines, such as Artificial Intelligence, Signal Processing, Mathematics, Physics and Informatics. Despite the many research projects in this area, more robust and efficient methods of Computational Imaging are still demanded in many application domains in Medicine, and their validation in real scenarios is matter of urgency.

These two important and predominant branches of Science are increasingly considered to be strongly connected and related. Hence, the main goal of the LNCV&B book series consists of the provision of a comprehensive forum for discussion on the current state-of-the-art in these fields by emphasizing their connection. The book series covers (but is not limited to):

- Applications of Computational Vision and Biomechanics
- Biometrics and Biomedical Pattern Analysis
- Cellular Imaging and Cellular Mechanics
- Clinical Biomechanics
- Computational Bioimaging and Visualization
- Computational Biology in Biomedical Imaging
- Development of Biomechanical Devices
- Device and Technique Development for Biomedical Imaging
- Digital Geometry Algorithms for Computational Vision and Visualization
- Experimental Biomechanics
- Gait & Posture Mechanics
- Multiscale Analysis in Biomechanics
- Neuromuscular Biomechanics
- Numerical Methods for Living Tissues
- Numerical Simulation
- Software Development on Computational Vision and Biomechanics
- Grid and High Performance Computing for Computational Vision and Biomechanics
- Imag-based Geometric Modeling and Mesh Generation
- Image Processing and Analysis
- Image Processing and Visualization in Biofluids
- Image Understanding
- Material Models
- Mechanobiology
- Medical Image Analysis
- Molecular Mechanics
- Multi-Modal Image Systems
- Multiscale Biosensors in Biomedical Imaging
- Multiscale Devices and Biomems for Biomedical Imaging
- Musculoskeletal Biomechanics
- Sport Biomechanics
- Virtual Reality in Biomechanics
- Vision Systems

L. K. Cheng · A. J. Pullan
G. Farrugia
Editors

New Advances in Gastrointestinal Motility Research

Springer

Editors
L. K. Cheng
A. J. Pullan
Auckland Bioengineering Institute
The University of Auckland
Auckland
New Zealand

G. Farrugia
Mayo Clinic
Rochester, MN
USA

ISSN 2212-9391 ISSN 2212-9413 (electronic)
ISBN 978-94-007-6560-3 ISBN 978-94-007-6561-0 (eBook)
DOI 10.1007/978-94-007-6561-0
Springer Dordrecht Heidelberg New York London

Library of Congress Control Number: 2013934099

© Springer Science+Business Media Dordrecht 2013
This work is subject to copyright. All rights are reserved by the Publisher, whether the whole or part of the material is concerned, specifically the rights of translation, reprinting, reuse of illustrations, recitation, broadcasting, reproduction on microfilms or in any other physical way, and transmission or information storage and retrieval, electronic adaptation, computer software, or by similar or dissimilar methodology now known or hereafter developed. Exempted from this legal reservation are brief excerpts in connection with reviews or scholarly analysis or material supplied specifically for the purpose of being entered and executed on a computer system, for exclusive use by the purchaser of the work. Duplication of this publication or parts thereof is permitted only under the provisions of the Copyright Law of the Publisher's location, in its current version, and permission for use must always be obtained from Springer. Permissions for use may be obtained through RightsLink at the Copyright Clearance Center. Violations are liable to prosecution under the respective Copyright Law.
The use of general descriptive names, registered names, trademarks, service marks, etc. in this publication does not imply, even in the absence of a specific statement, that such names are exempt from the relevant protective laws and regulations and therefore free for general use.
While the advice and information in this book are believed to be true and accurate at the date of publication, neither the authors nor the editors nor the publisher can accept any legal responsibility for any errors or omissions that may be made. The publisher makes no warranty, express or implied, with respect to the material contained herein.

Printed on acid-free paper

Springer is part of Springer Science+Business Media (www.springer.com)

This book is dedicated to the memory of Andrew J. Pullan (1963–2012).
A great friend, colleague, and mentor to us all. We will all miss you greatly

Contents

New Advances in Gastrointestinal Motility Research

Leo K. Cheng and Gianrico Farrugia

Abstract Gastrointestinal motility is an area of research that has gained renewed interest in recent years. However, it is evident that there still remains much to be learnt and discovered. The chapters in this volume entitled "New Advances in Gastrointestinal Motility Research" result from a meeting which took place at The University of Auckland, New Zealand in October/November 2011 and provide a summary of discussions. Both the meeting and this book were brainchilds of Professor Andrew Pullan. However, Professor Andrew Pullan tragically passed away between the inception and completion of this series. This book not simply dedicated to him and his family but is a reflection of his ideas and work. The 12 remaining chapters of this volume are arranged into 4 broad sections: covering gastrointestinal cellular activity and tissue structure; techniques for measuring, analyzing and visualizing high-resolution extra-cellular recordings; methods for modulating gastric electrical activity as well as sensing the resultant activity using non-invasive bio-electro-magnetic fields; and finally methods for assessing manometric and videographic motility patterns and the application of these data for predicting the flow and mixing behavior of luminal contents by using computational fluid dynamic techniques. As a result, this volume aims to provide both an overview of existing research techniques over a range of research areas as well as to highlight future directions and challenges for the community as a whole.

L. K. Cheng (✉)
Auckland Bioengineering Institute, The University of Auckland, Private Bag 92019, Auckland 1142, New Zealand
e-mail: l.cheng@auckland.ac.nz

L. K. Cheng
Department of Surgery, Vanderbilt University, Nashville, TN, USA

G. Farrugia
Enteric Neuroscience Program, Division of Gastroenterology & Hepatology, Mayo Clinic, Rochester, MN, USA

L. K. Cheng et al. (eds.), *New Advances in Gastrointestinal Motility Research*, Lecture Notes in Computational Vision and Biomechanics 10,
DOI: 10.1007/978-94-007-6561-0_1, © Springer Science+Business Media Dordrecht 2013

1 Introduction

There are 3 editors of this book. New Advances in Gastrointestinal Motility Research is a compilation of chapters written by experts who gathered in Auckland, New Zealand in late October and early November of 2011 to discuss both the recent progress in our understanding of gastrointestinal motility and what research still needs to be done. Both the meeting and the subsequent book were brainchilds of Professor Andrew Pullan. Professor Pullan was a force of nature, working tirelessly to advance the field by combining the best of the engineering and medical fields. Professor Andrew Pullan tragically passed away between the inception and completion of this series, yet his hand is visible in each and every chapter. This book not simply dedicated to him and his family but is a reflection of his ideas and work. We will all miss him very much.

The motility of the gastrointestinal (GI) tract is governed by rhythmic electrical patterns known as slow waves. These observations were first reported by Walter Alvarez in the 1920s and only followed the demonstration by Augustus Waller of the human electrocardiograms by approximately 30 years [2, 1, 9]. However, while electrophysiological recordings now play an integral part in cardiology, the understanding of gastrointestinal motility remains comparatively still in its infancy. The discovery that the presence and normal function of interstitial cells of Cajal (ICC) are necessary for normal GI motility has confirmed a hypothesis first proposed by Ramon y Cajal where he described a cell type that he speculated may modify smooth muscle contraction [3, 10, 6]. Even more recently, the degradation of ICC networks has been associated with a number of motility disorders such as gastroparesis, slow transit constipation and intestinal pseudo-obstruction [8, 4, 5, 11, 7]. Areas of current research include how the electrical patterns are generated, how they are altered in motility disorders, how that electrical activity correlates with changes in contractile patterns and how these factors correlates with alterations in underlying tissue structure.

Recent advances in the techniques for measuring the structure and function of gastrointestinal cells, tissue and organs now provides a wealth of data on physiological function. The ability to integrate these data into biophysically based computation models provides the ability to both confirm and aid in interpretation of experimental and clinical measurements and the refinement of measurement techniques.

Each chapter of this volume covers an area of gastrointestinal motility at a different spatial scale and includes historical, current and future perspectives on a research related to gastrointestinal motility. Loosely grouped into four sections: "Role of Ion Channel Mechanosensitivity in the Gut: Mechano-Electrical Feedback Exemplified by Stretch-Dependence of $Na_v1.5$" and "ICC Network Density: Regulation and Consequences" review the cellular function and the tissue structure of the GI tract in health and disease. The three chapters "The Principles and Practice of Gastrointestinal High-Resolution Electrical Mapping", "Quantitative Analysis of Electrical Activity in the Gastrointestinal Tract" and

"The Electrical Regulation of GI Motility at the Whole-Organ Level" describe the methods for measuring, analyzing and visualizing extracellular recordings from high-resolution tissue recordings. Following this, the chapters "Therapeutic Potential of Gastric Electrical Stimulation for Obesity", "Gastric Electrical Stimulation: Twentieth Century Development to Twenty First Century Implementation and Personalization of Programming", "Biomagnetic Signatures of Gastrointestinal Electrical Activity" and "Modelling Tissue Electrophysiology in the GI Tract: Past, Present and Future" review methods for modulating gastric electrical activity via electrical stimulation, non-invasive methods for characterizing GI electrical activity as well as computation techniques for simulating GI function. Finally, the three chapters "Colonic Manometry: What Do the Squiggly Lines Really Tell Us?", "Spatiotemporal Mapping Techniques for Quantifying Gut Motility" and "Computational Modeling of Gastrointestinal Fluid Dynamics" provide a review of current methods for assessing GI motility using manometric and videographic techniques as well as computational methods for simulating the resultant flow of luminal contents. Therefore, this volume aims to provide a review of a range of different research techniques in the field of gastrointestinal as well as a framework to consider the challenges and opportunities in the years to come.

Starting at the chapter "Role of Ion Channel Mechanosensitivity in the Gut: Mechano-Electrical Feedback Exemplified By Stretch-Dependence of $Na_v1.5$", Beyder et al. describe a voltage gated sodium channel, $Na_V1.5$, found in the human GI tract that regulates the resting potential of smooth muscle as well as slow wave upstroke and frequency. The existing computational models of GI cellular electrical activity and specifically a model of $Na_V1.5$ mechanosensitivity that has been incorporated into one of the cell models are presented. The ICCs are known to regulate the normal function of the gut by generating rhythmic electrical activity and the depletion of these cells have been associated with several gastrointestinal motility disorders. In the chapter "ICC Network Density: Regulation and Consequences", Gibbons et al. describe methods and techniques for measuring ICC morphology and function from tissue. In addition, the applications of novel mathematical metrics to quantify variations in the network structure and the creation of realistic virtual ICC networks to enable structure–function relationships to be investigated.

The chapters "The Principles and Practice of Gastrointestinal High-Resolution Electrical Mapping", "Quantitative Analysis of Electrical Activity in the Gastrointestinal Tract" and "The Electrical Regulation of GI Motility at the Whole-Organ Level" describe the principals of measuring, analyzing and patterns of electrical activity in the gastrointestinal tract. O'Grady et al. review the current status of GI multi-electrode mapping, with a particular focus on extracellular recordings, the design of mapping devices, and the practical considerations for successful experimental work. Erickson et al. then describe the development of novel signal processing and visualization methods for the automated analysis of extracellular slow wave recordings. Finally, in the chapter "The Electrical Regulation of GI Motility at the Whole-Organ Level", Angeli et al. present the current state of knowledge of electrical slow wave regulation of GI contractions in

the stomach, small intestine and colon. Emphasis is placed on data obtained from extracellular recordings over large areas of tissue.

In the chapters "Therapeutic Potential of Gastric Electrical Stimulation for Obesity" and "Gastric Electrical Stimulation: Twentieth Century Development to Twenty First Century Implementation and Personalization of Programming" review the ability to manipulate gastric motility for therapeutic purposes are discussed. Yin et al. review the current established methods for treating obesity: diet and exercise, pharmacotherapy and surgical treatment. Gastric electrical stimulation (GES) is a potential therapeutic potential for obesity. Patients, physicians and surgeons have shown enthusiasm towards GES compared to existing surgical options as it is much less invasive and more importantly is reversible or can be tuned over time. However, to date, controlled studies have failed to reach significant weight loss. Yin et al. also review various methods of GES that have been applied for treating obesity and provide insight into a future viable GES therapy for obesity. In chapter "Therapeutic Potential of Gastric Electrical Stimulation for Obesity", Griffith et al. review the use of GES for treating gastroparesis, an incompletely understood disorder characterized by vomiting, nausea, abdominal pain, and related symptoms. Recent work with temporary GES by way of endoscopically placed electrodes has shown as an important technique in the valuation of stimulation devices. These recent studies offer the potential for personalization of stimulation parameters in a given patient. In view of the significant issues still surrounding GES, this chapter also discusses the requirements before GES can be more widely accepted and adopted. Bradshaw et al. review in "Biomagnetic Signatures of Gastrointestinal Electrical Activity" non-invasive methods for sensing GI electrical activity—primarily by cutaneous electrical recordings or non-contact magnetic recordings. This chapter reviews the historical development of both electrical and magnetic field measurements of the GI tract. It also illustrates the application of these methods for assessing clinical conditions such as gastroparesis and mesenteric ischemia. In "Modelling Tissue Electrophysiology in the GITract: Past, Present and Future", by Corrias et al. provide a review of the historical and existing methods and software packages for conducting computational simulations of GI electrical activity. Such simulations provide a unique method for interpreting and analyzing a variety of experimental measurements.

The final group of chapters, review current techniques for the measurement of GI mechanical function. Manometric catheters are a primary technique used to record motility patterns. However, as explained in chapter "Colonic Manometry: What Do the Squiggly Lines Really Tell Us?" by Dinning the interpretation of these measurements remains uncertain. In this chapter, the motor patterns recorded by colonic manometry are compared to actual measurements of colonic wall motion and luminal transit. In doing the chapter aims to detail what manometry is really telling us about colonic function. In contrast, the chapter "Spatiotemporal Mapping Techniques for Quantifying Gut Motility" by Janssen et al. review the use of videographic methods for directly measuring the movement of the GI musculature in in vitro studies. From these videographic data, it is possible to produce two-dimensional spatio-temporal maps and also derive strain maps.

Practical considerations for performing such studies are also discussed. The final chapter "Computational Modeling of Gastrointestinal Fluid Dynamics" in this volume by Ferrua et al. reviews current research aimed at using computational fluid dynamic (CFD) techniques to predict the flow and mixing behavior of GI contents during digestion. The potential applications of this new approach to advance research in the food and health sectors as well as future challenges in this area are discussed.

Our goal in this focused volume is to provide a brief overview of a range of research areas and highlight future directions and challenges for the community as a whole. It is clear that not all aspects of research in gastrointestinal motility have been equally represented (e.g., research into enteric neurons, clinical imaging techniques which have been reviewed recently elsewhere). Although significant advances have been made in the recent decades, it is evident that there remains much to be learnt by the research community as a whole. Many exciting challenges await us in the near future!

Acknowledgments LKC was supported in part by the New Zealand Health Research Council, and the NIH (R01 DK64775). GF was supported in part by grants from the NIH (R01 DK57061, P01 DK 68055-P1 and R01 DK 52766). The New Advances in Gastrointestinal Motility Research Meeting held in Auckland, New Zealand was made possible by a grant from The University of Auckland Faculty Development Research Fund. The authors would like to acknowledge the contributions of Professor Andrew Pullan who tragically passed away between the inception and completion of this series.

References

1. Alvarez WC, Mahoney LJ (1922) Action currents in stomach and intestine. Am J Physiol 58:476–493
2. Alvarez WC (1992) The electrogastrogram and what it shows. JAMA 78:1116–1119
3. Cajal RR (1911) Rev Clin, 5th edn. Madrid 1911, pp 206–209
4. Grover M, Farrugia G, Lurken MS, Bernard CE, Faussone-Pellegrini MS, Smyrk TC, Parkman HP, Abell TL, Snape WJ, Hasler WL, Unalp-Arida A, Nguyen L, Koch KL, Calles J, Lee L, Tonascia J, Hamilton FA, Pasricha PJ (2011) Consortium NGCR. Cellular changes in diabetic and idiopathic gastroparesis. Gastroenterology 140(5):1575–1585 e1578
5. He CL, Burgart L, Wang L, Pemberton J, Young-Fadok T, Szurszewski J, Farrugia G (2000) Decreased interstitial cell of cajal volume in patients with slow-transit constipation. Gastroenterology 118(1):14–21
6. Huizinga JD, Thuneberg L, Kluppel M, Malysz J, Mikkelsen HB, Bernstein A (1995) W/kit gene required for interstitial cells of Cajal and for intestinal pacemaker activity. Nature 373(6512):347–349
7. Isozaki K, Hirota S, Miyagawa J, Taniguchi M, Shinomura Y, Matsuzawa Y (1997) Deficiency of c-kit + cells in patients with a myopathic form of chronic idiopathic intestinal pseudo-obstruction. Am J Gastroenterol 92(2):332–334
8. Miller SM, Narasimhan RA, Schmalz PF, Soffer EE, Walsh RM, Krishnamurthi V, Pasricha PJ, Szurszewski JH, Farrugia G (2008) Distribution of interstitial cells of Cajal and nitrergic neurons in normal and diabetic human appendix. Neurogastroenterol Motil 20(4):349–357

9. Waller AD (1887) A demonstration on man of electromotive changes accompanying the heart's beat. J Physiol (Lond) 8:229–234
10. Ward SM, Burns AJ, Torihashi S, Sanders KM (1994) Mutation of the proto-oncogene c-kit blocks development of interstitial cells and electrical rhythmicity in murine intestine. J Physiol (Lond) 480(Pt 1):91–97
11. Wedel T, Spiegler J, Soellner S, Roblick UJ, Schiedeck TH, Bruch HP, Krammer HJ (2002) Enteric nerves and interstitial cells of Cajal are altered in patients with slow-transit constipation and megacolon. Gastroenterology 123(5):1459–1467

Role of Ion Channel Mechanosensitivity in the Gut: Mechano-Electrical Feedback Exemplified By Stretch-Dependence of $Na_v1.5$

Arthur Beyder, Rachel Lees-Green and Gianrico Farrugia

Abstract $Na_V1.5$ is a voltage-gated sodium channel found in the human gastrointestinal tract. In smooth muscle cells (SMC) and interstitial cells of Cajal (ICC), $Na_V1.5$ regulates the resting potential as well as slow wave upstroke and frequency. Mutations in *SCN5A*, the gene coding for $Na_V1.5$, are associated with gastrointestinal functional disorders. Some patients with irritable bowel syndrome (IBS) have *SCN5A* mutations that result in functionally abnormal channels. $Na_V1.5$ is mechanosensitive, and some of the mutations associated with gastrointestinal (GI) motility disorders have impaired mechanosensitivity. $Na_V1.5$ mechanosensitivity involves the actin cytoskeleton and associating proteins as well as the lipid bilayer. Mechanical stimulation of $Na_V1.5$ results in an increase in peak current, acceleration of the voltage-dependent activation & inactivation and slowed recovery from inactivation. Biophysical modeling is increasingly used as a tool for investigating the effect of $Na_V1.5$ and other mechanosensitive components in slow wave generation. We summarize the existing models of gastrointestinal cellular electrical activity, and specifically a model of $Na_V1.5$ mechanosensitivity that has been incorporated into one of the cell models. In agreement with the experimental data, mechanical stimulation of $Na_V1.5$ results in increased excitability of the cell model in silico. In this chapter we discuss the current knowledge of the molecular mechanism of $Na_V1.5$ mechanosensitivity, mechano-electrical consequences of $Na_V1.5$ stretch in cells and propose physiologic and pathophysiologic consequences.

All organisms, even unicellular organisms and plants, are sensitive to mechanical input. In the larger organisms mechanosensitivity modulates a variety of physiological processes at the organ, cellular and molecular levels. Effective mechanical

A. Beyder (✉) · G. Farrugia
Enteric Neuroscience Program and Division of Gastroenterology and Hepatology,
Mayo Clinic, Rochester, MN, USA
e-mail: beyder.arthur@mayo.edu

R. Lees-Green
Auckland Bioengineering Institute, The University of Auckland, Auckland, New Zealand

L. K. Cheng et al. (eds.), *New Advances in Gastrointestinal Motility Research*,
Lecture Notes in Computational Vision and Biomechanics 10,
DOI: 10.1007/978-94-007-6561-0_2, © Springer Science+Business Media Dordrecht 2013

function is central for the gastrointestinal system. Mechanosensitivity underlies several fundamental processes involved in digestion, absorption and motility. Abnormalities in mechanosensitivity have been implicated in a variety of gastrointestinal diseases such as achalasia, gastroparesis, irritable bowel syndrome, intestinal pseudo-obstruction and slow transit constipation. Mechanical force is usually transduced at the plasma membrane level by mechano sensitive ion channels. While there have been significant advances in our understanding of bacterial mechanosensitive ion channels, much less is known about their mammalian counterparts. This chapter will focus on an example of a mechanically sensitive voltage-gated sodium selective ion channel $Na_V1.5$ found in the heart and in the human gastrointestinal tract. We will discuss the current knowledge of the molecular mechanism of $Na_V1.5$ mechanosensitivity, mechano-electrical consequences of $Na_V1.5$ stretch in cells and propose physiologic and pathophysiologic consequences.

1 Mechanosensitivity of Voltage-Gated Ion Channels May Contribute to Mechano-Electrical Feedback

In the gastrointestinal tract the interstitial cells of Cajal (ICC) generate cyclical electrical activity called slow waves (Fig. 1). These periodic electrical depolarizations are largely responsible for the impressive coordinated autonomous activity of the gastrointestinal tissue, even upon tissue excision. Slow waves are transmitted to the smooth muscle cells (SMC), thereby depolarizing the SMC membrane. Depolarization of the SMC membrane beyond the activation threshold of the voltage-gated calcium channels (Ca_V) results in channel opening and Ca^{2+} influx. This calcium influx then initiates the contractile activity that underpins gastrointestinal motility.

The generation, amplification and propagation of the slow waves require a large repertoire of voltage-gated ion channels. A particular type of voltage-gated channels—the voltage-gated sodium channels (Na_V), both TTX-sensitive [56, 69, 82] and TTX-resistant [26, 33, 58, 72]—are found in both the SMC and ICC of the gastrointestinal tract of many animals including humans. In humans $Na_V1.5$ is expressed in the jejunum circular layer [33, 72], and this channel is also found in the dog [71] and rat small intestine. This channel is functionally relevant, as block by lidocaine and QX-314 slows the upstroke and shortens the duration of the slow wave, with both effects contributing to the decrease in slow wave frequency [72]. Furthermore, abnormalities in $Na_V1.5$ are associated with pathology. The patients with mutations in *SCN5A* gene, which codes for $Na_V1.5$, have more abdominal symptoms [45] and increased IBS prevalence [64, 65] compared to controls. Recent studies also suggest that $Na_V1.5$ channels from patients with IBS are functionally abnormal [9, 64]. Abnormalities in the Na_V channel macromolecular complex are also associated with intestinal pseudo-obstruction [53].

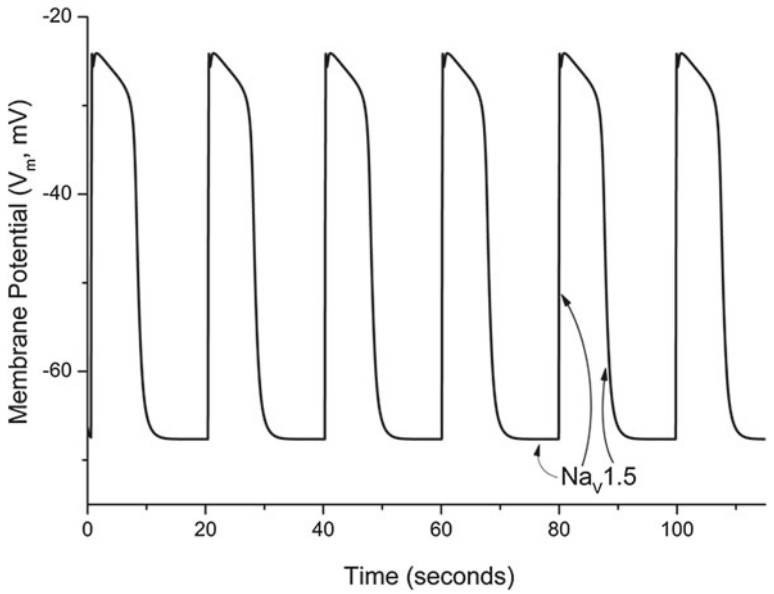

Fig. 1 Simulated gastric ICC slow waves. An established gastric ICC slow wave computational model [16] used to simulate 120 s of the periodic depolarization of slow waves. Na^+ current contributes to the slow wave during the upstroke, downstroke and the baseline of the slow waves

The mechanical state of the electromechanical organs alters the electrical activity, a so-called mechano-electrical feedback. Multiple mechanisms are responsible for the mechano-electrical feedback in the gastrointestinal tract. To a large degree, stretch stimuli within the gut are processed by the mechanisms residing in the wall by enteroendocrine cells [57], by the enteric nervous system [40], the ICC [81] and the SMC [23]. Since voltage-gated channels participate in the generation and coordination of the slow waves, the most direct mechano-electrical feedback mechanism may involve mechanosensitivity of voltage-gated ion channels. A subset of voltage-gated ion channels is mechanically sensitive. For these channels mechanical input regulates voltage-dependent activity. The voltage-dependent properties of these channels are of overriding importance to the electrical and electro-mechanical activity in the gut [6]; mechano-electrical feedback on voltage gated channels may be an important physiologic and patho-physiologic mechanism.

Pressure sensitivity of voltage-gated ion channels was realized even in the early squid axon experiments [13, 14]. As the tools to probe mechano-electrical feedback at the molecular level have improved, representatives from all voltage-gated ion channel families (K_V [30, 41, 42, 75], Ca_V [12, 23, 50], Na_V [7, 55, 74]) have been shown to be mechanically sensitive. In the sections below we will detail the current state of knowledge on the mechanism of $Na_V1.5$ mechanosensitivity.

2 Cellular Mechanosensitivity is Multifaceted

Multiple mechanisms are involved in cellular mechanosensation, including intracellular (e.g., cytoskeleton) [77] and extracellular (e.g., extracellular matrix) [67] response elements as well as the stretch-sensitive ion channels [63]. We propose that mechanosensation by voltage-gated ion channels in cells of electrically active tissues provides mechano-electrical feedback to the cell in order to modify the underlying electrical behavior. To achieve this goal the stretch-sensitive ion channels need to be able to receive input on the mechanical state of the surrounding environment. It is known that the eukaryotic stretch sensitive channels receive a variable amount of input from each of the above components, depending on cell type, channel type, level of connection to the anchoring protein and location within the membrane. Below, we review the evidence that the mechanism of $Na_V1.5$ mechanosensitivity involves both cytoskeletal connections and lipid membrane.

3 Actin Cytoskeleton is Critical for $Na_V1.5$ Shear-Stress Mechanosensitivity

$Na_V1.5$ is known to connect to multiple intracellular accessory proteins [1], including some that have been implicated in mechanosensation. Some established mechano-relevant associating proteins include ankyrin B [5], actin [70] via dystrophin [61] via syntrophin $\gamma 2$ [59] and titin via telethonin [53] (Fig. 2). Disruption or alteration of these associations has been linked to $Na_V1.5$ dysfunction.

The initial studies demonstrating $Na_V1.5$ mechanosensitivity were conducted in voltage clamped freshly dissociated ICC and SMC from human jejunum. In one study, freshly isolated ICC were stimulated by 10 mL/min perfusion. Flow of

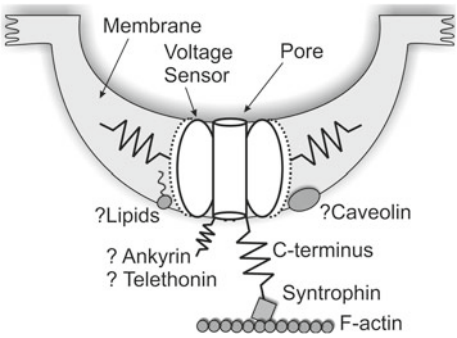

Fig. 2 $Na_V1.5$ mechanosensitivity components. A $Na_V1.5$ protein complex is associated with multiple intracellular proteins. Syntrophin and actin have been directly linked to $Na_V1.5$ mechanosensitivity. Other targets include ankyrin and telethonin. Multiple potential targets exist in the membrane, including caveolin and bilayer lipids

solution over a cell is known to induce shear stress, and this is a common mode of mechano-stimulation in vitro. This shear stress increased $Na_V1.5$ peak currents up to 40 % (from 146 ± 30 to 191 ± 43 pA) [72]. Na_V current was also identified in the SMC [33], and the responsible channel was later found to be $Na_V1.5$ [58]. Similar to the ICC, in SMC $Na_V1.5$ current was also shear sensitive, with shear increasing peak currents by 27 ± 3 % (from 147 ± 21 to 175 ± 23 pA) (Fig. 3a). Shear stress also accelerated activation, evidenced as shortening time to peak for activating voltages (−50 to −2 mV). On the other hand, inactivation kinetics were not affected by shear [70]. The change in the activation kinetics without a change in the inactivation kinetics suggested that the increase in peak current seen with shear-stress is unlikely simply from insertion of channels into the membrane.

It is generally known that the mechanism of shear sensitivity involves the cytoskeleton [29], and that $Na_V1.5$ function in the cardiac myocyte is modified by cytoskeletal components, such as actin [78]. Thus, the involvement of the actin, microtubule and intermediate filament cytoskeletal components in $Na_V1.5$ shear

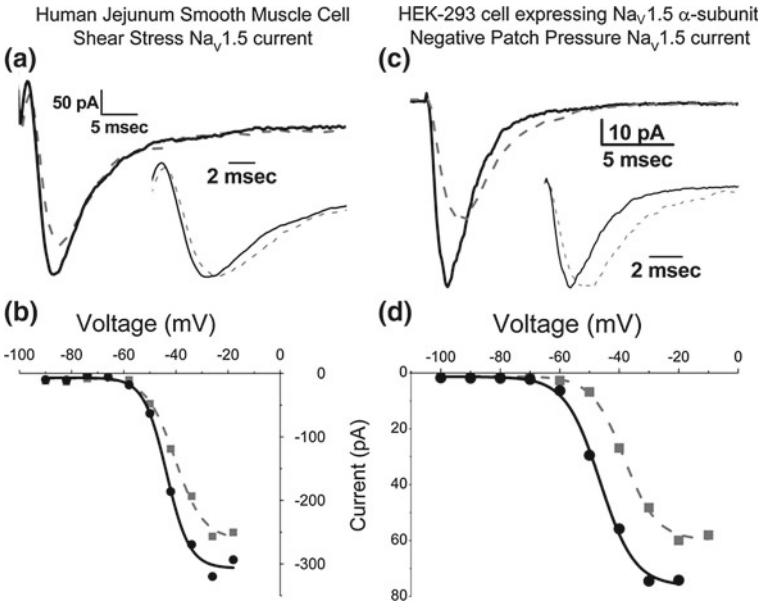

Fig. 3 Mechanosensitivity of $Na_V1.5$ to shear and patch pressure. **a** In a whole-cell voltage-clamped human jejunum smooth muscle cell, time-dependence of $Na_V1.5$ current is shown at −20 mV (*grey dash trace*). Flow at 10 mL/min increases peak current (*black trace*). When normalized to peak current, the acceleration in activation kinetics is notable (*inset*). **b** Current–voltage (IV) curves at rest (*grey dash*) and during flow (*black*) demonstrate an increase in peak current. **c** In a cell-attached patch from HEK293 cell, time-dependent $Na_V1.5$ current is shown at rest (0 mmHg, *grey dash*) and an increase in peak current with negative pressure (−30 mmHg, *black*). The kinetics of activation and inactivation are noticeably accelerated as shown in the traces normalized to peak current (*inset*). **d** IV curves for this patch at rest (*grey dash*) and with −30 mmHg pressure (*black*) showing a hyperpolarizing shift in the voltage-dependence of activation

mechanosensitivity was tested next. Pharmacological disruption of multiple cytoskeletal components did not affect $Na_V1.5$ function at rest, and disruption of the microtubule and intermediate filament networks did not affect $Na_V1.5$ shear sensitivity. However, actin cytoskeleton disruption by cytochalasin D and gelsolin effectively abolished shear sensitivity. On the other hand, actin network stabilization by phalloidin preserved $Na_V1.5$ mechanosensitivity [70]. Actin is not known to directly associate with ion channels. Instead, actin connection to ion channels, including $Na_V1.5$, involves adapter proteins. In the case of $Na_V1.5$, one of the adapter proteins is syntrophin $\gamma 2$ (Fig. 2). In the human gastrointestinal SMC syntrophin $\gamma 2$ PDZ domain was found to directly interact with the last 10 amino acids of $Na_V1.5$ and this interaction altered $Na_V1.5$ function at rest [59]. In a series of subsequent experiments, the disruption of this interaction eliminated $Na_V1.5$ shear stress mechanosensitivity [59].

It appears that $Na_V1.5$ shear stress mechanosensitivity is dependent on the connection between the channel's cytoplasmic C-terminus and syntrophin $\gamma 2$ connecting to the f-actin cytoskeleton. This mechanism of $Na_V1.5$ mechanosensitivity requires further exploration. Three broad outstanding questions remain regarding the mechanism of $Na_V1.5$ shear sensitivity. (1) Are other mechano-relevant associating proteins (e.g., ankyrin and telethonin) involved (Fig. 2)? (2) What is the rate-limiting mechanotransducer? (3) How does shear actually gate $Na_V1.5$?

4 The Mechanism of Stretch-Dependent $Na_V1.5$ Peak Current Increase

The details of mechanosensitivity by the ion-channel forming $Na_V1.5$ α-subunit can be determined in some detail using heterologous expression, such as HEK293 cells transfected with $Na_V1.5$. Shear stress mechanosensitivity was confirmed in this system, and effects were similar to those in native cells [64]. In such a system $Na_V1.5$ mechanosensitivity can be tested down to single channel level by using pressure- and voltage-clamped membrane patches, which provide an opportunity for well defined mechanical stimuli [73]. The mechanical stimulus applied to the patch is pressure, while the mechanical stimulus relevant to the ion channel is membrane tension [51]. Pressure is related to tension (T) in the simplest terms through Laplace's law,

$$\Delta T = P\Delta r/2, \tag{1}$$

where pressure is P and the radius of curvature is r. Thus for accurate estimation of tension, imaging of the patch is required [73]. In reality the stress–strain relationship of membrane complex is non-linear, so caution is required when interpreting data, but to date patch pressure has been the most robust mechanical stimulus for ion channels. In the few patch studies reported to date, $Na_V1.5$ has been consistently

mechanosensitive [7, 55]. Similar to the shear stress findings, patch pressure increases peak current and accelerates kinetics. In the patch, both positive and negative pressure produced an increase in peak current, with a −30 mmHg stimuli resulting in a 33 % peak current increase [7]. The increase in pressure-induced current appears even larger for voltages near activation, where a roughly 50 % increase was noted in a different study [55]. Since total patch current,

$$I = NP_o i, \tag{2}$$

where N is the number of channels, P_o is open probability and i is single channel current, one of these variables is responsible for the pressure-dependent current increase. Single channel experiments found that patch pressure 10–50 mmHg does not change single channel conductance, which remains fixed at ~17 pS. In this study pressure was found not to change the maximum probability of channel opening ($P_{o,max}$) and the increase in pressure-induced current was a result of an increase in the number of active channels by about 20 % [7]. However, it is unclear what mechanism is responsible for the increase in the active channel number. Two distinct possibilities exist. The first possibility is pressure-induced recruitment of channels either from additional membrane or changes in membrane fluidity. The second possibility is an awaking of a subset of previously "sleepy channels," which are channels that have been previously shown to awake with changes in temperature [52]. It is also unclear whether the mechanism of shear-induced peak current increase is similar to that experienced in the patch.

5 Pressure-Induced Acceleration in Kinetics and Shifts in Voltage-Sensitivity

Patch pressure increased peak current, accelerated kinetics and hyperpolarized voltage-sensitivity [7, 55]. Morris and Juranka [55] found a reversible acceleration of both activation and inactivation rate constants by about 40 % for $Na_V1.5$ channels expressed in Xenopus oocytes. Beyder and colleagues used $Na_V1.5$ expressed in HEK293 cells and found similar acceleration in the kinetics for all activating voltage steps, but this was only partially reversible [7] (Fig. 3c). In both studies, a single scaling constant was used to normalize kinetics, suggesting that pressure did not introduce novel gating states. The acceleration of the kinetics can be due to a shift in voltage-sensitivity. Indeed, when the current–voltage (IV) relationship was fit to a two-state Boltzmann function (described in Sect. 9.1), pressure (10–50 mmHg) shifted the voltage dependence of activation and inactivation by a remarkable 0.7 mV per mmHg [7] (Fig. 3d). These shifts in voltage sensitivity markedly hyperpolarized the voltage range of the window current with likely physiological consequences. The shift in voltage-dependence can be due to mechanical sensitivity of the voltage-sensitive activation steps or the relatively voltage-insensitive but rate-limiting gate opening, or a combination of both.

Kinetics can be normalized using a single constant, suggesting that pressure did not introduce novel kinetic states and that likely a single kinetic step was affected. Since closed-state inactivation follows voltage-activation but precedes gate opening, this transition can be used to assess the likely transition affected by pressure. It was found that closed-state inactivation appeared enhanced, suggesting that a voltage-sensing step was accelerated by pressure. These data suggested that the voltage-sensitive transitions were pressure sensitive, thereby suggesting mechanosensitivity of the voltage sensors.

Voltage sensor mechanosensitivity awaits confirmation by a more direct approach, but there are several supporting pieces of evidence for their involvement. Mechanosensitivity of an ion channel requires that at least one of the conformational transitions undergoes an area change, such that undergoing a mechanosensitive transition involves a change in free energy,

$$\Delta G = T\Delta A, \tag{3}$$

where T is tension and A is in-plane area [63]. Since ion channels are residents of the lipid bilayer, expansion within the bilayer is very likely to be sensitive to the protein-lipid interface. Indeed, previous studies have demonstrated that Na_V function is sensitive to the surrounding lipids [54] and amphiphiles [49]. In the recently published crystal structure of Na_V, the voltage-sensors have significant exposure to lipid membrane and based on that structure (discussed below), the voltage sensors would be expected to have a significant impact from a stretched bilayer. Previous studies also show that even the isolated voltage sensor domains have a dimpling effect on the lipid bilayer [10, 27, 39], adding a third dimension to the mechanical sensitivity of bilayer-voltage sensor interface.

In addition to the in-plane area expansion, the curvature of the lipid bilayer may add a third dimension in the consideration of $Na_V1.5$ mechanosensitivity. For example, highly curved areas called caveoli are known to be mechanosensitive [68], and thus molecules found within these domains would be exposed to mechanical input. In fact, it is known that in the cardiac myocytes $Na_V1.5$ are targeted to specific membrane domains with intrinsic curvature, including caveoli [79, 83] and T-tubules [66].

While it is likely that the voltage sensor domains are the mechanically sensitive parts of $Na_V1.5$, it is unclear whether (1) all four of the voltage sensors are equally involved, (2) there is a connection to the cytoskeletal mechanism described above.

6 Pressure Stabilizes $Na_V1.5$ Entry into Inactivation and Slows Recovery

In cell-attached patches pressure consistently accelerates inactivation, which is not seen in whole cell bath perfusion experiments. The kinetic acceleration of fast inactivation and the hyperpolarizing shift in the voltage-dependence of

inactivation mirrors those of kinetic acceleration of activation, and the shift in the voltage-dependence of activation, respectively. It is most likely that the changes in fast inactivation are secondary to the changes seen in the activation. In single channel studies the process of activation appears to be rate limiting, so the appearance of kinetic link and voltage-dependence of the much more rapid inactivation reflect those measures in activation [2]. This explanation is also consistent with the results of the pressure-induced changes in $Na_V1.5$. Namely, pressure accelerated the kinetics of activation and inactivation by the same linear constant, and the shift in voltage dependence was also equivalent in the direction and magnitude over a range of pressures [7, 55]. Thus, the appearance of the change in the kinetics and voltage-dependence of inactivation with pressure was likely linked to the activation.

An additional finding was that the recovery from inactivation of $Na_V1.5$ was significantly slowed with pressure. At -30 mmHg, for all but one holding potential the recovery from fast inactivation was slowed. While the left-shift in the voltage-dependence of inactivation explains some of the slowing of the recovery from inactivation, the experiments were done at the voltages that were sufficiently hyperpolarized to provide full channel availability.

7 Na_V Crystal Structure Provides Some Answers

The data presented above detail the currently known functional aspects of $Na_V1.5$ mechanosensitivity. Our understanding is incomplete and more data are needed to understand the mechanisms of $Na_V1.5$ mechanosensitivity. Specifically, fine details of protein structure are required to pinpoint further experimentation. Major recent advances in transmembrane protein X-ray crystallography have resulted in significant advances in visualizing ion channel structure. Recently, the first Na_V crystal structure was published [60]. Although this is the first Na_V structure available, a significant progress has been made over the last decade as K_V crystal structures of multiple channel species and in several conformations have been worked out [36, 37, 46–48]. None of these crystals were grown in a well-controlled mechanical environment. Nevertheless, several structural aspects are of interest given the body of the above functional data. First, crystal structures of all voltage-sensitive channels show that voltage sensor domains are loosely associated with the pore domain and have significant exposure to the lipid bilayer. Since the bilayer is known to be important for mechanotransduction, it is likely that this extensive interaction between the lipid bilayer and the voltage-sensor mediates at least some mechanical input. Second, water filled vestibules were found within the voltage-sensor domains, and these likely change during the activation process of the channels, and are also potential sites for mechanosensitivity. Third, the attachment of the voltage-sensor domains to the intracellular gate is via a string-like linker. This linker is another potential area of mechanosensitivity [8, 41].

8 $Na_V1.5$ Mechanosensitivity Abnormalities May be Pathologic

It is already known that for some mutations of *SCN5A*, the $Na_V1.5$ channels have disrupted mechanosensitivity [3, 64]. $Na_V1.5$ is expressed in the cardiac muscle and in the human gastrointestinal tract. $Na_V1.5$ mutations in both of these tissues are linked to disease. In the heart, $Na_V1.5$ dysfunction leads to LQT3 if gain-of-function [4] and Brugada syndrome if loss-of-function [76]. In the gut, $Na_V1.5$ mutations have been linked to abdominal pain syndromes [45] and specifically IBS [65]. $Na_V1.5$ mutants with impaired mechanosensitivity have been described in LQT3 [3] and IBS [65]. A G298S mutation discovered in a cohort of IBS patients resulted in $Na_V1.5$ channels with decreased peak currents in four known common backgrounds. In addition, in one of the backgrounds G298S led to a significant decrease in mechanosensitivity to shear stress [64]. Multiple other $Na_V1.5$ mutations have been described in a larger cohort of IBS patients [65], and several of these have also been found to be functionally abnormal [9], but their mechanosensitive behavior awaits further exploration. In the heart, two classic mutations linked to LQT3 were found to have mechanosensitive behavior different from the controls [3]. More specifically, $Na_V1.5$ R1623Q and R1626P were found to be mechanosensitive, but the typical coupling in the acceleration of activation and inactivation with stretch was disrupted. Thus, while in the control channels stretch accelerates both activation and inactivation to the same degree, the 1623 mutant has a typical acceleration of the activation, but the acceleration in inactivation is sped up to a smaller degree. The result is a larger and prolonged Na^+ current with stretch in 1623, which would predispose to early after-depolarizations and therefore arrhythmias.

9 Modeling the Effects of Ion Channel Mechanosensitivity in Silico

Mechanosensitivity and mechano-electrical feedback is difficult to study experimentally. Experimental tools necessary to obtain high fidelity data in both mechanical and electrical domains continue to be developed, but major limitations exist. Biophysically-based computational models are an ideal tool for integrating diverse findings from a wide variety of experimental scales and systems. This approach uses experimental data, but also allows the experimental conditions to be simulated by changing appropriate parameter values. An in-silico approach enables models to be used to test theories about cell electrophysiology and to predict the results for difficult experiments.

9.1 Introduction to Biophysically-Based Cell Models

Biophysically-based cell models simulate the electrical activity of excitable cells like ICC and SMC by modeling the components and processes that are believed to underlie the cellular electrical activity [20]. Different types of ion channels, pumps and other ion transport mechanisms can be integrated into a global model of the homogenized membrane potential and ion concentrations in the cell. Ion fluxes between different subcellular compartments in the cell may also be included, such as between endoplasmic reticulum and cytoplasm.

These biophysical cell models are modular and multi-scale, as each of the components in a model can be independently replaced or updated when new data become available. In this way, mechanosensitivity can be introduced into multiple components of a cell model. In addition, the influence of individual components on whole cell behavior can be predicted by altering the relative contribution of the component to the cell model.

The equations for the voltage-gated ion currents in biophysical cell models are typically developed using the classical Hodgkin-Huxley type approach. The whole cell ion currents are simulated by modeling the voltage dependence of activation and inactivation using voltage clamp data. The ion current through a particular type of ion channel is modeled as,

$$I_{\text{ion}} = g_{ion} \cdot d \cdot f \cdot (V_m - E_{rev}), \tag{4}$$

where g_{ion} is the maximum whole cell conductance, V_m is the cell membrane potential, E_{rev} is the equilibrium potential of the ion (also called the reversal or Nernst potential), and d and f are the activation and inactivation gating variables respectively [20, 32]. The equilibrium potential for a particular ion, E_{rev}, is the membrane potential at which the concentration gradient and the electrical gradient across the cell membrane are balanced such that there is no net ionic current across the membrane. Thus, the equilibrium potential is determined by the intracellular and extracellular ion concentrations.

The gating variables, d and f, used to model the sensitivity of the ion channel open state to various stimuli including voltage, mechanical stimuli, and ligand concentrations, are calculated using:

$$\frac{dx}{dt} = \frac{x_\infty - x(t)}{\tau_x}, \tag{5}$$

where x_∞ is the steady-state value for gating variable x, and τ_x is the time constant. The steady-state of the gating variables, d_∞ and f_∞, are often described using a Boltzmann function of the form:

$$\frac{I_{ion}}{I_{\max}} = \frac{1}{1 + e^{\left(V_{1/2} - V_m\right)/dV}}, \tag{6}$$

where I_{max} is the maximum current recorded through the ion channel, V_m is the membrane potential, $V_{1/2}$ is the voltage at which I_{ion} is half-maximal, and dV represents the slope of a sigmoidal curve describing the voltage dependence of the current [22].

These simple ion current models, while elegant and effective for describing the activation and inactivation of whole cell or macroscopic currents within a cell model, can be insufficient to capture the full complexity of ion currents, especially at the level of single ion channels or small clusters of channels.

An alternative way to model ion currents is as a Markov process, in which the kinetics of the ion channel at any point in time depend only on the current state of the channel, and not on any of the previous channel transitions. This enables simulation of the stochastic opening and closing of individual ion channels [31, 38].

The Hodgkin-Huxley formulation starts from the assumption that a channel has two states: open and closed. A Markov model can incorporate multiple open, closed and inactive states. The transition rates between each of the different states can be dependent on factors such as membrane potential, ion and ligand concentrations, and mechanical stretch. Unlike the Hodgkin-Huxley model, Markov models are able to capture the varied responses of ion channels in different states. For example, sodium channel activation and inactivation kinetics are known to be linked [2, 17, 31], and Beyder et al. [7] observed that stretch caused acceleration of $Na_V1.5$ inactivation secondary to accelerated activation kinetics. Markov models can incorporate the direct kinetic link between activation and inactivation of $Na_V1.5$ [62], whereas in a Hodgkin-Huxley type model activation and inactivation kinetics are independent [17].

Hodgkin-Huxley models are a subclass of Markov models, and therefore can indirectly include the behavior of channels with multiple closed, open and inactivated states, as well as recovery from inactivation, and multiple inactivation time constants, as evidenced by Markov adaptations of Hodgkin-Huxley models. Nonetheless, Markov models are essential for simulating the stochastic nature of individual or small groups of ion channels, and for describing more complex behaviors including the relationship between the state of an ion channel and its response to a stimulus [17].

Due to the extra states in Markov models, they are more difficult to develop and more computationally expensive to solve than Hodgkin-Huxley ion channel models. For modeling studies that aim to investigate the behavior of ion currents, Markov models provide a more accurate and detailed representation, but Hodgkin-Huxley type models are often sufficient for studies that aim to simply reproduce dynamic membrane potential activity like slow waves [17].

9.2 Established Models of Slow Waves

Four biophysically-based models of cellular level gastrointestinal slow wave activity have been published: a small intestine ICC slow wave model by Youm et al. [84], Corrias and Buist gastric SMC [15] and ICC [16] models, and a small intestine mouse ICC slow wave model by Faville et al. [24], which was based on a preceding model of ICC unitary potentials [25]. Each model will be briefly discussed below; for more detail see the recent review by Lees-Green et al. [44].

The ICC model developed by Youm et al. [84] was based on cardiac cell models, so the ion channels and calcium signaling pathways implemented in the model do not match well with the current understanding of ICC electrophysiology. This model contained a complex description of inositol trisphosphate (IP_3) production and degradation, as well as calcium ion (Ca^{2+}) transport within the sarcoendoplasmic reticulum (ER or SR). However, it did not incorporate mitochondria, which have been implicated in slow wave generation [80]; nor did it incorporate $Na_V1.5$ [72] or Cl^- channels [35, 85], both of which are now believed to play an important role in slow wave generation [44].

Both the Faville et al. [24, 25] and the Corrias and Buist [16] ICC models were based on a hypothesis of pacemaking mechanisms that has since been called into question [34, 44, 85]. Nevertheless, these models provide a good system for testing various aspects of ICC function, as the majority of the ion channels and other components in the models are still consistent with the present understanding of ICC electrophysiology. The Corrias and Buist model incorporated $Na_V1.5$ and a calcium-activated chloride current [16].

Faville et al. [24] developed a highly detailed model in which the slow waves are produced by the summation of unitary potentials, which are believed to be the underlying electrical activity responsible for generating slow waves. In contrast, Corrias and Buist [16] developed a model that reproduces the aggregate electrical activity of an ICC. It is less demanding computationally; therefore it is much more suitable than the Faville model for inclusion in tissue- and organ-level multi-scale models of the gastrointestinal tract. For example, two modeling studies have used the Corrias and Buist ICC model to test the viability of different entrainment mechanisms in networks of ICC—a voltage-dependent Ca^{2+} influx [11] and a voltage-dependent intracellular Ca^{2+} release mechanism [21].

Only one model of gastrointestinal SMC electrical activity from the stomach is currently available [15]. Unlike the ICC models, the SMC model is not self-excitable; slow waves are generated by the SMC model in response to a pacing stimulus current, and the signal generated by the model depends in large part on the shape of the input stimulus current.

The SMC model has been used to test the effects of different gastric electrical stimulation protocols on gastric slow waves in order to evaluate the motility outcomes and energy efficiency of each protocol [18]. Experiments on isolated rodent gastric SMC were used to validate the simulation results for a handful of selected stimulation protocols. This study demonstrated the utility of cell models

for investigating a comprehensive range of protocols while reducing reliance on animal experiments [18].

The SMC model [15] has also been used in several multi-scale modeling studies in conjunction with the Corrias and Buist ICC model [16] to investigate the electrical activity of the whole stomach, as discussed by Corrias et al. in "Modelling Tissue Electrophysiology in the GI Tract: Past, Present and Future". Two recent studies include that of Buist et al. [11] who developed a model of slow wave propagation along the stomach and Du et al. [19] who used a multi-scale model to predict a body surface EGG recording corresponding to a known slow wave activity on the stomach surface.

9.3 Introducing Stretch Sensitivity to Existing Cell Models

The existing cell models of gastrointestinal slow wave activity do not contain mechanosensing mechanisms, while only two models of ICC [16] and SMC [15] included a description of voltage-dependent $Na_V1.5$ currents. However, mechanosensitive ion channels can be easily incorporated into existing slow wave models by substituting a stretch-dependent $Na_V1.5$ model in place of an existing model of $Na_V1.5$ [15, 16] or another appropriate cation current, such as the phenomenological cation leak current [24], as demonstrated recently [43].

A highly detailed $Na_V1.5$ model is required to incorporate all of the experimentally observed $Na_V1.5$ mechanosensitive parameters. However, this may not be necessary for simulating the main effects of stretch on slow waves at a cell or tissue level. We integrated several aspects of $Na_V1.5$ pressure-sensitivity [7] using a Hodgkin-Huxley formulation into the available small intestine ICC slow wave model [24]. Specifically, the pressure-dependent hyperpolarizing shift in the voltage half-points of activation and inactivation were incorporated into calculations of the activation and inactivation steady-state parameters and time constants.

To simulate the effects of stretch with this model, negative pressures of −40 to −60 mmHg were applied to $Na_V1.5$ channels (Fig. 4). The largest pressure-induced changes in the simulated slow wave were observed at the highest pressure of −60 mmHg, as detailed in Table 1. Although the increase in frequency was small, a similar increase has also been observed in a study on strips of human small intestine tissue, where stretch caused slow wave frequency to increase from 7 to 7.3 cycles per minute [72].

These changes all suggest an excitatory role for $Na_V1.5$ during stretch, which is in agreement with the effects of stretch on sections of human small intestine [72], confirming that $Na_V1.5$ mechanosensitivity is likely to contribute to the effects of stretch on slow waves in GI tissue.

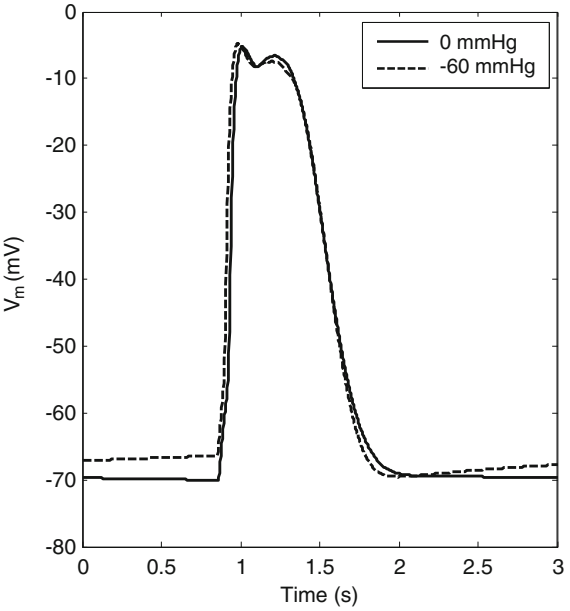

Fig. 4 Simulated slow waves from the modified Faville ICC model with no pressure (0 mmHg) and with −60 mmHg pressure applied to $Na_V1.5$

Table 1 Effects of applying −60 mmHg pressure on four key characteristics of simulated ICC slow wave activity

	0 mmHg	−60 mmHg	% Change
Resting membrane potential	−70.2 mV	−66.4 mV	5.3
Upstroke rate	623 mV s^{-1}	693 mV s^{-1}	11.4
Duration	615 ms	645 ms	4.9
Frequency	17.0 cpm	17.1 cpm	0.85

Slow waves were simulated using a modified version of the Faville small intestine ICC model with pressure-dependent changes in $I_{Nav1.5}$

9.4 The Future of Modeling $Na_V1.5$ Mechanosensitivity

The initial results from modeling $Na_V1.5$ mechanosensitivity in small intestine ICC are promising. Further modeling and experimental studies can provide additional insight into the role of $Na_V1.5$ in mediating stretch-dependent changes of slow waves in the gastrointestinal tract.

The stretch-dependent shift in voltage half-points implemented in the Hodgkin-Huxley formulation of $Na_V1.5$ in small intestine ICC altered the slow wave by causing a hyperpolarizing shift in the window current towards the resting membrane potential, thus increasing the baseline Na^+ current during the resting phase. It is likely that the resultant depolarization of the resting membrane potential contributed to the increased frequency and upstroke rate of the slow waves [43].

Some aspects of $Na_V1.5$ mechanosensitivity were not included in the Hodgkin-Huxley formulation [43]. These include the stabilization of inactivated states and slowed recovery from inactivation [7], which may affect the repolarization phase of slow waves and further contribute to the resting potential and excitability. A Markov formulation of $Na_V1.5$ [62] could be adopted to directly model the effect of stretch on the inactivated states and the kinetic link between activation and inactivation.

An important goal of modeling stretch is to expand this work to investigate mechanosensitivity on the tissue scale. The dynamic effects of mechanoelectrical and electromechanical feedback cycles on the tissue and organ level can be further explored by modeling, using both ICC and SMC models with an integrated model of $Na_V1.5$ mechanosensitivity.

It is likely that most channels in the GI tract have some mechanosensitivity. In general, any channel that has changes in its in-plane area during gating should be mechanically sensitive. Many channels found in the GI tract have already been shown to be mechanosensitive, including L-type Ca^{2+} channels [50] as well as $Na_V1.5$, but the level of available data, especially from primary cells, is limited. Tissue level models will be enhanced by incorporating each of these ion channel models into both ICC and SMC, where appropriate.

10 The Future of Mechano-Electrical Feedback Experimentation and Modeling

In this chapter we summarized the experimental and modeling data available for gut mechano-electrical feedback at the cellular and molecular scale using $Na_V1.5$ as an example. It is clear that much more remains to be done in both the experimental and modeling arenas. The experimentalists will need to continue to develop the experimental tools for the study of molecular electro mechanics, to expand the focus to other ion channels and to assess mechano sensitive states of ion channels comprehensively. The modelers will need to refine the existing cellular and molecular models to include a more comprehensive repertoire of ion channels, to have the flexibility to integrate multiple kinetic states into the molecular models and to couple mechano-electrical feedback with electro-mechanical output [28]. This combined work will allow the exciting opportunity to examine mechano-electrical feedback at enlarging anatomic scales, to predict the impact of the individual molecular components on tissue physiology, to understand the pathophysiology relating to ion channel mechanosensitivity, and to most importantly discover therapeutic options for our patients.

Acknowledgments Work supported in part by a grant from the NIH (R01 DK52766) (GF) and American Physiological Society Career Enhancement Award (AB).

References

1. Abriel H (2010) Cardiac sodium channel Na(v)1.5 and interacting proteins: Physiology and pathophysiology. J Mol Cell Cardiol 48(1):2–11
2. Aldrich RW, Corey DP, Stevens CF (1983) A reinterpretation of mammalian sodium channel gating based on single channel recording. Nature 306(5942):436–441
3. Banderali U, Juranka PF, Clark RB, Giles WR, Morris CE (2010) Impaired stretch modulation in potentially lethal cardiac sodium channel mutants. Channels (Austin) 4(1):12–21
4. Bennett PB, Yazawa K, Makita N, George AL Jr (1995) Molecular mechanism for an inherited cardiac arrhythmia. Nature 376(6542):683–685
5. Bennett V, Healy J (2008) Organizing the fluid membrane bilayer: diseases linked to spectrin and ankyrin. Trends Mol Med 14(1):28–36
6. Beyder A, Farrugia G (2012) Targeting ion channels for the treatment of gastrointestinal motility disorders. Therap Adv Gastroenterol 5(1):5–21
7. Beyder A, Rae, JL, Bernard, C, Strege, PR, Sachs, F, Farrugia, G (2010) Mechanosensitivity of Nav1.5, a voltage-sensitive sodium channel. J Physiol 588(24):4969–4985
8. Beyder A, Sachs F (2009) Electromechanical coupling in the membranes of Shaker-transfected HEK cells. Proc Natl Acad Sci U S A 106(16):6626–6631
9. Beyder A, Strege P, Mazzone A, Bernard C, Tester DJ, Saito YA, Ackerman M, Farrugia G (2011) Mutations in SCN5A from patients with IBS result in abnormal Nav1.5 function. Digestive Diseases Week, Chicago, IL
10. Bjelkmar P, Niemela PS, Vattulainen I, Lindahl E (2009) Conformational changes and slow dynamics through microsecond polarized atomistic molecular simulation of an integral Kv1.2 ion channel. PLoS Comput Biol 5(2):e1000289
11. Buist ML, Corrias A, Poh YC (2010) A model of slow wave propagation and entrainment along the stomach. Ann Biomed Eng 38(9):3022–3030
12. Calabrese B, Tabarean IV, Juranka P, Morris CE (2002) Mechanosensitivity of N-type calcium channel currents. Biophys J 83(5):2560–2574
13. Conti F, Fioravanti R, Segal JR, Stuhmer W (1982) Pressure dependence of the sodium currents of squid giant axon. J Membr Biol 69(1):23–34
14. Conti F, Inoue I, Kukita F, Stuhmer W (1984) Pressure dependence of sodium gating currents in the squid giant axon. Eur Biophys J 11(2):137–147
15. Corrias A, Buist ML (2007) A quantitative model of gastric smooth muscle cellular activation. Ann Biomed Eng 35(9):1595–1607
16. Corrias A, Buist ML (2008) Quantitative cellular description of gastric slow wave activity. Am J Physiol Gastrointest Liver Physiol 294(4):G989–G995
17. Destexhe A, Huguenard JR (2009) Modeling voltage-dependent channels. In: Schutter ED (ed) Computational modeling methods for neuroscientists. MIT Press, Cambridge, pp 107–137
18. Du P, Li S, O'Grady G, Cheng LK, Pullan AJ, Chen JD (2009) Effects of electrical stimulation on isolated rodent gastric smooth muscle cells evaluated via a joint computational simulation and experimental approach. Am J Physiol Gastrointest Liver Physiol 297(4):G672–G680
19. Du P, O'Grady G, Cheng LK, Pullan AJ (2010) A multiscale model of the electrophysiological basis of the human electrogastrogram. Biophys J 99(9):2784–2792
20. Du P, O'Grady G, Davidson JB, Cheng LK, Pullan AJ (2010) Multiscale modeling of gastrointestinal electrophysiology and experimental validation. Crit Rev Biomed Eng 38(3):225–254
21. Du P, O'Grady G, Gibbons SJ, Yassi R, Lees-Green R, Farrugia G, Cheng LK, Pullan AJ (2009) Tissue-specific mathematical models of slow wave entrainment in wild-type and 5-HT(2B) knockout mice with altered interstitial cells of Cajal networks. Biophys J 98(9):1772–1781

22. Dubois JM, Ouanounou G, Rouzaire-Dubois B (2009) The Boltzmann equation in molecular biology. Prog Biophys Mol Biol 99(2–3):87–93
23. Farrugia G, Holm AN, Rich A, Sarr MG, Szurszewski JH, Rae JL (1999) A mechanosensitive calcium channel in human intestinal smooth muscle cells. Gastroenterology 117(4):900–905
24. Faville RA, Pullan AJ, Sanders KM, Koh SD, Lloyd CM, Smith NP (2009) Biophysically based mathematical modeling of interstitial cells of Cajal slow wave activity generated from a discrete unitary potential basis. Biophys J 96(12):4834–4852
25. Faville RA, Pullan AJ, Sanders KM, Smith NP (2008) A biophysically based mathematical model of unitary potential activity in interstitial cells of Cajal. Biophys J 95(1):88–104
26. Fernandez-Tenorio M, Gonzalez-Rodriguez P, Porras C, Castellano A, Moosmang S, Hofmann F, Urena J, Lopez-Barneo J (2010) Short communication: genetic ablation of L-type Ca2+ channels abolishes depolarization-induced Ca2+ release in arterial smooth muscle. Circ Res 106(7):1285–1289
27. Freites JA, Tobias DJ, von Heijne G, White SH (2005) Interface connections of a transmembrane voltage sensor. Proc Natl Acad Sci U S A 102(42):15059–15064
28. Gajendiran V, Buist ML (2011) A quantitative description of active force generation in gastrointestinal smooth muscle. Int J Numer Methods Biomed Eng 27(3):450–460
29. Geiger B, Bershadsky A (2002) Exploring the neighborhood: adhesion-coupled cell mechanosensors. Cell 110(2):139–142
30. Gu CX, Juranka PF, Morris CE (2001) Stretch-activation and stretch-inactivation of Shaker-IR, a voltage-gated K+ channel. Biophys J 80(6):2678–2693
31. Hille B (2001) Ion channels of excitable membranes, 3rd edn. Sinauer Associates, Inc., Sunderland
32. Hodgkin AL, Huxley AF (1952) A quantitative description of membrane current and its application to conduction and excitation in nerve. J Physiol 117(4):500–544
33. Holm AN, Rich A, Miller SM, Strege P, Ou Y, Gibbons S, Sarr MG, Szurszewski JH, Rae JL, Farrugia G (2002) Sodium current in human jejunal circular smooth muscle cells. Gastroenterology 122(1):178–187
34. Huang F, Rock JR, Harfe BD, Cheng T, Huang X, Jan YN, Jan LY (2009) Studies on expression and function of the TMEM16A calcium-activated chloride channel. Proc Natl Acad Sci U S A 106(50):21413–21418
35. Hwang SJ, Blair PJ, Britton FC, Odriscoll KE, Hennig G, Bayguinov JR, Rock JR, Harfe BD, Sanders KM, Ward SM (2009) Expression of anoctamin 1/TMEM16A by interstitial cells of Cajal is fundamental for slow wave activity in gastrointestinal muscles. J Physiol 587(20):4887–4904
36. Jiang Y, Lee A, Chen J, Ruta V, Cadene M, Chait BT, MacKinnon R (2003) X-ray structure of a voltage-dependent K+ channel. Nature 423:33–41
37. Jiang Y, Ruta V, Chen J, Lee A, MacKinnon R (2003) The principle of gating charge movement in a voltage-dependent K+ channel. Nature 423:42–48
38. Keener JP, Sneyd J (2009) Mathematical physiology: cellular physiology. Springer, New York
39. Krepkiy D, Mihailescu M, Freites JA, Schow EV, Worcester DL, Gawrisch K, Tobias DJ, White SH, Swartz KJ (2009) Structure and hydration of membranes embedded with voltage-sensing domains. Nature 462(7272):473–479
40. Kunze WA, Clerc N, Bertrand PP, Furness JB (1999) Contractile activity in intestinal muscle evokes action potential discharge in guinea-pig myenteric neurons. J Physiol 517(2):547–561
41. Laitko U, Juranka PF, Morris CE (2006) Membrane stretch slows the concerted step prior to opening in a Kv channel. J Gen Physiol 127(6):687–701
42. Laitko U, Morris CE (2004) Membrane tension accelerates rate-limiting voltage-dependent activation and slow inactivation steps in a Shaker channel. J Gen Physiol 123:135–154
43. Lees-Green R, Beyder A, Farrugia G, O'Grady G, Poh YC, Buist ML, Pullan AJ (2011) Computational modeling of the sodium channel mechanical stretch effects on the electrical function of human interstitial cells of Cajal and smooth muscle cells. Digestive Diseases Week, Chicago, IL, May 2011

44. Lees-Green R, Du P, O'Grady G, Beyder A, Farrugia G, Pullan AJ (2011) Biophysically-based modelling of the interstitial cells of Cajal: Current status and future perspectives. Frontiers Comput Physiol Med 2:29
45. Locke GR 3rd, Ackerman MJ, Zinsmeister AR, Thapa P, Farrugia G (2006) Gastrointestinal symptoms in families of patients with an SCN5A-encoded cardiac channelopathy: evidence of an intestinal channelopathy. Am J Gastroenterol 101(6):1299–1304
46. Long SB, Cambell EB, MacKinnon R (2005) Crystal structure of a mammalian voltage-dependent Shaker family K+ channel. Science 309(5736):897–903
47. Long SB, Cambell EB, MacKinnon R (2005) Voltage sensor of Kv1.2: structural basis of electromechanical coupling. Science 309(5736):903–908
48. Long SB, Tao X, Campbell EB, MacKinnon R (2007) Atomic structure of a voltage-dependent K+ channel in a lipid membrane-like environment. Nature 450(7168):376–382
49. Lundbaek JA, Birn P, Hansen AJ, Sogaard R, Nielsen C, Girshman J, Bruno MJ, Tape SE, Egebjerg J, Greathouse DV, Mattice GL, Koeppe RE 2nd, Andersen OS (2004) Regulation of sodium channel function by bilayer elasticity: the importance of hydrophobic coupling. Effects of Micelle-forming amphiphiles and cholesterol. J Gen Physiol 123(5):599–621
50. Lyford GL, Strege PR, Shepard A, Ou Y, Ermilov L, Miller SM, Gibbons SJ, Rae JL, Szurszewski JH, Farrugia G (2002) Alpha(1C) (Ca(V)1.2) L-type calcium channel mediates mechanosensitive calcium regulation. Am J Physiol Cell Physiol 283(3):C1001–C1008
51. Markin VS, Sachs F (2004) Thermodynamics of mechanosensitivity. Phys Biol 1(1–2):110–124
52. Matteson DR, Armstrong CM (1982) Evidence for a population of sleepy sodium channels in squid axon at low temperature. J Gen Physiol 79(5):739–758
53. Mazzone A, Strege PR, Tester DJ, Bernard CE, Faulkner G, De Giorgio R, Makielski JC, Stanghellini V, Gibbons SJ, Ackerman MJ, Farrugia G (2008) A mutation in telethonin alters Nav1.5 function. J Biol Chem 283(24):16537–16544
54. Milescu M, Bosmans F, Lee S, Alabi AA, Kim JI, Swartz KJ (2009) Interactions between lipids and voltage sensor paddles detected with tarantula toxins. Nat Struct Mol Biol 16(10):1080–1085
55. Morris CE, Juranka PF (2007) Nav channel mechanosensitivity: activation and inactivation accelerate reversibly with stretch. Biophys J 93(3):822–833
56. Muraki K, Imaizumi Y, Watanabe M (1991) Sodium currents in smooth muscle cells freshly isolated from stomach fundus of the rat and ureter of the guinea-pig. J Physiol 442:351–375
57. Nozawa K, Kawabata-Shoda E, Doihara H, Kojima R, Okada H, Mochizuki S, Sano Y, Inamura K, Matsushime H, Koizumi T, Yokoyama T, Ito H (2009) TRPA1 regulates gastrointestinal motility through serotonin release from enterochromaffin cells. Proc Natl Acad Sci U S A 106(9):3408–3413
58. Ou Y, Gibbons SJ, Miller SM, Strege PR, Rich A, Distad MA, Ackerman MJ, Rae JL, Szurszewski JH, Farrugia G (2002) SCN5A is expressed in human jejunal circular smooth muscle cells. Neurogastroenterol Motil 14(5):477–486
59. Ou Y, Strege P, Miller SM, Makielski J, Ackerman M, Gibbons SJ, Farrugia G (2003) Syntrophin gamma 2 regulates SCN5A gating by a PDZ domain-mediated interaction. J Biol Chem 278(3):1915–1923
60. Payandeh J, Scheuer T, Zheng N, Catterall WA (2011) The crystal structure of a voltage-gated sodium channel. Nature 475(7356):353–358
61. Petitprez S, Zmoos AF, Ogrodnik J, Balse E, Raad N, El-Haou S, Albesa M, Bittihn P, Luther S, Lehnart SE, Hatem SN, Coulombe A, Abriel H (2011) SAP97 and dystrophin macromolecular complexes determine two pools of cardiac sodium channels Nav1.5 in cardiomyocytes. Circ Res 108(3):294–304
62. Poh YC, Beyder A, Strege PR, Farrugia G, Buist ML (2011) Quantification of gastrointestinal sodium channelopathy. J Theor Biol 293C:41–48
63. Sachs F (2010) Stretch-activated ion channels: what are they? Physiology (Bethesda) 25(1):50–56

64. Saito YA, Strege PR, Tester DJ, Locke GR 3rd, Talley NJ, Bernard CE, Rae JL, Makielski JC, Ackerman MJ, Farrugia G (2009) Sodium channel mutation in irritable bowel syndrome: evidence for an ion channelopathy. Am J Physiol Gastrointest Liver Physiol 296(2): G211–G218
65. Saito YA, Tester DJ, Mazzone A, Beyder A, Locke GR, 3rd, Talley NJ, Ackerman M, Farrugia G (2009) Sodium channel mutations in irritable bowel syndrome. Neurogastroenterology & Motility, Chicago, IL, 2009
66. Scriven DR, Dan P, Moore ED (2000) Distribution of proteins implicated in excitation-contraction coupling in rat ventricular myocytes. Biophys J 79(5):2682–2691
67. Shi ZD, Abraham G, Tarbell JM (2010) Shear stress modulation of smooth muscle cell marker genes in 2-D and 3-D depends on mechanotransduction by heparan sulfate proteoglycans and ERK1/2. PLoS One 5(8):e12196
68. Sinha B, Koster D, Ruez R, Gonnord P, Bastiani M, Abankwa D, Stan RV, Butler-Browne G, Vedie B, Johannes L, Morone N, Parton RG, Raposo G, Sens P, Lamaze C, Nassoy P (2011) Cells respond to mechanical stress by rapid disassembly of caveolae. Cell 144(3):402–413
69. Smirnov SV, Zholos AV, Shuba MF (1992) Potential-dependent inward currents in single isolated smooth muscle cells of the rat ileum. J Physiol 454:549–571
70. Strege PR, Holm AN, Rich A, Miller SM, Ou Y, Sarr MG, Farrugia G (2003) Cytoskeletal modulation of sodium current in human jejunal circular smooth muscle cells. Am J Physiol Cell Physiol 284(1):C60–C66
71. Strege PR, Mazzone A, Kraichely RE, Sha L, Holm AN, Ou Y, Lim I, Gibbons SJ, Sarr MG, Farrugia G (2007) Species dependent expression of intestinal smooth muscle mechanosensitive sodium channels. Neurogastroenterol Motil 19(2):135–143
72. Strege PR, Ou Y, Sha L, Rich A, Gibbons SJ, Szurszewski JH, Sarr MG, Farrugia G (2003) Sodium current in human intestinal interstitial cells of Cajal. Am J Physiol Gastrointest Liver Physiol 285(6):G1111–G1121
73. Suchyna TM, Markin VS, Sachs F (2009) Biophysics and structure of the patch and the gigaseal. Biophys J 97(3):738–747
74. Tabarean IV, Juranka P, Morris CE (1999) Membrane stretch affects gating modes of a skeletal muscle sodium channel. Biophys J 77(2):758–774
75. Tabarean IV, Morris CE (2002) Membrane stretch accelerates activation and slow inactivation in Shaker channels with S3–S4 linker deletions. Biophys J 82(6):2982–2994
76. Tfelt-Hansen J, Winkel BG, Grunnet M, Jespersen T (2010) Inherited cardiac diseases caused by mutations in the Nav1.5 sodium channel. J Cardiovasc Electrophysiol 21(1):107–115
77. Trepat X, Deng L, An SS, Navajas D, Tschumperlin DJ, Gerthoffer WT, Butler JP, Fredberg JJ (2007) Universal physical responses to stretch in the living cell. Nature 447(7144):592–595
78. Undrovinas AI, Shander GS, Makielski JC (1995) Cytoskeleton modulates gating of voltage-dependent sodium channel in heart. Am J Physiol 269(1 Pt 2):H203–H214
79. Vatta M, Ackerman MJ, Ye B, Makielski JC, Ughanze EE, Taylor EW, Tester DJ, Balijepalli RC, Foell JD, Li Z, Kamp TJ, Towbin JA (2006) Mutant caveolin-3 induces persistent late sodium current and is associated with long-QT syndrome. Circulation 114(20):2104–2112
80. Ward SM, Baker SA, de Faoite A, Sanders KM (2003) Propagation of slow waves requires IP3 receptors and mitochondrial Ca2+ uptake in canine colonic muscles. J Physiol 549(1):207–218
81. Won KJ, Sanders KM, Ward SM (2005) Interstitial cells of Cajal mediate mechanosensitive responses in the stomach. Proc Natl Acad Sci U S A 102(41):14913–14918
82. Xiong Z, Sperelakis N, Noffsinger A, Fenoglio-Preiser C (1993) Fast Na+ current in circular smooth muscle cells of the large intestine. Pflugers Arch 423(5–6):485–491
83. Yarbrough TL, Lu T, Lee HC, Shibata EF (2002) Localization of cardiac sodium channels in caveolin-rich membrane domains: regulation of sodium current amplitude. Circ Res 90(4):443–449

84. Youm JB, Kim N, Han J, Kim E, Joo H, Leem CH, Goto G, Noma A, Earm YE (2006) A mathematical model of pacemaker activity recorded from mouse small intestine. Philos Trans A Math Phys Eng Sci 364(1842):1135–1154
85. Zhu MH, Kim TW, Ro S, Yan W, Ward SM, Koh SD, Sanders KM (2009) A Ca2+-activated Cl- conductance in interstitial cells of Cajal linked to slow wave currents and pacemaker activity. J Physiol 587(20):4905–4918

ICC Network Density: Regulation and Consequences

Simon J. Gibbons, Jerry Gao and Gianrico Farrugia

Abstract Interstitial cells of Cajal (ICC) are mesoderm-derived mesenchymal cells found in the smooth muscle layers of the gastrointestinal tract. They contribute to the normal function of the gut by generating rhythmic electrical activity, as intermediaries in neuromuscular signalling, altering the membrane potential of adjacent smooth muscle and responding to mechanical stretch. Depletion of ICC is associated with several gastrointestinal motility disorders including diabetic gastroparesis, slow transit constipation and intestinal pseudo-obstruction. This chapter reviews the information that can be obtained from measuring and characterizing networks of interstitial cells of Cajal in health and disease, the applications of that information in computer modelling and about how mathematical modelling might inform further efforts to characterize and/or reverse ICC network depletion. We describe the appropriate techniques for tissue collection and handling when investigating effects on ICC networks. Methods for identifying, accurately quantifying and mapping ICC are presented together with new analyses that can identify changes to the geometry as well as the density of the ICC networks. Finally we discuss the information that is obtained on the relationship between ICC network changes and alterations to gastrointestinal function and show how computer modelling of virtual ICC networks could be used to predict those relationships.

S. J. Gibbons (✉) · G. Farrugia
Enteric Neurosciences Program, Department Physiology and Biomedical Engineering, Mayo Clinic College of Medicine, Guggenheim 838, 200 First Street SW, Rochester, MN 55905, USA
e-mail: gibbons.simon@mayo.edu

J. Gao
Auckland Bioengineering Institute, The University of Auckland, Auckland, New Zealand

L. K. Cheng et al. (eds.), *New Advances in Gastrointestinal Motility Research*, Lecture Notes in Computational Vision and Biomechanics 10,
DOI: 10.1007/978-94-007-6561-0_3, © Springer Science+Business Media Dordrecht 2013

1 Introduction

Interstitial cells of Cajal (ICC) are morphologically, functionally and developmentally discrete populations of cells in the muscularis propria of the gastrointestinal tract [10, 55]. Other smooth muscles contain cells that are apparently similar to ICC [3, 39, 45] but it is studies on the gastrointestinal tract that have principally defined the functions and properties of ICC. There are also populations of interstitial cells that are distinct from the well-defined cells of Cajal. These "fibroblast-like" cells [25, 66] and ICC may have overlapping developmental lineages and also have some similar functional roles [37] but there has been limited characterization of the "fibroblast-like" cells.

Intact networks of ICC contribute to normal motility patterns in the gastrointestinal tract by functioning as electrical pacemaker cells [27, 64, 69], by amplifying neuronal inputs to smooth muscle cells [4], by being a factor in the establishment of membrane potential gradients in the tissues [11] and by being responsive to stretch [61, 72]. Depletion of ICC is frequently observed in patients with gastroparesis [24, 46], slow transit constipation [23, 71], and intestinal pseudo-obstruction [12, 29]. ICC networks also decrease in density during the normal ageing process [20], which likely puts the aged individual at increased risk of GI problems in response to an insult such as an infection or partial obstruction. In mice, the development of diabetic gastroparesis is directly correlated with depletion of ICC networks with the reversal of delayed gastric emptying being associated with restoration of the ICC [6]. In humans, the delay in gastric emptying seen in gastroparesis inversely correlates with the number of ICC [21]. There are also inbred strains of rodents [30, 44, 68] as well as gene-targeted mutant animals [54] with impaired gastrointestinal function and altered ICC networks. The animals with mutations at the White Spotting (W) and Steel Dickie (Sld) genetic loci have been of particular interest due to the determination that the W locus contain the genes for the receptor tyrosine kinase receptor, Kit, and Sld is the locus for its ligand, stem cell factor. Kit is the most widely used marker for ICC and immunochemical detection of Kit is a standard method in the pathological assessment of ICC network integrity [16].

Functional studies on human, mouse and pig tissue have shown that in the stomach, pacemaking originates from ICC in a region of the gastric body close to fundus and that organized propagation of electrical slow waves down to the pyloric sphincter is dependent on the tightly coupled networks of ICC [34, 38, 47, 62]. Recent research has focused on the important questions of how the electrical patterns are altered in motility disorders, how that electrical activity correlates with changes in contractile patterns and how it correlates with alterations in ICC networks. Older studies made sharp electrode recordings from multiple locations in the stomach using in vitro preparations from mouse muscularis propria to demonstrate that depletion of ICC was associated with dysrhythmias [48]. More recently, multi-electrode mapping has made it possible to record the propagation of the electrical activity in several regions of the gastrointestinal tract from other

species including humans (this volume, "The Principles and Practice of Gastrointestinal High-Resolution Electrical Mapping" and "The Electrical Regulation of GI Motility at the Whole-Organ Level"). The underlying hypotheses of these studies are that ICC networks, specifically in the myenteric region (ICC-MY), generate and propagate the electrical slow wave. Clear demonstration of this relationship can be achieved by quantification of the ICC networks from tissues on which electrical and mechanical recordings have been made.

Although ICC networks are known to be depleted in diseased states, the functional outcomes of ICC loss have not been well elucidated. Experimental strategies for quantifying the structure–function relationship of ICC networks are limited, as the morphology of the ICC networks on a large scale can only be examined qualitatively, and recorded indicators of function such as electrical activity at small scales may prove to be challenging. In this chapter, we will describe the histochemical and image analysis approaches necessary for accurate and complete mapping of ICC networks and introduce an alternative approach of using mathematical and computational modelling to investigate the structure–function relationship. The objective of this modelling is to predict the limits for degradation of the ICC networks before the functional reserve of cells is depleted to the point that dysmotility will occur. In addition, we will discuss how the analysis and modelling can report and predict the limits for network dimensions and geometry to ensure preservation of function.

2 Measurement of ICC Morphology and Function

2.1 Tissue Collection and Handling

The accurate and reproducible measurement of ICC requires care and consistency in the collection of the tissues and proper collection of specimens is outlined in a recent position paper [35]. We have observed that immunoreactivity to Kit is very sensitive to the time it takes to get the tissue and process it. Waste surgical tissue subjected to simulated ischemia by storage on ice in F12 medium had significantly less Kit-immunoreactivity than samples from the same patient that were processed immediately after resection [10]. Others have shown that changes to ICC at the ultrastructural level occur quite rapidly if the tissue is not processed for analysis immediately [8]. As a result it is important to ensure that all specimens are collected in a consistent manner. It should be borne in mind that changes to the surgical technique can have unintended consequences on the quality of the material that reaches the laboratory. For example, laparoscopic procedures where clamping blood vessels early during surgery can mean longer periods of ischemia than conventional laparotomies. Control and diseased tissues should also be carefully matched by age due to the documented decline in ICC numbers with age [20], and samples used in comparative studies should be collected from same regions of the organ.

2.2 Markers of ICC

Studies on the morphology of ICC networks have depended on the use of specific markers for the cells. Ramon Y Cajal identified ICC as distinct from both neurons and smooth muscle cells in the rabbit gastrointestinal tract [50] by staining the tissues with methylene blue. This was the only commonly used method for identifying ICC by light microscopic techniques until the first demonstration that ICC were immunoreactive for Kit [44]. At this point, Kit became the default antigenic marker for ICC. The alternative to light microscopy was to identify ICC by their ultrastructural characteristics, which was an approach described in a succession of careful and detailed studies from the groups of Thuneberg, Rumessens, Komuro and Faussone-Pellegrini [36, 55]. Recently Ano1, a Ca^{2+}-activated Cl^- channel subunit, was found to be restricted to ICC in the muscle layers of the gastrointestinal tract [9, 19].

Kit and Ano1 immunoreactivities are very useful as markers of ICC because they permit labelling of the whole cell structure and assessment of volume changes in the ICC network. However, the level of Kit expression changes during the maturation and aging of ICC. Specifically, ICC progenitor cells express low but detectable levels of Kit when compared to mature ICC [31]. The ICC progenitor cells do express Ano1 and can only be distinguished from mature ICC by the difference in Kit expression and the immunoreactivity for CD34 of the progenitors. At the other end of the time-scale, aged or senescent ICC may lose expression of one or more of these markers prior to loss of function or the death of the cell. Our studies on human colonic tissue from patients with slow transit constipation indicate that both Ano1 and Kit levels decline in parallel even though there is no evidence that the two molecules are functionally or physically linked in the cell [32]. This suggests that the cells are lost when the markers are lost in these tissues. Studies on cultured explants of mouse gastric muscles does detect a Kit-negative, CD44 immunoreactive population of cells that do not generate pacemaker potentials and appear to represent senescent but not dead ICC [42]. When assessing the changes in ICC networks in health, disease and ageing it is important to bear in mind that loss of immunoreactivity may be due to changes in protein expression or antigen accessibility rather than depletion of, or damage to the cells.

The densities of ICC networks and the high levels of connectivity of the cells, particularly in the region of the myenteric plexuses, make it difficult to count the numbers of cells. Quantification of enteric neurons has been greatly facilitated by the identification of an antigen that is highly enriched in the nucleus (Hu C/D, ANNA1 [41]). It would be very useful to have a similar, nuclear restricted antigen specific to ICC. For neurons, loss of cells is not always associated with a reduced density of innervation because the remaining cells can compensate by neurite outgrowth (e.g., [2]). There is reason to expect that enumeration of ICC using a nuclear marker, combined with measurement of network volume using a membrane marker, will similarly detect changes to the volumes of cells during development or in diseased tissues.

The principle limitation of all immunochemical labels for cell types are the properties of the antibodies chosen for the study. This has been discussed extensively in descriptions of techniques in immunobiology but it is worth noting that both Kit and Ano1 immunoreactivity are quite sensitive to fixation conditions in some species [19, 65]. Variations in the effectiveness of different lots of antibodies are quite common so it behoves the investigator to do all of the necessary controls. Even reagents sold specifically for clinical pathology applications can be inconsistent due to the practice of doing quality control of antisera for human tissues based on labelling Kit-bright mast cells rather than somewhat dimmer ICC (see [17] for a discussion).

2.3 Quantification of ICC

There are many studies that have measured ICC numbers and distribution in a wide range of vertebrates including fish [52], most standard laboratory animals and humans. As outlined above, it is useful to measure the volume and distribution of the ICC network and the number of cells within the network. The network can be best visualized using an en-face preparation such as a whole mount, or by taking thick sections of the tissue. In both cases, the limitations are the ability of the labels or stains to penetrate the tissue and the ability of the imaging system to collect faithful images of the labelled cells. The muscularis propria of most small rodents is thin enough for easy detection of ICC networks using antibodies to Kit and Ano1. However, the muscle layers of human gastrointestinal tissues are much thicker and so immune-labelling is typically done using tissues cut in cross section at varying thicknesses from 10 μm slices of paraffin embedded tissue (e.g., [17]) up to 150 μm (e.g., [23]). ICC in the human small intestine can also be visualized in flat sheet preparations with the longitudinal muscle peeled away or in 0.5–1 mm thick cross sectional preparations [40].

2.3.1 Counting ICC

In histochemical studies, counting ICC is best done in tissue sections that have been counterstained for a nuclear marker such as 4',6-diamidino-2-phenylindole (DAPI). ICC in non-adjacent sections should be counted and the number of microscopic fields examined should be high enough to assure that the values are representative. Our studies have established that for ICC in human gastric body it is sufficient to count the cells in the circular muscle layer in a total of 40×0.04 μm^2 fields from three non-adjacent sections [22]. These numbers will vary for other populations of ICC in other tissues. In whole mount preparations from rodent gastrointestinal tract, the ICC in the myenteric plexus region can be particularly difficult to count. The density of the positively labelled structures makes it hard to separate ICC nuclei from the nuclei of other cell types.

One approach that we have attempted is to volume render stacks of confocal images of both the Kit-positive structures and the DAPI-positive nuclei. A 3D digital map of the individual nuclei was generated by thresholding and a map of the objects subjected to principle component analysis [56]. Several classes of objects were identified including one population of small spherical nuclei that were associated with Kit immunoreactive ICC-MY. Validation of this approach is not complete but it appears to offer promise. The use of flow cytometry to sort cells dissociated from gastrointestinal muscles is an effective approach that not only gives clear quantitative data but has also been refined to separate different populations of ICC, ICC stem cells and senescent ICC [5, 42]. The only limitation to flow cytometry is the need to destroy the sample to sort the cells and therefore the loss of information on the distribution of the cells and their connectedness.

2.3.2 Quantification of Network Density

Experienced investigators can obtain reliable and reproducible qualitative scores for the density of ICC networks in tissue sections by direct visual inspection of specimens. In unpublished studies (direct communication S Gibbons), three investigators acting independently and blind to whether the tissue was healthy or diseased, obtained excellent agreement in the results using a 4 point scale to score ICC networks. However this method requires training, is difficult to report and hard to standardize between laboratories. In whole mount preparations and thick sections, it is more difficult to assess the 3D networks. Unless big changes in the networks are observed then a qualitative appraisal is unreliable and it is not possible to detect less than a 30 % change in network volume in such complex samples.

The most rigorous approach to assessing network density is the measurement of the volume of labelled cell structures. This can be achieved by applying confocal laser scanning microscopy to image fluorescently labelled, antigen-positive cells in tissue preparations of varying thickness. Confocal microscopy generates stacks of images that represent thin optical sections through the tissue for viewing as single 2D images or rendering into 3D volumes to be mapped and analysed. The method is dependent on even and complete penetration of the reagents and the quality of the microscopic imaging. The limits on the resolution of the collected images are the quality of the microscope objectives and distortion of the image due to differences in the refractive indices of the media in the imaging light path. The diffraction limit (d) is calculated using the equation:

$$\mathrm{d} = \frac{\lambda}{2NA}$$

For imaging green fluorescence ($\lambda = 530$ nm), this is theoretically about 200 nm but when using the best lenses with acceptable working distances and high numerical apertures (NA), the practical limit is about 400 nm. Some of the image

distortion [67] can be corrected by applying a correction factor obtained from imaging fluorescent spheres [58] but in very thick tissues (>150 μm) not only is the brightness of the signal attenuated but the coherence of the collected image is reduced. Imaging in thicker specimens has been reported in tissues subjected to clearing [13]. Also longer wavelength light passes more effectively through tissue with less interference from endogenous autofluorescence so fluorophores with spectra in the far-red range will be visible at greater depths in tissue. However resolution is reduced by the larger diffraction limit for far-red fluorophores.

High resolution 3D images provide the opportunity to extract not only a measure of ICC network volume but also information on the shape, connectedness and orientation of the cells and processes in the tissue. The first step in this procedure is to generate accurate bitmaps of the networks, which can be achieved by thresholding out the labelled structures, filtering for connectedness between adjacent positive voxels and applying image conditioning techniques to detect boundaries between the positively labelled structures and the surrounding tissues. The tools to do these analyses have been developed for many applications other than segmenting confocal microscope data. We use the Analyze™ program developed by the Mayo Clinic Biomedical Imaging Resource and available commercially (AnalyzeDirect, Overland Park KS) but other software is capable of doing the same types of analysis. Images of ICC networks are complex; the cell bodies tend to be comparatively thick and brightly labelled whereas the processes are thinner and not so bright. The cells are distributed in an uneven fashion across the thickness of the muscle layer with the network in the myenteric plexus region being dense and thin enough to be practically two dimensional unlike the ICC in the muscle layers that are more diffusely distributed in three dimensions. Altogether, no more than 15 % of the total image volume is represented by the positively labelled ICC. Due to these factors, many automated segmentation algorithms that work on other 3D images cannot create accurate maps of ICC networks from confocal microscopic images. Manual segmentation is effective but does take time. ICC in the rodent small intestine present particular problems due to the lower expression of Kit in the ICC from the deep muscular plexus region compared to ICC in myenteric plexus region. However, if there is a low level of background fluorescence in the un-labelled regions of the image, then well-labelled networks can be thresholded using two or three steps to produce a map of the ICC network that accurately matches the raw data. The process can be standardized so that two different trained analysts obtain volume measurements with a high level of correlation for multiple different images and with less than 10 % difference in the calculated values for the image volumes.

2.3.3 Sampling Issues

The power of any scientific study depends on making measurements in a sufficiently large sample. Due to the variability in ICC distribution and numbers in different gastrointestinal tissues it is important to have enough tissues and enough

samples per tissue to calculate the range of normal values for the specific organ under study and to detect any differences in ICC number and morphology between diseased and healthy tissue. A further critical consideration is whether any detected differences are sufficient to cause effects on gastrointestinal physiology.

Sample availability can be a significant problem for studies on human gastrointestinal tissues. For tissues from experimental animals, there is usually sufficient sample but the limitation is on the amount of time and resources necessary to process all the samples. For studies on human ICC, the majority of studies on healthy tissue have been on surgical waste collected at the time of resection for either cancer (mostly large intestine) or procedures to treat morbid obesity (small intestine and stomach). The appendix has also been used as a bellwether for changes to ICC in the rest of the gastrointestinal tract [46, 53]. Specimens from patients with motility disorders are usually only obtained when the patient has had symptoms for significant amount of time and is refractory to medical treatment. The problem with these specimens is that the change(s) that produced the original functional impairment may be obscured by changes occurring in the long period leading up to surgery. Paradoxically, although the patients may have had their symptoms for years, they are still generally younger than the patients having surgery for gastrointestinal cancer so age-matching can also be a problem. It would be ideal if we could obtain full-thickness biopsies of a sufficient size when the disease first presents itself. Studies on pigs have demonstrated the practicality of this approach for doing gastric biopsies [49] but techniques still need further validation. At present, good animal models of disease are the only way to investigate possible changes during the initial stages of impaired gastrointestinal function.

Sources of variability in ICC density other than age and sample handling include ensuring that the sampling locations are consistent and having sufficient sample to allow for uneven loss of ICC and patchiness in the network integrity. In the normal, healthy mouse [7, 59] and human [28, 51], it is well established that ICC network density from the fundus to the pylorus and from the greater to lesser curvature changes in all dimensions. In the stomach from mice with diabetic gastroparesis the loss of ICC in the gastric body and antrum is patchy [48]. However in gastric body samples from patients with long-standing diabetic gastroparesis this does not appear to be the case [22] perhaps because those patients have particularly severe and long-standing problems. In the large intestine, the density of ICC in the rodent does change significantly between the proximal and distal colon [1]. In human colon, there is limited data and although a comprehensive study from our group detected no significant differences in network density from proximal to distal colon [43], differences have been reported in a study on what appear to be smaller tissue samples [71]. Regardless, when studying ICC in the small and large intestines it is still best to take samples from the closest matching regions possible.

2.3.4 Quantification of Structural Properties of Networks Using Novel Metrics

ICC network structure assessments remain qualitative as metrics for quantifying the structural properties of these networks have not been developed. Yet, these metrics are essential for understanding the structure–function relationship of ICC networks, as functional outcomes can be related to the specific structural properties measured by the metrics, and differences in networks can be quantitatively described. Measurement of network volume and ICC number does not provide much information on the spatial distribution and arrangement of ICC. Recently, two new metrics for assessing ICC networks have been introduced: the density and connectivity metrics [14, 15]. These metrics have been successfully applied to quantify spatial properties of 2D image stacks of ICC networks and can be readily extended to 3D analysis. The metrics are formulated based upon a continuum approach, so the ICC network is viewed as a syncytium. Only whether a pixel/voxel is occupied by ICC or not is considered, and the individual cell boundaries are neglected. Below is a description of the two metrics:

(1) Density metric (ρ) is defined as the proportion of ICC present in the image:

$$\rho = \frac{N_{ICC}}{N_{Total}} \tag{1}$$

where N_{ICC} and N_{Total} are the number of ICC pixels and total number of pixels in the image respectively. The density metric ranges from 0 to 1, with 0 indicating that no ICC are present, and 1 indicating that only ICC are present.

(2) Connectivity metric (c) reflects the connectivity of the ICC network. Defining a group of immediately connected ICC pixels as an ICC island, the connectivity of the network can be measured by:

$$c = \frac{\sqrt{\sum_{i=1}^{n} I_i^2}}{N_{ICC}} \tag{2}$$

where I_i is the number of pixels in the ith ICC island, n is the total number of ICC islands throughout the network, and N_{ICC} is defined as in (1). For this metric, each ICC island is viewed as a separate object, and the normalized weighted average of island sizes is calculated with more weight placed on larger islands. The connectivity metric ranges from 0 to 1, with a larger metric value indicating a higher level of connectivity throughout the network.

The density metric exhibits similar information to that of the existing ICC volume measure, but has been normalized to allow for comparison of different sized images. More importantly, the connectivity metric is the first metric to quantify the structure of ICC networks.

3 Correlating ICC Changes to Changes in Gastrointestinal Function

Studies designed to correlate changes in the function of the gastrointestinal tract with the amount and location of ICC depletion have identified a clear link between ICC loss and several diseases but also have led to the conclusion that there is a significant functional reserve of ICC in the healthy gastrointestinal tract.

In the case of gastroparesis, the loss of ICC corresponds with onset of delayed gastric emptying in non-obese diabetic (NOD) mice. In mice treated to reverse the delay, levels of ICC return to normal [6, 48, 70]. In a subset of humans with diabetic gastroparesis, there were significantly fewer than normal ICC in the circular muscle layers in samples obtained from the gastric body [22]. It should be noted that this phenomenon of significant ICC depletion was found in a large subset of, but not all patients with severe and long-standing symptoms [22] and that there were other cellular changes including inflammatory cell infiltrate and alterations in nerve fibres. Therefore, gastroparesis appears to be a consequence of ICC depletion in both humans and mice but under some circumstances the symptoms can occur when cells are not depleted. Whether there is a change to the function of the ICC remains to be determined either by recording electrical activity in the intact organ (G. O'Grady, personal communication) or by investigating ICC function in tissues obtained from experimental animals with gastroparesis.

Some results from studies on the relationship between ICC networks and gastrointestinal dysfunction can seem unexpected. For example the Klotho mouse, a model of progeria (or accelerated ageing), has extensive loss of ICC in the stomach that are not associated with alterations in gastric emptying but clear changes in food intake and a failure to grow [31]. Close examination reveals that delayed emptying, likely due to loss of pacemaker activity and abnormal motility patterns, is balanced by accelerated emptying due to increased stiffness of the stomach wall and impaired accommodation.

A functional reserve in ICC networks is indicated by studies in both mice and humans. A progressive decrease in ICC numbers with age in both the stomach and large intestine of healthy human tissue results in levels of ICC in aged individuals that are more than 60 % lower than the numbers reported for young adults [20]. The patients in these studies reported normal gastrointestinal function but it is noteworthy that none of the samples obtained from stomachs of aged individuals had ICC levels as low as the levels detected in patients with gastroparesis [22]. Using our method of quantification a level of ICC in the circular smooth muscle layer of the human gastric body that is below approximately 3 cells per field (0.12 mm^2 area, 12 μm thick sections) is likely to result in a functional impairment. We have not established the quantitative limits of this relationship in mouse tissues but we do know from our work on the serotonin 2B receptor (5-HT_{2B}) that 5-HT_{2B} receptor knockout mice have a 30 % depletion in the ICC-MY network with an insignificant decrease in intestinal transit [63].

It is not particularly surprising that there is a functional reserve in ICC networks given the importance of effectively handling food intake for any organism and these observations do suggest that injury to ICC networks can occur without impacting gastrointestinal function. Later in life the injury might have an impact on function in older individuals as their ICC numbers decline to the point where an effect occurs. However, there may be opportunities to protect or restore networks given the increasing amounts of information that are available on the maintenance and regeneration of ICC.

4 Regulation of ICC Numbers and Networks

ICC must make and sustain contact with other cells and must be dispersed through the tissue at densities that assure normal function of the gastrointestinal tract. The mechanisms by which the distribution of ICC is established and maintained are becoming clearer and appear to involve a balance between maintenance, replacement and depletion of the mature cells (Fig. 1). Maintenance of cells involves the activation of pathways to prevent cell death and cell senescence as well as up-regulation of factors that combat oxidative injury or promote cell repair. Replacement of cells can be mediated by replenishment from pools of committed or pluripotent stem cells or by proliferation of mature ICC. Depletion of cells can be due to either programmed cell death pathways such as apoptosis or by senescence. The consequence of these balancing factors is that ICC in the healthy mouse gastrointestinal tract appear to turnover on a 3–6 month time scale. The apparent rates of apoptosis in human colon have been estimated [18] but the replacement rate is not known. However based on the rate of cell loss, the rate of ICC in turnover in the human colon is likely to be similar to the rates detected in mouse tissues.

The best studied growth factor for ICC networks is the stem cell factor/Kit signalling pathway, which must be intact for normal development of ICC networks [27, 44, 69] and controls the mechanisms for differentiation of committed stem cells into mature ICC [42]. Insulin-like growth factor-1 (IGF-1) contributes to the integrity of ICC networks by being a key upstream regulator of stem cell factor availability from smooth muscle [42]. Serotonin acting on 5-HT_{2B} receptors [73] and nitric oxide (NO) derived from neuronal nitric oxide synthase [7] are other factors that play a role in supporting ICC networks and it is likely that the formation of specialized contacts between enteric motor neurons and ICC, between ICC and smooth muscle cells and between individual ICC are dependent on signalling by small molecules. In the same way that there is a functional reserve of cells in ICC networks, the reports indicate some redundancy in the mechanisms for establishing and populating those networks. Some of these mechanisms may affect the geometry of the ICC networks and others may affect the density of the processes or the distribution of the cells. As reported above (Sect. 2.3.4), the effects of

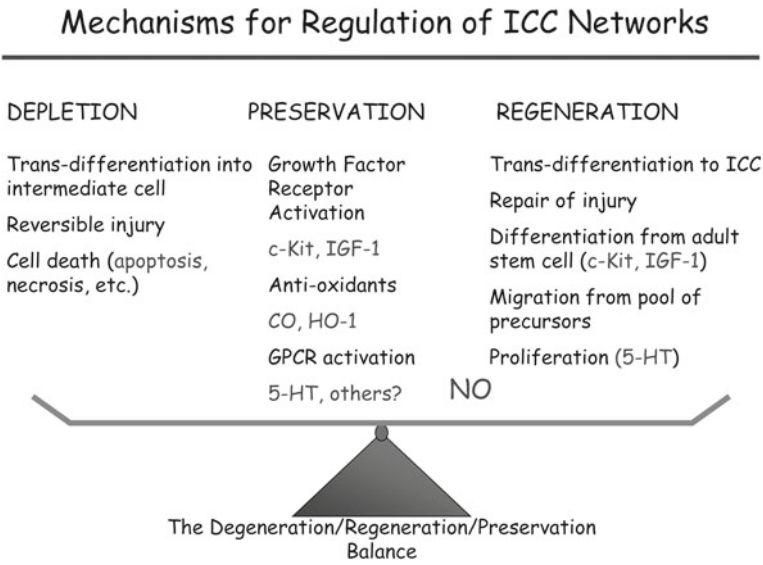

Fig. 1 ICC numbers depend on a balance between depletion, preservation and regeneration

gene-targeted knockout of the 5-HT_{2B} receptor, which reduces proliferation of mature ICC [63], is anisotropic alteration in the ICC-MY network.

In diseased tissue, the preservation of normal gastric emptying and normal ICC networks in mice with diabetes appears to be mediated by up-regulation of heme oxygenase-1 (HO1) expression in alternatively activated macrophages. This cellular response combats injury caused by high glucose and oxidative stress in the stomachs of diabetic mice. The product of HO1 activity that is most important for reversing diabetic gastroparesis appears to be carbon monoxide (CO), as CO alone is sufficient as a substitute for HO1 up-regulation [33]. However the mechanisms by which ICC networks in mice with diabetic gastroparesis recover following treatment with CO have not been established.

5 Virtual ICC Network Generation for Studying Structure–Function Relationships

Generation of virtual ICC networks is an approach to facilitate the investigation of ICC network structure–function relationships when large-scale tissue volume ICC imaging data are not available. These networks make it possible to test the impact of differing levels of ICC network depletion on function and to examine how different structures can theoretically produce different functional outcomes.

Realistic virtual ICC networks that possess spatial properties similar to real ICC networks can be generated *in silico*. Virtual networks of various levels of depletion

can be generated and then coupled to multi-scale computational models (as described by Corrias et al. in "Modelling Tissue Electrophysiology in the GI Tract: Past, Present and Future in this volume") to predict the biophysical electrical activity of these networks [14] and hence aid in understanding the structure–function relationship of ICC networks. Two existing algorithms capable of generating an unlimited number of virtual ICC networks of any size and through a range of depletion levels are briefly discussed here and the respective performances are compared.

(1) Stochastic-Based Modelling Algorithm (SBMA)
SBMA is a heuristic algorithm developed by inspecting the spatial properties of jejunum myenteric plexus ICC networks [15] from wild-type (WT) and 5-HT_{2B}-receptor knockout ($Htr2b^{-/-}$) mice (Fig. 2). The black pixels represent ICC whereas the white pixels are assumed to be the background tissue matrix. These network images are 512 × 512 pixels and represent tissue with physical dimensions of 316 × 316 × 7 μm and 316 × 316 × 8 μm respectively.
The primary observation of ICC network structure from the WT and $Htr2b^{-/-}$ networks is that both exhibited a grid-like structure. The $Htr2b^{-/-}$ network was thinner, less connected, and more anisotropic, that is having a stronger preferential direction, than the WT network. These observations formed the basis of the SBMA.
The SBMA generates virtual ICC networks in three steps (Fig. 3). Firstly, a grid structure backbone composed of one-pixel width lines is generated. Secondly, the grid structure backbone is thickened, and thirdly, the image is post-processed to remove small artefacts. The level of depletion severity of the generated image is controlled by the user via an input parameter. Although the

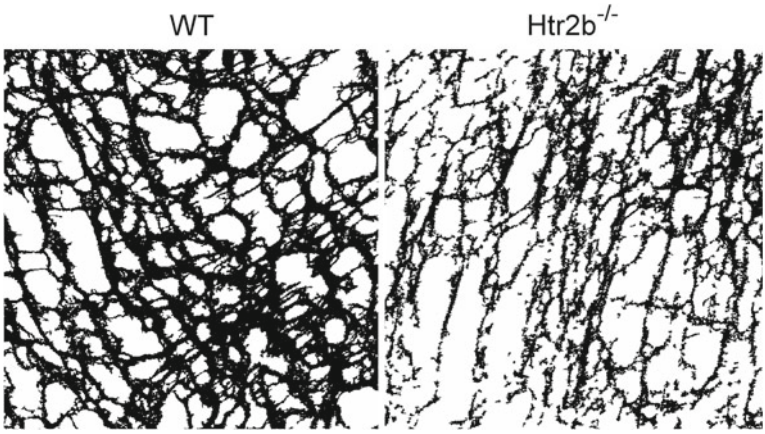

Fig. 2 Real myenteric ICC (*black*) networks from small intestine of WT and $Htr2b^{-/-}$ mice. These network images are 512 × 512 pixels and represent tissue with physical dimensions of 316 μm × 316 μm × 7 μm and 316 μm × 316 μm × 8 μm respectively

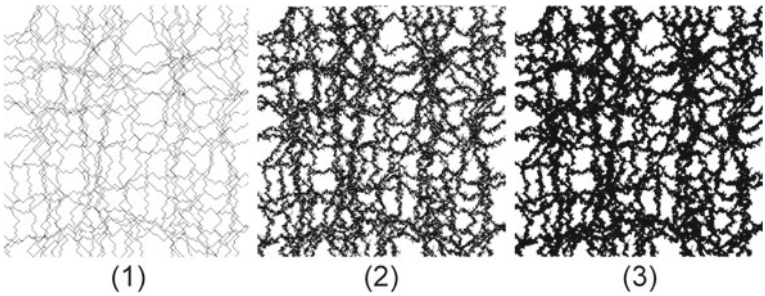

Fig. 3 The three steps of SBMA in generating virtual ICC networks: **a** Backbone structure generation; **b** Network thickening; and **c** Post-processing. The virtual network being generated mimics the WT network in Fig. 2, and has the same image resolution and reflects the same physical dimensions

output from each of the three steps depends upon random processes, decision making thresholds in the algorithm are affected by the user-input value through empirically derived relationships.

(2) Modified Single Normal Equation Simulation (SNESIM)
The original SNESIM algorithm is employed in the petroleum industry to build models of geological formations that host oil reservoirs using a statistical approach [60]. This algorithm was then adapted for the generation of ICC networks [14, 15].
The modified SNESIM algorithm requires two user-supplied images, one representing a normal network, and the other representing a severely depleted network. The multiple-point statistics, which express the conditional probability of finding ICC in two or more locations simultaneously, of each image is extracted and a weighted sum of these statistics is calculated with weights dependent upon the target density of the virtual network set by the user. Then, the virtual network is generated recursively with a pixel-based technique from the user-defined coarsest to finest scale using the weighted statistics.

The SBMA was developed solely based on observations from two ICC network images, and hence many generic ICC network structure assumptions are made. Also, as the real ICC network images inspected were 2D image stacks, the SBMA is only capable of generating 2D virtual ICC networks. Conversely, the modified SNESIM algorithm extracts the desired properties from a user-supplied image, and minimal underlying assumptions are present. Therefore, although the modified SNESIM algorithm is applicable in many more circumstances, including the capability to generate virtual 3D ICC network image volumes, and generates more realistic virtual networks, it is also more computationally expensive than the SBMA. This demonstrates that different approaches will yield in different strengths and weaknesses, and the most suitable technique for the desired purpose should be selected.

6 Future Challenges

The future challenges in research on ICC network morphology are primarily questions of scale and application of the tools. The tools are available to image, map and model networks of labelled cells and sufficient tissue can be obtained from small experimental animals to have the power to correlate changes in the network with functional and physiological properties of the tissues. From the modelling perspective, more metrics need to be developed to examine the various aspects of ICC network structures. The functional outcomes can then be correlated against each of the aspects of the networks to determine the structural changes during ICC depletion that lead to the loss of function. The development of a comprehensive set of network structure metrics can also be used to validate whether the generated virtual ICC networks are realistic, which is necessary before these networks can be used as a substitute for real imaging data. Once the network generation algorithm is validated to be capable of creating realistic ICC networks, the virtual networks can be coupled with multi-scale computational models of the biophysical electrical activity to investigate the relationship of the structure of ICC networks to the various functions of ICC including pacemaking and amplification of neuronal signalling.

It is also necessary to get a clearer understanding of the source of the electrical slow waves in human tissues and the mechanism by which the slow waves are propagated to the smooth muscle. Compared to the networks in the myenteric region of mouse stomach, the ICC in the myenteric region of the human gastric body are rather sparse and slow waves appear to be generated in part through ICC in the muscle layers [22, 28, 51]. Innovative solutions will be necessary to image and map ICC in very thick tissue preparations or by registering the images obtained from adjacent thinner preparations. The final objective will be to assess the relationship between dysrhythmias, impaired function and distribution of ICC on the larger scale represented by human tissues.

In regions of the gastrointestinal tract other than the stomach, there is even less information on the correlation between ICC network disruption and changes to function. Two populations of ICC in the colon appear to generate oscillating electrical activity [26, 40] but no direct relationship between the integrity of the ICC networks and colon function has been demonstrated. High resolution mapping by manometry of contractile activity (refer to "Colonic Manometry: What do the Squiggly Lines Really Tell us?" by Dinning, this volume) combined with assessment of ICC network integrity at discrete locations in the colon might be a productive approach to address the relationship between ICC and function in experimental animals. In addition, further development of non-invasive methods for assessing local gastrointestinal transit changes offer opportunities for timing and localizing the collection of tissues to the points at which network changes can be most productively assessed. For humans, it would be ideal if we could assess network changes in patients with recently developed motility issues or better, to determine the network changes that predict vulnerability to future motility

problems. As outlined in the introduction, the function of ICC is not limited to pacemaker activity. The quantitative limits on the number of ICC necessary for normal neuro-muscular transmission in the gastrointestinal tract are not known. Similarly the relationship between ICC depletion and the trans-mural membrane potential gradient has only been investigated in mice with impaired Kit signalling [57]. Clearly more studies that integrate physiological measurements and functional studies with mapping and quantification of ICC are necessary.

Assessing the relationship between ICC and the surrounding tissue and cells will be one of the key links in understanding the changes in the gastrointestinal tract that lead to ICC-associated motility disorders. At the cellular level, macrophages, nerves, Kit-negative fibroblast-like cells and smooth muscle cells all interact with ICC. ICC stem cell numbers might give an indication of the regenerative capacity of a tissue. Numbers of senescent cells could provide a measure of the amount of on-going damage. At the ultrastructural level, gap junctions, postsynaptic specializations and the distribution of intracellular structures are indicators of the functional integrity and connectivity of the cells. We only have limited quantitative information on these relationships and have very little spatial information.

Computer models can integrate information on the integrity of ICC networks, the connections of the networks to other cells and the effects of localized inputs to cells in the networks. However this can only be achieved by putting accurate experimental information into the models and the results must be carefully validated by returning to the biological system and determining if the predictions are correct.

In summary, ICC network integrity is necessary for normal gastrointestinal function. Measurement and mapping of the networks provides the tools for assessment of the relationship between the network and function. Computer modelling using maps of ICC networks can predict the impact of changes to the ICC network on function. Improved methods for measurement and mapping of ICC from larger regions of the tissues under study are needed but modelling does offer the ability to create virtual networks for hypothesis testing.

Acknowledgments We wish to thank the members of the Enteric Neuroscience Program, especially Dr Joseph Szurszewski and Mrs Kristy Zodrow, and members of the Gastrointestinal Research Group at the Auckland Bioengineering Institute for their support and assistance with this work. We are especially grateful to Dr Andrew Pullan for his leadership in establishing and maintaining the collaboration that is a key component in the studies described here. Thanks Andrew. These studies were supported by the following NIH Grants R01 DK57061 (GF, SJG), P01 DK 68055–P1 (GF, SJG), P01 DK 68055–B (SJG), R01 DK 52766 (GF, SJG), 1P30DK084567 (GF, SJG). Jerry Gao is supported by the University of Auckland Health Research Doctoral Scholarship, the Freemasons Postgraduate Scholarship and the R. H. T. Bates Postgraduate Scholarship.

References

1. Alberti E, Mikkelsen HB, Larsen JO, Jimenez M (2005) Motility patterns and distribution of interstitial cells of Cajal and nitrergic neurons in the proximal, mid- and distal-colon of the rat. Neurogastroenterol Motil 17:133–147
2. Bernard CE, Gibbons SJ, Gomez-Pinilla PJ, Lurken MS, Schmalz PF, Roeder JL, Linden D, Cima RR, Dozois EJ, Larson DW, Camilleri M, Zinsmeister AR, Pozo MJ, Hicks GA, Farrugia G (2009) Effect of age on the enteric nervous system of the human colon. Neurogastroenterol Motil 21:746–e746
3. Bolton TB, Gordienko DV, Povstyan OV, Harhun MI, Pucovsky V (2004) Smooth muscle cells and interstitial cells of blood vessels. Cell Calcium 35:643–657
4. Burns AJ, Lomax AE, Torihashi S, Sanders KM, Ward SM (1996) Interstitial cells of Cajal mediate inhibitory neurotransmission in the stomach. Proc Natl Acad Sci USA 93:12008–12013
5. Chen H, Redelman D, Ro S, Ward SM, Ordog T, Sanders KM (2007) Selective labeling and isolation of functional classes of interstitial cells of Cajal of human and murine small intestine. Am J Physiol Cell Physiol 292:C497–C507
6. Choi KM, Gibbons SJ, Nguyen TV, Stoltz GJ, Lurken MS, Ordog T, Szurszewski JH, Farrugia G (2008) Heme oxygenase-1 protects interstitial cells of Cajal from oxidative stress and reverses diabetic gastroparesis. Gastroenterology 135:2055–2064
7. Choi KM, Gibbons SJ, Roeder JL, Lurken MS, Zhu J, Wouters MM, Miller SM, Szurszewski JH, Farrugia G (2007) Regulation of interstitial cells of Cajal in the mouse gastric body by neuronal nitric oxide. Neurogastroenterol Motil 19:585–595
8. Christensen J, Rick GA, Lowe LS (1992) Distributions of interstitial cells of Cajal in stomach and colon of cat, dog, ferret, opossum, rat, guinea pig and rabbit. J Auton Nerv Syst 37:47–56
9. Espinosa I, Lee CH, Kim MK, Rouse BT, Subramanian S, Montgomery K, Varma S, Corless CL, Heinrich MC, Smith KS, Wang Z, Rubin B, Nielsen TO, Seitz RS, Ross DT, West RB, Cleary ML, van de Rijn M (2008) A novel monoclonal antibody against DOG1 is a sensitive and specific marker for gastrointestinal stromal tumors. Am J Surg Pathol 32:210–218
10. Farrugia G (2008) Interstitial cells of Cajal in health and disease. Neurogastroenterol Motil 20(Suppl 1):54–63
11. Farrugia G, Lei S, Lin X, Miller SM, Nath KA, Ferris CD, Levitt M, Szurszewski JH (2003) A major role for carbon monoxide as an endogenous hyperpolarizing factor in the gastrointestinal tract. Proc Natl Acad Sci USA 100:8567–8570
12. Feldstein AE, Miller SM, El-Youssef M, Rodeberg D, Lindor NM, Burgart LJ, Szurszewski JH, Farrugia G (2003) Chronic intestinal pseudoobstruction associated with altered interstitial cells of Cajal networks. J Pediatr Gastroenterol Nutr 36:492–497
13. Fu YY, Lin CW, Enikolopov G, Sibley E, Chiang AS, Tang SC (2009) Microtome-free 3-dimensional confocal imaging method for visualization of mouse intestine with subcellular-level resolution. Gastroenterology 137:453–465
14. Gao J, Du P, Archer R, O'Grady G, Gibbons SJ, Farrugia G, Cheng LK, Pullan AJ (2011) A stochastic multi-scale model of electrical function in normal and depleted ICC networks. IEEE Trans Bio-Med Eng 58:3451–3455. doi:10.1109/TBME.2011.2164248
15. Gao J, Du P, Archer R, Gibbons SJ, O'Grady G, Farrugia G, Pullan AJ (2011) Virtual ICC network generation algorithms for modeling the physiological consequences of ICC depletion. Gastroenterology 140:S-373
16. Garrity MM, Burgart LJ, Mahoney MR, Windschitl HE, Salim M, Wiesenfeld M, Krook JE, Michalak JC, Goldberg RM, O'Connell MJ, Furth AF, Sargent DJ, Murphy LM, Hill E, Riehle DL, Meyers CH, Witzig TE, North Central Cancer Treatment Group (2004) Prognostic value of proliferation, apoptosis, defective DNA mismatch repair, and p53 overexpression in patients with resected Dukes' B2 or C colon cancer: a North Central Cancer Treatment Group Study. J Clin Oncol 22:1572–1582

17. Garrity MM, Gibbons SJ, Smyrk TC, Vanderwinden JM, Gomez-Pinilla PJ, Nehra A, Borg M, Farrugia G (2009) Diagnostic challenges of motility disorders: optimal detection of CD117+ interstitial cells of Cajal. Histopathology 54:286–294
18. Gibbons SJ, De Giorgio R, Pellegrini MS, Garrity-Park MM, Miller SM, Schmalz PF, Young-Fadok TM, Larson DW, Dozois EJ, Camilleri M, Stanghellini V, Szurszewski JH, Farrugia G (2009) Apoptotic cell death of human interstitial cells of Cajal. Neurogastroenterol Motil 21:85–93. doi:10.1111/j.1365-2982.2008.01185.x
19. Gomez-Pinilla PJ, Gibbons SJ, Bardsley MR, Lorincz A, Pozo MJ, Pasricha PJ, Van de Rijn M, West RB, Sarr MG, Kendrick ML, Cima RR, Dozois EJ, Larson DW, Ordog T, Farrugia G (2009) Ano1 is a selective marker of interstitial cells of Cajal in the human and mouse gastrointestinal tract. Am J Physiol Gastrointest Liver Physiol 296:G1370–G1381
20. Gomez-Pinilla PJ, Gibbons SJ, Sarr MG, Kendrick ML, Shen KR, Cima RR, Dozois EJ, Larson DW, Ordog T, Pozo MJ, Farrugia G (2011) Changes in interstitial cells of Cajal with age in the human stomach and colon. Neurogastroenterol Motil 23:36–44
21. Grover M, Bernard CE, Pasricha PJ, Lurken MS, Faussone-Pellegrini MS, Smyrk TC, Parkman HP, Abell TL, Snape WJ, Hasler WL, McCallum RW, Nguyen L, Koch KL, Calles J, Lee L, Tonascia J, Unalp-Arida A, Hamilton FA, Farrugia G (2012) Clinical-histological associations in gastroparesis: results from the Gastroparesis Clinical Research Consortium. Neurogastroenterol Motil 24(6)531–9, e249
22. Grover M, Farrugia G, Lurken MS, Bernard CE, Faussone-Pellegrini MS, Smyrk TC, Parkman HP, Abell TL, Snape WJ, Hasler WL, Unalp-Arida A, Nguyen L, Koch KL, Calles J, Lee L, Tonascia J, Hamilton FA, Pasricha PJ, NIDDK Gastroparesis Clinical Research Consortium (2011) Cellular changes in diabetic and idiopathic gastroparesis. Gastroenterology 140:1575–85.e8
23. He CL, Burgart L, Wang L, Pemberton J, Young-Fadok T, Szurszewski J, Farrugia G (2000) Decreased interstitial cell of Cajal volume in patients with slow-transit constipation. Gastroenterology 118:14–21
24. He CL, Soffer EE, Ferris CD, Walsh RM, Szurszewski JH, Farrugia G (2001) Loss of interstitial cells of Cajal and inhibitory innervation in insulin-dependent diabetes. Gastroenterology 121:427–434
25. Horiguchi K, Komuro T (2000) Ultrastructural observations of fibroblast-like cells forming gap junctions in the W/W(nu) mouse small intestine. J Auton Nerv Syst 80:142–147
26. Huizinga JD, Martz S, Gil V, Wang XY, Jimenez M, Parsons S (2011) Two independent networks of interstitial cells of Cajal work cooperatively with the enteric nervous system to create colonic motor patterns. Front Neurosci 5:93. doi:10.3389/fnins.2011.00093
27. Huizinga JD, Thuneberg L, Kluppel M, Malysz J, Mikkelsen HB, Bernstein A (1995) W/kit gene required for interstitial cells of Cajal and for intestinal pacemaker activity. Nature 373:347–349
28. Ibba Manneschi L, Pacini S, Corsani L, Bechi P, Faussone-Pellegrini MS (2004) Interstitital cells of Cajal in the human stomach: distribution and relationship with enteric innervation. Histol Histopathol 19:1153–1164
29. Isozaki K, Hirota S, Miyagawa J, Taniguchi M, Shinomura Y, Matsuzawa Y (1997) Deficiency of c-kit+ cells in patients with a myopathic form of chronic idiopathic intestinal pseudo-obstruction. Am J Gastroenterol 92:332–334
30. Isozaki K, Hirota S, Nakama A, Miyagawa J, Shinomura Y, Xu Z, Nomura S, Kitamura Y (1995) Disturbed intestinal movement, bile reflux to the stomach, and deficiency of c-kit-expressing cells in Ws/Ws mutant rats. Gastroenterology 109:456–464
31. Izbeki F, Asuzu DT, Lorincz A, Bardsley MR, Popko LN, Choi KM, Young DL, Hayashi Y, Linden DR, Kuro-o M, Farrugia G, Ordog T (2010) Loss of Kitlow progenitors, reduced stem cell factor and high oxidative stress underlie gastric dysfunction in progeric mice. J Physiol 588:3101–3117
32. Kashyap P, Gomez-Pinilla PJ, Pozo MJ, Cima RR, Dozois EJ, Larson DW, Ordog T, Gibbons SJ, Farrugia G (2011) Immunoreactivity for Ano1 detects depletion of Kit-positive interstitial cells of Cajal in patients with slow transit constipation. Neurogastroenterol Motil 23:760–765

33. Kashyap PC, Choi KM, Dutta N, Linden DR, Szurszewski JH, Gibbons SJ, Farrugia G (2010) Carbon monoxide reverses diabetic gastroparesis in NOD mice. Am J Physiol Gastrointest Liver Physiol 298:G1013–G1019. doi:10.1152/ajpgi.00069.2010
34. Kelly KA, Code CF, Elveback LR (1969) Patterns of canine gastric electrical activity. Am J Physiol 217:461–470
35. Knowles CH, De Giorgio R, Kapur RP, Bruder E, Farrugia G, Geboes K, Lindberg G, Martin JE, Meier-Ruge WA, Milla PJ, Smith VV, Vandervinden JM, Veress B, Wedel T (2010) The London Classification of gastrointestinal neuromuscular pathology: report on behalf of the Gastro 2009 International Working Group. Gut 59:882–887
36. Komuro T, Seki K, Horiguchi K (1999) Ultrastructural characterization of the interstitial cells of Cajal. Arch Histol Cytol 62:295–316
37. Kurahashi M, Zheng H, Dwyer L, Ward SM, Don Koh S, Sanders KM (2011) A functional role for the 'fibroblast-like cells' in gastrointestinal smooth muscles. J Physiol 589:697–710
38. Lammers WJ, Ver Donck L, Stephen B, Smets D, Schuurkes JA (2009) Origin and propagation of the slow wave in the canine stomach: the outlines of a gastric conduction system. Am J Physiol Gastrointest Liver Physiol 296:G1200–G1210
39. Lang RJ, Zoltkowski BZ, Hammer JM, Meeker WF, Wendt I (2007) Electrical characterization of interstitial cells of Cajal-like cells and smooth muscle cells isolated from the mouse ureteropelvic junction. J Urol 177:1573–1580
40. Lee HT, Hennig GW, Fleming NW, Keef KD, Spencer NJ, Ward SM, Sanders KM, Smith TK (2007) Septal interstitial cells of Cajal conduct pacemaker activity to excite muscle bundles in human jejunum. Gastroenterology 133:907–917
41. Lin Z, Gao N, Hu HZ, Liu S, Gao C, Kim G, Ren J, Xia Y, Peck OC, Wood JD (2002) Immunoreactivity of Hu proteins facilitates identification of myenteric neurones in guinea-pig small intestine. Neurogastroenterol Motil 14:197–204
42. Lorincz A, Redelman D, Horvath VJ, Bardsley MR, Chen H, Ordog T (2008) Progenitors of interstitial cells of Cajal in the postnatal murine stomach. Gastroenterology 134:1083–1093
43. Lyford GL, He CL, Soffer E, Hull TL, Strong SA, Senagore AJ, Burgart LJ, Young-Fadok T, Szurszewski JH, Farrugia G (2002) Pan-colonic decrease in interstitial cells of Cajal in patients with slow transit constipation. Gut 51:496–501
44. Maeda H, Yamagata A, Nishikawa S, Yoshinaga K, Kobayashi S, Nishi K (1992) Requirement of c-kit for development of intestinal pacemaker system. Development 116:369–375
45. McCloskey KD (2011) Interstitial cells of Cajal in the urinary tract. Handb Exp Pharmacol 202:233–254
46. Miller SM, Narasimhan RA, Schmalz PF, Soffer EE, Walsh RM, Krishnamurthi V, Pasricha PJ, Szurszewski JH, Farrugia G (2008) Distribution of interstitial cells of Cajal and nitrergic neurons in normal and diabetic human appendix. Neurogastroenterol Motil 20:349–357
47. O'Grady G, Du P, Cheng LK, Egbuji JU, Lammers WJ, Windsor JA, Pullan AJ (2010) Origin and propagation of human gastric slow-wave activity defined by high-resolution mapping. Am J Physiol. Gastrointest Liver Physiol 299:G585–G592. doi:10.1152/ajpgi.00125.2010
48. Ordog T, Takayama I, Cheung WK, Ward SM, Sanders KM (2000) Remodeling of networks of interstitial cells of Cajal in a murine model of diabetic gastroparesis. Diabetes 49:1731–1739
49. Rajan E, Gostout CJ, Lurken MS, Talley NJ, Locke GR, Szarka LA, Sumiyama K, Bakken TA, Stoltz GJ, Knipschield MA, Farrugia G (2008) Endoscopic "no hole" full-thickness biopsy of the stomach to detect myenteric ganglia. Gastrointest Endosc 68:301–307
50. Ramon Y Cajal S (1911) Histologie du systéme nerveux de l'Homme et des Vertébrés. Maloine Paris
51. Rhee PL, Lee JY, Son HJ, Kim JJ, Rhee JC, Kim S, Koh SD, Hwang SJ, Sanders KM, Ward SM (2011) Analysis of pacemaker activity in the human stomach. J Physiol. doi:10.1113/jphysiol.2011.217497

52. Rich A, Leddon SA, Hess SL, Gibbons SJ, Miller S, Xu X, Farrugia G (2007) Kit-like immunoreactivity in the zebrafish gastrointestinal tract reveals putative ICC. Dev Dyn 236:903–911
53. Richter A, Wit C, Vanderwinden JM, Wit J, Barthlen W (2009) Interstitial cells of Cajal in the vermiform appendix in childhood. Eur J Pediatr Surg 19:30–33
54. Rubin BP, Antonescu CR, Scott-Browne JP, Comstock ML, Gu Y, Tanas MR, Ware CB, Woodell J (2005) A knock-in mouse model of gastrointestinal stromal tumor harboring kit K641E. Cancer Res 65:6631–6639
55. Rumessen JJ, Vanderwinden JM (2003) Interstitial cells in the musculature of the gastrointestinal tract: Cajal and beyond. Int Rev Cytol 229:115–208
56. Sagstetter AM, Camp JJ, Lurken MS, Szurszewski JH, Farrugia G, Gibbons SJ, Robb RA (2007) Computer-aided classification of cell nuclei in the gastrointestinal tract by volume and principal axis. Proc SPIE 6514:1–9
57. Sha L, Farrugia G, Harmsen WS, Szurszewski JH (2007) Membrane potential gradient is carbon monoxide-dependent in mouse and human small intestine. Am J Physiol Gastrointest Liver Physiol 293:G438–G445. doi:10.1152/ajpgi.00037.2007
58. Sha L, Ou LL, Miller SM, Ma R, Szurszewski JH (1996) Cat pancreatic neurons: morphology, electrophysiological properties, and responses to 5-HT. Pancreas 13:111–124
59. Song G, Hirst GDS, Sanders KM, Ward SM (2005) Regional variation in ICC distribution, pacemaking activity and neural responses in the longitudinal muscle of the murine stomach. J Physiol 564:523–540
60. Strebelle S, Journel A (2001) Reservoir modeling using multiple-point statistics. SPE Annual Technical Conference and Exhibition 71324:1–11
61. Strege PR, Ou Y, Sha L, Rich A, Gibbons SJ, Szurszewski JH, Sarr MG, Farrugia G (2003) Sodium current in human intestinal interstitial cells of Cajal. Am J Physiol Gastrointest Liver Physiol 285:G1111–G1121
62. Szurszewski JH (ed) (1987) Electrical basis of gastrointestinal motility. Raven, New York
63. Tharayil VS, Wouters MM, Stanich JE, Roeder JL, Lei S, Beyder A, Gomez-Pinilla PJ, Gershon MD, Maroteaux L, Gibbons SJ, Farrugia G (2010) Lack of serotonin 5-HT2B receptor alters proliferation and network volume of interstitial cells of Cajal in vivo. Neurogastroenterol Motil 22:462–469, e109–410. doi:10.1111/j.1365-2982.2009.01435.x
64. Thomsen L, Robinson TL, Lee JC, Farraway LA, Hughes MJ, Andrews DW, Huizinga JD (1998) Interstitial cells of Cajal generate a rhythmic pacemaker current. Nat Med 4:848–851
65. Torihashi S, Yokoi K, Nagaya H, Aoki K, Fujimoto T (2004) New monoclonal antibody (AIC) identifies interstitial cells of Cajal in the musculature of the mouse gastrointestinal tract. Auton Neurosci-Basic Clin 113:16–23
66. Vanderwinden JM, Rumessen JJ, De Laet MH, Vanderhaeghen JJ, Schiffmann SN (1999) CD34 + cells in human intestine are fibroblasts adjacent to, but distinct from, interstitial cells of Cajal. Lab Invest 79:59–65
67. Visser TD, Oud JL, Brakenhoff GJ (1992) Refractive index and axial distance measurements in 3-D microscopy. Optik 90:17–19
68. Ward SM, Burns AJ, Torihashi S, Harney SC, Sanders KM (1995) Impaired development of interstitial cells and intestinal electrical rhythmicity in steel mutants. Am J Physiol 269:C1577–C1585
69. Ward SM, Burns AJ, Torihashi S, Sanders KM (1994) Mutation of the proto-oncogene c-kit blocks development of interstitial cells and electrical rhythmicity in murine intestine. J Physiol 480:91–97
70. Watkins CC, Sawa A, Blackshaw S, Barow RK, Snyder SH, Ferris CD (2000) Insulin restores neuronal nitric oxide synthase expression and function that is lost in diabetic gastropathy. J Clin Invest 106:373–384
71. Wedel T, Spiegler J, Soellner S, Roblick UJ, Schiedeck TH, Bruch HP, Krammer HJ (2002) Enteric nerves and interstitial cells of Cajal are altered in patients with slow-transit constipation and megacolon. Gastroenterology 123:1459–1467

72. Won KJ, Sanders KM, Ward SM (2005) Interstitial cells of Cajal mediate mechanosensitive responses in the stomach. Proc Natl Acad Sci USA 102:14913–14918
73. Wouters MM, Gibbons SJ, Roeder JL, Distad M, Ou Y, Strege PR, Szurszewski JH, Farrugia G (2007) Exogenous serotonin regulates proliferation of interstitial cells of Cajal in mouse jejunum through 5-HT2B receptors. Gastroenterology 133:897–906. doi:10.1053/j.gastro.2007.06.017

The Principles and Practice of Gastrointestinal High-Resolution Electrical Mapping

Gregory O'Grady, Timothy R. Angeli and Wim J. E. P. Lammers

Abstract High resolution (multi-electrode) electrical mapping has become a prominent technique for investigating the propagation of electrical activity in the gastrointestinal (GI) tract. This technique involves the placement of dense arrays of many electrodes over the surface of the tissue, in order to reconstruct the spread of electrical activation in accurate spatiotemporal detail. Multi-electrode mapping can be performed in-vivo and in-vitro in a variety of animal models, and clinical methods for human mapping are also advancing. This chapter reviews the current status of GI multi-electrode mapping, with a particular focus on the principles of extracellular recordings, the design of mapping devices, the discrimination of artifacts, and the practical considerations for successful experimental work. Potential future directions for the field are considered.

1 Introduction

Extracellular electrical recordings taken directly from the surface of the gastrointestinal (GI) tract have been a central technique in motility research for almost a century. Whereas intracellular recordings allow investigations into ion channel

G. O'Grady (✉)
Department of Surgery, The University of Auckland, Private Bag 92019,
Auckland 1142, New Zealand
e-mail: ogrady.greg@gmail.com

G. O'Grady · T. R. Angeli · W. J. E. P. Lammers
Auckland Bioengineering Institute, The University of Auckland, Auckland, New Zealand

T. R. Angeli
Riddet Institute, Palmerston North, New Zealand

W. J. E. P. Lammers
Department of Physiology, UAE University, Al Ain, United Arab Emirates

L. K. Cheng et al. (eds.), *New Advances in Gastrointestinal Motility Research*,
Lecture Notes in Computational Vision and Biomechanics 10,
DOI: 10.1007/978-94-007-6561-0_4, © Springer Science+Business Media Dordrecht 2013

function and cellular electrophysiology, extracellular recordings enable investigations into integrated electrophysiological function in intact tissues and whole organs.

In recent years, extracellular multi-electrode (high-resolution; HR) mapping has become an increasingly important technique for analyzing GI electrical behaviors. This technique involves the placement of dense arrays of many electrodes over the surface of an organ, in order to reconstruct the sequence of electrical activation in accurate spatiotemporal detail. This spatial detail is necessary to accurately resolve the propagation patterns that underpin normal motility, and is critical for defining the more complex patterns of abnormal electrical behavior [41, 48]. Whereas multi-electrode mapping has been used for many years in cardiac and neural electrophysiology, now playing essential roles in routine clinical practice, methods for GI tract mapping are only a relatively recently innovation [31], and have not yet entered clinical practice.

This chapter discusses the foundations, principles and practice of multi-electrode GI mapping. Current mapping techniques are reviewed, device design is addressed, and future directions discussed. Particular attention is given to the practical methods of both in-vivo and in-vitro GI mapping, toward the aim of promoting and expanding the use of these research techniques.

2 Historical Background

GI extracellular research can be considered in three eras, through which technical advances have underpinned experimental advances: early foundations, modern foundations, and the current era of multi-electrode mapping.

2.1 Early Foundations

The first rigorous investigations into GI electrical activity were undertaken by Walter C. Alvarez in the early decades of the twentieth century [3]. Alvarez attached silver-plated and chloridized steel wires to the serosa of GI tissues, connected to a D'Arsonval galvanometer, and captured pointer movements via the shadow cast from a light source onto moving bromide paper. Mechanical activity could be simultaneously captured via a small aluminum lever. Using this system, Alvarez and colleagues recorded bioelectrical events and laid a foundation for the field [1]. Alvarez described slow waves as 'typical church steeples rising from a constant baseline', and observed that electrical activity occurred continuously in tissue that was not visibly contracting [2, 3].

Bozler was another notable early investigator, introducing technical refinements that enabled significant experimental contributions, including establishing that GI tissues form an interconnected electrical syncytium [11, 12]. Bozler prepared his

intestinal segments within shielded boxes and vigilantly controlled for temperature and humidity [12], demonstrating an attention to detail that remains essential for successful recordings. By using calomel electrodes attached to flexible thin cotton wicks soaked in a conductive fluid, which moved freely with contractions, Bozler also developed the foundations for investigating GI spike behavior (smooth muscle action potentials) [11].

2.2 Modern Foundations

A range of improved techniques enabled an expansion of extracellular research during the 1960s-1970s, including recordings in humans. Improved efficiency and accuracy of recordings was enabled by current amplifiers and polygraph recorders, and later, by digital acquisition and computerized analysis. Implantable electrodes were developed that facilitated in-vivo implantation for chronic awake animal studies, such as those outlining normal gastric slow wave propagation by Kelly and Code [25], and the migrating motor complex by Szurszewski [58]. Bortoff conducted investigations into the relationship between intracellular and extracellular recordings, explaining the configuration of extracellular recordings, thereby establishing a more rational basis for applying these techniques [9].

During this era, investigators commonly attempted to reconstruct the patterns of electrical activation from sparse arrangements of few electrodes attached at regular distances along the GI tract serosa [25, 59]. While this strategy enabled a basic outlining of electrical activation, sparse sampling precluded an accurate estimation of electrical wavefront movements. Significant assumptions had to be made regarding what was occurring in the unmeasured areas, and it rapidly became difficult or impossible to reliably track the origin and propagation of electrical patterns, particularly when the activity became dysrhythmic, or when multiple pacemakers interacted [57].

2.3 Multi-Electrode (High-Resolution) Mapping and the Current Era

The need for an accurate spatiotemporal analysis of GI electrical activation motivated Lammers et al. to perform the first GI tract multi-electrode mapping study in 1993 [31]. This work was performed on rabbit duodenum in-vitro, using a custom-made platform of 240 silver-wire electrodes bound into a regular array in a block of dental resin. Recordings were made on an acquisition system adapted from cardiac use, and the data was manually analyzed. This pioneering work demonstrated proof of principle for GI mapping, and produced the first spatiotemporal maps of the origin and spread of slow wave activation fronts in GI

tissues. Technical and experimental advances have continued to progress over the last two decades, leading to the first human multi-electrode GI mapping study in 2010 [48].

3 Principles of Gastrointestinal Extracellular Recordings

3.1 The Biophysical Basis of GI Extracellular Recordings

Gastrointestinal slow waves are generated and propagated by networks of interstitial cells of Cajal (ICC), and conduct into the adjacent smooth muscle cell (SMC) layers [19]. Although this mechanism of slow wave 'entrainment' through ICC is a specialized adaptation, the general principles of extracellular recordings are universal to bioelectrical systems and are well established [55].

Extracellular electrodes detect the extracellular fields that are generated as activation fronts excite tissue. During the propagation of an activation front, current flows from the inactive (source) to activated (sink) tissue regions. Extracellular electrodes detect these currents, with the resultant potentials appearing as positive ahead of the wavefront, zero at the site of the wavefront, and negative behind it, generating a typically biphasic waveform (Fig. 1) [9]. These waveforms approximate the second derivative of the intracellularly—recorded slow wave in

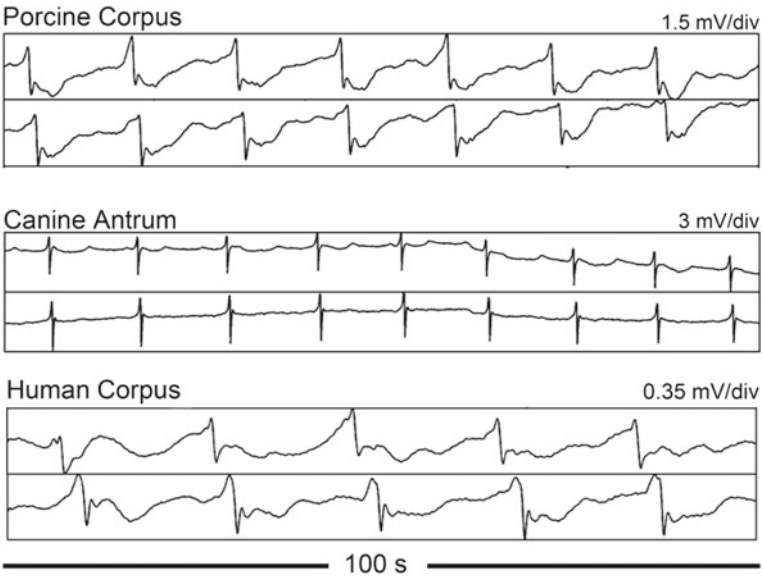

Fig. 1 Examples of extracellular slow wave recordings. Extracellular amplitudes, SNR and morphologies vary across different gastric regions and species. Recorded as per the methods in Egbuji et al. [16]

morphology, but are much briefer than the intracellular potentials, because the voltage gradient is only substantial near to the site of depolarization. The point of maximum negative gradient on the extracellular slow wave downstroke corresponds with the arrival of the wavefront at the site of the electrode, and is determined to be the 'time of activation' for extracellular mapping [18, 37]. Repolarization events result in very small extracellular potentials that are substantially more difficult to reliably resolve, and which have not yet been studied in any detail in the GI tract.

In view of the above, it should be clear that surface contact electrodes record the summative activity from a large population of many cells [24]. The detected field is generated from a hemisphere of tissue, with potentials falling away at an exponential relationship with distance from the electrode. Recent recordings of GI double potentials at the center of gastric re-entrant circuits, which reflect the detection of wavefronts by a single electrode across both sides of a functional conduction block, suggest that the radius of the detected extracellular field may extend several hundred micrometers in all directions beyond the edges of the electrode [52]. Detection sensitivity of this field has been greatly aided by the high-fidelity of modern amplifiers.

The morphology of extracellular slow wave waveforms varies between species and regions of the GI tract, due to several known and unknown factors. In humans and dogs, the gastric pacemaker and distal antral regions show a high-amplitude, high signal-to-noise ratio (SNR) signal, whereas corpus signals are of lower amplitude, with a reduced SNR (Fig. 1) [40, 48]. These differences are partly related to conduction velocity (conduction speed being rapid in the pacemaker region and in the antrum), as velocity has a direct relationship with extracellular amplitudes [51]. This relationship is due to proportionality between conduction velocity and total transmembrane current entering the extracellular space [51]. Extracellular slow wave morphologies can also be fractionated, showing multiple components [40, 48], perhaps reflecting the heterogeneous spread of activation fronts through the layered GI wall.

Technical factors also contribute to waveform variability during extracellular recordings; for example, different slow wave morphologies will be achieved by unipolar and bipolar approaches [7]. Digitization, amplification and filtering can also markedly change slow wave morphology [24], as will variable electrode contact, and electrode design considerations (discussed below). During gastric dysrhythmia, the variability of extracellular waveforms may become pronounced, for reasons including the emergence of anisotropic velocity profiles, interference at wavefront collisions, wave fragmentation into multiple propagating wavelets, and double potentials [41, 51, 52]. Such complexity in dysrhythmic electrograms presents challenges for reliable signal interpretation and particularly activation time marking.

Other than slow waves, there is a second type of electrical activity occurring in the GI tract known as 'spikes', which are true smooth muscle action potentials. Slow waves alone can induce sufficient SMC depolarization to induce contractions, particularly in the stomach. However, spikes are understood to play a central

role in generating functionally meaningful and sustained contractions throughout much of the GI tract, particularly in the distal antrum and the intestines. Spikes occur when depolarization from slow waves and co-regulatory neurohormonal mechanisms reaches a threshold, resulting in the increased activation of voltage-dependent calcium channels and action potentials, and enhanced contractility [56]. The propagation of spikes in 'patches' has been mapped by Lammers et al. in several studies [27, 29, 32]; however, the exact mechanisms governing the organization and propagation of these spike patches at the tissue level remains poorly understood. Further detail on the propagation of spikes vs slow waves is provided in by Angeli et al. in "The Electrical Regulation of GI Motility at the Whole-Organ Level" of this volume.

To date, slow wave patterns have been mapped in the stomach and small intestine, but have not been recordable in the colon, either in-vivo or in-vitro. The propagation of spike patches has been mapped in the gastric antrum, small intestine and rectum [29, 32, 40].

3.2 Electrode Design for Multi-Electrode Mapping

The type of electrode platform chosen for any particular experimental applications depends on several factors, including the context of the study, cost, ease of use, biocompatibility, species under study, need for sterility, and anticipated SNR of the target tissue. Significant design differences must be considered for in-vivo and in-vitro applications. The principles for electrode design are discussed in this section, while further discussion of specific platforms in current use is presented later in this chapter.

The diameter of the contact electrode is one of several important design variables. A compromise must be reached between making the electrode large enough to resolve small GI extracellular voltages, and small enough to ensure that the recorded events represent sharp, relatively localized activation. There have been no studies definitively quantifying the optimal electrode diameter, however 0.3 mm is a standard size that is commonly used in current mapping devices [15, 31, 40]. Electrode diameters within a range from around 0.2 up to 0.5 mm have been validated in many studies and contexts and should prove effective in general use [5, 8, 45, 61]. If the electrodes protrude from the platform before contacting the tissue, they should be insulated, save for the tip, to prevent diffuse contact with a large area of tissue or fluid against the exposed surface [31].

A number of electrode materials can achieve reliable signal transduction, and again a trade-off is presented between several factors, notably optimizing charge transfer and stability, biocompatibility and material properties. Silver is well known to have advantages for bioelectrical signal transduction, such as a more stable electrode potential, low intrinsic noise, and a small interface impedance, particularly when chloridized to facilitate charge transfer at the electrode–electrolyte interface [43], and silver wire is commonly used for in-vivo and in-vitro mapping applications

[30]. Silver may be prone to oxidation under the effect of potent sterilization agents such as ethylene oxide and hydrogen peroxide plasma (Sterrad) [53]; however, silver wire has been used in laparoscopic devices without noting excessive corrosion after ethylene oxide treatment over several uses [49]. Sintered silver-chloride electrodes have been used effectively in other extracellular fields and could be an attractive option for customized GI devices in future [42]. The most inert noble metals, such as gold and platinum, are potentially best suited to chronic clinical applications [15], and combinations such as platinum-iridium are also a theoretically strong option [43]. Stainless steel has also been preferred in some extracellular applications for its desirable material properties [45].

As noted above, pure silver electrodes are sometimes 'chloridized' prior to use, for example by soaking them in a solution such as bleach prior to rinsing and use, in order to improve the stability of electrical recordings [43]. This may be appropriate for animal work, but poses toxicity and sterilization concerns for human research. We do not chloridize our silver electrodes; however, this is partly achieved in-vivo by the sustained electrode contact with a thin film of NaCl rich tissue fluid that naturally covers the GI tract serosa.

Electrode cabling must also be thoughtfully designed to ensure optimal signal transmission to the acquisition device. Ideally, cable shielding should be employed to reduce pick-up of ambient noise [49]. Unshielded SCSI (Small Computer System Interface) ribbon cables have been effectively used in several studies, and are cheap and easy to produce, but these do not perform as well as custom made cables constructed with Teflon-coated stainless steel and comprehensive shielding [15, 53]. The number and quality of contact junctions between the electrode and the acquisition box is also significant, because signal quality may degrade across each one of these contacts, indicating that such junctions should be minimized and optimized.

For in-vivo mapping, the electrodes may be flush with the recording platform, helping to facilitate uniform contact with the array that is brought into gentle apposition with the tissue [15, 40]. For in-vitro recordings, where the normal circulation of the isolated tissue is removed and tissue viability now fully depends on adequate perfusion from the tissue bath fluid, attention to tissue condition is paramount, and arrays should therefore be built with the electrode wires extending 2.5–10 mm beyond the end of the platform, enabling the tissue-bath perfusion fluid to freely circulate between the electrodes [30, 31, 36].

All GI extracellular mapping to date has been performed with passive electrodes. Active electrode systems have a form of amplifier physically built into the electrode. While active electrodes can achieve cleaner, superior-quality signals, they convey a disadvantage of increased circuitry complexity and cost, and sterilization could be more difficult. Nevertheless, active electrode approaches would be one possible pathway to improve signal quality if found necessary in future work. Noise-cancelling electrode designs could also be considered.

3.3 Bipolar Versus Unipolar Recordings

An area that has received little attention to date in the GI field is the relative merits of bipolar vs unipolar (monopolar) recordings. Bipolar recordings measure the bioelectrical potential difference between adjacent pairs of electrodes, whereas unipolar electrodes measure the potential difference between each electrode and a common indifferent reference. Bipolar electrode configurations have been used for extracellular GI tract recordings in several previous studies, including in humans [10, 14]. However, all multi-electrode GI mapping studies to date have been conducted with unipolar electrodes.

One advantage of the unipolar approach is that the potential difference is recorded irrespective of the orientation of the advancing wavefront (an 'omnidirectional' field of view) [26]. Bipolar recordings, in contrast, are directionally sensitive, such that the voltage gradient detected is dependent on the orientation of the wavefront relative to the electrode pair. Unipolar electrograms also offer a better-defined local activation time for mapping, although bipolar electrograms offer other potential advantages, particularly extraneous noise reduction (i.e., when noise occurs simultaneously in a bipolar electrode pair, it cancels), and a more localized 'field of view', enabling more reliable recordings of low-level local activities [26]. In the cardiac field, these trade-offs mean that unipolar and bipolar electrodes can offer useful complimentary information. However, it is unknown if the potential benefits of bipolar approaches translate meaningfully to the GI field. Until further research is performed, we recommend unipolar approaches for multi-electrode mapping. Multi-electrode unipolar recordings can also readily be converted into bipolar recordings.

3.4 Data Acquisition Systems and Software

A range of data acquisition systems are available for extracellular GI recordings, including from National Instruments (Austin, Texas, USA), BIOPAC Systems (Goleta, California, USA) and BioSemi (Amsterdam, The Netherlands). The different systems offer a range of configuration options, and, in general, systems with high channel recording capability require a high cost outlay. Lammers et al. have used a customized 256-channel acquisition system originally developed for myocardial use [31], whereas the group based in Auckland use a 256-channel BioSemi ActiveTwo system that was modified for passive recordings [16, 48]. The BioSemi has several useful attributes, notably, a very high-quality capability, small size, high portability, fiber-optic isolation to ensure patient safety, and long-life battery power, all of which make this system particularly well suited to clinical use [44].

Acquisition software for GI mapping is currently receiving increased attention. Previously, simple software interfaces in programs such as LabView (National

Instruments, Texas) enabled real-time visualization of selected channels to provide limited feedback on the adequacy of the recorded data and activity under investigation [15]. Recently, Bull et al. have developed a more sophisticated on-line analysis software program in the Python programing language, which enables accurate spatial visualization of the activity being recorded, in near real-time [13]. This software allows investigators to reposition their recording array if found to be imperfect, or to respond in real time to other experimental observations. Acquisition frequencies are an important aspect of conducting GI recordings, and are discussed further by Erickson et al. in "Quantitative Analysis of Electrical Activity in the Gastrointestinal Tract".

3.5 Artifacts in GI Extracellular Recordings

Noise is ubiquitous in bioelectrical recordings, and a number of biological and extraneous noise sources can cause artifacts in extracellular signals. Like in the cardiac and neural fields, some competing extracellular artifacts can mimic true slow wave activity, and educated caution is therefore needed to reliably differentiate artifact from fact [46]. It is, perhaps, easier to tell noise from signal in multi-channel recordings than it is in sparse electrical recordings. For example, it is helpful to observe that extrinsic and non-GI biological noise sources, such as cable movements, electronic interference, and cardiac and respiratory noise, are registered as simultaneous deflections in all electrograms (e.g., Fig. 2), whereas slow waves show a velocity-appropriate lag between adjacent channels [37]. The differing frequencies of slow waves and competing noise sources can also be useful to discriminate signal of interest from competing signal content, the notable exception being that in-vivo intestinal slow wave recordings occur at a similar frequency to the ventilator. Ventilator pauses can then become a helpful tool to discriminate ventilation artifact.

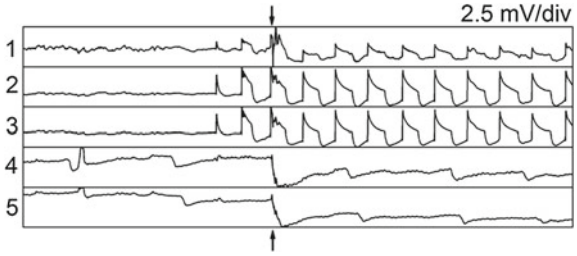

Fig. 2 Examples of artifacts in noisy 100 s human corpus extracellular recordings. Extrinsic noise sources including cable movements (at time indicated by *arrows*), and ventilator artifacts (the regular waveforms in channels 1–3). These artifacts can be readily differentiated from true slow wave activity because they appear simultaneously in all channels, whereas slow waves show a time lag between adjacent channels

Contraction artifacts are potentially more problematic than other artifacts, because in some tissues (e.g., stomach), they propagate at the same velocity as slow waves. Carefully observing morphological differences in the signal content then becomes essential. Fortunately, depending on filtering settings, contraction artifacts typically appear quite different to slow waves, having a more symmetrical appearance (or an oscillating spike-like appearance), and lacking the typical biphasic morphology with downstroke, making them readily distinguishable [46].

Recording artifacts are further discussed by Erickson et al. in "Quantitative Analysis of Electrical Activity in the Gastrointestinal Tract" of this volume.

4 Experimental Practice of Serosal Multi-Electrode Mapping

4.1 In-Vivo GI Mapping

4.1.1 Electrode Platforms

Two general classes of electrode platforms have been used in in-vivo GI serosal mapping (Fig. 3). Custom built arrays were developed by Lammers et al. using silver-wire arrays embedded in resin (www.smoothmap.org), and have been

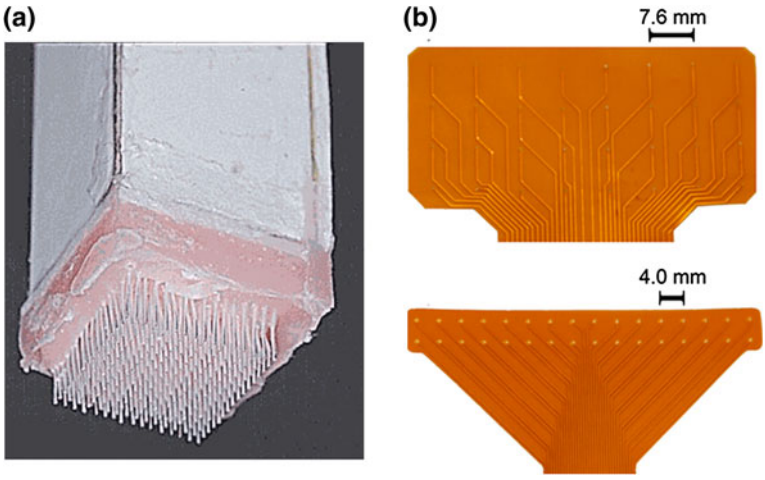

Fig. 3 Examples of electrode platforms for multi-electrode mapping. **a** Custom-made brush electrode for in-vitro mapping, showing 256 silver wires from a resin base-plate. The wires extend 3 mm from the platform to enable fluid to readily perfuse the excised tissues. **b** Two different flexible printed circuit board (PCB) designs for in-vivo mapping, each with 32 electrodes of 7.6 mm (*top*) and 4 mm (*bottom*) inter-electrode spacing. Multiple flexible PCBs can be arranged in parallel alignment to map a large area of tissue

successively applied in many in-vivo studies, achieving a high signal quality (e.g., [40, 41]). In order to facilitate human GI multi-electrode mapping, Du et al. more recently adapted flexible printed circuit board (PCB) electrodes, which had previously been used for cardiac mapping [15]. Flexible PCB arrays have silver or gold contacts and copper channels laid into a polyimide ribbon base, are mass produced with high-fidelity and low cost, and can be easily sterilized and disposed of, if necessary. Flexible PCBs also have the advantage of being able to conform to highly curved anatomical surfaces, such as around the gastric curvatures or intestinal circumference [4,16]. However, the signal quality of flexible PCBs is, generally, somewhat inferior and more variable than the custom-built arrays, potentially making analyses more challenging when recordings have a lower SNR [15, 18]. Multiple flexible PCBs can be joined together in close adjacent alignment to map a larger surface area, by using a sterile adhesive such as Tegaderm (3M, Minneapolis, MN, USA).

4.1.2 Animal models

Dogs, pigs and cats have been the most commonly used large animal models for intra-operative in-vivo serosal electrical recordings, and high-resolution porcine and canine baseline gastric slow wave data is now available for reference [16, 40]. These animals are chosen because, like humans, they are monogastric omnivores. However, investigators should be aware of important species differences in anatomy and physiology when selecting the appropriate model for their work [48]. The canine stomach is the most similar to humans, with similar anatomy, and comparable regional physiological variations including a low-velocity corpus activity and a sharp transition to a higher amplitude and velocity activity in the distal antrum [40]. The pig stomach has significant anatomical differences, including a relatively large fundus, an esophagus that enters at the mid-point of the lesser curvature, and the electrically-quiescent 'torus pylorus' in the distal stomach [16]. Common pig breeds are known to have Kit mutations, which contribute to their white coat color [20]; however, it is not known if ICC function is affected. Physiologically, pigs also have a large area of quiescence along the whole lesser curvature of the stomach, and lack the antral sharp increase in amplitude and velocity seen in humans and dogs [16].

In our experience, gastric electrical activity is less stable in pigs than in humans and dogs, with a high dysrhythmia rate being observed during routine intra-operative studies [52]. However, high-frequency tachygastria occurs infrequently in pigs, perhaps due to the lack of an 'electrophysiological antrum' [16]. Despite these issues, the ready availability and relatively low cost of pigs makes them a convenient and acceptable model for many experimental applications, particularly device development work.

4.1.3 Anesthesia

The effects of anesthesia on slow wave activity have not been extensively studied, however, mapping studies have been successfully performed under anesthesia in several species [16, 33, 40, 48]. Some investigators have reported a decline in slow wave frequency associated with anesthesia [23], but this may simply reflect a reduced ability to regulate body temperature, such that the frequency falls with cooling. Dysrhythmias have also been observed during intra-operative mapping in pigs and dogs, and an effect of anesthetic drugs cannot be excluded [40, 52].

A wide variety of anaesthetic agents are available. One recent intra-operative human mapping study of 12 patients with normal stomachs used a common regimen of prophylactic antibiotics, benzodiazepines, epidural anesthesia (ropivacaine/bupivacaine), short-acting opiates (e.g., fentanyl), muscle relaxant (suxamethonium/rocuronium), propofol, and an inhalational anesthetic (e.g., isoflurane or sevoflurane). Reassuringly, no instances of intraoperative dysrhythmia were observed in this cohort, and the general pattern of human gastric slow wave activity under anesthesia closely matched the known pattern of contractions occurring during the awake fed state on MRI [48]. Hotokozeka et al. reported that time under anesthesia was not a significant variable for the presence of gastric dysrhythmia in the post operative period [22].

Spike activity is known to be relatively reduced or absent during anesthesia, which is to be expected considering the state of reduced gut contractile activity during fasting, and the stress response to laparotomy. Nevertheless, spike activation has been successfully mapped in the anaesthetized state [29, 32, 40].

Our current large animal anesthetic regimen is to use Zoletil for induction (Tiletamine HCl 50 mg mL-1 and Zolazepam HCl 50 mg mL-1), and isoflurane for maintenance (2.5–5 % with an oxygen flow of 400 mL within a closed circuit system). Opiates have been associated with gastric dysrhythmias, so we avoid these agents in baseline anesthetic regimens in animals [41] [60]. In humans, short-acting opiates are routinely used peri-operatively, including to cover the sympathetic effects of laryngoscopy and intubation, so these agents may be difficult to avoid in patients.

4.1.4 Physiological Monitoring and Reference Electrodes

It is standard practice to monitor vital signs during experimental studies. However, temperature monitoring is particularly critical for mapping. Temperature changes have highly significant effects on the frequency and conductivity of slow wave activity [54], and if the target tissue is allowed to cool significantly, slow wave activity may cease altogether or become disorganized. In animal studies, we monitor both core and abdominal temperatures, and employ a warming pad, blankets, and a heat lamp when necessary to maintain the normal physiological range. In clinical studies, we employ forced-air warming devices.

For reference electrodes, we employ standard electrocardiogram skin pads, positioning them on the shaved abraded cutaneous abdomen and/or hind-leg in animals. In humans, we typically place these reference electrodes over the shoulders, away from the sterile field, and where the chest movement is minimal with respiration.

4.1.5 Positioning of Mapping Arrays

The surgical incision should be selected to best match the required organ access. We routinely use either a subcostal or midline laparotomy for gastric work, and midline laparotomy is generally sufficient for intestinal studies. It is worthwhile to keep the peritoneum closed and the abdominal walls approximated until the arrays are immediately ready to position, to prevent unnecessary drying and cooling of the viscera.

Handling of the viscera should be kept to a minimum during mapping, and should be as gentle as possible when needed. Gentle contact with the serosa does not affect the speed and pattern of slow wave propagation, but firm handling can slow conduction [31], or induce electrical disorganization, so must be avoided. Tissues can be manipulated without serosal contact with the aid of judiciously-positioned tissue-grasping forceps, and the recording arrays can be gently slid over the serosal surface into the desired position. A small amount of warmed saline-soaked gauze can be packed onto and/or around the upper surface of the electrodes to maintain sound contact between the arrays and serosa. Once the electrodes are positioned, the wound edges should be re-approximated to prevent visceral drying and cooling, and a stabilization period of several minutes can then be allowed for equilibration before the recordings commence.

Once the arrays are positioned, it is important that the electrode cables are steadily secured and not moved, to prevent the positioned electrodes slipping out of place, and to avoid introducing artifacts into the recordings. In human studies, we use 2 m lengths of sterile SCSI ribbon connector cable, fixed to a retractor arm [48]. Some slack is allowed such that the electrodes can move freely with the viscera during respiratory excursion, with the remaining cable being of adequate length to connect to an acquisition system clear of the sterile field.

Electrode contact is much more difficult in the small intestine than the stomach, due to the significant curvature of the organ in both the longitudinal and circumferential axes. Lammers et al. have effectively mapped both slow wave and spike conduction small intestinal patterns using custom-built resin-embedded platforms, by resting the platforms against one side of the intestinal surface at a time [32, 39]. However, because they are flexible, the PCB electrodes can be wrapped around the intestinal surface to map both sides in continuity. Angeli et al. recently applied flexible PCBs in silicone cradles around segments of small intestine to reveal the interesting finding that slow waves can propagate around the circumference of the GI tract [4].

4.1.6 In-Vitro GI Mapping

Although the general principles are the same as in-vivo work, specific technical modifications are necessary for successful in-vitro mapping. Tissue condition is paramount, and in addition to electrode design adjustments described earlier, high fluid flow rates are employed through the fluid bath (100–400 ml/min) to ensure thorough tissue oxygenation and waste elimination [31, 38]. The electrodes should be applied against the tissue with the gentlest of pressure, or kept very slightly above the tissues [9, 28]. Using these techniques, and with careful attention to experimental variables like temperature, Lammers et al. have successfully mapped slow waves and spikes in-vitro in a variety of animal models including mouse, rat, rabbit, and cat [31, 35, 62].

5 Future Directions

5.1 Improving the Scientific Foundation of GI Mapping

This review has highlighted several knowledge gaps that could be filled to provide a more robust scientific foundation for GI multi-electrode mapping. There have been few experimental or technical studies assessing the biophysical basis of extracellular recordings, including the size of the field mapped by a single electrode. Additionally, the contributions of specific ICC and muscle layers through the thickness of the GI wall to the measured extracellular potentials are unknown. The causes of complex electrogram patterns, such as fractionation and dysrhythmic signal morphologies, also require more research, as do the potential advantages and disadvantages of bipolar versus unipolar approaches. There is scope for further optimizing the contact electrode size for GI mapping, and for developing plunge electrodes, for recording 3-dimensional activation patterns through the tissue wall [21].

5.2 Reducing Research Barriers to Serosal Mapping

Despite its apparent potential, and the striking precedent for multi-electrode mapping in cardiac electrophysiology, the uptake of GI multi-electrode mapping has been slow. Barriers to entry in this research field have included the cost of multi-channel acquisition systems, difficulty in electrode construction, and the high complexity and time-intensiveness of analytical tasks. There are also common misconceptions about extracellular recordings in the GI field, including confusion about what is actually being measured, the significance of artifacts, underestimation of the necessity of spatial data for understanding activation

patterns, and cases of misunderstanding which techniques should be applied in-vivo versus in-vitro [6, 46]. However, the growing number and prominence of published mapping studies, the emergence of affordable mass produced electrodes [15], and the growing availability of automated analysis software tools suitable for non-specialists in signal processing have greatly reduced some of these barriers in recent times [17, 18, 63].

Although the present generation of flexible PCB arrays has enabled clinical translation, there is a need for higher quality human arrays with a superior SNR [53]. If a clinical benefit for multi-electrode mapping could be demonstrated, in terms of guiding or improving patient management, then this would stimulate array development and increase demand for acquisition systems and software. Research in this direction is progressing and is proving promising, with the first mapping studies of aberrant slow wave patterns in patients with gastroparesis recently published [47]. There is also potential to standardize development and production of in-vitro mapping arrays, which would usefully expand the application of mapping to the wide array of small animal models now available for motility research [30].

5.3 Chronic Studies

Enabling chronic (awake) multi-electrode mapping studies would be another useful direction for future research. At present, all mapping studies have been performed under anaesthesia or in-vitro. However, chronic studies are ultimately needed to investigate motility patterns in the fed state, and to understand the functional and symptomatic significance of dysrhythmic patterns. Preliminary work in developing miniature implantable arrays and on-line analysis systems has demonstrated feasibility for awake animal mapping [34, 61], and the development of wireless data transfer would be a particularly valuable adjunct to support chronic studies, with potential for clinical applications in monitoring human dysrhythmias.

5.4 Minimally Invasive Mapping and Therapies

Clinical interest in GI multi-electrode mapping is expanding, partly reflecting the recent successful translation of the techniques to humans [48], and partly reflecting the growth in understanding of the role played by the interstitial cells of Cajal (ICC) in motility disorders. ICC loss or dysfunction is now associated with several significant diseases, such as gastroparesis, in which ICC networks show damage and depletion, and irritable bowel syndrome, where ICC channelopathies have been identified in a patient subset [19]. Multi-electrode mapping offers potential to elucidate the functional consequences of such pathologies at the tissue and organ

levels, in order to guide the development of improved diagnostic and therapeutic approaches for these difficult diseases, for example, through gastric pacing [50].

A major impediment to the clinical translation of multi-electrode mapping, however, is the invasiveness of current technologies, which require open surgical access. In recent years, early attempts have, therefore, been made to develop and apply miniature arrays of fewer electrodes for endoscopic or laparoscopic applications [14, 49]. Devices with as few as four electrodes can provide reliable information about velocity and amplitude, further supporting the utility of small array systems [49].

Ultimately, we anticipate that improved endoscopic tools will become available for the routine minimally-invasive mapping of the human GI tract. Such endoscopic systems, coupled with real-time software applications, have the potential to revolutionize the understanding and management of gastric dysrhythmias in clinical practice, and could, therefore, underpin important advances in the care of patients with motility diseases in future years.

Acknowledgments GOG is supported by grants from the American Neurogastroenterology & Motility Society, the NZ Health Research Council, and the NIH (R01 DK64775). TRA is supported by the Riddett Institute and the Royal Society of NZ.

References

1. Alvarez WC (1922) The electrogastrogram and what it shows. JAMA 78:1116–1119
2. Alvarez WC (1929) Physiologic studies on the motor activities of the stomach and bowel in man. Am J Physiol 88(4):650–662
3. Alvarez WC, Mahoney LJ (1922) Action currents in stomach and intestine. Am J Physiol 58(3):476–493
4. Angeli TR, O'Grady G, Erickson JC, Du P, Paskaranandavadivel N, Bissett IP et al (2011) Mapping small intestine bioelectrical activity using high-resolution printed-circuit-board electrodes. In: Conference Proceedings—IEEE Engineering in Medicine and Biology Society, pp 4951–4954
5. Bass P, Code CF, Lambert EH (1961) Motor and electric activity of the duodenum. Am J Physiol 201:287–291
6. Bayguinov O, Hennig GW, Sanders KM (2011) Movement artifacts may contaminate extracellular electrical recordings from GI muscles. Neurogastroenterol Motil 23:1029–e498
7. Berkson J, Baldes EJ, Alvarez WC (1932) Electromyographic studies of the gastrointestinal tract: I. The correlations between mechanical movement and changes in electrical potential during rhythmic contraction of the intestine. Am J Physiol 102(3):683–692
8. Bortoff A (1961) Slow potential variations of small intestine. Am J Physiol 201(1):203–208
9. Bortoff A (1967) Configuration of intestinal slow waves obtained by monopolar recording techniques. Am J Physiol 213(1):157–162
10. Bortolotti M, Sarti P, Barara L, Brunelli F (1990) Gastric myoelectrical activity in patients with chronic idiopathic gastroparesis. J Gastroint Motil 2:104–108
11. Bozler E (1942) The action potentials accompanying conducted responses in visceral smooth muscles. Am J Physiol 136(4):553–560
12. Bozler E (1939) Electrophysiological studies on the motility of the gastrointestinal tract. Am J Physiol 127(2):301–307

13. Bull S, O'Grady G, Cheng LK, Pullan AJ (2011) A framework for the online analysis of multi-electrode gastric slow wave recordings. In: Conference Proceedings—IEEE Engineering in Medicine and Biology Society, pp 1741–1744
14. Coleski R, Hasler WL (2009) Coupling and propagation of normal and dysrhythmic gastric slow waves during acute hyperglycaemia in healthy humans. Neurogastroenterol Motil 21(5):492–499, e1–e2
15. Du P, O'Grady G, Egbuji JU, Lammers WJ, Budgett D, Nielsen P et al (2009) High-resolution mapping of in vivo gastrointestinal slow wave activity using flexible printed circuit board electrodes: methodology and validation. Ann Biomed Eng 37(4):839–846
16. Egbuji JU, O'Grady G, Du P, Cheng LK, Lammers WJEP, Windsor JA et al (2010) Origin, propagation and regional characteristics of porcine gastric slow wave activity determined by high-resolution mapping. Neurogastroenterol Motil 22:e292–e300
17. Erickson JC, O'Grady G, Du P, Egbuji JU, Pullan AJ, Cheng LK (2011) Automated cycle partitioning and visualization of high-resolution activation time maps of gastric slow wave recordings: the region growing using polynomial surface-estimate stabilization (REGROUPS) algorithm. Ann Biomed Eng 39(1):469–483
18. Erickson JC, O'Grady G, Du P, Obioha C, Qiao W, Richards WO et al (2010) Falling-edge, variable threshold (FEVT) method for the automated detection of gastric slow wave events in serosal high-resolution electrical recordings. Ann Biomed Eng 38(4):1511–1529
19. Farrugia G (2008) Interstitial cells of Cajal in health and disease. Neurogastroenterol Motil 20(suppl 1):54–63
20. Fontanesi L, D'Alessandro E, Scotti E, Liotta L, Crovetti A, Chiofalo V et al (2010) Genetic heterogeneity and selection signature at the KIT gene in pigs showing different coat colours and patterns. Anim Genet 41(5):478–492
21. Hooks DA, Trew ML (2008) Construction and validation of a plunge electrode array for three-dimensional determination of conductivity in the heart. IEEE Trans Biomed Eng 55(2 Pt 1):626–635
22. Hotokezaka M, Mentis EP, Patel SP, Combs MJ, Teates CD, Schirmer BD (1997) Recovery of gastrointestinal tract motility and myoelectric activity change after abdominal surgery. Arch Surg 132(4):410–417
23. Hou X, Yin J, Liu J, Pasricha PJ, Chen JD (2005) In vivo gastric and intestinal slow waves in W/WV mice. Dig Dis Sci 50(7):1335–1341
24. Ideker RE, Smith WM, Blanchard SM, Reiser SL, Simpson EV, Wolf PD et al (1989) The assumptions of isochronal cardiac mapping. Pacing Clin Electrophysiol 12(3):456–478
25. Kelly KA, Code CF, Elveback LR (1969) Patterns of canine gastric electrical activity. Am J Physiol 217(2):461–470
26. Kimber S, Downar E, Masse S, Sevaptsidis E, Chen T, Mickleborough L et al (1996) A comparison of unipolar and bipolar electrodes during cardiac mapping studies. Pacing Clin Electrophysiol 19(8):1196–1204
27. Lammers WJ (2000) Propagation of individual spikes as "patches" of activation in isolated feline duodenum. Am J Physiol Gastrointest Liver Physiol 278(2):G297–G307
28. Lammers WJ (2005) Spatial and temporal coupling between slow waves and pendular contractions. Am J Physiol Gastrointest Liver Physiol 289(5):G898–G903
29. Lammers WJ, Abazer FA, Ver Donck L, Smets D, Schuurkes JA, Coulie B (2006) Electrical activity in the rectum of anaesthetized dogs. Neurogastroenterol Motil 18(7):569–577
30. Lammers WJ, Al-Bloushi HM, Al-Eisae SA, Al-Dhaheri FA, Stephen BS, John R et al (2011) Slow wave propagation and ICC plasticity in the small intestine of diabetic rats. Exp Physiol 96(10):1039–1148
31. Lammers WJ, al-Kais A, Singh S, Arafat K, el-Sharkawy TY (1993) Multielectrode mapping of slow-wave activity in the isolated rabbit duodenum. J Appl Physiol 74(3):1454–1461
32. Lammers WJ, Donck LV, Schuurkes JA, Stephen B (2003) Longitudinal and circumferential spike patches in the canine small intestine in vivo. Am J Physiol Gastrointest Liver Physiol 285(5):G1014–G1027

33. Lammers WJ, el-Kays A, Manefield GW, Arafat K, el-Sharkawy TY (1997) Disturbances in the propagation of the slow wave during acute local ischaemia in the feline small intestine. Eur J Gastroenterol Hepatol 9(4):381–388
34. Lammers WJ, Michiels B, Voeten J, Ver Donck L, Schuurkes JA (2008) Mapping slow waves and spikes in chronically instrumented conscious dogs: automated on-line electrogram analysis. Med Biol Eng Comput 46(2):121–129
35. Lammers WJ, Slack JR, Stephen B, Pozzan O (2000) The spatial behaviour of spike patches in the feline gastroduodenal junction in vitro. Neurogastroenterol Motil 12(5):467–473
36. Lammers WJ, Stephen B (2008) Origin and propagation of individual slow waves along the intact feline small intestine. Exp Physiol 93(3):334–346
37. Lammers WJ, Stephen B, Arafat K, Manefield GW (1996) High resolution electrical mapping in the gastrointestinal system: initial results. Neurogastroenterol Motil 8(3):207–216
38. Lammers WJ, Stephen B, Slack JR (2002) Similarities and differences in the propagation of slow waves and peristaltic waves. Am J Physiol Gastrointest Liver Physiol 283(3):G778–G786
39. Lammers WJ, Ver Donck L, Schuurkes JA, Stephen B (2005) Peripheral pacemakers and patterns of slow wave propagation in the canine small intestine in vivo. Can J Physiol Pharmacol 83(11):1031–1043
40. Lammers WJ, Ver Donck L, Stephen B, Smets D, Schuurkes JA (2009) Origin and propagation of the slow wave in the canine stomach: the outlines of a gastric conduction system. Am J Physiol Gastrointest Liver Physiol 296:1200–1210
41. Lammers WJEP, Ver Donck L, Stephen B, Smets D, Schuurkes JAJ (2008) Focal activities and re-entrant propagations as mechanisms of gastric tachyarrhythmias. Gastroenterology 135(5):1601–1611
42. Lapatki BG, Van Dijk JP, Jonas IE, Zwarts MJ, Stegeman DF (2004) A thin, flexible multielectrode grid for high-density surface EMG. J Appl Physiol 96(1):327–336
43. McAdams E (2006) Bioelectrodes. In: Webster JG (ed) Encyclopedia of Medical Devices and Instrumentation, 2nd edn. Wiley, New York, pp 120–166
44. Metting Van Rijn AC, Kuiper AP, Linnenbank AC, Grimbergen CA (1993) Patient isolation in multichannel bioelectric recordings by digital transmission through a single optical fiber. IEEE Trans Biomed Eng 40(3):302–308
45. Monges H, Salducci J (1970) A method of recording the gastric electrical activity in man. Am J Dig Dis 15:271
46. O'Grady G (2012) Gastrointestinal extracellular electrical recordings: fact or artifact? Neurogastroenterol Motil 24(1):1–6
47. O'Grady G, Angeli TR, Du P, Lahr C, Lammers WJEP, Windsor JA, Abell TL, Farrugia G, Pullan AJ, Cheng LK (2012) Abnormal initiation and conduction of slow-wave activity in gastroparesis, defined by high-resolution electrical mapping. Gastroenterology 143(3):589–598
48. O'Grady G, Du P, Cheng LK, Egbuji JU, Lammers WJ, Windsor JA et al (2010) The origin and propagation of human gastric slow wave activity defined by high-resolution mapping. Am J Physiol Gastrointest Liver Physiol 299(3):585–592
49. O'Grady G, Du P, Egbuji JU, Lammers WJ, Wahab A, Pullan AJ et al (2009) A novel laparoscopic device for measuring gastrointestinal slow-wave activity. Surg Endosc 23:2842–2848
50. O'Grady G, Du P, Lammers WJ, Egbuji JU, Mithraratne P, Chen JDZ et al (2010) High-resolution entrainment mapping for gastric pacing: a new analytic tool. Am J Physiol Gastrointest Liver Physiol 298:314–321
51. O'Grady G, Du P, Paskaranandavadivel N, Angeli T, Lammers WJEP, Farrugia G et al (2012) Rapid high-amplitude circumferential slow wave conduction during normal gastric pacemaking and dysrhythmias 24(7):e299–312
52. O'Grady G, Egbuji JU, Du P, Lammers WJ, Cheng LK, Windsor JA et al (2011) High-resolution spatial analysis of slow wave initiation and conduction in porcine gastric dysrhythmia. Neurogastroenterol Motil 23(9):e345–e355

53. O'Grady G, Paskaranandavadivel N, Angeli T, Du P, Windsor JA, Cheng LK et al (2011) A comparison of gold vs silver electrode contacts for high-resolution gastric electrical mapping using flexible printed circuit board electrodes. Physiol Meas 32:N13–N22
54. Ohba M, Sakamoto Y, Tomita T (1975) The slow wave in the circular muscle of the guinea-pig stomach. J Physiol 253(2):505–516
55. Plonsey R, Barr RC (2007) Extracellular fields. In: Plonsey R, Barr RC (eds) Bioelectricity: a quantitative approach. Springer, New York, pp 223–265
56. Sanders KM (2008) Regulation of smooth muscle excitation and contraction. Neurogastroenterol Motil 20(suppl 1):39–53
57. Suzuki N, Prosser CL, DeVos W (1986) Waxing and waning of slow waves in intestinal musculature. Am J Physiol 250(1 Pt 1):G28–G34
58. Szurszewski JH (1969) A migrating electric complex of canine small intestine. Am J Physiol 217(6):1757–1763
59. Szurszewski JH, Elveback LR, Code CF (1970) Configuration and frequency gradient of electric slow wave over canine small bowel. Am J Physiol 218(5):1468–1473
60. Thorn SE, Wattwil M, Lindberg G, Sawe J (1996) Systemic and central effects of morphine on gastroduodenal motility. Acta Anaesthesiol Scand 40(2):177–186
61. Ver Donck L, Lammers WJ, Moreaux B, Smets D, Voeten J, Vekemans J et al (2006) Mapping slow waves and spikes in chronically instrumented conscious dogs: implantation techniques and recordings. Med Biol Eng Comput 44(3):170–178
62. Wang XY, Lammers WJ, Bercik P, Huizinga JD (2005) Lack of pyloric interstitial cells of Cajal explains distinct peristaltic motor patterns in stomach and small intestine. Am J Physiol Gastrointest Liver Physiol 289(3):G539–G549
63. Yassi R, O'Grady G, Paskaranandavadivel N, Du P, Angeli TR, Pullan AJ, Cheng LK, Erickson JC (2012) The Gastrointestinal Electrical Mapping Suite (GEMS): Software for analysing and visualising gastrointestinal multi-electrode recordings. BMC Gastroenterol 12(60):1–14

Quantitative Analysis of Electrical Activity in the Gastrointestinal Tract

Jonathan C. Erickson, Niranchan Paskaranandavadivel and Simon H. Bull

Abstract High resolution electrical mapping of the gastrointestinal tract provides us with vital information about the coordination of motility. Due to the nature of the recording setup, an enormous amount of information is collected which needs to be processed and analysed. In recent years, novel methods and software packages have been developed in order to automate the processes which were previously manually done with judicious selection. This chapter outlines the methods performed in order to analyse and visualize the electrical activity in an efficient and effective manner, with potential applications and future work.

1 Introduction to GI Analysis

High resolution (HR) electrical mapping is an essential research and clinical tool that has advanced our knowledge of the electrophysiology of the major organs in our body. HR electrical mapping techniques have been used successfully to study the heart and the brain, both on the surface of the organ and on the body surface. This has led to develop diagnostic capabilities and treatment options in the field of neuroscience and cardiology. In recent years HR electrical mapping has been used to understand the gastrointestinal (GI) tract in greater detail and elucidate the mechanisms and differences between normal and abnormal activity [26, 38].

J. C. Erickson (✉)
Washington and Lee University, Lexington, USA
e-mail: ericksonj@wlu.edu

N. Paskaranandavadivel · S. H. Bull
Auckland Bioengineering Institute, The University of Auckland, Auckland, New Zealand
e-mail: npas004@aucklanduni.ac.nz

S. H. Bull
e-mail: s.bull@auckland.ac.nz

L. K. Cheng et al. (eds.), *New Advances in Gastrointestinal Motility Research*,
Lecture Notes in Computational Vision and Biomechanics 10,
DOI: 10.1007/978-94-007-6561-0_5, © Springer Science+Business Media Dordrecht 2013

There is an underlying bio-electrical activity present in the GI tract, termed slow waves, which coordinates motility. Slow waves are generated and propagated through a specialized network of cells known as 'Interstitial Cells of Cajal (ICCs)', which are present in the musculature of the GI tract [13]. In canines, gastric slow waves recur around 5 cycles per minute (cpm) [27], and intestinal slow waves recur from around 10–17 cpm depending on the location [23]. Along with slow waves, electrical spike activity and migrating motor complexes are known to occur during motility [17] (see Angeli et al. "The Electrical Regulation of GI Motility at the Whole-Organ Level" of this volume for further information). In order to study the underlying GI electrical activity in a robust and reliable manner qualitative and quantitative techniques are required.

This chapter will focus on the methods and approaches that have been used in HR GI electrical mapping, and their application to clinical mapping. With HR electrical mapping there is an enormous amount of information which needs to be analysed and visualized using effective approaches. A brief overview of signal processing in relation to GI electrical signals is given, after which event detection and clustering methods are discussed. Methods to estimate the velocity and amplitude of the slow wave propagation are presented with their applications to clinical experimental recordings. This chapter concludes by exploring potential methodologies that are aimed at studying the electrical activity in the GI tract in a qualitative and quantitative manner.

2 Gastrointestinal Electrical Recording Techniques

Electrical recording of the GI tract was first attempted by Alvarez et al. [1], where he probed the stomach and intestine using Einthoven's and D'Arsonval's galvanometers to record electrical activity. Since then, and over the years researchers have recorded electrical activity from the GI tract intracellular (see Beyder et al. "Role of Ion Channel Mechanosensitivity in the Gut: Mechano-Electrical Feedback Exemplified by Stretch-Dependence of $Na_v1.5$" of this volume) and extracellularly from the mucosal and serosal surface of the organ and from the body surface (see Bradshaw et al. "Biomagnetic Signatures of Gastrointestinal Electrical Activity" in this volume), which is commonly referred to as cutaneous electrogastrograms (EGG). The signal morphology of intracellular recordings approximately matches the morphology of serosal extracellular recordings via a temporal second derivative [4, 46]. Intracellular signals provide the most detailed identifiable current movements from and into the cell, leading to the electrical activity present in the GI tract. Extracellular recordings provide a summed and distributed view of the intracellular recordings, while EGG recordings provide a summed and smoothed representation of the electrical activity present in the GI tract and body surface.

Initially few electrodes (around 4–8) were used to record the electrical activity on the surface of the gut [6, 19, 44]. This provided a valuable insight into the

electrophysiology of the GI tract, and began to elucidate and generate hypotheses about the mechanisms present in the GI tract. However spatial information about the electrical activity was not addressed adequately (see Fig.1), thus motivating the development of high resolution electrical recording techniques by Lammers et al. and Du et al. [8, 25].

Currently high resolution mapping electrodes which were developed for use in the GI tract have an inter-electrode distance spacing ranging from 2 to 7.62 mm, with the number of electrodes ranging from 192 to 256 [7, 8, 27]. These configurations have provided adequate coverage to map the stomach [27], intestines [23], and recently the ureter [16] of many species, including humans [34] (see O'Grady et al. "The Principles and Practice of Gastrointestinal High-Resolution Electrical Mapping" of this volume). HR mapping is attractive for mapping and tracking the electrophysiological propagation, but produces large amounts of data which require effective methods to analyse in a quantitative and qualitative manner.

3 Signal Processing

GI mapping recordings—like all bioelectric recordings—are often contaminated by various sources of noise, and noise removal is, therefore, an essential first step of signal (pre-)processing. Noise in the raw recordings can be eliminated or minimized by shielding the cables and using effective electrodes to improve signal to noise ratio (see O'Grady et al. "The Principles and Practice of Gastrointestinal High-Resolution Electrical Mapping" of this volume). In this section a brief overview of potential noise sources in gastric HR electrical mapping is given along with approaches used to eliminate them. Noise is omnipresent and its sources include: power line interference (at 50 or 60 Hz), thermally generated (Johnson) noise, other nearby electrical devices, and physiological artefacts. The commonly observed physiological artefacts for GI electrical recordings come in the form of respiration from the subject, and electrical and mechanical activity from the heart and other organs.

Noise components in bio-electrical recordings can span the entire relevant frequency range, from essentially DC to several hundred cycles per second. The low frequency noise mainly manifests as baseline wander in the signals, which is due to the time-varying electrode-serosa impedance.

Respiration typically occurs at about 8–15 cpm, which can be particularly problematic due to the large degree of spectral overlap with the small intestine slow wave frequency range.

Power line interference and other noise artefacts (frequency above 15 cpm) are classified as high frequency noise. Noise removal primarily depends on three factors: type of analysis to be performed, which frequencies of the bio-signal are of interest, and the recording hardware. With in-vivo gastric slow wave recordings, the signals have both slow (frequency below 15 cpm) and fast (frequency above

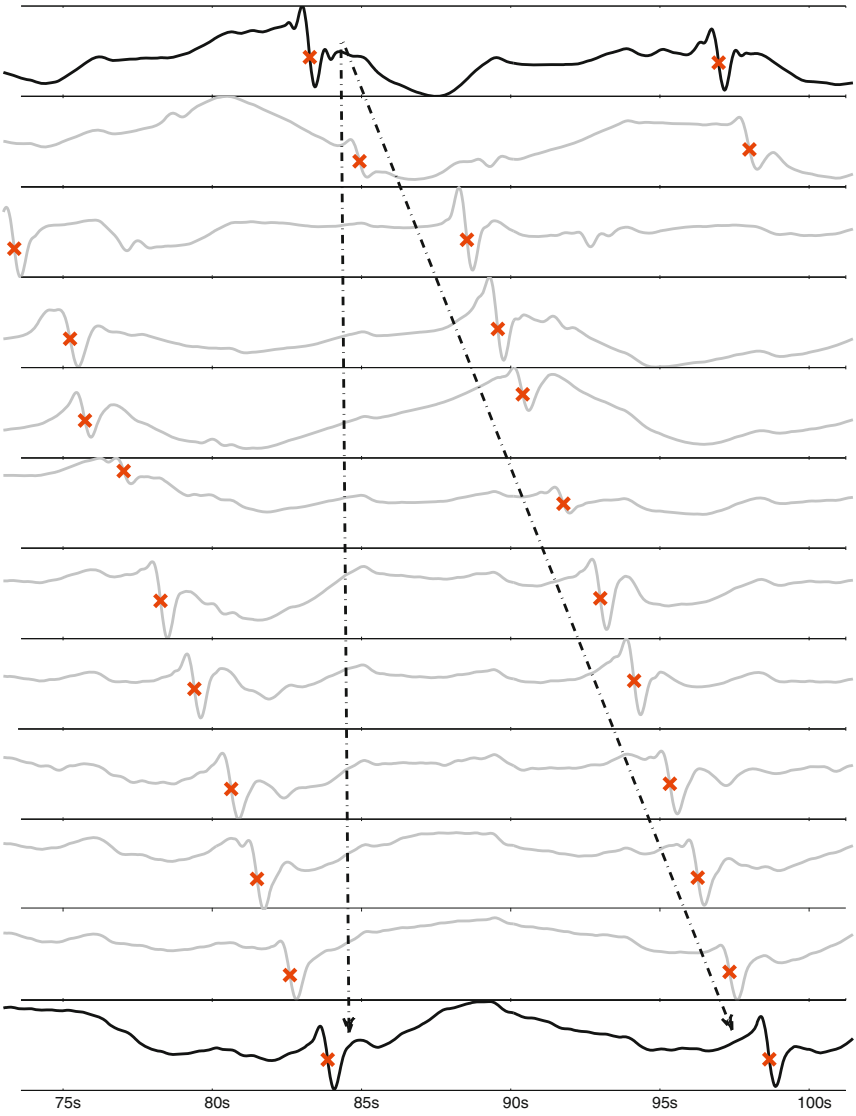

Fig. 1 Identification of gastric slow wave spatial propagation using high resolution and sparse electrodes. Slow wave events are marked by a *cross*, and *dotted arrow* marks the mapping of the spatial propagation of slow waves. All of the signal traces (in *gray* and *black*) are from a high resolution electrode array [8], but the *top* and *bottom* signal traces have been shown in *black* to represent sparse recordings. High resolution mapping facilitates a more certain tracking and identification of the slow wave. The *dashed arrows* suggest possible slow wave tracking interpretations; both could be valid interpretations given only the first and last channels, but the *right hand arrow* is selected as correct of the slow wave given the extra information provided by the intermediate electrodes

15 cpm) components. We shall examine some of the filters that have been used in sparse and HR GI mapping to eliminate noise.

With sparse gastric serosal recording, Sarna et al. [44] recorded the electrical data using analog filters with a passband of 0.35–22 Hz, while Chen et al. [6] recorded the data using analog filters with a passband of 0.05–35 Hz.

Lammers et al. [25] was among the first to start recording and analysing slow waves using HR, and applied a 20 point moving average filter. Such a filter acts as a low pass filter and eliminates power line interference (at 50 Hz) and other higher frequency components without distorting the morphology of the signal, provided its components are much less than 50 Hz. Baseline wander was not present in these studies as the recording hardware was band limited from 2 to 400 Hz.

Following on, Du et al. [8] developed HR flexible printed circuit board electrode arrays to analyse electrical activity in the GI tract. Different second order low pass Bessel filters with cut-off frequencies ranging from 2 to 10 Hz were applied in various studies to study slow waves in the stomach [8, 10, 34, 35]. Butterworth filters were also to study slow wave activity in the stomach, offline (passband 1–60 cpm) [11, 12], and in real time (passband 0.5–4 Hz) [5] using these flexible PCB electrodes. Time domain filters were also applied to the flexible PCBs, which were the moving median filter for baseline removal and a Savitzky Golay filter for high frequency noise removal, and were shown to outperform the Butterworth filter (passband 1–60 cpm) [40]. One of the advantages of time domain filters such as a Savitzky Golay filter over a frequency domain filter such as a Butterworth filter is that they can maintain the peaks and do not distort the morphology of the signal.

With GI electrical recordings, there can be both slow wave and spike activity at varying frequencies. Thus, depending on the type of analysis to be performed, appropriate filtering techniques must be used. In HR GI mapping, the common analytical tool is the use of slow wave isochronal activation time maps where the signals are marked at the point of most negative deflection. For this purpose, the signal does not need to have all of its morphological characteristics (e.g. the slow return to baseline), and a 'harsh' filter setting may be used. A 'harsh' filter is one which distorts the morphology of the slow wave (mainly eliminating the slow return to baseline component of the slow wave) and reduces its signal amplitude from the raw recording, while a 'soft' filter better maintains these features but is not as effective at removing unwanted signals. If the amplitude or morphology of the slow waves are to be analysed, 'soft' filter settings can be used, so the amplitude of the signal does not erode and also the morphology would not get distorted. Examples of 'soft' and 'harsh' filtering on a slow wave signal obtained from the serosal surface of the stomach are shown in Fig. 2. With the 'soft' filtering approach the baseline is removed via a moving median filter (20 second window), while with the 'harsh' filtering approach a high pass butterworth filter with a cut-off frequency of 20 cpm is used.

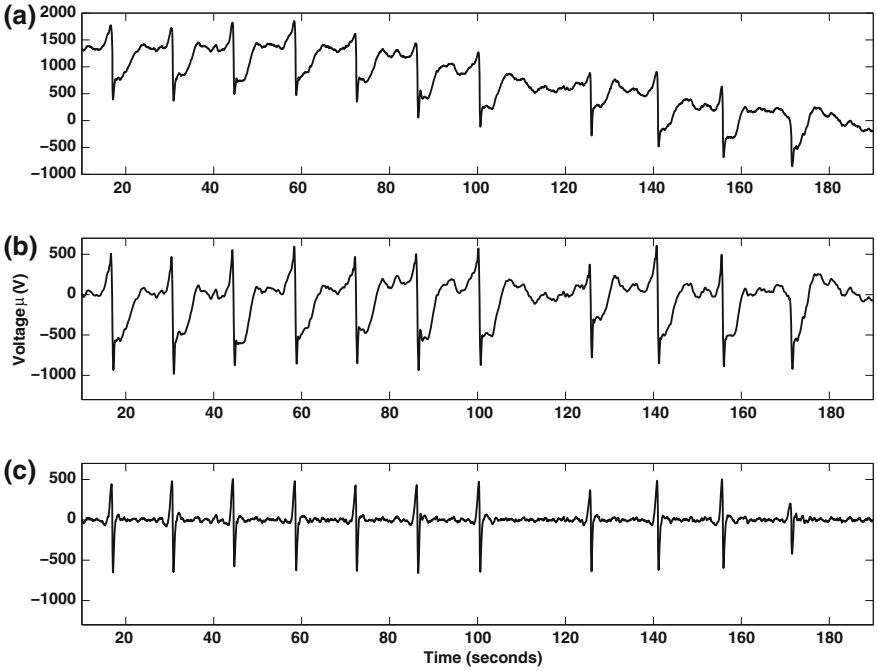

Fig. 2 Illustration of baseline removal using two filtering techniques on serosal gastric slow waves in a porcine subject. **a** Gastric slow wave recording where high frequency noise has been eliminated using a Savitzky Golay filter with a polynomial order of 9 and a window size of 1.7 s. **b** Removal of baseline wander using a moving median window (20 s window). **c** Removal of baseline wander using a high pass butterworth filter with a cut-off frequency of 20 cpm. As can be seen the morphology and amplitude of the slow is altered when using a 'harsh' filter, but might be able to provide a more accurate fiducial point for the point of activation

4 Slow Wave Event Detection: The FEVT Algorithm

One of the key features in GI electrical recordings is the slow wave. The onset (activation time, AT) of the slow wave defines when the traveling slow wave has arrived at a particular electrode location. Once activation times are detected across the entire array, isochronal maps depicting the spatiotemporal wave activity can be generated (see Sect. 5).

In gastric serosal electrical recordings, the onset of the slow wave is typically manifested by a relatively large amplitude with a fast time-scale (high frequency) and a negative deflection in the signal. This is followed by a relatively slow recovery to baseline (Fig. 3a). The fiducial point of interest to be detected is the fast initial large transient.

Several automated methods have been developed to perform this task which vary in complexity and performance. The most basic method is simple thresholding. In this method an AT is detected when the amplitude of the recorded

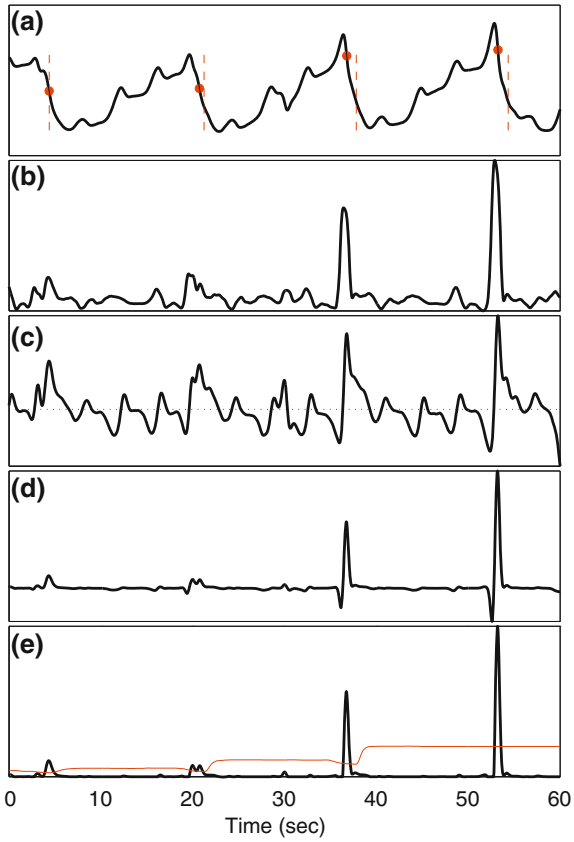

Fig. 3 Illustration of signal processing sequence for falling-edge-detector method with variable detection threshold. **a** Example serosal electrode recording. *Red vertical dashes* denote hand-marked TOAs, while *filled red circles* indicate ATs detected with the Falling-Edge, Variable-Threshold algorithm. **b** SNEO signal computed from **a**. **c** Edge-detector signal computed from **a**. The *horizontal dashed line* marks the value of 0. Local maxima in **C** correspond to a falling edge in a (and vice-versa). **d** The result of multiplying signals **b** and **c**. **e** Falling Edge (FE) signal, equal to Signal **d** with all negative-values set to 0. The *red curve* represents the detection threshold which varies over time. The four "pulses" corresponding to each AT are properly detected. Reproduced from Erickson et al. [12]

voltage signal ($V(t)$) crosses a constant threshold, which is usually set equal to the estimated noise in the signal (σ) multiplied by a constant (k)—i.e., where $|V(t)| \geq k\sigma$. A more sophisticated method developed by Lammers et al. detects ATs based on an "amplitude sensitive differentiator" (ASD) transform of the recorded signal: $ASD = |V(t)|\frac{dV}{dt}$ [24]. A constant threshold was similarly used. More recently, the Falling Edge-Variable Threshold (FEVT) algorithm was designed to improve the accuracy of an automated analysis.

In brief, FEVT works by emphasizing the large amplitude, high frequency content of the original signal via a 2nd-order non-linear energy operator (NEO) transform [31] (also commonly referred to as the Teager Energy Transform [18]). Sharp downward transients are additionally emphasized by applying an edge-detector kernel [45]. Thus, the falling edge (FE) signal used to detect ATs is given by:

$$FE(t) = (V(t+1)V(t-1) - V(t)V(t)) \times \left(V(t) * d_{N_{edge}}\right) \quad (1)$$

where t denotes an integer time index, and $d_{N_{edge}}$ is the edge-detector kernel defined in [45], and $\times$ indicates an element-wise multiplication and $*$ indicates a convolution.

A time-varying threshold, which is used to identify slow wave events, is computed to account for the fact that even small variations in the slow wave waveform can produce relatively large changes in the amplitude of FE signal. Figure 3 illustrates the key steps of the algorithm. Full mathematical details of the FEVT algorithm can be found in Erickson et al. [12].

Some noteworthy points on the FEVT algorithm are as follows:

1. The NEO transform, which is computed in the first step of the FEVT algorithm, belongs to a class of differential energy operators [29]. Its original intended usage was for radio signal detection. It was first adapted and adopted into the biomedical realm for detecting spikes in extracellular neural recordings [31].
2. The edge detector kernel which is convolved with the gastric serosal recording was originally used for edge detection in digital images by Sezan [45]. Explicitly zeroing out regions of the FE signal that are negative focuses the algorithm to look for downward deflections only.
3. The threshold signal varies in time (hence the "VT" in the algorithm's name), and is set to a constant factor multiplied by the median of the absolute deviation. The latter is essentially a robust statistic for estimating the noise in a signal, thereby allowing for robust detection of peaks in the FE signal, which correspond to the negative deflection of the respective slow waves. This noise estimator was originally proposed and implemented by Nenadic and Burdick with application to detecting spikes in neural recordings [32]. It is beneficial in our context because the FE transform can have large peaks whose amplitude can vary from one event to the next due to small variations in the recorded signal, whether due to noise, or due to slight changes in underlying electrical signal or changing electrode impedance.

Optimizing the performance of FEVT involves judicious selection of three parameters:

1. Smoothing window size. The outcome is not particularly sensitive to this parameter, and generally the smoothing window size is in the range of 0–1 s for best performance.
2. Moving median window length. The outcome is dependent on this parameter. It should be made long enough such that the median is not strongly affected by any

peaks (slow wave events) in the FE signal. It should also be made short enough that it avoids "washing out" the fine detail of peaks which could possibly vary in magnitude. In general, it should be chosen to be about 1.5 times the period at which slow waves occur. For example, for gastric slow waves occurring at 3 cpm, this parameter is usually set to about 30 s (1.5 cycles).
3. Detection threshold multiplier, η. The outcome is dependent on this parameter. For higher sensitivity, η should be kept low; for greater specificity (avoidance of false positives), η should be set higher. Typically recommended values are $\eta = 4–7$.

The FEVT algorithm has been found to robustly detect slow waves from gastric recordings [12]. Already, it has been utilized to accelerate the analyses of slow wave spatiotemporal dynamics during normal and dysrhythmic pacemaking activity [36, 38]. It has also proven useful, though slightly less effective, at detecting slow waves in small intestine [2].

The current shortcomings of the algorithm are:

1. Computational expense: The computational overhead is fairly intensive, mostly due to computing the running median, but not prohibitively so. A real-time implementation [5] requires that the user wait an initial $\approx$20 s for the first marks to be made, but there is no additional delay in automated marking thereafter.
2. Improperly marking artifacts: Large transient artifacts which are not of biological origin can be marked as false positives (see Fig. 4, channel 7). This issue is not particularly problematic because actual slow wave ATs can be validated based on the magnitude of the signal: false positive artifacts are almost always much larger in magnitude than an actual slow wave signal.
3. Generally difficult signals: Fractionated waveforms, or signals with a "wandering baseline" (see Fig. 4, channel 27) are still difficult to properly analyze. Future research directions will explore whether machine learning algorithms such as support vector machines can aid in properly classifying a putative AT as an artifact, or an actual slow wave. The main idea is to send a window of data centered on the (putative) AT mark to the classifier for rendering the final decision.

5 Clustering of Propagating Waves: The REGROUPS Algorithm

In order to analyze slow-wave propagation patterns over multiple cycles, it is often highly beneficial and/or necessary to create a sequence of isochronal activation time (AT) maps (see Fig. 5b and d). These maps can be utilized to assess the spatiotemporal dynamics of slow wave conduction, i.e., direction and speed of propagation (see Sect. 6). A prerequisite for generating AT maps is to properly group or cluster all of the identified slow wave event activation times

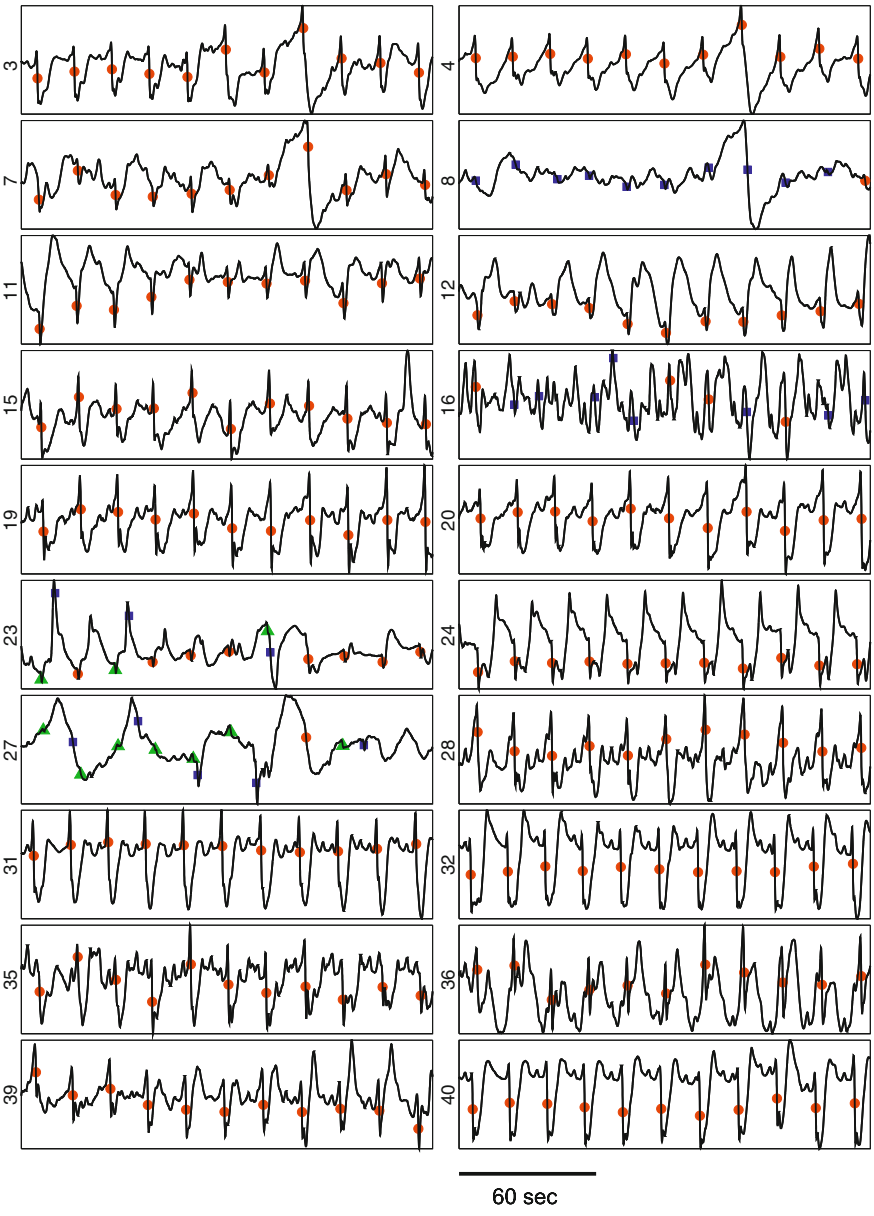

Fig. 4 Signals recorded with PCB electrodes, with the results illustrating outcome of automated AT detection using the FEVT method. Each of 20 panels shows a 180 s long signal recorded with a PCB electrode. Automarking results are marked as true positives (TPs, *filled red circles*), false positives (FPs, *filled blue squares*), and false negatives (FNs, *filled green triangles*). For most electrodes, the FEVT detection algorithm succeeding in finding all ATs without finding any FPs. However, some electrodes (23 and 27, for example) show a significant fraction of FPs and FNs due to their relatively complex waveforms. Adapted from [14]

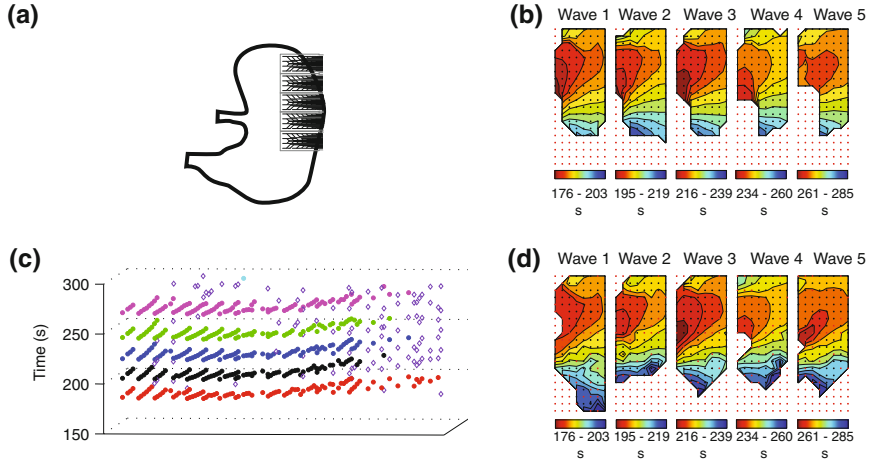

Fig. 5 Cycle partitioning result and corresponding AT maps for manual and REGROUPS methods. **a** Approximate placement of electrode array on stomach. **b** Isochronal AT map generated via manual clustering. **c** Clustering of points defining each wave cycle using the REGROUPS method, and **d** corresponding AT maps. The wave spreads from regions colored *red* (earliest activation times) to *blue* (latest activation times). The results of manual and REGROUPS cycle partitioning are highly similar, both illustrating the slow wave conducting radially away from a pacemaker site. Adapted from [11]

corresponding to an individual wave. The Region Growing utilizing Polynomial Stabilization (REGROUPS) method was designed expressly for this purpose. Full details of this algorithm can be found in Erickson et al. [11].

Similar to previously described wave-mapping algorithms by Lammers et al. [21], and Rogers and Ideker [42, 43], one key step in REGROUPS involves clustering points by starting at a seed point and searching neighboring electrodes for an AT that is temporally "close enough". A "point" refers to a spatiotemporal 3-element coordinate $(x_i, y_i, t_i^{(k)})$ where x_i and y_i specify the position of the of the ith electrode in the array, and $t_i^{(k)}$ is the kth AT at that site. All neighboring electrode sites of a point just added to the cluster are also searched to see if they are temporally close.

The REGROUPS method was designed to handle two issues commonly encountered during routine measurement:

1. Missing data or bad electrodes: Electrode sites with no marked ATs, mainly due to insufficient contact or erosion of electrode tips due to the sterilization [39]. This algorithm is not hindered by a small amount of missing data by design, as described below.
2. Velocity gradient: REGROUPS takes into account any changes in wavefront propagation velocity by utilizing a second-order model to describe its spatio-temporal dynamics (see Eq. 2).

This method explicitly utilizes a continuously updating spatiotemporal filter to estimate the ATs at a given location. The filter is essentially a second-order polynomial surface of the form:

$$AT(x, y) = p_1x^2 + p_2y^2 + p_3xy + p_4x + p_5y + p_6 \quad (2)$$

where x and y denote spatial coordinates, and the coefficients p_1 through p_6 define the exact shape of the surface. The coefficients, p_i, are updated each time a point is added to the cluster defining the waveform. The estimate of an AT at a nearby electrode site (x_n, y_n) not yet included in the cluster is computed simply by extending the surface to that spatial coordinate, i.e, $AT(x_n, y_n)$. The REGROUPS temporal closeness criterion stipulates that a point at a nearby site be added to the cluster if:

$$\delta T = |AT(x_n, y_n) - \text{ marked ATs at}(x_n, y_n)| \leq \text{ time tolerance.} \quad (3)$$

The value of δT should be chosen as a compromise between keeping it large enough to not be too stringent on the estimate for $AT(x, y)$, while also keeping it small enough so as to discriminate which points are properly clustered. REGROUPS terminates clustering of an individual wave when all electrode sites have been considered.

Figure 6 shows the polynomial surface updating as more points are continually added to the cluster. Notice how the curvature, slope, and twist of the surface change as more points are added. Thus, this data-driven model utilizes an updating spatiotemporal filter that takes into account any velocity gradients or non-uniformities in the wavefront propagation.

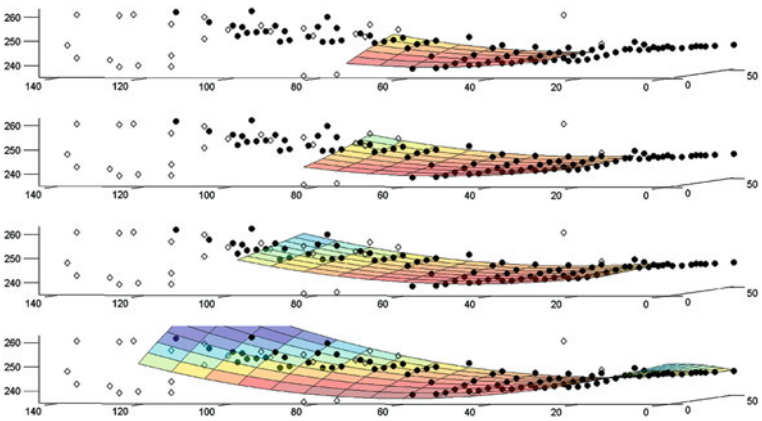

Fig. 6 The second order surface $AT(x, y)$ updating according to the points already in the cluster. *Filled circles* represent points which, at the end of clustering, are clustered into the cycle; *unfilled diamonds* represent points which were rejected during clustering (*orphans*). The subpanels (*top* to *bottom*) show the second-order surface when clustering is approximately 1/4, 1/2, 3/4, and fully complete. Time is represented on the vertical axis (units of seconds). The (x, y) coordinates represent the electrode site positions (units of mm). Reproduced from Erickson et al. [11]

By incorporating a model of the wavefront propagation, the REGROUPS method is able to "jump" across bad electrode sites, in order to prevent early or inappropriate termination of the algorithm. It is also capable of properly clustering points that represent a clashing slow wave pattern [11]. Recently O'Grady et al. have employed the algorithm to investigate circumferential slow wave conduction [37]; to compare slow wave initiation and conduction during normal and dysrhythmic behavior in a porcine model [38]; and to slow wave activity in human patients suffering from gastroparesis [33].

While REGROUPS has proven useful for studying (relatively) simple gastric slow wave activity patterns, it cannot properly group ATs when an electrical activity pattern is too chaotic, or when there is no sensible notion of coherent wavefront propagation of individual slow waves as has been occasionally observed in small intestine. In such instances, a second-order polynomial surface proves inadequate to describe the details of wave propagation, hence the predicted activation times are not accurate, and the points can not be clustered properly. Future research will investigate ways of extending the REGROUPS method or developing an alternate method for complex gastric or intestine slow wave patterns, where the spatiotemporal nature of the slow wave propagation is more variable from one wave to the next.

6 Velocity and Amplitude Estimation

6.1 Velocity

Once the slow waves events have been grouped into its respective propagating waves, an isochronal activation time map can be created (see Fig. 7a). This will show the general direction of slow waves propagation across the serosal surface of where the electrode array has been placed. From the activation time map, velocity vectors can be computed which will give a complimentary qualitative and quantitative view of slow wave propagation. A brief definition of velocity in GI slow wave mapping will be provided along with a discussion on methods to estimate velocity.

Velocity in simple terms is defined as the speed of an object in a specified direction. In GI slow wave mapping, it is the speed and direction of a propagating slow wave as mapped on the serosal surface on the stomach or other organs in the GI tract. In the cardiac field, velocities are defined with respect to fibre orientations [20]. In extracellular serosal mapping studies it is assumed the ICC layers are a 2D plane along the serosal surface of the stomach, and that there are no transmural components, although in reality, the ICC layers are a complex 3D structure [28]. When transmural mapping studies are done, and fibre orientations can be accurately identified in the GI tract, velocity estimates could be reported accordingly.

Velocity in two dimensions is defined as follows,

$$\begin{bmatrix} V_x \\ V_y \end{bmatrix} = \begin{bmatrix} \frac{T_x}{T_x^2+T_y^2} \\ \frac{T_y}{T_x^2+T_y^2} \end{bmatrix} \tag{4}$$

where $T_x = \partial T/\partial x$ and $T_y = \partial T/\partial y$ are the gradients of the isochronal time map with respect to the x and y directions of the recording array.

One approach to estimate velocities is to take a simple finite difference of the time array, and estimate the velocities. This method has been used in clinical mapping studies [22, 23, 34] in both stomach and small intestine. However this method has two disadvantages which has been observed in practice. One is that any noise in the activation time map would be amplified by taking a difference in time values. Secondly as mentioned by Bayly et al. [3], any missing activation time value in the map would lead to missing velocity estimates around that electrode. To eliminate this problem, the activation time map or the difference in time values can be interpolated based on the values around it.

The latter technique was used with smoothing applied to it in a method called the "smoothed finite difference" [41]. In this method, once $\partial T/\partial x$ and $\partial T/\partial y$ were found, an inverse distance weighting scheme was used to interpolate missing data points. V_x and V_y were then smoothed using a Gaussian filter to reduce any noise due to noise amplification. In Fig. 7, the velocity of a porcine gastric propagating wavefront is estimated using the method.

Another approach to estimating velocities is via the use of polynomial fitting as introduced by Bayly et al. [3]. In this method, a second order polynomial of the form Eq. (2) was fitted to the 2D activation time map. The same polynomial model described in Sect. 5 was applied, with a different application. The polynomial fit acts as an interpolant and smoothing function while estimating velocities. Ideally a window size of four or five times the sampling interval is chosen to estimate velocities in an overlapping manner. One disadvantage with this method is that there can be overshoots at the edges of the electrode array, leading to misleading velocity estimates. In some GI mapping studies for normal slow wave propagation

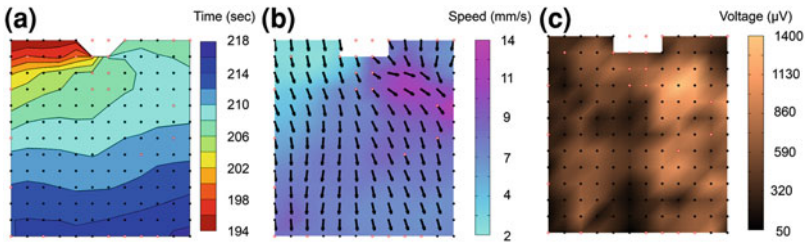

Fig. 7 Porcine gastric slow wave propagation. **a** Activation time map with isochrones at two second intervals. **b** Velocity field estimated using smoothed finite difference and plotted as a magnitude colormap with velocity directions overlaid. **c** Amplitude estimates of slow waves during the slow wave propagation

this method of velocity estimation has been used to estimate velocity vector directions with the polynomial fit applied to the whole array [10, 34].

There are other approaches to velocity estimation as seen in HR cardiac electrical mapping. Some of the methods include the use of wavelets [15] and the use of radial basis functions to estimate velocity [30], but have not been validated for use in gastric HR mapping. With velocity vectors, further analysis can be performed which may be able to provide vital information about slow wave propagation patterns. Recently a method utilising the change in direction of the velocity vectors was used to differentiate between normal and abnormal slow wave propagation patterns [9].

6.2 Amplitude

Signal amplitude can reveal information about the strength of the underlying activity. With sparse gastric electrical recordings, signal amplitude would reveal the strength of slow waves at a particular site, and most often an average value is quoted. This is also possible with high resolution mapping, but it also offers information in the spatial domain allowing signal amplitude of the slow wave propagation to be estimated and viewed as a map. Two approaches of amplitude estimation are discussed.

The first approach works by placing a window of specified width around detected slow wave, and taking the difference between the maximum and minimum values. This approach works extremely well when the morphology of the slow wave is static and well defined, and the window size can be specified as 1 s. The downside with this method is that slow wave morphologies can be varied and dynamic.

Another approach is to identify the peak and troughs of the slow wave event and then take the difference between the peak signal value and the trough signal value. The roots of the derivatives of a function provide its maxima, minima and inflection points, and this can assist in finding the peak and trough of the slow wave. In signal processing terms, it translates as the zero crossings of the derivatives of the slow waves signal provides us with its peak, trough and point of inflections on the slow wave (Fig. 8). The points of inflection can be found via the use of second derivatives as in some slow wave signals there are double potentials, where the peak or trough positions could be misleading. The main reason for adopting this approach is because there is a recovery component in the gastric slow wave morphology which falls below the trough of the slow waves, leading to misleading estimates of the amplitude of the slow wave. One of the limiting factors of this method is that it can be sensitive to noise, and thus a smoothing function needs to be applied on the derivative signals. A Savitzky Golay derivative filter can used to obtain a smooth derivative signal if the signal is noisy [40]. One of the downside with this implementation is that a prescribed set of parameters for different set of noise levels are required. However, in practice only one set of parameters are used.

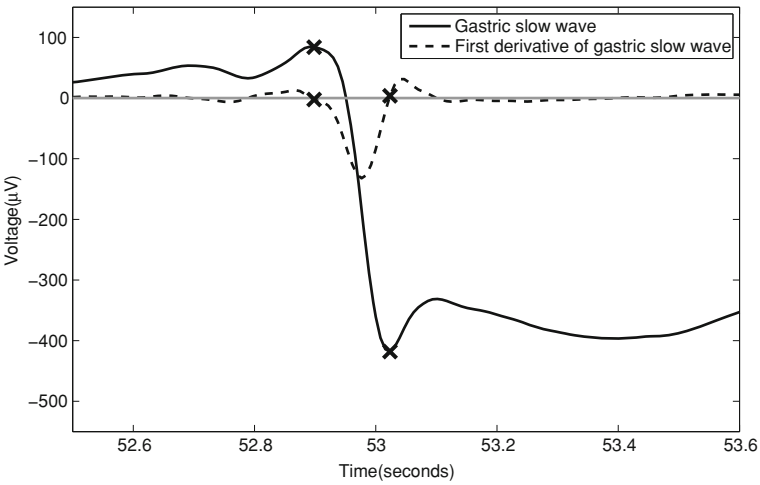

Fig. 8 Estimation of slow wave amplitude via detection of the peak and trough of the slow wave. The zero crossing positions (marked as *cross*) on the first derivative of the slow wave gives the location of the peak and trough of the signal. The zero crossing position closest to the fiducial marked slow waves are chosen as the time positions for the peak and trough of the slow wave

When comparing amplitude across experimental studies, certain aspects should be taken into account such as type of hardware used for bio-electrical recordings, software processing techniques, and experimental set-up. Based on the recording hardware used, and weather the electrodes are passive or active, the recorded amplitude could have different signal values and morphology. Also the use of digital or analog filters to eliminate noise, may dampen the amplitude of the slow wave.

7 Software Packages

The previously described methods and techniques have been incorporated into two software packages.

The Gastrointestinal Electrical Mapping Suite (GEMS) provides a user interface supported by implementations of the FEVT and REGROUPS algorithms as well as filtering procedures and algorithms for calculating amplitudes and velocities [47]. GEMS allows users to analyse high resolution serosal recordings in a mostly automated way while still giving users the opportunity to manually intervene by changing parameters or manually marking and grouping slow waves.

An online package analyses data recorded by from the Biosemi system during recordings, displaying wave propagation as the signals are being recorded, facilitating the checking of electrode placement and the monitoring of experimental effects.

7.1 GEMS

The Gastrointestinal Electrical Mapping Suite is a software package developed for analysing gastrointestinal signals primarily from the stomach and small intestine [47]. GEMS gives users the ability to analyse the large quantities of data recorded from HR recording arrays in an efficient manner, with as little manual intervention as possible.

GEMS is designed to be used by operators who may not be completely familiar with signal processing concepts. It leads users through a fixed set of steps to load data, orient the electrodes, filter the data and create output images and animations. The key features of GEMS are:

1. The ability to load data and rotate it to match the orientation of electrodes on the stomach.
2. The ability to filter data using the predetermined "best" parameters, select from one of several good set of options, or define a completely custom filtering configuration.
3. The ability to automatically mark large quantities of data using FEVT (Sect. 4) and REGROUPS (Sect. 5).
4. The ability to produce publication-ready map images, such as Fig. 7.

As the rectangular electrode patch can be placed in different orientations it is sometimes necessary to rotate it to understand the direction of propagation. GEMS presents users with various predefined filtering options which have been tuned for slow wave detection, but users are given more control over the filtering settings if they want it. Users may use the FEVT and REGROUPS algorithm to automatically mark slow wave activation times and group these into waves, though these marks and groups may be manually screened and grouped.

Figure 9 shows a row of electrodes from the electrode array after having been automatically marked with the FEVT algorithm. The user may remove those that they believe to be incorrect or manually add any slow wave activations that may have been missed, before using REGROUPS to partition the marks into individual slow wave events.

GEMS is able to produce publication-ready maps of slow wave activation time, amplitude, velocity (Fig. 7), or activation animations that can in some cases give a clearer view of the activity than subsequent isochronal maps can.

GEMS has been used for a number of different studies, and is used for analysing all high-resolution data recorded in our lab. Du et al. [9] and O'Grady et al. [38] have both used GEMS extensively in studies of dysrhythmic gastric electrical activity in porcine studies. Angeli et al. [2] found appropriate FEVT and REGROUPS parameters for detecting small intestine slow waves and used GEMS for the analysis of high-resolution recordings from porcine intestinal studies.

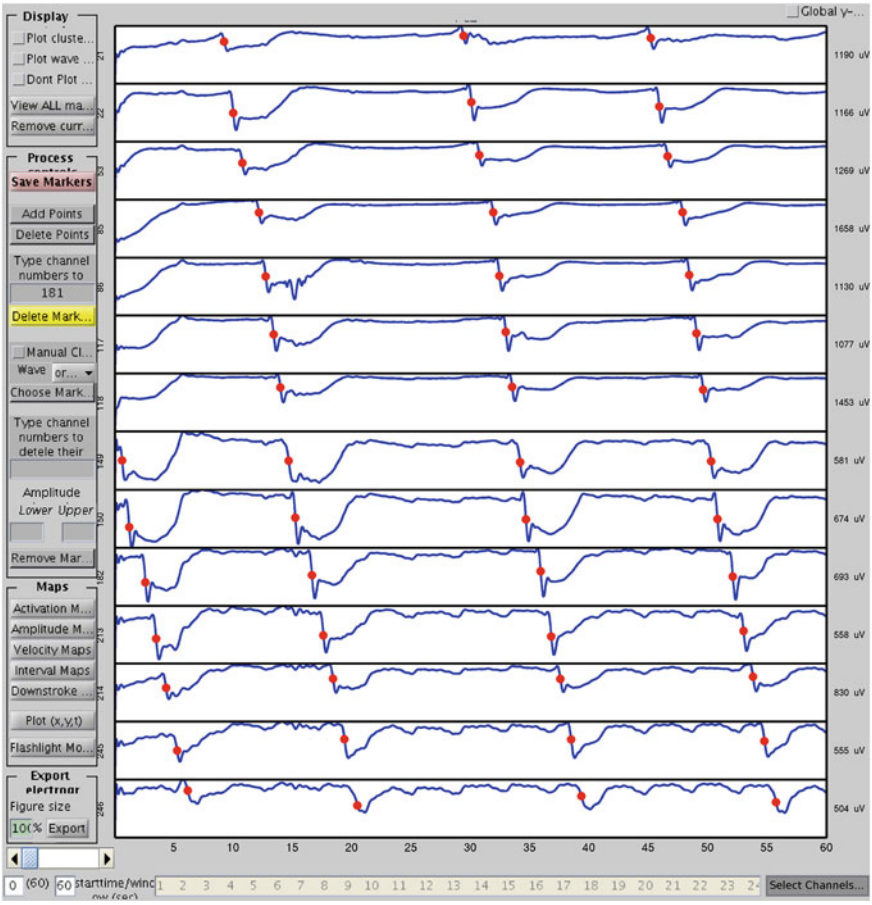

Fig. 9 A row of electrode traces from a pig stomach recording after being downsampled, filtered and having the FEVT algorithm applied. The *red dots* indicate the times identified as slow wave events by FEVT. This interface facilitates adding and removing activation time markings manually, or the removal of entire channels

7.2 Online Software Package

Some aspects of the analysis of slow wave activity have been incorporated into and online system running during experiments are performed [5]. This system filters the incoming data and processes it with the FEVT algorithm and is able to show show activation animation and isochronal maps as they are detection during recording. The isochronal maps are grouped with a simpler method than REGROUPS and is close to the wave mapping method [21]. Using the same methods as are used in offline analysis gives operators familiar with slow wave analysis the same parameters to alter for the best performance in different situations. In addition to FEVT, channels are classified as either being ‘good’ or ‘bad’

using a moving Kurtosis classifier. This helps in the interpretation of the activity by removing distracting false marks and also draws attention to recording problems such as poor electrode contact or placement by showing a majority of channels recording 'bad' signals. A screen capture showing the system being used is shown in Fig. 10, which shows it in a configuration that displays animations and isochronal maps similar to those used for offline analysis.

The online analysis does not replace offline analysis but rather gives operators better information about the information being recorded which can in many cases reduce time spent in the operating room. For example it is possible to move the electrode array to best cover objects of interest such as pacemakers or conduction blocks immediately where without any information it is possible that such features of the electrical will be missed or only partially recorded. It also allows allows new types of dynamic experiments where the effect of drugs, stimulation or other controlled influences on the propagation of slow waves can be monitored and responded to.

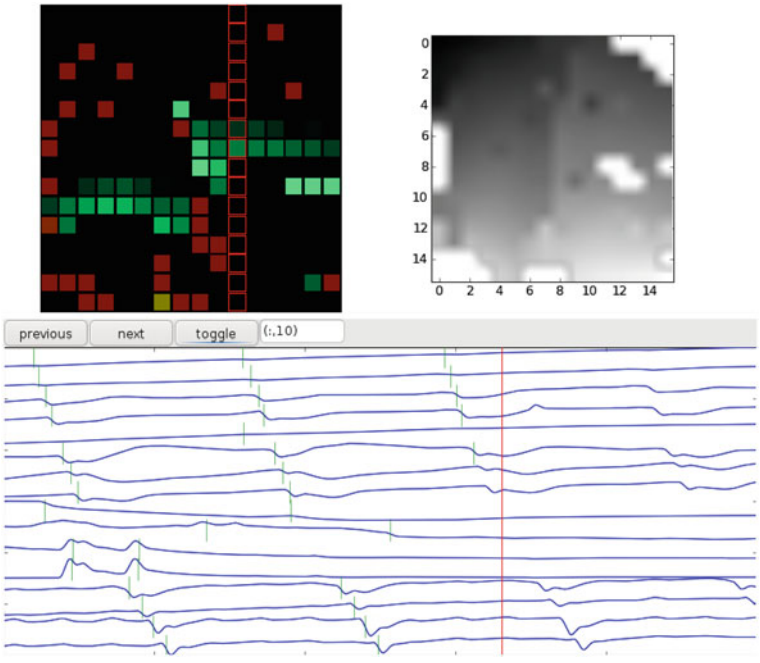

Fig. 10 A screen capture of the online software detector being used in a gastric mapping study with the slow wave activity propagating from the *top left* to *bottom right* of the array. The *top left* panel shows the detection of a slow wave event in the electrode array. The green squares indicate electrodes where slow wave events have been detected and red square indicate where events have been detected but determined to artifacts. The *bottom* panel displays a column of electrode traces that continuously updates. The vertical green line on the signal shows the detection of the activation time for a slow wave event. The *top right* panel shows the most recently captured propagating slow-wave wavefront using an automated online method. The unshaded area of this map indicates the region where no slow-wave activity was captured

8 Future Work and Conclusions

This chapter presents a summary of the recent advances in the analysis of gastrointestinal electrical activity, with a focus on gastric serosal activity. Future approaches are discussed, along with its potential clinical application.

The techniques described in this chapter have aided in reducing the time spent on laborious tasks (e.g., slow wave marking), and has focused the analysis on the clinical implications of the recorded data. It has also served to provide a standardized framework for GI HR electrical mapping, so that comparison can be made across studies [40]. This framework can be applied to the study of other gastrointestinal organs such as the small and large intestines. Although the same methodologies can be applied, the algorithms may need to be optimized for proper use [2].

One other important aspect of the GI electrical activity are the spikes. They are known to propagate and its identification be can be time consuming and tedious. Methods to automate and track spike activity along with slow waves is an area currently under development.

Further, there are opportunities to quantitatively and qualitatively asses normal and abnormal GI activity. One potential area of development is the use of velocity vectors. Du et al. has recently developed a method of identifying regions of interest using a change in direction from normal activity [9]. Further, use of mathematical operators such as the curl and divergence may provide useful information about the characteristics of the underlying electrical activity [14].

These methods of analysis could potentially be used for diagnostic purposes and could one day could be useful in strategizing treatment plans.

Acknowledgments This work was funded in part by research grants from the Health Research Council of New Zealand and the NIH (R01 DK64775).

References

1. Alvarez WC, Mahoney LJ (1922) Action currents in stomach and intestine. Am J Physiol 58(3):476–493
2. Angeli TR, O'Grady G, Erickson JC, Du P, Paskaranandavadivel N, Bissett I, Cheng LK, Pullan AJ (2011) Methods and validation of mapping small intestine bioelectrical activity using high-resolution printed-circuit board electrodes. In: Conference proceedings—IEEE engineering in medicine and biology society, IEEE, pp 4951–4954
3. Bayly PV, KenKnight BH, Rogers JM, Hillsley RE, Ideker RE, Smith WM (1998) Estimation of conduction velocity vector fields from epicardial mapping data. IEEE Trans Biomed Eng 45(5):563–571
4. Bortoff A (1967) Configuration of intestinal slow waves obtained by monopolar recording techniques. Am J Physiol 213(1):157–162
5. Bull SH, O'Grady G, Cheng LK, Pullan AJ (2011) A framework for the online analysis of multi-electrode gastric slow wave recordings. In: Conference proceedings—IEEE engineering in medicine and biology society, 2011, pp 41–1744

6. Chen JDZ, Qian L, Ouyang H, Yin J et al (2003) Gastric electrical stimulation with short pulses reduces vomiting but not dysrhythmias in dogs. Gastroenterology 124(2):401–409
7. Cheng Leo K, O'Grady Gregory, Egbuji John U, Windsor John A, Pullan Andrew J (2010) Gastrointestinal system. Wiley Interdiscip Rev Syst Biol Med 2(1):65–79
8. Du P, O'Grady G, Egbuji JU, Lammers WJ, Budgett D, Nielsen P, Windsor JA, Pullan AJ, Cheng LK (2009) High-resolution mapping of in vivo gastrointestinal slow wave activity using flexible printed circuit board electrodes: methodology and validation. Ann Biomed Eng 37(4):839–846
9. Du P, O'Grady G, Paskaranandavadivel N, Angeli TR, Lahr C, Abell TL, Cheng LK, Pullan AJ (2011) Quantification of velocity anisotropy during gastric electrical arrhythmia. In: Conference proceedings—IEEE engineering in medicine and biology society, pp 4402–4405
10. Egbuji JU, Ogrady G, Du P, Cheng LK, Lammers WJEP, Windsor JA, Pullan AJ (2010) Origin, propagation and regional characteristics of porcine gastric slow wave activity determined by high-resolution mapping. Neurogastroenterol Motil 22(10):e292–e300
11. Erickson JC, O'Grady G, Du P, Egbuji JU, Pullan AJ, Cheng LK (2011) Automated gastric slow wave cycle partitioning and visualization for high-resolution activation time maps. Ann Biomed Eng 39:1–15
12. Erickson JC, O'Grady G, Du P, Obioha C, Qiao W, Richards WO, Bradshaw LA, Pullan AJ, Cheng LK (2010) Falling-edge, variable threshold (FEVT) method for the automated detection of gastric slow wave events in high-resolution serosal electrode recordings. Ann Biomed Eng 38(4):1511–1529
13. Farrugia G (2008) Interstitial cells of Cajal in health and disease. Neurogastroenterol Motil 20:54–63
14. Fitzgerald TN, Brooks DH, Triedman JK (2005) Identification of cardiac rhythm features by mathematical analysis of vector fields. IEEE Trans Biomed Eng 52(1):19–29
15. Gaudette RJ, Brooks DH, MacLeod RS (1997) Epicardial velocity estimation using wavelets. In: Computers in cardiology, IEEE, pp 339–342
16. Hammad FT, Lammers WJ, Stephen B, Lubbad L (2011) Propagation of the electrical impulse in reversible unilateral ureteral obstruction as determined at high electrophysiological resolution. J Urol 185(2):744–750
17. Huizinga JD, Lammers WJEP (2009) Gut peristalsis is governed by a multitude of cooperating mechanisms. Am J Physiol Gastrointest Liver Physiol 296(1):G1–G8
18. Kaiser JF (1993) Some useful properties of teager's energy operators. In: IEEE transactions on acoustics, speech, and signal processing, vol 3, IEEE, pp 149–152
19. Kelly KA, Elveback LR (1969) Patterns of canine gastric electrical activity. Am J Physiol 217(2):461–470
20. Kleber AG, Janse MJ, Wilms-Schopmann FJ, Wilde AA, Coronel R (1986) Changes in conduction velocity during acute ischemia in ventricular myocardium of the isolated porcine heart. Circulation 73(1):189–198
21. Lammers WJ, el Kays A, Arafat K, el Sharkawy TY (1995) Wave mapping: detection of co-existing multiple wavefronts in high-resolution electrical mapping. Med Biol Eng Comput 33:476–481
22. Lammers WJEP (2009) Smoothmap v3.05. Al Ain, United Arab Emirates (Online)
23. Lammers WJEP, Donck LV, Schuurkes JAJ, Stephen B (2005) Peripheral pacemakers and patterns of slow wave propagation in the canine small intestine in vivo. Can J Physiol Pharmacol 83(11):1031–1043
24. Lammers WJEP, Michiels B, Voeten J, Donck LV, Schuurkes JAJ (2008) Mapping slow waves and spikes in chronically instrumented dogs: automated on-line electrogram analysis. Med Biol Eng Comput 46:121–129
25. Lammers WJEP, Stephen B, Arafat K, Manefield GW (1996) High resolution electrical mapping in the gastrointestinal system: initial results. Neurogastroenterol Motil 8(3):207–216
26. Lammers WJEP, Ver Donck L, Stephen B, Smets D, Schuurkes JAJ (2008) Focal activities and re-entrant propagations as mechanisms of gastric tachyarrhythmias. Gastroenterolerology 135(5):1601–1611

27. Lammers WJEP, Ver Donck L, Stephen B, Smets D, Schuurkes JAJ (2009) Origin and propagation of the slow wave in the canine stomach: the outlines of a gastric conduction system. Am J Physiol Gastrointest Liver Physiol 296(6):G1200–G1210
28. Lee HT, Hennig GW, Fleming NW, Keef KD, Spencer NJ, Ward SM, Sanders KM, Smith TK (2007) The mechanism and spread of pacemaker activity through myenteric interstitial cells of Cajal in human small intestine. Gastroenterology 132(5):1852–1865
29. Maragos P, Potamianos A (1995) Higher order differential energy operators. IEEE Signal Process Lett 2(8):152–154
30. Mase M, Ravelli F (2010) Automatic reconstruction of activation and velocity maps from electro-anatomic data by radial basis functions. In: Conference proceeding—IEEE engineering in medicine and biology society, IEEE, pp 2608–2611
31. Mukhopadhyay S, Ray GC (1998) A new interpretation of nonlinear energy operator and its efficacy in spike detection. IEEE Trans Biomed Eng 45(2):180–187
32. Nenadic Z, Burdick JW (2005) Spike detection using the continuous wavelet transform. IEEE Trans Biomed Eng 52(1):74–87
33. O'Grady G, Angeli TR, Du P, Lahr C, Lammers WJ, Windsor JA, Abell TL, Farrugia G, Pullan AJ, Cheng LK (2012) Abnormal initiation and conduction of slow-wave activity in gastroparesis, defined by high-resolution electrical mapping. Gastroenterology 143(3):589–98
34. O'Grady G, Du P, Cheng LK, Egbuji JU, Lammers WJEP, Windsor JA, Pullan AJ (2010) Origin and propagation of human gastric slow-wave activity defined by high-resolution mapping. Am J Physiol Gastrointest Liver Physiol 299(3):G585–G592
35. O'Grady G, Du P, Lammers WJEP, Egbuji JU, Mithraratne P, Chen JDZ, Cheng LK, Windsor JA, Pullan AJ (2010) High-resolution entrainment mapping of gastric pacing: a new analytical tool. Am J Physiol Gastrointest Liver Physiol 298(2):G314–G321
36. O'Grady G, Du P, Paskaranandavadivel N, Angeli TR, Lammers WJ, Farrugia G, Asirvatham S, Windsor JA, Pullan AJ, Cheng LK (2011) High-resolution spatial analysis of slow wave initiation and conduction in porcine gastric dysrhythmia. Neurogastroenterol Motil 23(9):e345–e355
37. O'Grady G, Du P, Paskaranandavadivel N, Angeli TR, Lammers WJEP, Farrugia G, Asirvatham S, Windsor JA, Pullan AJ, Cheng LK (2012) Rapid high-amplitude circumferential slow wave propagation during normal gastric pacemaking and dysrhythmias. Neurogastroenterol Motil 24(7):e299–e312
38. O'Grady G, Egbuji JU, Du P, Lammers W, Cheng LK, Windsor JA, Pullan AJ (2011) igh-resolution spatial analysis of slow wave initiation and conduction in porcine gastric dysrhythmia. Neurogastroent Motil 23(9):e345–e355
39. O'Grady G, Paskaranandavadivel N, Angeli TR, Du P, Windsor JA, Cheng LK, Pullan AJ (2011) A comparison of gold versus silver electrode contacts for high-resolution gastric electrical mapping using flexible printed circuit board arrays. Physiol Meas 32(3):N13–N22
40. Paskaranandavadivel N, Cheng LK, Du P, O'Grady G, Pullan AJ (2011) Improved signal processing techniques for the analysis of high resolution serosal slow wave activity in the stomach. In: Conference proceeding—IEEE engineering in medicine and biology society, pp 1737–1740
41. Paskaranandavadivel N, O'Grady G, Du P, Pullan AJ, Cheng LK (2012) An improved method for the estimation and visualization of velocity fields from gastric high-resolution electrical mapping. IEEE Trans Biomed Eng 59(3):882–889
42. Rogers JM, Bayly PV, Ideker RE, Smith WM (1998) Quantitative techniques for analyzing high-resolution cardiac-mapping data. IEEE Eng Med Biol Mag 17:62–72
43. Rogers JM, Usui M, KenKnight BH, Ideker RE, Smith WM (1997) A quantitative framework for analyzing epicardial activation patterns during ventricular fibrillation. Ann Biomed Eng 25:749–760
44. Sarna SK, Daniel EE, Kingma YJ (1972) Effects of partial cuts on gastric electrical control activity and its computer model. Am J Physiol 223(2):332–340

45. Sezan MI (1990) A peak detection algorithm and its application to histogram-based image data reduction. Comput Vis Graph Image process 49(1):36–51
46. Spach MS, Barr RC, Serwer GA, Kootsey JM, Johnson EA (1972) Extracellular potentials related to intracellular action potentials in the dog purkinje system. Circ Res 30(5):505–519
47. Yassi R, O'Grady G, Paskaranandavadivel N, Du P, Angeli TR, Pullan AJ, Cheng LK, Erickson JC (2012) The gastrointestinal electrical mapping suite (GEMS): software for analyzing and visualizing high-resolution (multi-electrode) recordings in spatiotemporal detail. BMC Gastroenterol 12(60):1–14

The Electrical Regulation of GI Motility at the Whole-Organ Level

Timothy R. Angeli, Gregory O'Grady and Wim J. E. P. Lammers

Abstract A rhythmic bioelectrical activity, composed of slow waves and spikes, plays a central role in coordinating contractions in much of the gastrointestinal tract. This chapter addresses the current state of knowledge of the electrical activity contributing to the regulation of GI contractions, with a specific focus on organ-level excitation in the stomach and small intestine. Emphasis is placed on data obtained from extracellular recordings, which effectively profile patterns of bioelectrical propagation over large tissue scales. Recent advances in understanding whole-organ excitation from high-resolution (HR) electrical mapping studies are discussed in particular detail. Lastly, clinical and research questions of current interest are identified.

1 Introduction

The motility of the GI tract is governed by several integrated mechanisms, encompassing neural, hormonal, myenteric and bioelectrical systems. Among these mechanisms, a rhythmic electrical 'slow wave' activity, generated and propagated by the interstitial cells of Cajal (ICC), imparts a controlling pattern of

T. R. Angeli (✉) · G. O'Grady · W. J. E. P. Lammers
Auckland Bioengineering Institute, University of Auckland, Private Bag 92019Auckland 1142, New Zealand
e-mail: tang010@aucklanduni.ac.nz

T. R. Angeli
Riddet Institute, Palmerston North, New Zealand

G. O'Grady
Department of Surgery, University of Auckland, Auckland, New Zealand

W. J. E. P. Lammers
Department of Physiology, UAE University, Al Ain, United Arab Emirates

L. K. Cheng et al. (eds.), *New Advances in Gastrointestinal Motility Research*,
Lecture Notes in Computational Vision and Biomechanics 10,
DOI: 10.1007/978-94-007-6561-0_6, © Springer Science+Business Media Dordrecht 2013

excitability that influences the timing, frequency, direction and organization of contractions [24]. Further bioelectrical events, termed 'spikes', are superimposed on slow waves in some parts of the GI tract, influencing the degree of excitation and contraction that is ultimately achieved in gut smooth muscles.

The biological behavior of slow waves and spikes, and their precise role in regulating GI motility, has been the subject of sustained investigation for almost a century [1], and these subjects remain a focus of vigorous enquiry. This chapter addresses the current state of knowledge in the electrical regulation in GI organs, identifies several research questions of current interest, and offers clinical and future perspectives.

The scope of the chapter is restricted to electrical activity, with particular emphasis on the large-scale organization of slow waves and spikes at the whole-organ level. Although brief consideration is given to slow wave conduction through ICC networks, readers are referred to the more in-depth discussions by Beyder et al. in "Role of Ion Channel Mechanosensitivity in the Gut: Mechano-Electrical Feedback Exemplified by Stretch-Dependence of $Na_V1.5$", and Gibbons et al. in "ICC Network Density: Regulation and Consequences" regarding the cellular mechanisms and cell-network structures that underpin these organ-level events.

Whereas intracellular measurements are important for investigating cell-level physiology, extracellular measurements are the predominant technique for evaluating whole-organ electrical activity because this method enables the summative investigation and reconstruction of the profile and patterns of slow wave propagation over large tissue scales, as discussed by O'Grady et al. in "The Principles and Practice of Gastrointestinal High-Resolution Electrical Mapping". The major focus of this chapter is, therefore, on reviewing extracellular recording studies, with particular regard to the stomach and small intestine. Extracellular recordings have played a much smaller role in understanding colonic electrical excitation to date, and for a more comprehensive review of current theories of the electrical control of colonic motility, readers are referred to a recent discussion by Huizinga et al. [25]. The colon and esophagus are not discussed in detail in this chapter.

As reviewed by O'Grady et al. in "The Principles and Practice of Gastrointestinal High-Resolution Electrical Mapping", until recently, much of the data describing whole-organ GI slow wave and spike patterns was achieved using linear configurations of few electrodes (e.g., [27, 57]). Such studies enabled a general understanding of slow wave frequencies, and velocities could be estimated by tracking sequential cycles in adjacent electrograms based on slight variations in cycle length. However, the lack of spatial resolution inherent in sparse recordings meant that spatial propagation dynamics, pacemaker locations and behaviors, and wavefront interactions could not be reliably described. More recently, high-resolution (HR), multi-electrode platforms have been developed for mapping GI electrical events in fine spatiotemporal detail, allowing deeper insights into whole-organ patterns of electrical regulation [12, 31]. This chapter emphasizes experimental results from GI HR techniques.

The organ-level electrical activity of the GI tract has been studied in a wide range of small and large animal models. The purpose of this chapter is to present a current, integrated and coherent perspective on whole-organ stomach and small intestine electrophysiology, and its control on motility, in order to help inform and guide clinical motility studies and research. Therefore, the focus of the chapter is primarily on large animal studies, and, where possible, the human studies that have been performed with extracellular techniques.

2 Fundamentals of Electrical Regulation

2.1 Slow Waves and Spikes

Slow waves are a continuous, cyclical change in membrane potential that propagates through the GI wall in a coordinated fashion. Slow waves serve to move the resting membrane potential of smooth muscle cell (SMC) from a typical range of −75 to –55 mV to a peak potential of around –40 to –25 mV, thereby modulating their propensity for contraction. Although each slow wave is associated with SMC calcium influx, and at least small contractility can be registered by sensitive transducers for every slow wave [23], co-regulatory mechanisms, such as neuronal and stretch stimuli, are necessary to effect functionally-significant contractions [24].

In some SMC, such as in gastric antrum, small intestine, and to a lesser extent, gastric corpus, threshold depolarization may elicit regenerative action potentials (i.e., 'spikes'), involving brief intense bursts of Ca^{2+} entry [50]. These spikes generally lead to stronger contractile responses.

2.2 Slow Wave Entrainment

The pacemaker system of the GI tract does not have specific point sources or 'nodes', as in the heart, but rather consists of a continuous network of coupled ICC. In isolated cell cultures, ICC will generate slow waves at different intrinsic frequencies, but in an intact network, the frequencies of the ICC synchronize to the single fastest frequency in the syncytium, in a process known as entrainment. ICC are interconnected via intricate networks of gap junctions, and slow wave entrainment occurs through these networks in a regenerative manner, such that electrical events may continue to propagate for distances of up to many centimeters, or even meters in-vitro [39]. Entrainment is vital in achieving the organized slow wave propagation patterns that are associated with healthy motility patterns. The exact mechanisms of ICC entrainment are a focus of ongoing research, but may result from a voltage-dependent IP_3-mediated Ca^{2+} release from

intracellular stores [59]. Different hypotheses exist for the exact mechanism of Ca^{2+} release, including calcium-induced calcium release via IP_3 receptors and voltage-dependent IP_3 concentration modulation [30, 43].

2.3 Slow Wave Conduction through ICC Networks

Theories regarding how slow waves propagate through ICC networks are important for understanding whole-organ excitation patterns in normal and pathological states. As discussed by Gibbons et al. in "Role of Ion Channel Mechanosensitivity in the Gut: Mechano-Electrical Feedback Exemplified by Stretch-Dependence of $Na_V1.5$" of this volume, several types of ICC have been classified according to their location. Hirst et al. previously suggested that in guinea pig antrum, potentials primarily conduct slowly through ICC-MP (myenteric plexus ICC), which depolarize successive networks of ICC-IM (intramuscular ICC) along their course [22]. Once ICC-IM are activated, it was suggested that at each propagation step, conduction then rapidly spreads in the circumferential direction through ICC-IM, manifesting at the whole-organ level as a slowly descending ring of contraction.

However, recent evidence from HR mapping has now suggested that a refinement to this theory is necessary, because during normal longitudinal conduction, circumferential propagation is not actually observed [14, 41, 45]. Instead, circumferential propagation is only normally observed at pacemaker regions. Thereafter, ring wavefronts are quickly established, such that propagating wavefronts move as a 'sleeve' of excitation, and circumferential conduction ceases to exist [13]. Rapid circumferential conduction may reflect different conduction rates through ICC layers, or different gap junction distributions [48].

2.4 Slow Waves and SMC

Unlike ICC, SMC lack the conductance responsible for generating slow wave activity. However, SMC do maintain a 'latent' pacemaker activity, that allows them to regenerate slow waves on depolarization (reviewed in [24]), and thus, SMC support the active propagation of slow waves into muscle layers. It is generally considered that electrical coupling of ICC and SMC is achieved by small sparse gap junctions. Coupling has been evaluated by concurrent intracellular recordings of slow wave activity in SMC and ICC [9], confirming that slow waves originate in ICC, and conduct to SMC, with the two cell networks effectively acting as a common electrical syncytium. The coupling between ICC and SMC occurs without draining excessive current, such that ongoing ICC entrainment is not disrupted.

2.5 Electrical Activity in Context

Excitation–contraction coupling is highly regulated by neural, hormonal, paracrine and mechanosensitivity mechanisms, ensuring that the energy-consuming contractile machinery is only activated in the fed state [19]. The function and role of the co-regulatory systems is not a focus of this chapter, and readers are referred elsewhere for this detail (e.g., [24, 17]). However, these regulatory factors are assimilated by SMC in parallel (amplifying or inhibiting each other), with additional modulating influences from within SMC, to produce a highly regulated output suited to the functional context. The key direct influence on contraction is increased cytoplasmic Ca^{2+}, which affects actin-myosin attachment and cross-bridge cycling.

SMC resting membrane potentials (RMPs), spike thresholds, and external modulation responses vary throughout the gut, preconditioning SMC contractile behavior, and contributing to the differentiation of regional gut functions. Some regions (e.g., the gastric fundus) have a relatively depolarized RMP, lying in a range where sustained low level activation of voltage-dependent calcium channels (in combination with co-regulatory inputs) may lead to continuous influx of Ca^{2+} [50]. Other voltage-independent sources act to co-regulate RMP, such as the dependence of RMP on carbon monoxide, likely also playing a role in regional variations of RMP [53].

3 The Electrical Activity of the Stomach

3.1 Overview of Gastric Function

Physiologically, the stomach is often considered in two parts [29], as explained by Ferrua et al. in "Computational Modeling of Gastrointestinal Fluid Dynamics". The 'proximal unit' (primarily fundus and upper corpus) fulfills a tonic reservoir function, achieved by vagally-mediated 'receptive relaxation', whereby the stomach relaxes to accept the anticipated food bolus, and 'accommodation', whereby increasing food volumes are accepted without significant further increases in intragastric pressure. The distal 'gastric unit' (lower corpus and antrum) is a highly efficient homogenizer. This role encompasses continence to solid matter, and the coordinated trituration (mixing and grinding) of these solids via mechanical and chemical means, into a fine slurry (chyme), which empties with the liquid phase of the meal into the duodenum. Trituration is achieved by propulsive gastric contractions that are patterned by slow waves.

Normal gastric emptying is highly regulated, and is dependent on the coordinated functions of the proximal stomach, distal stomach, and the proximal small intestine. The primary driver of emptying is likely the pressure gradient that normally exists between the stomach and duodenum (the so-called 'pressure-pump') [26].

Following a meal, during emptying, this pressure gradient is maintained at a constant level by the continuous adaption of gastric tone and rapid clearance of contents from the duodenum. Antral contractions (the 'peristaltic pump') may play a lesser role in emptying.

There is a characteristic gradient of resting membrane potential along the stomach, from ~ -48 mV in the fundus to ~ -71 mV in the antrum, as well as a ~ 10 mV gradient through the gastric wall thickness. These gradients function as a 'biological rheostat', allowing circular smooth muscle to vary its recruitment, such that contraction strength may vary from weak to propulsive and occluding, depending on the stimulus [58]. It is partly due to this gradient that tonic contractions are the predominant fundal motor pattern.

During the fasted state, slow waves continue to propagate, while contractions are less intense in general, with the main exception being the migrating motor complex (MMC). In particular, phase III of the MMC is characterized by the appearance of a migratory band of prolonged bursts of spike activity superimposed on the slow wave activity, with the resultant contractions serving to force indigestible solids, shed epithelial cells and secretions through a relaxed pylorus [8]. Refer to Sect. 4.4 for a more thorough description of the phases of the MMC.

3.2 The Origin and Propagation of Gastric Slow Waves

Historically, sparse electrode recordings provided a useful general outline of gastric slow wave initiation and conduction. By arranging 4–8 electrodes in lines along the stomach, it was established, in dogs and humans, that the whole stomach normally has a single pacemaker system, all tissue being 'coupled' to a single point of slow wave origin [21, 28]. Hinder et al. localized this pacemaker region in humans to a region of the greater curvature, $\sim$5–7 cm aborad to the cardia, and showed that slow waves do not propagate proximally into the fundus [21].

Many studies have documented human gastric slow waves to occur at a frequency of around 3 cycles per minute (cpm). The normal range is often defined as around 2–4 cpm [50], but is not clearly established. After eating, this frequency reduces in a manner that is partly dependent on the temperature of the ingested meal [60]. An intrinsic ICC frequency gradient in the aboral direction has been shown in-vivo, which underpins slow wave entrainment. T across the fundus produced no change in slow wave rate or rhythm distally. However, a declining frequency gradient from $\sim$3.0 to 0.8–1.8 cpm was uncovered when transections were made progressively more distally through corpus and antrum, and gastric bisection (i.e., down the midline axis) also revealed a reduced frequency in the lesser curvature half [21, 28].

Recent HR mapping studies have added significant further detail to this general outline of the gastric conduction system [14, 41, 45]. It was traditionally assumed that only one gastric slow wave is typically propagating at a time and that there is a gradual increase in slow wave velocity and amplitude from corpus to antrum.

These assumptions have now been shown to be incorrect in HR mapping studies, but probably arose from a tendency to 'alias' the signals generated from sparse electrode recordings; i.e., events recorded in consecutive corpus electrodes can be assigned to the wrong cycle when the spatial sampling density is low [45].

HR studies in pigs, dogs and humans have all confirmed that the normal pacemaker region is located high on the greater curvature, and is associated with a high-amplitude and high-velocity activity [14, 41, 45]. It has recently been shown that this specific pacemaker profile is a consequence of the circumferential conduction that occurs at the pacemaker region, and the activity in this region returns to the normal corpus range when entrained by retrograde-travelling wavefronts from a paced distal source [48]. Rapid circumferential conduction is discussed above, while the high amplitude is likely a consequence of proportionality between the conduction velocity and the total transmembrane current entering the extracellular space [48].

After 2–3 s of propagation time, the amplitude and velocity fall by ~66 %, by which time wavefronts rapidly organize in circumferential bands traveling organoaxially, such that a circumferential conduction component is no longer observed [14, 41, 45]. Propagation over the anterior and posterior serosal surfaces has been shown to be largely symmetrical [14].

It was often previously considered that there was a gradual increase in amplitude and velocity during propagation from corpus to antrum during aborad propagation. However, HR mapping studies have more recently demonstrated a consistent velocity throughout the corpus (~3 mm/s in humans), with a relatively rapid transition in activity (>2 × increase in amplitude and velocity), at a point within the distal antrum [41, 45]. The slow corpus conductance leads to the accrual of several wavefronts (3–4 in humans, at a spacing of ~60 mm), which then spread out on entry into the distal rapid-conductance zone [13, 41, 45].

A quiescent area has been identified at the pylorus, where slow waves are blocked [41, 61]. Besides being a critical mechanical barrier, the pylorus also, therefore, serves an electrical barrier function, whereby gastric slow waves are decoupled from intestinal slow waves allowing differentiated patterns and functions.

Gastric contractions are initiated and coordinated by gastric slow waves, and recent HR mapping in humans closely matches the motility patterns revealed by MRI [45]. This pattern is summarized in Fig. 1, which shows a 20 s simulation based on HR mapping data and integrative modeling [13, 45]. One cycle occurs approximately each 20 s. Gastric slow waves originate near the greater curvature of the upper corpus and propagate radially for only a short distance toward the fundus and cardia. In the corpus, wavefronts organize into rings traveling organoaxially, with the slow corpus velocity (~3 mm/s) leading to the accrual of several wavefronts at spacing ~60 mm. Within the antrum, there is a rapid transition to a higher amplitude and faster velocity (~2 × corpus). Anterior and posterior activity is symmetrical, and gastric slow waves terminate at the pylorus [14].

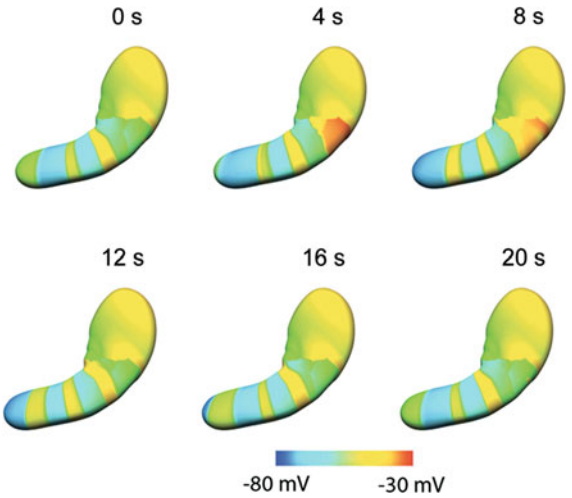

Fig. 1 The origin and propagation of gastric slow wave activity: A 20 s simulation based on HR mapping data and integrative modeling [45, 46], showing approximately one complete cycle. Gastric slow waves originate near the greater curvature of the upper corpus, propagate radially for a short distance, then organize into rings traveling organoaxially down the corpus. Several wavefronts are present at one time, at spacing ~60 mm. Within the antrum, amplitude and velocity increase to approximately twice that of the corpus before terminating at the pylorus. An animation of this figure is available at: http://www.youtube.com/v/ROeH9LGeD54. [With thanks to Dr. Peng Du, Auckland Bioengineering Institute]

3.3 Gastric Spike Activity

Spike potentials are readily seen in extracellular recordings, and their propagation may be tracked over several millimeters, independent of slow waves [33, 41]. Gastric spike activity has been described in several studies, always being superimposed on the slow wave plateau period, and being more clearly and commonly documented in the antrum than corpus [5, 27 41]. Excitatory neural input increases the probability of spike generation, such that they are not commonly observed during HR mapping studies, which have been conducted under anesthesia and fasting conditions [45]. Patches of spike activity may traverse the pylorus, but the functional significance of this finding is currently unclear [33].

4 Electrical Activity of the Small Intestine

4.1 Overview of Small Intestine Function

In humans, the small intestine (SI) averages ~4–6 m in length, comprising three physiologically-distinct but anatomically-continuous divisions: duodenum (proximal ~30 cm), jejunum (mid ~2.5 m), and ileum (distal ~2.5 m). Chyme enters the SI at a controlled rate, and is continuously mixed and transported along the tract. After ~3–5 h of transport, undigested material is delivered to the colon via the ileocaecal valve for fermentation, final absorption, desiccation, and ultimately, expulsion of waste.

In the duodenum, acidic chyme is neutralized with alkaline secretions and mixed with digestive enzymes and bile, initiating the intestinal breakdown of solids. Gastric, biliary and pancreatic functions are highly regulated by duodenal neurohormonal feedback loops, which are responsive to chyme volume, nutrient content (calories, fat and protein content), and acidity. The jejunum and ileum are primarily responsible for the absorption of nutrients and water, aided by the densely-folded mucosal surface and microvilli, with certain functions being specific to ileum, such as vitamin B12 absorption and bile salt cycling.

In the fed state, the small intestine exhibits two main contractile patterns: mixing and propulsion. During mixing, serial 'segmenting' contractions repeatedly divide intestinal loops into uniform divisions, moving intestinal contents in both directions [3]. In the fasted state, as in the stomach, organized, phasic motor patterns periodically occur as part of the MMC, including large-scale contractions that traverse the length of the small intestine, again serving a 'housekeeper' debris-clearance role, further discussed in Sect. 4.4, The Migrating Motor Complex [56].

Slow waves and spikes, in conjunction with co-regulatory stimuli including neural, hormonal, and mechanosensitive mechanisms, play central roles in both fasted and fed motility, by 'patterning' excitation. For example, as originally demonstrated by Alvarez and Mahoney, the maximal frequencies of slow waves and rhythmic segmenting contractions are identical along the SI [1]. However, the nature of the motor pattern superimposed on the slow wave also depends in large part on the controlling influence of the enteric nervous system (ENS) plexuses. The ENS supplies the intrinsic innervation of the GI tract, exerting local neural control over small intestine motility and serving as a coordinating mechanism of mixing and propulsive movements in the small intestine [17].

4.2 The Origin and Propagation of Small Intestine Slow Waves

As in the stomach, historical sparse electrode recordings formed the foundation of our knowledge of SI slow waves (e.g., [1, 7, 57]), with more recent HR studies

adding a spatial understanding of slow wave pacemakers, wave interactions, and propagation dynamics (e.g., [37, 39]).

A declining slow wave frequency gradient has been defined to occur along the length of the small intestine in multiple species [10, 37, 57]. In humans, the frequency decreases from ~11–12 cpm in the duodenum, down to ~8–9 cpm in the ileum [6, 16]. The nature of SI pacesetting and the mechanisms of this frequency gradient have been the subject of extensive investigation, and are still debated.

Unlike the single-pacesetter system of the stomach, in-vivo SI slow wave activity has been shown to be governed by a series of pacemakers, with an initial pacemaker located in the proximal duodenum, and a series of transient peripheral pacemakers located along the length of the tract [10, 37, 55]. From sparse electrode studies, it was suggested that these pacemakers compete to determine slow wave frequency and propagation patterns across segmental regions of the SI [10, 57]. Specifically, the standard model suggests that proximal regions, where the intrinsic ICC frequency is higher, entrain distal tissue until the disparity in driving frequency and intrinsic frequency is too great for the distal region to follow (reviewed in [17]). A short section of irregular activity is suggested to then occur, distal to which, a new plateau of lower frequency activity is established. The interaction between peripheral pacemakers at these sites of frequency transition were proposed as the cause of the 'waxing and waning' (or 'spindling') phenomenon, whereby the amplitude of slow waves cyclically increases and decreases over time, as a consequence of the frequencies in these segments operating slightly out of phase [55].

Within these 'frequency plateaus', the overall conductance of slow waves still progresses from oral to anal. However, variability in propagation direction is known to occur. In anesthetized canines, for example, HR mapping has shown that slow wave propagation is mainly aboral (84 % of recordings), but also exhibits oral propagation (11 %), propagation blocks (2 %), and circumferential propagation at peripheral pacemakers (3 %) along the intestinal length [37].

The theory that there is proximal entrainment of distal SI segments of lower intrinsic frequency is supported by transection studies of the SI. These studies have shown that the slow wave frequency drops immediately distal to the site of a transection, and further declines if another transection is performed distal to the first, demonstrating a hierarchical entrainment of slow waves above the inherent frequency along the length of the intestine [7, 11].

Recently, the traditional model of competing SI pacemakers and slow wave frequency plateaus was challenged by a feline in-vitro study presented by Lammers et al. [39]. This study, employing a linear array of 240 electrodes at 4–8 mm inter-electrode spacing, showed that slow waves could propagate the full length of the feline SI in-vitro, and that the declining SI frequency gradient was caused by occasional conduction blocks of the anally-propagating wavefronts (i.e., with some waves 'dropping out' along the way) [39]. Furthermore, the occurrence and extent of 'frequency plateaus' was highly variable between individual animals, and no 'waxing and waning' was detected, potentially due to the different type and size of the recording electrodes compared to those used previously [10].

Reconciling the conflicting theories of the 'traditional model' of slow wave pacesetting and conduction, and the more recent findings by Lammers et al., is now an interesting research focus. It is likely that both mechanisms are operational to some extent in different contexts. For example, Suzuki et al. previously reported that slow wave activity in-vitro was highly regular, and that 'spindling' was rarely observed, suggesting that peripheral pacesetter interaction may mainly manifest in-vivo [55]. To add further complexity, Angeli et al. and Lammers et al. have separately reported the finding of slow-wave re-entrant circuits in healthy intestinal segments, in-vivo and in-vitro respectively, suggesting that tissue-level mechanisms may also dictate segmental SI frequencies, rather than just intrinsic frequencies alone [2, 42]. The significance of this work for normal intestinal function is currently unknown.

The velocity of small intestine slow waves varies between species and, like their frequencies, declines along the length of the intestine. The duodenum shows a particularly rapid velocity. For example, the slow wave velocity in the anesthetized dog decreases from an average of 105 mm/s in the duodenum to 8 mm/s in the terminal ileum [37]. Additionally, small intestine slow waves propagate in an anisotropic conduction pattern, being slightly faster circumferentially than longitudinally (ratio 1.3:1 in feline SI) [34]. As in the stomach, this anisotropy is likely to be of significance in causing wavefronts to rapidly orient transversely (and, thereafter, to propagate longitudinally as a 'sleeve' of excitation), in order to promote SI content transit.

Extracellular slow wave amplitudes also decrease along the length of the intestine, from duodenum to terminal ileum (possibly being caused by the decline in velocity, because extracellular amplitudes and velocities are biophysically correlated [48]). For example, extracellular slow wave amplitudes decrease by approximately 75 % (1.20 to 0.31 mV average) from proximal duodenum to terminal ileum in the anesthetized canine [37].

The origin and propagation of small intestine slow waves are summarized in Fig. 2a, where an isochronal map and accompanying electrograms illustrate the pattern of slow wave propagation at a pacemaker site recorded from the serosa of an isolated segment of feline small intestine in-vitro. The slow wave initially travels in all directions from the site of pacemaking, with slightly faster propagation in the circumferential than in the longitudinal direction, serving to orient the slow wave into a wavefront that propagates in the organoaxial direction away from the site of pacemaking.

4.3 Small Intestine Spike Activity

Spike potentials in the small intestine have been observed across a wide range of extracellular studies and vary in quantity and intensity, correlated to the magnitude of the contractile force.

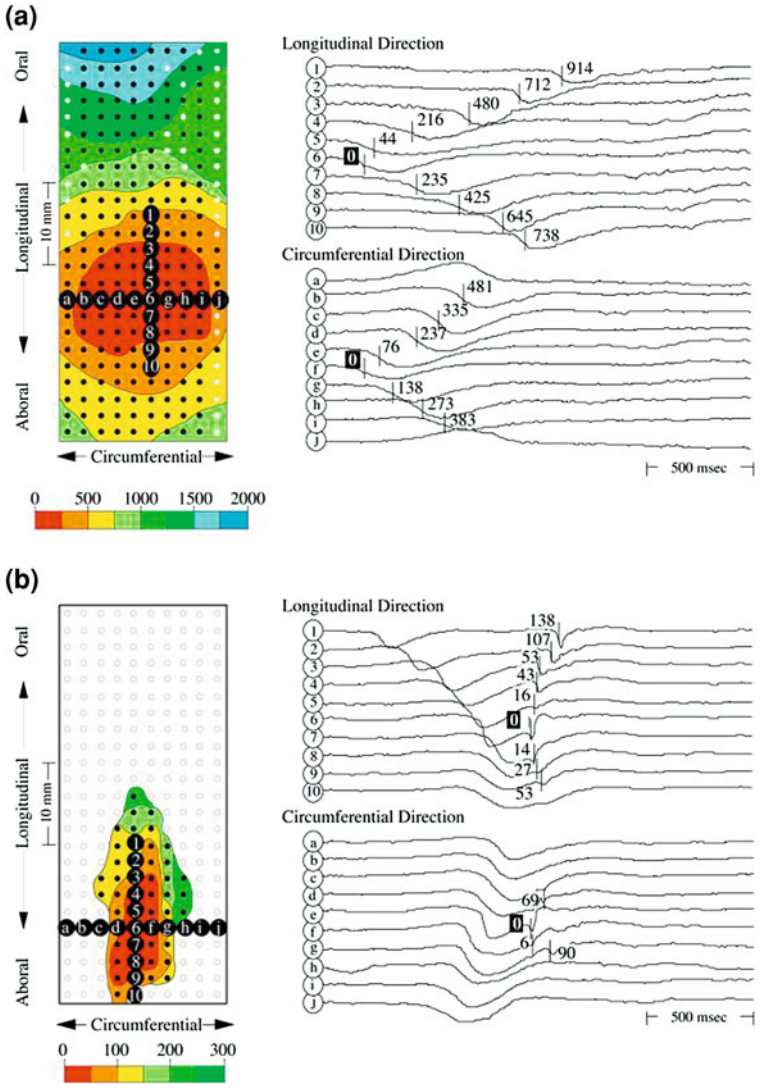

Fig. 2 Propagation characteristics of a slow wave **a** and longitudinal spike patch **b**. *Left* panels display the propagation maps of both impulses, which were recorded from the serosa of an isolated segment of feline small intestine in-vitro. Isochronal areas (250 ms in a and 50 ms in b) were drawn in several colors to illustrate the patterns of propagation. Initial slow wave propagation **a** occurred from the site of pacemaking (electrode 6) in all directions, with slightly faster propagation in the circumferential than in the longitudinal direction, serving to orient the slow wave into a wavefront that propagated in the organoaxial direction away from the site of pacemaking. The spike patch, in contrast, showed much faster propagation in the longitudinal than in the circumferential direction and terminated abruptly, both in the longitudinal and circumferential direction after 150–300 ms. (Modified from [24, 34])

The propagation characteristics of spikes are significantly different from those of SI slow waves. Spikes are best described to occur on the plateau of slow waves, where their propagation has been mapped to occur in small 'patches' conducting in all directions within the depolarized tissue [34]. Two directions of spike propagation have been observed in the small intestine, the first oriented predominately in the longitudinal direction (Fig. 2b) and the second oriented predominately in the circumferential direction, presumed to propagate in the longitudinal and circular muscle layers, respectively [36]. Spike activity can propagate independent of slow wave propagation characteristics, often exhibiting different velocity and propagation patterns than the corresponding slow wave activity [34, 36]. However, the mechanisms of spike patch propagation and cessation are currently unknown.

Multiple spikes may occur following on the depolarization of the slow wave, leading to multiple propagating spike patches and, thereby, inducing summated contraction in that area. The direction of propagation of the slow wave, together with the population of spike patches in its wake, may determine the type of overall contraction, as investigated in the case of pendular contractions [38]. Spike bursts, probably related to major contractions, have also been observed in the absence of slow waves, likely being induced by co-regulatory depolarizing inputs, and resulting in orally and aborally propagating contractions [35].

4.4 The Migrating Motor Complex

In the fasted state, the migrating motor complex (MMC) acts as a band of large-scale segmentation, originating in the duodenum and propagating caudally along the small intestine, propelling residual food and sloughed enterocytes down the intestine and into the colon. The MMC is underpinned by a number of co-regulatory mechanisms, including neural, hormonal and electrical. Hormones like motilin and ghrelin play an integral part in coordinating the MMC, but it is also characterized by the migrating myoelectrical complex, an excitatory band of spike activity that sweeps down the length of the small intestine [20, 56]. The coordinated propagation of the MMC occurs in recurrent cycles, and it is not disturbed by transection, suggesting that the ENS provides the key pathway for initiation and coordination of the MMC [4]. The MMC consists of four phases, lasting for a total duration of 84–112 min [20]. Phase I (40–60 % of cycle length) is characterized by relative mechanical quiescence and the absence of spike activity; Phase II (20–30 %) is characterized by irregular phasic contractions, exhibiting spike activity associated with approximately half of the slow wave cycles; Phase III (5–10 min) is characterized by rhythmic contractions occluding the lumen, with spike activity correlated to every slow wave cycle, the majority of which propagate aborally, although contractions occasionally propagate orally as well; Phase IV is characterized by irregular contractions and is a transition between the rhythmic contractions of Phase III and the relatively quiescent state of Phase I [4, 20].

5 Future Directions

It is seen from the above discussion that a century of investigations have achieved a considerable understanding of GI whole-organ excitation. However, substantial knowledge gaps still remain, and to date, meaningful clinical translation of this research to motility disorders has been lacking.

In recent years, GI HR mapping has proved a key advance for understanding large-scale electrical conduction events, and one research priority is, therefore, to further progress human studies using HR techniques. Recent human HR gastric mapping work, employing purpose-built sterilizable arrays [45], has proven the relevance and viability of this approach, and similar techniques now wait to be applied to the human SI. This research direction has significant potential to better inform the nature of human SI pacesetting, wavefront interactions, and frequency gradient mechanisms. Additionally, this research may prove valuable to answer longstanding questions in the field like if the waxing and waning phenomenon is related to spatial slow wave dynamics [55]. In future, we also anticipate that HR mapping may be applied in conjunction with other techniques, such as spatio-temporal motility mapping and HR manometry (e.g., as described by Lentle et al. in "Spatiotemporal Mapping Techniques for Quantifying Gut Motility" and Dinning et al. in "Colonic Manometry: What do the Squiggly Lines Really Tell Us?") in multimodal studies, to provide an improved understanding of integrated motility function.

Extracellular recordings of colonic electrical activity have been reported in the past (e.g., [54]). However, in our experience, these studies have proven difficult to reproduce. To date, no studies of colonic electrical activity have been conducted using HR methods. If they could be achieved, such studies would have the potential to introduce new levels of detail to our understanding of colonic motility, especially if combined with HR manometry studies.

5.1 Future Clinical Directions

There currently remains no established role for the evaluation of GI electrical activity in clinical practice. However, associations between disordered electrical activity and dysmotility are well established [24, 49], and research continues to be directed toward elucidating the role of electrical dysfunction in pathophysiology and symptom generation. In recent years, an expanding body of evidence associating disorders of ICC with dysmotility has reinvigorated efforts to clinically evaluate GI electrical patterns in order to understand and interpret the functional consequences of ICC loss for whole-organ function [15]. Brief attention is now given to some example areas of current enquiry and future potential.

Gastric dysrhythmias are abnormal electrical rhythms or patterns that are known to accompany several motility disorders, notably gastroparesis and

functional dyspepsia [49, 50]. The functional and pathophysiological significance of dysrhythmias remains poorly understood. One focus of current enquiry is the roll of ICC network degradation in dysrhythmogenesis, especially in idiopathic and diabetic gastroparesis, where ICC loss is recognized as the most significant cellular defect in affected patients [18].

Another highly significant recent development in dysrhythmia research has been the application of HR mapping to study dysrhythmic slow wave patterns [40, 47]. These studies have revealed that patterns and mechanisms of gastric dysrhythmias are spatially complex, and include focal activities, re-entrant circuits, circular propagations, conduction blocks and fibrillation-like behaviors [40, 47]. Tissue-level properties, including refractory patterns, activation heterogeneity, excitation delays, and circus-movements are now known to be critical to the genesis and maintenance of dysrhythmic patterns [40, 47]. Potential also now exists to apply HR mapping to develop more rational gastric pacing protocols for gastric dysrhythmias [46].

Intestinal dysrhythmias, by comparison, continue to remain poorly understood, having been the subject of very few studies. The most detailed of such studies have been conducted in the context of induced ischemia, where dynamic conduction blocks, ectopic pacemakers and tachyarrhythmias have been observed [32, 52]. Conditions such as post-surgical dysmotility have also shown possible associations with aberrant slow wave activity [44]. However, there are few available details concerning the occurrence, source, and nature of dysrhythmic intestinal patterns, and more research is needed.

Intestinal channelopathies are another area of growing research interest and significance. The description of specific ICC channelopathies in association with irritable bowel syndrome has been an exciting development (reviewed by Beyder et al. in "Role of Ion Channel Mechanosensitivity in the Gut: Mechano-Electrical Feedback Exemplified by Stretch-Dependence of $Na_V1.5$"). This work has paved the way for future studies to investigate the impact of ion channelopathies on slow waves and spikes, and, therefore, whole-organ excitation and function.

Acknowledgments TRA is supported by the Riddet Institute, the Royal Society of NZ, and the NZ Society of Gastroenterology. GOG is supported by the American Neurogastroenterology & Motility Society, the NZ Health Research Council, and the NIH (R01 DK64775).

References

1. Alvarez WC, Mahoney LJ (1922) Action currents in stomach and intestine. Am J Physiol 58:476–493
2. Angeli TR, O'Grady G, Du P, Paskaranandavadivel N, Pullan AJ, Bissett IP, Cheng LK (2013) Circumferential and functional re-entry of in vivo slow-wave activity in the porcine small intestine. Neurogastroenterol Motil [Epub ahead of print] doi: 10:1111/nmo.12085
3. Cannon WB (1902) The movements of the intestines studied by means of the Rontgen rays. Am J Physiol 6:251–277

4. Carlson GM, Bedi BS, Code CF (1972) Mechanism of propagation of intestinal interdigestive myoelectrical complex. Am J Physiol 222:1027–1030
5. Carlson HC, Code CF, Nelson RA (1966) Motor action of the canine gastroduodenal junction: a cineradiographic, pressure and electric study. Dig Dis Sci 11:155–172
6. Christensen J, Schedl HP, Clifton JA (1966) The small intestinal basic electrical rhythm (slow wave) frequency gradient in normal men in patients with variety of diseases. Gastroenterology 50:309–315
7. Code CF, Szurszewski JH (1970) The effect of duodenal and mid small bowel transection on the frequency gradient of the pacesetter potential in the canine small intestine. J Physiol 207:281–289
8. Code CF, Marlett JA (1975) The interdigestive myo-electric complex of the stomach and small bowel of dogs. J Physiol 246:289–309
9. Cousins HM, Edwards FR, Hickey H, Hill CE, Hirst GDS (2003) Electrical coupling between the myenteric interstitial cells of Cajal and adjacent muscle layers in the guinea-pig gastric antrum. J Physiol 550:829–844
10. Diamant NE, Bortoff A (1969) Nature of the intestinal slow-wave frequency gradient. Am J Physiol 216:301–307
11. Diamant NE, Bortoff A (1969) Effects of transection on the intestinal slow-wave frequency gradient. Am J Physiol 216:734–743
12. Du P, O'Grady G, Egbuji JU, Lammers WJ, Budgett D, Neilsen P, Windsor JA, Pullan A, Cheng LK (2009) High-resolution mapping of in vitro gastrointestinal slow wave activity using flexible printed circuit board electrodes: methodology and validation. Ann Biomed Eng 37:839–846
13. Du P, O'Grady G, Cheng LK, Pullan AJ (2010) A multi-scale model of the electrophysiological basis of the human electrogastrogram. Biophys J 99:2784–2792
14. Egbuji JU, O'Grady G, Du P, Cheng LK, Lammers WJEP, Windsor JA, Pullan AJ (2010) Origin, propagation and regional characteristics of porcine gastric slow wave activity determined by high-resolution mapping. Neurogastroenterol Motil 22:e292–e300
15. Farrugia G (2008) Interstitial cells of Cajal in health and disease. Neurogastroenterol Motil 20:54–63
16. Fleckenstein P, Oigaard A (1978) Electrical spike activity in the human small intestine: a multiple electrode study of fasting diurnal variations. Dig Dis Sci 23:776–780
17. Furness JB (2006) The Enteric Nervous System. Wiley-Blackwell, Oxford
18. Grover M, Farrugia G, Lurken MS et al (2011) Cellular changes in diabetic and idiopathic gastroparesis. Gastroenterology 140(1575–85):e8
19. Grundy D, Brookes S (2011) Neural Control of Gastrointestinal Function. Colloquium series on integrated systems physiology: from molecule to function to disease. Morgan & Claypool Life Sciences.
20. Hasler WL (2006) Small Intestine Motility. Physiology of the Gastrointestinal Tract, Fourth Edition 935–964
21. Hinder RA, Kelly KA (1977) Human gastric pacesetter potential. Site of origin, spread, and response to gastric transection and proximal gastric vagotomy. Am J Surg 133:29–33
22. Hirst GD, Edwards FR (2006) Electrical events underlying organized myogenic contractions of the guinea pig stomach. J Physiol 576:659–665
23. Hocke M, Schone U, Richert H, Gornert P, Keller J, Layer P, Stallmach A (2009) Every slow-wave impulse is associated with motor activity of the human stomach. Am J Physiol Gastrointest Liver Physiol 296:G709–G716
24. Huizinga JD, Lammers WJEP (2009) Gut peristalsis is coordinated by a multitude of cooperating mechanisms. Am J Physiol Gastrointest Liver Physiol 296:1–8
25. Huizinga JD, Martz S, Gil V, Wang X, Jimenez M, Parsons S (2011) Two independent networks of interstitial cells of Cajal work cooperatively with the enteric nervous system to create colonic motor patterns. Front Neurosci 5:93
26. Indireshkumar K, Brasseur JG, Faas H, Hebbard GS, Kunz P, Dent J, Feinle C, Li M, Boesiger P, Fried M, Schwizer W (2000) Relative contributions of "pressure pump" and

"peristaltic pump" to gastric emptying. Am J Physiol Gastrointest Liver Physiol 278:G604–G616
27. Kelly KA, Code CF, Elveback LR (1969) Patterns of canine gastric electrical activity. Am J Physiol 217:461–470
28. Kelly KA, Code CF (1971) Canine gastric pacemaker. Am J Physiol 220:112–118
29. Kelly KA (1980) Gastric emptying of liquids and solids. Roles of the proximal and distal stomach. Am J Physiol 239:G71–G76
30. Koh SD, Ward SM, Ordog T, Sanders KM, Horowitz B (2003) Conductances responsible for slow wave generation and propagation in interstitial cells of Cajal. Curr Opin Pharmacol 3:579–582
31. Lammers WJEP, Al-Kais A, Singh S, Arafat K, el-Sharkawy TY (1993) Multielectrode mapping of slow-wave activity in the isolated rabbit duodenum. J Appl Physiol 218:1454–1461
32. Lammers WJ, el-Kays A, Manefield GW, Arafat K, el-Sharkawy TY (1997) Disturbances in the propagation of the slow wave during acute local ischaemia in the feline small intestine. Eur J of Gastroenterol Hepatol 9:381–388
33. Lammers WJ, Slack JR, Stephen B, Pozzan O (2000) The spatial behaviour of spike patches in the feline gastroduodenal junction in vitro. Neurogastroenterol Motil 12:467–473
34. Lammers WJ, Stephen B, Slack JR, Dhanasekaran S (2002) Anisotropic propagation in the small intestine. Neurogastroenterol Motil 14:357–364
35. Lammers WJ, Stephen B, Slack JR (2002) Similarities and differences in the propagation of slow waves and peristaltic waves. Am J Physiol Gastrointest Liver Physiol 283:G778–G786
36. Lammers WJEP, Ver Donck L, Schuurkes JAJ, Stephen B (2003) Longitudinal and circumferential spike patches in the canine small intestine in vivo. Am J Physiol Gastrointest Liver Physiol 285:G1014–G1027
37. Lammers WJEP, Ver Donck L, Schuurkes JAJ, Stephen B (2005) Peripheral pacemakers and patterns of slow wave propagation in the canine small intestine in vivo. Can J Physiol Pharmacol 83:1031–1043
38. Lammers WJEP (2005) Spatial and temporal coupling between slow waves and pendular contractions. Am J Physiol 289:G898–G903
39. Lammers WJ, Stephen B (2008) Origin and propagation of individual slow waves along the intact feline small intestine. Exp Physiol 93:334–346
40. Lammers WJEP, Ver Donck L, Stephen B, Smets D, Schuurkes JAJ (2008) Focal activities and re-entrant propagations as mechanisms of gastric tachyarrhythmias. Gastroenterology 135:1601–1611
41. Lammers WJ, Ver Donck L, Stephen B, Smets D, Schuurkes JA (2009) Origin and propagation of the slow wave in the canine stomach: the outlines of a gastric conduction system. Am J Physiol Gastrointest Liver Physiol 296:1200–1210
42. Lammers WJEP, Stephen B, Karam SM (2012) Functional reentry and circus movement arrhythmias in the small intestine of normal and diabetic rats. Am J Physiol 302:G684–G689
43. Lees-Green R, Du P, O'Grady G, Beyder A, Farrugia G, Pullan AJ (2011) Biophysically based modeling of the interstitial cells of Cajal: current status and future perspectives. Front Physiol 2(29):1–19
44. Morrison P, Miedema BW, Kohler L, Kelly KA (1990) Electrical dysrhythmias in the roux jejunal limb: cause and treatment. Am J Surg 160:252–256
45. O'Grady G, Du P, Cheng LK, Egbuji JU, Lammers WJEP, Windsor JA, Pullan AJ (2010) The origin and propagation of human gastric slow wave activity defined by high-resolution mapping. Am J Physiol Gastrointest Liver Physiol 299:585–592
46. O'Grady G, Du P, Lammers WJEP, Egbuji JU, Mithraratne P, Chen JDZ, Cheng LK, Windsor JA, Pullan AJ (2010) High-resolution entrainment mapping of gastric pacing: a new analytical tool. Am J Physiol Gastrointest Liver Physiol 298:G314–G321
47. O'Grady G, Egbuji JU, Du P, Lammers WJEP, Cheng LK, Windsor JA, Pullan AJ (2011) High-resolution spatial analysis of slow wave initiation and conduction in porcine gastric dysrhythmia. Neurogastroenterol Motil 23:e345–e355

48. O'Grady G, Du P, Paskaranandavadivel N, Angeli TR, Lammers WJEP, Farrugia G, Asirvatham SJ, Windsor JA, Pullan AJ, Cheng LK (2012) Rapid high-amplitude cumferential slow wave conduction during normal gastric pacemaking and dysrhythmias. Neurogastroenterol Motil 24(7):e299–312
49. O'Grady G, Angeli TR, Du P, Lahr C, Lammers WJEP, Windsor JA, Abell TL, Farrugia G, Pullan AJ, Cheng LK (2012) Abnormal initiation and conduction of slow-wave activity in gastroparesis, defined by high-resolution electrical mapping. Gastroenterology 143(3):589–598
50. Parkman HP, Hasler WL, Barnett JL, Eaker EY (2003) Electrogastrography: a document prepared by the gastric section of the American Motility Society Clinical GI Motility Testing Task Force. Neurogastroenterol Motil 2003:89–102
51. Sanders KM (2008) Regulation of smooth muscle excitation and contraction. Neurogastroenterol Motil 20:39–53
52. Seidel SA, Hegde SS, Bradshaw A, Ladipo JK, Richards WO (1999) Intestinal tachyarrhythmias during small bowel ischemia. Am J Physiol Gastrointest Liver Physiol 277:G993–G999
53. Sha L, Farrugia G, Harmsen WS, Szurszewski JH (2007) Membrane potential gradient is carbon monoxide-dependent in mouse and human small intestine. Am J Physiol 293(2):G438–G445
54. Shafik A, Shafik AA, El-Sibai O, Mostafa M (2003) Electrical activity of the colon in subjects with constipation due to total colonic inertia: an electrophysiologic study. Arch Surg 138:1007–1011
55. Suzuki N, Prosser CL, DeVos W (1986) Waxing and waning of slow waves in intestinal musculature. Am J Physiol Gastrointest Liver Physiol 250:G28–G34
56. Szurszewski JH (1969) A migrating electric complex of the canine small intestine. Am J Physiol 217:1757–1763
57. Szurszewski JH, Elveback LR, Code CF (1970) Configuration and frequency gradient of electric slow wave over canine small bowel. Am J Physiol 218:1468–1473
58. Szurszewski JH, Farrugia G (2004) Carbon monoxide is an endogenous hyperpolarizing factor in the gastrointestinal tract. Neurogastroenterol Motil 16(Suppl 1):81–85
59. van Helden DF, Laver DR, Holdsworth J, Imtiaz MS (2010) The generation and propagation of gastric slow waves. Clin Exp Pharmacol Physiol 37:516–524
60. Verhagen MA, Luijk HD, Samsom M, Smout AJ (1998) Effect of meal temperature on the frequency of gastric myoelectrical activity. Neurogastroenterol Motil 10:175–181
61. Wang XY, Lammers WJ, Bercik P, Huizinga JD (2005) Lack of pyloric interstitial cells of Cajal explains distinct peristaltic motor patterns in stomach and small intestine. Am J Physiol Gastrointest Liver Physiol 289:G539–G549

Therapeutic Potential of Gastric Electrical Stimulation for Obesity

Jieyin Yin and Jiande Chen

Abstract Obesity is one of the major public health problems in the world. While various methods have been investigated or introduced, bariatric surgical procedures are currently the only effective long-term therapies for treating obesity. Due to mortality and morbidity, the bariatric surgery is limited to a subset of patients with morbid obesity. In this chapter we present an overview of an emerging anti-obesity therapy: gastric electrical stimulation (GES). First, the scientific basis for GES as a potential therapy for obesity is introduced. Secondly, GES methodologies and configurations are presented. Methods of GES that have been used for treating obesity are then introduced, and their effects on food intake and body weight are presented, followed with the discussion on possible mechanical, neural and hormonal mechanisms involved in the anti-obesity effect of GES. Finally, our viewpoint on the potential of GES for obesity and future development of the GES therapy are provided.

1 Introduction

Obesity is one of the most prevalent public health problems worldwide. About 1.7 billion individuals in the world are now estimated to be obese (body mass index or BMI $\geq$ 30 kg/m^2) [12] and approximately two-thirds of general population in USA are overweight and of those, about half are obese. The annual medical cost for the treatment of obesity in USA is estimated to be $147 billion in 2008 [17]. The analysis of five prospective cohort studies suggested that between 275,000 and 325,000 Americans die each year from obesity-related diseases [2]. Obesity is also

J. Yin (✉) · J. Chen
Division of Gastroenterology, GI Research, Route 0655, University of Texas Medical Branch, Galveston, TX 77555-0655, USA
e-mail: jiyin@utmb.edu

L. K. Cheng et al. (eds.), *New Advances in Gastrointestinal Motility Research*, Lecture Notes in Computational Vision and Biomechanics 10,
DOI: 10.1007/978-94-007-6561-0_7, © Springer Science+Business Media Dordrecht 2013

associated with an increased prevalence of socioeconomic hardship due to a higher rate of disability, early retirement, and widespread discrimination [18].

The treatment of obesity can be classified into three categories: general measures (diet and exercise), pharmacotherapy and surgical treatment.

Diet and Exercise are the first treatment/preventive option for obesity. The goal of this program is to integrate positive eating and physical activity behaviors into the patient's life. Although an acceptable weight loss may be achieved with such measures, maintaining weight loss is a lot more difficult, particularly for patients treated with caloric restriction. About 50 % of patients regain weight within one year after the treatment and almost all patients regain weight within 5 years [14].

Pharmacotherapy of obesity has been problematic. Various drugs have been developed for the treatment of obesity. These include amphetamine derivatives such as fenfluramine and dexfenfluramine, sibutramine, diethylpropion, mazindol, phentermine, phenylpropanolamine, orlistat, etc. [6, 28]. However, in general, the outcome of the medical treatment has been disappointing due to either adverse effects or a lack of long-term efficacy.

Surgical treatment is typically reserved for patients with morbid obesity (BMI $>$ 40) [20]. A number of surgical procedures have been used clinically, including vertical banded gastroplasty (also called gastric stapling) that restricts food intake, gastric bypass that promotes mal-digestion of ingested nutrients, such as Roux-en-Y and biliopancreatic diversion, duodenal switch and gastric banding (called lapbanding if the procedure is done laparoscopically) or adjustable gastric banding [7]. All these procedures have been shown to result in substantial weight loss with duodenal switch the most effective, whereas lapbanding is least invasive. However, it should be noted that the gastric bypass procedure as well as other surgical procedures have a number of drawbacks: (1) They alter the anatomy of the gut and are irreversible; (2) They involve morbidity and mortality; the mortality rate is about 0.2–2 % and the rate of major adverse events is about 5–8 % [26]; (3) They impair micronutrient absorption and results in metabolic and nutritional complications. Nutrient deficiencies following gastric bypass include protein-calorie malnutrition, fat malabsorption as well as deficiencies in iron, vitamin B_{12}, folate, riboflavin and calcium [26].

Recently gastric electrical stimulation (GES) has been introduced as a potential therapeutic potential for obesity. Compared with the surgical therapies, GES is less invasive and most importantly reversible and adjustable over time. During GES clinical studies, patients, physicians and surgeons have shown enthusiasm towards GES. However, controlled studies have failed to reach significant weight loss. The aim of this chapter is to critically review various methods of GES that have been applied for treating obesity and provide insight into a viable GES therapy for obesity.

2 Food Intake and Gastrointestinal Motility

While the brain makes the ultimate decision on eating or not eating, the most influential organ involving food intake and nutrient absorption is the gut. The gut plays a critical role in communicating with the brain both neurally and hormonally. The neural and hormonal signals from the gut to the brain are triggered by the interaction between food and various receptors including mechanical actions of the gut when the ingested food/nutrients travel along the gut. Therefore it is important to understand the role of gastrointestinal motility on food intake. Since the action of GES on the gastrointestinal system is primarily limited to the stomach, we focus our discussions on gastric motility.

Regulatory roles of gastric motility in food intake: The stomach functions as a reservoir to accommodate ingested food and a pump to empty gastric chyme into the small intestine. Upon ingestion of food, the stomach is relaxed to a certain degree to accommodate food, a process called the accommodation reflex mediated through the vagal activation and release of nitric oxide. If the volume of the ingested food is beyond the gastric accommodation, the pressure of the stomach will build up, leading to the sensation of bloating and fullness, and termination of food intake, a process defined as satiation in a recent publication [8]. A reduced gastric accommodation leads a reduction in food intake and/or enhanced post-prandial fullness/bloating. The second function of the stomach is to empty the ingested food to the small intestine, a process called gastric emptying. The speed of gastric emptying is believed to be associated with satiety or appetite that determines the amount of food intake of a subsequent meal [8]. A delay in gastric emptying leads to a reduced intake of a subsequent meal or a delay of the subsequent meal.

Gastric tone, gastric distention and satiation: In addition to genetic, neural and hormonal regulations, the stomach is involved in the process of satiation. Intuitively, one would expect that an obese subject has a large stomach or increased gastric accommodation. A review of the published studies in the literature however, does not support such a concept, i.e., statistically there is no difference in the size of the stomach or gastric accommodation between lean and obese subjects [8, 46]. However, a number of studies have demonstrated that gastric distention induced by an intragastric balloon leads to a reduction in food intake or early satiation [20, 27]. Despite a meta-analysis of 15 published clinical studies concluding its effectiveness in reducing weight within a period of about 6 months, its long-term efficacy could not be established [20]. The long-term failure of this method is attributed to the adaptation of the stomach: after a sufficiently long-term use of the intragastric balloon, the size of the stomach is increased to accommodation the balloon and therefore the intragastric balloon does not help in building up higher gastric pressure upon food intake and its effect on satiation is reduced as the stomach is adapted to the presence of the balloon.

GES with appropriate parameters/configurations in the fasting state is reported to reduce gastric tone and induce gastric distention measured by the barostat

system [47]. It was found that the GES-induced increase in gastric volume was inversely correlated with the reduced amount of food intake in dogs [34]. Furthermore, we have also found that the GES activates satiety neurons in the ventromedial hypothalamus in a similar way as the distention of the stomach using an intragastric balloon [42].

Gastric emptying and satiety: A number of studies have investigated the difference in gastric emptying between lean and obese subjects. Controversial results have been reported with some showing rapid emptying, some showing slower emptying and some others showing no changes [8]. However, intervention-induced delay in emptying has been linked to increased satiety, reduced food intake and/or weight loss. One good example of this is the use of anti-obesity medications. A number of these drugs have been shown to delay gastric emptying associated with increased satiety or weight loss. These include sibutramine [38, 45, 50], rimonabant [21, 15] and oleoylethanolamide [3]. Studies performed in our lab have shown the similar link between intervention-induced delay in gastric emptying and increased satiety. GES with appropriate parameters/configurations has been shown to delay gastric emptying in dogs and humans, associated with reduced intake of food or water as well as weight loss [25, 51, 52].

3 Gastric Electrical Stimulation

Different methods of GES have been introduced and studied for various applications. In this chapter, we classify GES methods in two ways: (1) based on stimulus configurations and (2) based on the effect of GES on gastric motility.

3.1 GES Configurations

The electrical stimulus is composed of a series of electrical pulses (usually square waveform). Based on the width of stimulation pulses, GES can be classified as long pulses, short pulses and pulse trains [54].

Long-pulse stimulation: This method is most frequently reported in the literature (but mostly limited to animals) because it is able to "pace" or entrain natural slow waves. In this method, the electrical stimulus is composed of repetitive single pulses with a pulse width in the order of milliseconds (10–600 ms), and a stimulation frequency in the vicinity or in the order of the physiological frequency of the gastric slow wave (see Fig. 1a). It is also called low frequency/high energy GES [29, 24]

Short-pulse stimulation: In contrast to long-pulse stimulation, the pulse width in this method is substantially shorter and is in the order of a few 100 microseconds (μs). The stimulation frequency is usually a few times higher than the physiological frequency of the gastric slow wave (see Fig. 1b).

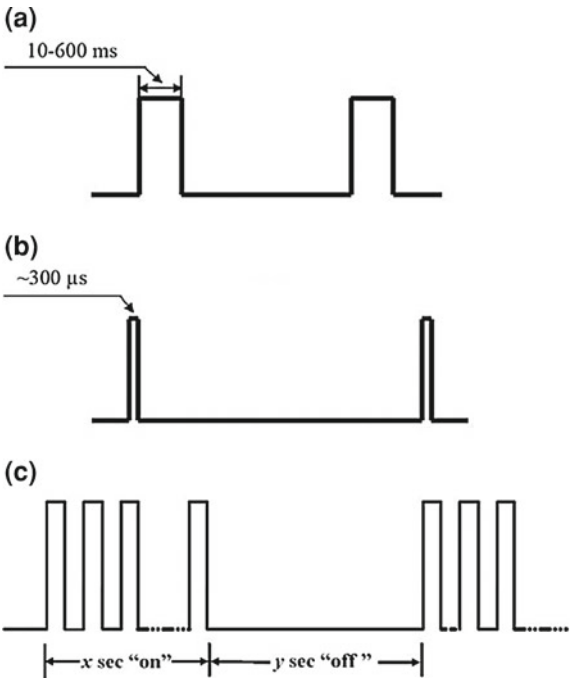

Fig. 1 Three types of electrical stimuli. **a** Repetitive long pulses with a pulse width of 10–600 ms. **b** repetitive short pulses with the pulse width in the order of μs. **c** Trains short pules

Trains of short-pulses: In this method, the stimulus is composed of repetitive trains of short pulses with an on-period and off-period (see Fig. 1c). This kind of stimulation has been frequently used in nerve stimulation. Commercially available implantable stimulators are capable of generating trains of pulses only with a pulse width of below 1 ms. Recently, however, a number of implantable pulse generators have been developed for clinical trials or animal research that are capable of generating pulses with a pulse width of >1 ms [31, 1, 4, 37].

3.2 eGES, nGES and iGES

According to the effects of GES on gastric motility, GES can be classified into the following categories:

eGES or excitatory GES: Any method of GES that enhances gastric motility is called eGES. According to this definition, eGES is able to either pace gastric slow waves (gastric intrinsic myoelectrical activity), enhance gastric contractions and/or accelerate gastric emptying. In the method of eGES, long pulses are typically used and the frequency of the stimulation should be the same as or slightly higher than the frequency of the intrinsic gastric slow waves. Examples of eGES include gastric pacing that normalize gastric dysrhythmia and synchronized GES that enhances antral contractions and speed up gastric emptying [57]. This method is

typically used for treating gastric motility disorders [23]. Long-pulse eGES at the electrophysiological frequency of the stomach has been applied to normalize gastric dysrhythmia in patients with gastroparesis (delayed gastric emptying) and accelerate delayed emptying of the stomach [9, 16, 19, 29]. Both human and canine studies have shown that the method of long-pulse eGES is capable of pacing the stomach and restoring the normal rhythm of gastric myoelectrical activity [29, 16, 9]. Improvement in clinical symptoms of dyspepsia and gastric emptying was also reported using long-pulse GES at the physiological frequency. However, no implantable device is available to assess the long-term effects of this method for the treatment of gastric motor disorders.

In the method of pulse train GES, if the pulse width is in the order of a few ms or higher, it is also capable of enhancing or inducing gastric contractions. Two examples are the one proposed by Mintchev et al [31, 1] and the device called the Tantalus [37, 40]. In both of these methods, pulse trains are given at a frequency (number of trains/min) that is in the vicinity of or lower than the physiological frequency of the intrinsic gastric contractions or synchronized with the intrinsic gastric contractions. Both of these methods have been reported to induce or enhance gastric contraction/emptying [31, 37].

nGES or neutral GES: Any method of GES that has no effects on gastric motility is called nGES. In this method, the stimuli of GES are usually composed of short pulses. Although this method of GES does not alter gastric motility, it typically changes neural activities. The method that has been used clinically for the treatment of nausea and vomiting in patients with gastroparesis (called Enterra Therapy) can be classified as nGES as it does not effectively alter gastric slow waves, antral contractions or gastric emptying [24, 40]. The anti-emetic effect of the Enterra therapy is discussed in detail by Griffith et al. in "Gastric Electrical Stimulation: Twentieth Century Development to Twenty-First Century Implementation and Personalization of Programming" of this volume. If GES uses short pulses or trains of short pulses with a width of <1 ms, it may also be called nGES because GES with these parameters do not alter gastric motility.

iGES or inhibitory GES: Any method of GES that inhibits gastric motility, such as inhibiting gastric tone, contractions and/or emptying, is called iGES in this chapter. Two methods of GES can be called iGES: (1) long pulse GES that inhibits motility (typically the stimulation frequency is higher than normal frequency of gastric slow waves); (2) pulse train GES that inhibits motility (typically the pulse width is >1 ms). The inhibition of gastric motility has been linked to reduced food intake and therefore iGES is expected to be an appropriate method for the treatment of obesity.

4 Gastric Electrical Stimulation for Obesity

The first GES method introduced to treating obesity is called implantable gastric stimulation (IGS). It uses trains of short pulses and has minimal effects on gastric motility, but alters central neuronal and hormonal activities (nGES). Another GES

method that was applied clinically to obese patients is called Tantalus. In that method, GES was designed to induce/enhance gastric motility (eGES). The third GES method that is used for treating obesity is is designed to inhibit gastrointestinal motility (iGES).

4.1 Implantable Gastric Stimulation

IGS was introduced for treating obesity about a dozen years ago [11, 10]. Trains of short-pulses are used with the following parameters: the duration of the train on-time 2 s and off-time: 3; pulses frequency: 40 Hz; width: 300 μs and amplitude: 6–10 mA. In clinical studies for obesity, the stimulation was performed via a pair of electrodes placed on the gastric serosa in the middle of the lesser curvature. While open-label studies in Europe have yielded promising results, about 25–35 % excess weight loss [11, 10] (See Fig. 2), its efficacy in reducing weight in morbid obesity has not been demonstrated in two multi-center randomized controlled studies [30, 42].

Mechanistic studies performed in our lab have shown that IGS exerts no effects on gastric contraction, gastric emptying or gastric tone [32]. Accordingly, this method can be classified as nGES. On the other hand, the IGS method was reported to activate satiety neurons in the ventromedial hypothalamus, decrease orexin and increase oxytocin in the hypothalamus [44]. Clinically, IGS was observed to reduce appetite and increase inter-meal satiety [13] in patients with obesity. However, it is apparent that the IGS-induced satiety was not strong enough to alter eating behaviors of obese patients.

4.2 Tantalus

The Tantalus system was designed to enhance gastric motility based on the hypothesis that the enhancement of gastric contractions at early stage of food

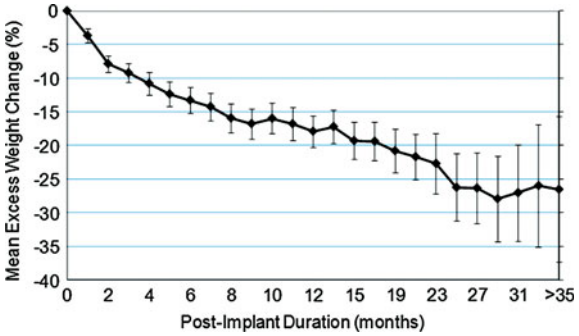

Fig. 2 European multi-center open-label trial using IGS in 50 obese patients. Reduction in body weight was observed during the 3-year follow ups. The final excess weight loss was about 26 %

ingestion enhances satiety and thereby reducing food intake. The system was composed of three pairs of electrodes and a subcutaneously implanted pulse generator. One pair of the electrodes was used to detect the impedance of the fundus and the other two pairs were used for the measurement of antral slow waves and delivery of stimulation [4]. Food ingestion was automatically detected according to a simultaneous increase in fundic impedance and a decrease in gastric slow wave frequency. Each stimulus was composed of a train of pulses with a train duration of 1.2 s, pulse frequency of 83 Hz, pulse width of 6 ms and pulse amplitude from 6–10 mA. The delivery of each pulse train was synchronized with the local slow waves.

The Tantalus system was originally proposed for the treatment of obesity; it was hypothesized that the system would enhance antral contractions during the early phase of the postprandial state and the enhanced antral contractions, together with gastric distention attributed to food ingestion, would increase vagal afferent signaling to the brain resulting in increased satiety [35]. In an open-label clinical study in patients with morbid obesity, there was a 17 % excess weight loss in 12 patients after 20 weeks of treatment and a 27 % excess weight loss in nine patients after 52 weeks of treatment [4]. No follow-up controlled studies were reported in the literature. It seems that the system is now under investigation for its role in treating diabetes [5].

While the Tantalus system uses advanced technologies of detecting food intake and synchronizing the stimulation with intrinsic gastric slow waves, its rationale for treating obesity is unclear. In one study a significant increase in gastric emptying was reported in 12 obese patients treated with the Tantalus system and the acceleration in gastric emptying was believed to be attributed to enhanced antral contractility [37]. It is however, unclear why accelerated gastric emptying may lead to a reduced food intake although this may be related to increased distension of the proximal small bowel.

4.3 Inhibitory Gastric Electrical Stimulation

While both IGS and Tantalus system were reported to be effective in reducing body weight in open-label studies, they did not produce significant weight loss in controlled studies. The major reason of failure, we believe is the lack of appropriate effects on gastric motility which plays a crucial role in the regulation of satiety and satiation as discussed above. IGS has minimal or no effects on gastric motility; whereas the Tantalus system actually speeds up gastric emptying. Acceleration in gastric emptying could lead to a reduction in satiety in between meals and shorten meal interval or increase food intake of the subsequent meal.

The iGES method is suited for treating obesity. Both long pulse iGES and pulse train iGES (pulse width at least 2 ms) have been shown to reduce food intake and produce weight loss in various animal models. Long pulse iGES delivered in the antrum (to disrupt the aboral propagation of intrinsic slow waves) at a frequency of

tachygastria (to induce antral hypomotility) has been demonstrated to reduce food intake and body weight in regular rats, obese Zucker rats and diet-induced obese rats [52] and dogs [53]. In healthy volunteers, acute iGES using temporary mucosal electrodes was also reported to reduce food intake [51, 25].

When GES is performed using pulse trains, its effects on gastric motility are determined by the following facts: (1) the pulse width must be long enough ($\geq$2 ms at 40 Hz) to be capable of altering smooth muscle functions [22]; (2) when the pulse width is sufficiently long, GES exerts an inhibitory effect on gastric contractions if the frequency of pulse trains is higher than the normal frequency of the gastric slow waves (3 cycles/min in humans and 5 cycles/min in dogs), but may enhance gastric contractions if the frequency of pulse trains is in the normal range of the gastric slow waves. At a fixed frequency of 40 Hz, GES produces inhibitory effects on gastric motility when the pulse width is increased from 0.3 ms (IGS method) to 2–3 ms, resulting in a significant decrease in food intake and body weight [56]. Since long pulse iGES may cause problems of current imbalance and electrode corrosion, pulse train iGES is expected to be more suitable for treating obesity.

5 Mechanisms of GES for Obesity

Mechanical (particularly gastric motility), neural and hormonal pathways have been reported to be involved in the application of GES for obesity. In this section we briefly discuss the effects of various methods of GES used in obesity treatment on gastric motility including, gastric tone, antral contractions and gastric emptying, satiety neurons in the hypothalamus via the vagal and spinal afferent pathways and certain central and gastrointestinal hormones.

5.1 Inhibitory Effects of iGES on Gastric Motility

Gastric tone: In a canine study, the effects of pulse train GES with different pulses widths were investigated and the results are shown in Fig. 3. GES was performed via a pair of stimulation electrodes in the distal antrum with parameters of train-on time of 2 s, off time of 3 s, 40 Hz, 6 mA and pulse width from 0.21 to 4 ms. Gastric tone was assessed by the measurement of intragastric volume using a barostat device. As shown in Fig. 3, GES increased the gastric volume at a pulse width of 2 ms ($p = 0.018$) and 4 ms ($p = 0.05$) in comparison with the corresponding baseline recording. However, GES had no effects on gastric volume with a pulse width of 0.21, 0.45 or 1 ms. Similar inhibitory effects on gastric tone were reported with iGES using long pulses [47, 34].

Antral contractions: Inhibition of antral contractions was reported with both methods of iGES using long pulses and pulse trains and the inhibitory effect was

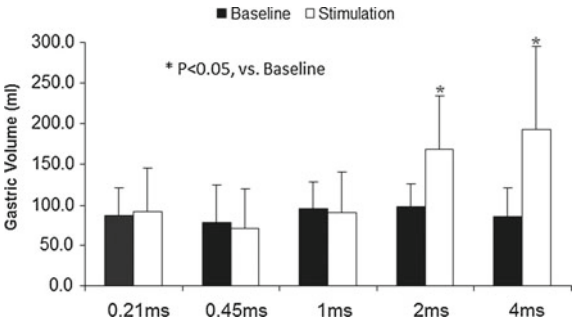

Fig. 3 Effects of pulse train GES with different pulse widths on gastric tone. Gastric volume was not altered with GES with a pulse width <2 m but significantly increase with a pulse width of 2 and 4 ms

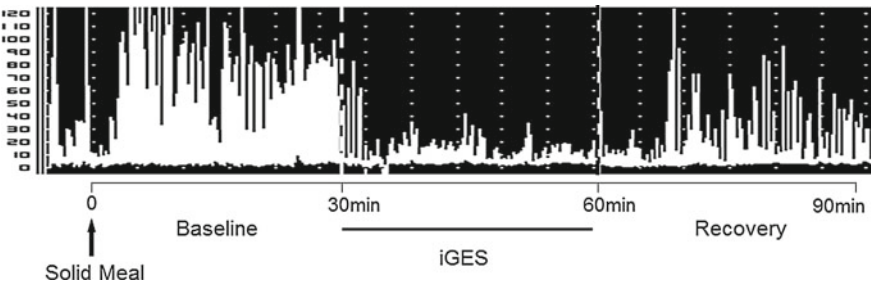

Fig. 4 Inhibition of postprandial antral contractions in a dog with long pulse iGES. Strong gastric contractions were noted immediately after a solid meal (baseline) but suppressed during the period when iGES was applied

found to be mediated via the sympathetic mechanism [33]. Figure 4 presents a typical recording of antral contractions in a dog at baseline, during iGES (long pulses) and after termination of iGES in the postprandial state. It can be seen clearly that antral contractions were substantially reduced during iGES and gradually recovered after iGES was terminated.

Gastric emptying: Inhibitory effects of iGES on gastric emptying were investigated in both canine and clinical studies. In one canine study, iGES was performed using pulse trains with a pulse width of 2 ms and delivered at the distal antrum [41]. Gastric emptying of solids was significantly decreased with iGES: The half-time gastric emptying was increased from 177.7 ± 27.1 min with sham iGES to 254.6 ± 71.7 min with GES ($P < 0.024$). In another canine study, iGES was performed using single long pulses repeated at a frequency of 10 or 30 pulses/min delivered at the pyloric area [49]. A significant and energy-dependent delay in gastric emptying of liquid was observed with iGES, as shown in Fig. 5.

Two clinical studies have been performed in healthy volunteers using temporary electrodes placed on gastric mucosa under endoscopy. iGES was performed using long pulses repeated at a frequency of 9 pulses/min. In one study iGES was

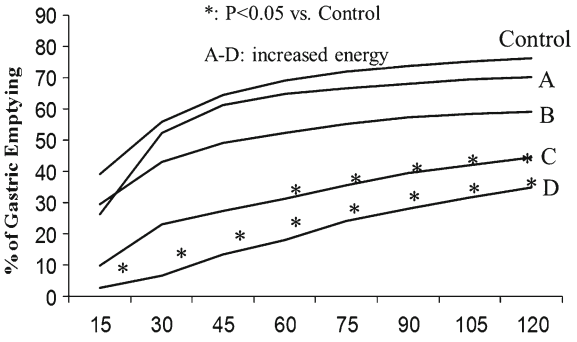

Fig. 5 iGES energy-dependently delayed gastric emptying of liquid in dogs. From *top* to *bottom* gastric emptying curves: control and iGES with parameters of *A*: 0.2 ms, 10 ppm (pulses/min) and 5 mA; *B*: 50 ms, 10 ppm and 5 mA; *C*: 50 ms, 30 ppm and 5 mA; *D*: 50 ms, 30 ppm and 10 mA

performed via the distal antrum and a significant reduction in gastric emptying of solid was observed [51]. In another study, iGES was delivered via the fundus and the reduction in gastric emptying was not significant or marginally significant at some points after ingestion of a solid meal [25].

5.2 Central Neuronal and Humoral Effects of GES

Different from gastric motility, central neuronal and humoral activities can be altered by both nGES (such as IGS) and iGES. This is because the central nervous system responds to electrical stimulation quickly (a short time constant). However, a comparative study revealed enhanced central effects with GES when its pulse width was increased from 0.3 to 3 ms as shown in Fig. 6 [55].

Involvement of vagal afferent pathway: Involvement of the vagal afferent pathway was noted in a recent rodent study using various methods of GES. GES was found to activate neurons responsive to gastric distention in the nucleus tractus solitarii, suggesting the involvement of the vagal afferent pathway. About 40 % of neurons responsive to gastric distention were activated with GES of long pulses or GES with trains of short pulses [36]. With GES of trains of short pulses, it was further noted that an increase in pulse width or amplitude resulted in activation of more neurons. In another rodent study, vagal afferent fibers were activated when antral contractions were induced with GES [35].

Central neuronal effects: Using the extracellular recording in the anesthetized rats, a recent study reported the activation of gastric distention-responsive neurons in the paraventricular nucleus with various methods of GES [43]. All three methods of GES (short pulse, long pulse and trains of short pulses) were able to activate these neurons. However, in one specific type of neurons (gastric distention-inhibitory neurons), opposite effects were noted between GES with trains of short pulses (with parameters used for treating obesity) and GES of short pulses (with parameters used for treating nausea and vomiting in patients with gastroparesis). These data suggest possible different central mechanisms with different methods of GES. Similar central neuronal effects with GES were also noted in the

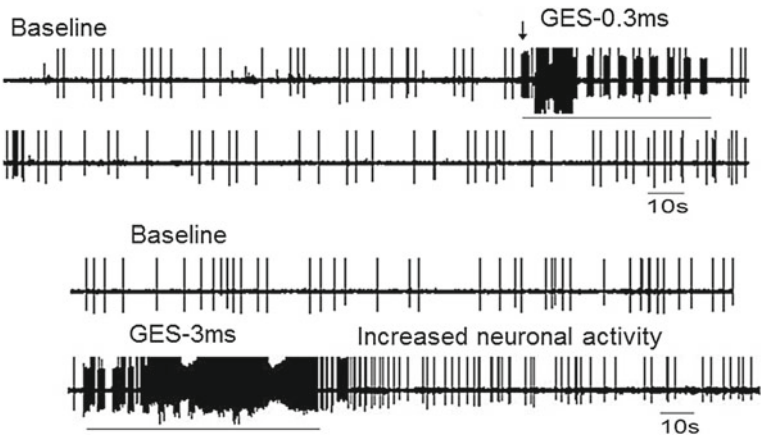

Fig. 6 Effects of GES on a satiety neuron in the ventromedial nucleus (VMH). GES with a pulse width of 3 ms (GES-3 ms) was noted to be more potent in activating the neuron (*lower* panel) than GES with a pulse width of 0.3 ms (GES-0.3 ms)

other areas of the brain, such as the hippocampus [48] and the ventromedial nucleus [42].

Central humoral effects: A few recent studies have investigated possible central humoral mechanisms of IGS and reported a decrease in certain orexignetic peptides and an increase in anorexigenic peptides. After 2-h GES with trains of short pulses, neurons expressing orexin was significantly decreased in the supra-optic nucleus and the lateral hypothalamic area, whereas neurons expressing oxytocin and cholecystokinin were increased in the parametricular nucleus and hippocampus, respectively [44, 48].

6 Perspectives on GES for Treating Obesity

In summary, current GES methods for obesity treatment can be classified into iGES and non-iGES (or IGS) according to their effects on gastric motility. While both methods of GES activate satiety neurons in the hypothalamus and alter satiety-related hormones, only iGES inhibits gastric motility. However, currently available devices are not able to deliver electrical stimuli for iGES and therefore a new generation device suitable for iGES is needed.

In addition to the required higher output, a new generation device for obesity may also be required to have the following features: (1) remote charging due to the high output nature of iGES. The technology for remotely charging an implantable pulse generator is already available; (2) on-demand stimulation. Since iGES is designed to reduce food intake, it is conceivable that stimulation may only be needed during and certain time period after food intake. This can be achieved by a

circuit imbedded in the implantable stimulator that detects certain physiological changes after food intake, such as the distention of the stomach or the change in gastric slow wave frequency as done in the Tantalus system. (3) feedback-controlled mechanism. It was reported in a previous study that the sensitivity of individuals to gastric electrical stimulation varied substantially among different subjects. That is, the selection of stimulation parameters may have to be optimized individually. Accordingly, a closed loop system may be required to control the output of the stimulator: the most crucial parameters of iGES are dynamically controlled based on the outcome measures of the stimulation, such as the inhibition on gastric contractions.

References

1. Aelen P, Neshev E, Cholette M, Crisanti K, Mitchell P, Debru E, Church N, Mintchev MP (2008) Manipulation of food intake and weight dynamics using retrograde neural gastric electrical stimulation in a chronic canine model. Neurogastroenterol Motil 20:358–368
2. Allison DB, Fontaine KR, Manson JE, Stevens J, VanItallie TB (1999) Annual deaths attributable to obesity in the United States. JAMA 282:1530–1538
3. Aviello G, Matias I, Capasso R, Petrosino S, Borrelli F, Orlando P, Romano B, Capasso F, Di Marzo V, Izzo AA (2008) Inhibitory effect of the anorexic compound oleoylethanolamide on gastric emptying in control and overweight mice. J Mol Med 86:413–422
4. Bohdjalian A, Prager G, Aviv R, Policker S, Schindler K, Kretschmer S, Riener R, Zacherl J, Ludvik B (2006) One-year experience with Tantalus: a new surgical approach to treat morbid obesity. Obes Surg 16:627–634
5. Bohdjalian A, Prager G, Rosak C, Weiner R, Jung R, Schramm M, Aviv R, Schindler K, Haddad W, Rosenthal N, Ludvik B (2009) Improvement in glycemic control in morbidly obese type 2 diabetic subjects by gastric stimulation. Obes Surg 19(9):1221–1227
6. Bray GA, Greenway FL (1999) Current and potential drugs for treatment of obesity. Endocr Rev 20(6):805–875
7. Buchwald H, Avidor Y, Braunwald E, Jensen MD, Pories W, Fahrbach K, Schoelles K (2004) Bariatric surgery: a systematic review and meta-analysis. JAMA 292:1724–1737
8. Camilleri M, Grudell AB (2007) Appetite and obesity: a gastroenterologist's perspective. Neurogastroenterol Motil 19:333–341
9. Chen JDZ, Qian LW, Ouyang H, Yin JY (2003) Gastric electrical stimulation with short pulses improves vomiting but not gastric dysrhythmia in dogs. Gastroenterology 124:401–409
10. Cigaina V (2004) Long-term follow-up of gastric stimulation for obesity: the Mestre 8-year experience. Obes Surg 14(Suppl 1):S14–S22
11. D'Argent J (2002) Gastric electrical stimulation as therapy of morbid obesity: preliminary results from the French study. Obes Surg 12(Suppl 1):21S–25S
12. Deitel M (2003) Overweight and obesity worldwide now estimated to involve 1.7 billion people. Obes Surg 13:329–330
13. De Luca M, Segato G, Busetto L, Favretti F, Aigner F, Weiss H, de Gheldere C, Gaggiotti G, Himpens J, Limao J, Scheyer M, Toppino M, Zurmeyer EL, Bottani G, Penthaler H (2004) Progress in implantable gastric stimulation: summary of results of the European multi-center study. Obes Surg 14(Suppl 1):S33–S39
14. Dickey RA, Bartuska CDG, Bray GW, Callaway CW, Davidson ET, Feld S, Ferraro RT, et al. (1998) AACE/ACE Position statement on the prevention, diagnosis, and treatment of obesity (1998 revision) Endocr Pract 4(5):297–350

15. Di Marzo V, Capasso R, Matias I, Aviello G, Petrosino S, Borrelli F, Romano B, Orlando P, Capasso F, Izzo AA (2008) The role of endocannabinoids in the regulation of gastric emptying: alterations in mice fed a high-fat diet. Br J Pharmacol 153:1272–1280
16. Eagon JC, Kelly KA (1993) Effects of gastric pacing on canine gastric motility and emptying. Am J Physiol 265:G767–G774
17. Finkelstein EA, Trogdon JG, Cohen JW, Dietz W (2009) Annual medical spending attributable to obesity: payer-and service-specific estimates. Health Aff (Millwood) 28:w822–w831
18. Gortmaker SL, Must A, Perrin JM, Sobol AM, Dietz WH (1993) Social and economic consequences of overweight in adolescence and young adulthood. N Engl J Med 329:1008–1012
19. Hocking MP, Vogel SB, Sninsky CA (1992) Human gastric myoelectrical activity and gastric emptying following gastric surgery and with pacing. Gastroenterology 103:1811–1816
20. Imaz I, Martinez-Cervell C, Garcia-Alvarez EE, Sendra-Gutierrez JM, Gonzalez-Enriquez J (2008) Safety and effectiveness of the intragastric balloon for obesity. A meta-analysis. Obes Surg 18:841–846
21. Krentz AJ, Patel MB, Bailey CJ (2008) New drugs for type 2 diabetes mellitus: what is their place in therapy? Drugs 68:2131–2162
22. Li S, Chen JD (2010) Cellular effects of gastric electrical stimulation on antral smooth muscle cells in rats. Am J Physiol Regul Integr Comp Physiol 298(6):R1580–R1587
23. Lin ZY, Chen JDZ (2002) Advances in gastrointestinal electrical stimulation. Crit Rev Biomed Eng 30:419–458
24. Lin Z, Forster J, Sarosiek I, McCallum RW (2003) Treatment of gastroparesis with electrical stimulation. Dig Dis Sci 48(5):837–848
25. Liu J, Hou X, Song G, Cha H, Yang B, Chen JD (2006) Gastric electrical stimulation using endoscopically placed mucosal electrodes reduces food intake in humans. Am J Gastroenterol 101:798–803
26. Malinowski SS (2006) Nutritional and metabolic complications of bariatric surgery. Am J Med Sci 331:219–225
27. Mathus-Vliegen EM (2008) Intragastric balloon treatment for obesity: what does it really offer? Dig Dis 26:40–44
28. Mayer MA, Höcht C, Puyó A, Taira CA (2009) Recent advances in obesity pharmacotherapy. Curr Clin Pharmacol 4:53–61
29. McCallum RW, Chen JD, Lin Z, Schirmer BD, Williams RD, Ross RA (1998) Gastric pacing improves emptying and symptoms in patients with gastroparesis. Gastroenterology 114(3):456–461
30. McCallum RW, Sarosiel, Lin Z, Moncure M, USA Study Group (2002) Preliminary results of gastric electrical stimulation on weight loss and gastric emptying in morbidly obese patients—randomized double blinded trial. Neurogastroenterol Motil 14:422
31. Neshev E, Onen D, Jalilian E, Mintchev MP (2006) Pre-pyloric neural electrical stimulation produces cholinergically-mediated reverse peristalsis in the acute canine model of microprocessor-invoked gastric motility for the treatment of obesity. Obes Surg 16:510–520
32. Ouyang H, Yin JY, Chen JDZ (2003) Inhibitory effects of chronic gastric electrical stimulation on food intake and weight and their possible mechanisms. Dig Dis Sci 48:698–705
33. Ouyang H, Xing J, Chen JD (2005) Tachygastria induced by gastric electrical stimulation is mediated via alpha- and beta-adrenergic pathway and inhibits antral motility in dogs. Neurogastroenterol Motil 17(6):846–853
34. Ouyang H, Yin J, Chen JD (2006) Gastric or intestinal electrical stimulation-induced increase in gastric volume is correlated with reduced food intake. Scand J Gastroenterol 41:1261–1266
35. Peles S, Petersen J, Aviv R, Policker S, Abu-Hatoum O, Ben-Haim SA, Gutterman DD, Sengupta JN (2003) Enhancement of antral contractions and vagal afferent signaling with

synchronized electrical stimulation. Am J Physiol Gastrointest Liver Physiol 285:G577–G585
36. Qin C, Sun Y, Chen JDZ, Foreman R (2005) Gastric electrical stimulation modulates neuronal activity in nucleus tractus solitarii in rats. Auton Neurosci Basic Clin 119:1–8
37. Sanmiguel CP, Haddad W, Aviv R, Cunneen SA, Phillips EH, Kapella W, Soffer EE (2007) The TANTALUS system for obesity: effect on gastric emptying of solids and ghrelin plasma levels. Obes Surg 17:1503–1509
38. Scheen AJ, Lefebvre PJ (2000) Antiobesity pharmacotherapy in the management of type 2 diabetes. Diabetes Metab Res Rev 16:114–124
39. Shikora SA, Bergenstal R, Bessler M, Brody F, Foster G, Frank A, Gold M, Klein S, Kushner R, Sarwer DB (2009) Implantable gastric stimulation for the treatment of clinically severe obesity: results of the SHAPE trial. Surg Obes Relat Dis 5:31
40. Soffer E, Abell T, Lin Z, Lorincz A, McCallum R, Parkman H, Policker S, Ordog T (2009) Review article: gastric electrical stimulation for gastroparesis–physiological foundations, technical aspects and clinical implications. Aliment Pharmacol Ther 30(7):681–694
41. Song GQ, Hou X, Sun Y, Yang B, Qian W, Chen JD (2007) Effects of retrograde gastric electrical stimulation with pulse trains on gastric emptying of solids and plasma hormones in dogs. Am J Surg 194(1):122–127
42. Sun X, Tang M, Zhang J, Chen JD (2006) Excitatory effects of gastric electrical stimulation on gastric distension responsive neurons in ventromedial hypothalamus (VMH) in rats. Neurosci Res 55:451–457
43. Tang M, Zhang J, Chen JDZ (2006) Central mechanisms of gastric electrical stimulation involving neurons in paraventricular nucleus of hypothalamus in rats. Obes Surg 16:344–352
44. Tang M, Zhang J, Xu L, Chen JD (2006) Implantable gastric stimulation alters expression of oxytocin- and orexin-containing neurons in the hypothalamus of rats. Obes Surg 16(6):762–769
45. Vazquez Roque MI, Camilleri M, Clark MM, Tepoel DA, Jensen MD, Graszer KM, Kalsy SA, Burton DD, Baxter KL, Zinsmeister AR (2007) Alteration of gastric functions and candidate genes associated with weight reduction in response to sibutramine. Clin Gastroenterol Hepatol 5:829–837
46. Xing J, Chen JD (2004) Alterations of gastrointestinal motility in obesity. Obes Res 12:1723–1732
47. Xing JH, Chen JD (2006) Effects and mechanisms of long-pulse gastric electrical stimulation on canine gastric tone and accommodation. Neurogastroenterol Motil 18:136–143
48. Xu L, Tang M, Chen JDZ (2005) Effect of gastric electrical stimulation on gastric distention responsive neurons and expression of nNOS in rodent hippocampus. Gastroenterology 128:A624
49. Xu X, Zhu H, Chen JD (2005) Pyloric electrical stimulation reduces food intake by inhibiting gastric motility in dogs. Gastroenterology 128(1):43–50
50. Xu J, Chen JDZ (2008) Effects of sibutramine on gastric emptying, intestinal motility and rectal tone in dogs. Dig Dis Sci 53:155–162
51. Yao S, Ke M, Wang Z, Xu D, Zhang Y, Chen JD (2005) Retrograde gastric pacing reduces food intake and delays gastric emptying in humans: a potential therapy for obesity? Dig Dis Sci 50:1569–1575
52. Yin J, Chen JD (2005) Retrograde gastric electrical stimulation reduces food intake and weight in obese rats. Obes Res 13:1580–1587
53. Yin J, Chen J (2006) Inhibitory effects of gastric electrical stimulation on ghrelin-induced excitatory effects on gastric motility and food intake in dogs. Scand J Gastroenterol 41(8):903–909
54. Zhang J, Chen JD (2006) Systematic review: applications and future of gastric electrical stimulation. Aliment Pharmacol Ther 24(7):991–1002
55. Zhang J, Tang M, Chen JD (2009) Gastric electrical stimulation for obesity: the need for a new device using wider pulses. Obesity 17(3):474–480

56. Zhang J, Maude-Griffin R, Zhu H, Sun Y, Starkebaum W, Firestone E, Chen JD (2011) Gastric electrical stimulation parameter dependently alters ventral medial hypothalamic activity and feeding in obese rats. Am J Physiol Gastrointest Liver Physiol 301:G912–G918
57. Zhu H, Sallam H, Chen DD, Chen JD (2007) Therapeutic potential of synchronized gastric electrical stimulation for gastroparesis: enhanced gastric motility in dogs. Am J Physiol Regul Integr Comp Physiol 293(5):R1875–R1881

Gastric Electrical Stimulation: Twentieth Century Development to Twenty-First Century Implementation and Personalization of Programming

James Griffith, Sumanth Daram, Ben Boatright, Joy Hughes, Christopher J. Lahr, Archana Kedar and Thomas L. Abell

Abstract Gastroparesis is an incompletely understood disorder characterized by vomiting, nausea, abdominal pain, and related symptoms amongst evidence of delayed gastric emptying often refractory to medical therapy. Gastric electrical stimulation (GES), using higher than physiologic frequency and low energy, has been shown to be effective in many patients with refractory symptoms and received Humanitarian Use Device approval in 2000. A meta-analysis suggests GES is effective for symptom control and favorable in gastric emptying, nutritional status, and quality of life analysis. Recent work with endoscopically placed, temporary GES indicates trial stimulation is important in the evaluation of stimulation devices. In addition, approximately 50 % of patients responded to standard settings [4, Neurogastroenterol Motil 18(4):334–338, 2006] while other patients require higher energy settings for optimal response. These recent studies offer the potential for personalization of stimulation parameters in a given patient. For GES to be accepted and adopted on more widespread basis, further evaluation of individual responses to simulation must be determined and then correlated with individual histologic, electrophysiological and biochemical findings to optimally help patients. This chapter will discuss the historical development of current GES therapy.

J. Griffith · J. Hughes
School of Medicine, University of Mississippi Medical Center, 2500 North State Street, Jackson, MS 39216, USA

S. Daram · B. Boatright · A. Kedar · T. L. Abell (✉)
Division of Digestive Diseases, Department of Medicine, University of Mississippi Medical Center, 2500 North State Street, Jackson, MS 39216, USA
e-mail: thomas.abell@louisville.edu

C. J. Lahr
Department of Surgery, University of Mississippi Medical Center, 2500 North State Street, Jackson, MS 39216, USA

L. K. Cheng et al. (eds.), *New Advances in Gastrointestinal Motility Research*, Lecture Notes in Computational Vision and Biomechanics 10,
DOI: 10.1007/978-94-007-6561-0_8, © Springer Science+Business Media Dordrecht 2013

1 Introduction

Some patients with clinical gastroparesis (Gp) remain severely affected by Gp symptoms, including nausea, vomiting, bloating, abdominal pain, and early satiety, despite pharmacologic treatment. In this medically refractory Gp subgroup, gastric electric stimulation (GES) therapy appears to be an effective treatment modality as supported by two meta-analysis review of the literature, further discussed in Sect. 5 of this chapter. Still, GES's role as a therapeutic treatment of gastroproparesis remains controversial.

At present, GES therapy relies on a surgically implanted stimulator or endoscopically implanted electrodes attached to an external device for the delivery of exogenous electrical stimulus. Investigations to determine the exact mechanism through which this stimulus may modify abnormal slow wave activity remain ongoing. However, reports documenting beneficial effects of GES on Gp symptoms, particularly nausea and vomiting, as well as associated improvements in patient-reported quality of life scores, continue to emerge [22, 8]. As investigations demonstrated sufficient evidence of the device's safety along with probable efficacy, the US Food and Drug Administration (FDA) designated GES as a humanitarian device in 2000.

In addition to a brief overview of what is now known about Gp and impaired gastric motility, we will discuss the development and history of (1) surgically implanted, permanent GES, with its delivery of stimulation to the gastric serosa, and (2) temporary GES, with endoscopically implanted leads that deliver stimulation to the gastric mucosa, and finally (3) measures to tailor GES stimulation to an individual patient's needs.

2 Gastroparesis

Despite investigations dating back to 1812 [15], the characterization and appropriate treatment of Gp remain controversial and an area of much ongoing investigation. Kassander is heralded as begetting the term gastroparesis in his 1958 description of gastroparesis diabeticorum in type 1 diabetics with gastric retention [18]. Following a period of research, radiologic gastric emptying scintigraphy became the standard method for evaluating gastroparesis and has since lead to the current clinical definition of gastroparesis: symptoms of and delayed gastric emptying in the absence of mechanical obstruction [23]. However, utilizing new technological advances, the continuous investigation of Gp by several groups of researchers in the 1960's–1980's moved the scientific community's discussions of Gp beyond gastric emptying into the topics of abnormal gastric electrophysiology and associated Gp symptoms [9].

The importance of electrophysiology has grown as the past decade of research demonstrates symptoms manifested by disordered gastric electrophysiology to be

independent from gastric emptying. Furthermore, some patients with symptoms and abnormal histologic and electrogastrogram (EGG) characteristics associated with Gp are found to have normal gastric emptying [24, 14]. As these studies demonstrated limited diagnostic use for gastric emptying studies in identifying gastroparesis, one of the directions for Gp identification turned was investigating electrical recordings of the stomach. With high resolution, electrical recordings from the stomach's serosa, aberrations similar to pathologic electrophysiologic dysfunctions of the heart were identified in patients with known Gp [22]. Appreciation of Gp's multifactorial etiologies prompting electrical abnormalities of the stomach and circumspection of delayed gastric emptying time (GET) as part of the diagnostic assessment has lead to continued controversy for how to define gastroparesis [22, 14, 30].

While debates on Gp's definition and etiologies continue including a recent exchange of expert opinions over potential overlap between diagnoses of functional dyspepsia [17] and gastroparesis [13], experts are increasingly in agreement that deficits of neuromuscular cells within the gastrointestinal tract are the likely pathways contributing to the onset of gastroparesis and the basis for using electrical stimulation as a medical therapy in Gp (see "ICC Network Density: Regulation and Consequences" by Gibbons et al. in this volume for additional information).

3 Electrical Stimulation

The role of electrical stimulation in modulating gastrointestinal electrophysiologic motility deficits has been discussed since its debut as a therapy for post-operative ileus in 1911 [10]. Early application of electricity on the gut continued in the 1960s by Debakey et al. until the practice was abandoned when non-randomized and non-controlled trials did not demonstrate therapeutic benefit in post-operative ileus [25, 6, 29]. However, electrical stimulation in animal studies continued with the goals of re-establishing normal gastric wave rates and rhythms in a manner similar to a cardiac pacemaker [19].

In 1988, Familoni, Abell and Voeller at the University of Tennessee, Memphis conducted an animal study using a custom device to test the ability of different electrical stimulation parameters to 'correct' disordered gastrointestinal function, as measured by implanted manometry and sutured recording GES leads. In the Memphis group's work, high frequency (supraphysiologic) stimulation was superior to low frequency (physiologic) stimulation in the canine stomach for improving gastric motility [12]. After a successful trial in one human subject, the animal study's findings provided the basis for what is now approved as Gastric Electrical Stimulation (GES) therapy [12, 11].

The successful use of high-frequency/low-energy gastric stimulation in this one patient in 1992 led to the submission of a proposal for an *Investigational Device Exemption* (IDE) to the US FDA. With approval gained in 1995, a formal United States trial of the new protocol using an early stimulator from *Medtronic* began,

with parallel trials in Canada and Europe; these trials later came to be known as the *GEMS* study, published in *Digestion* [1]. GES has been used for other non-approved indications, such as the investigational research involving obesity, which is discussed by Yin et al. in "Therapeutic Potential of Gastric Electrical Stimulation for Obesity" of this volume.

4 Trials Leading to Humanitarian Device Status: The *GEMS* and *WAVESS* studies

4.1 GEMS

The international, multicenter *GEMS* study investigated whether GES therapy safely elicits sustained therapeutic benefit [1]. Measures of patient-reported symptoms and gastric emptying time were used to characterize any therapeutic benefit. Patients with documented intractable symptoms for greater than 1 year and significant weight loss despite standard prokinetic and anti-emetic drug therapy were initially recruited for this study, pending exclusion of *DSM-IV* eating disorders. Prokinetic and/or antiemetic medication use was allowed during the study if being taken before the start of the study.

Phase I of the study utilized a novel trial of temporary stimulation placing leads either by endoscopy, laparoscopy, or laparotomy prior to permanent device implantation. Five patients who showed no symptomatic improvement during temporary stimulation were then excluded from Phase II, permanent GES placement, as this procedure was presumed to lack therapeutic benefit for these select patients.

At the conclusion of the *GEMS* trial, no cardiac arrhythmias were observed. The morbidity and infection rates were equivalent to those expected for laparotomy or laparoscopy, and aside from rapid recurrence of symptoms, no severe side effects occurred when the stimulator was inadvertently deactivated. Symptomatically, patients reported rapid and sustained improvements lasting greater than 1-year post-permanent GES implantation along with reduced use of prokinetics, antiemetics, and nutritional support. Gastric emptying improvements greater than one standard deviation from baseline studies only occurred following long-term stimulation. Interestingly, only idiopathic gastroparesis, not diabetic, had improvements in gastric emptying, but as the study noted, any clinical implications of this difference could not be drawn without further investigation.

Although the *GEMS* study demonstrated results indicating GES as a safe method with sustained symptomatic improvements in drug-refractory gastroparesis patients, the finding that 80 % of participating patients have an immediate, antiemetic response to the technique prompted the *WAVESS* trial in which permanent stimulators were implanted directly without prior temporary stimulation [1, 2].

4.2 WAVESS

To determine and standardize normal gastric emptying parameters for the *WAVESS* trial and future studies, a separate initial study was conducted with normal volunteers. This preliminary investigation was eventually published as the low-fat meal, gastric-emptying protocol, now used by many gastroenterologists, in 2000 [27].

This *WAVESS* study, a two month randomized, placebo controlled, double-blinded crossover design followed by conversion to a 10 month open-label study period, was conducted at a number of sites across three continents. After permanent GES implantation, the stimulator was either turned ON or OFF for the first month and then switched to the opposite setting. Patients reported weekly vomiting frequency, symptom severity and health-related quality of life (collected using *HQOL SF-36* Health Status Survey) at one and two month blinded follow-ups along with 6 and 12 month un-blinded evaluations. Prior to becoming an open-label trial, patients stated their preference between the two months. Overall, the results of this trial showed improvements in symptoms, especially weekly vomiting, and *HQOL* when the stimulator was turned ON which became statistically significant at 6 and 12 months during the open phase of the trial. GET improvements were statistically significant at 12 months when patients were analyzed as a cohort and diabetic, but not idiopathic. Similar to the *GEMS* trial, symptom reduction did not correlate to GET improvements in this trial. The original design to this trial was altered as it was initially powered for 80 patients, but due to withdrawal of sponsor funding, only 33 patients were recruited and the trial duration was shortened to what is described above and published in 2002 [2].

At the conclusion of these studies, a humanitarian use device designation for a high frequency, low amplitude gastric electrical stimulator, *Enterra*®, was approved by the US FDA for patients with medication refractory, diabetic and idiopathic gastroparesis [28]. With commercial availability of the stimulator, the *Medtronic Enterra* stimulator has since been implanted in thousands of people worldwide.

5 Trials on GES Efficacy Since HUD Exemption Obtained

Following the approval of GES with Humanitarian Use Device (HUD) exemption, this relatively new treatment modality for drug-refractory gastroparesis has spurred a number of clinical studies summarized in a meta-analysis to evaluate the device's impact on clinical outcomes [22]. In this meta-analysis, studies were screened for duplicate outcomes from a prior published study so as to prevent multiple publication bias, and also those studies, which utilize temporary GES potentially creating selection bias by identifying probable GES responders.

Of the 13 included studies collected from Jan 1992 to Aug 2008, most lacked controls and only one study was conducted using a randomized, blinded design. The GES meta-analysis found statistically significant benefits in patients receiving

GES for refractory gastroparesis including significant reductions in vomiting, nausea, and total symptom severity scores. Validated quality of life scores and dependence on enteral and parenteral nutrition also showed clinical and statistically significant improvements too. Furthermore, this collection of studies showed both an overall improvements in 2 and 4 h gastric scintigraphy that were statistically significant, albeit the 2 h GET range varied greatly between studies. Of note, one study, which was included in this meta-analysis, demonstrated a drastic difference in the survival of patients with diabetic Gp receiving GES implantation when compared to controls that had not yet received stimulation due to insurance approval/reimbursement issues [5]. In this evolution, implanted diabetics' 30-month mean survival was 95.4 %, and that for non-implanted diabetics was 33.3 %. The survival difference for diabetic patients was statistically significant, unlike differences between idiopathic implanted versus non-implanted survivals [5]. Similar significant findings to the 2009 meta-analysis for symptoms and GET were noted in a 2011 meta-analysis [7]. However, the authors in the 2011 meta-analysis felt the strongest impact of GES occurred in patients with diabetic gastroparesis. While the authors of the 2009 meta-analysis do caution data interpretation based on concerns of the quality of evidence lacking controls or shams, they do advocate continued investigations with controlled trials to confirm these potentially significant benefits of GES therapy in drug-refractory gastroparesis.

Designing such randomized, double-masked, placebo controlled cross-over trials to evaluate GES under a higher quality of scientific evidence proved to contain unforeseen complications as the *ENDOStim* trial [3] and *Enterra* clinical trial [21] demonstrated. The 2005–2006 analyzed temporary GES effects over two consecutive 3-day sessions of stimulation and sham-stimulation with a one day washout in between. Two patient groups were formed as one group received stimulation in the first three-day session while the second group received stimulation in the second three-day session. A comparison between the initial session groups demonstrated statistically significant decrease in vomiting which remained statistically significant throughout the washout period as well (Fig. 1—adapted from ref 26). During the second session, vomiting slightly decreased with stimulation and increased without stimulation. However, the compilation of the vomiting scores in this second session was not significant. Similar irregularities in study results were published in the *Enterra* clinical trial, which stimulated patients for a prolonged period followed by sham-stimulation [21]. In both of these studies, possible remodeling while being stimulated may have elicited a potential carry-over into cessation of stimulation results. Based upon these experiences, utilizing parallel groups, longer wash-out periods or stepped-wedge designs should be considered in future double-masked, randomized, placebo controlled trials [3] to help substantiate whether: (1) GES provides clinical benefit to patients with medically—refractory gastroparesis and (2) temporary GES defines the patient subset likely to benefit from permanent stimulation.

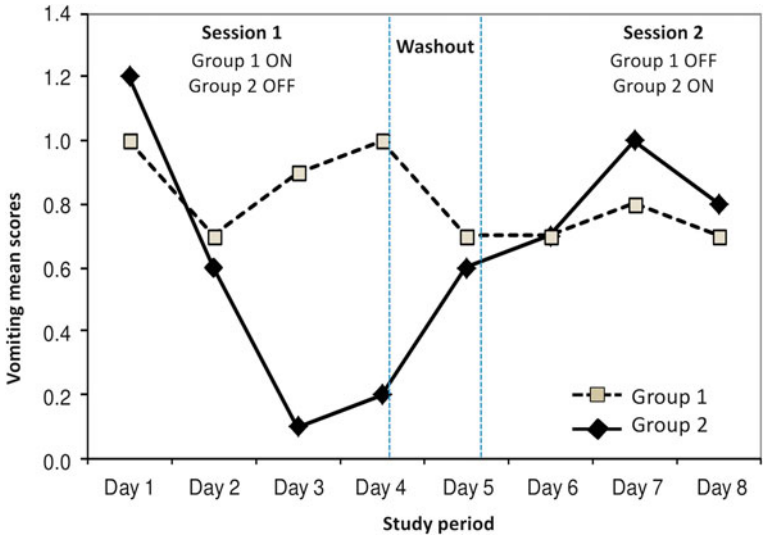

Fig. 1 Vomiting symptom scores for all patients who completed the study

6 Personalization of GES

Patient characterization strategies in the treatment of drug-refractory gastroparesis have evolved with improved understanding of gastroparesis and greater experience treating this disorder with electricity. Upon implantation, GES is initially set to a factory set energy output based upon initial animal work and the published trials used for approval. However, the device is capable of altering the voltage, frequency, duration (both ON and OFF periods), and pulse width; these settings combine to determine the ultimate energy output over a wide spectrum of possible total energies and delivery parameter combinations. Although multiple studies have indicated Gp symptom relief following GES therapy, a subset of these patients implanted with GES fail to respond or do not respond optimally to initial GES energy settings. Similar findings are noted in other fields of electrical stimulation, like thalamic stimulation, where algorithmic-based energy adjustments are implemented to affect symptom outcomes [20].

The team of Abidi, Starkebaum, and Abell hypothesized that energy, like most medications, requires titration to determine the appropriate dose a patient needs. This hypothesis prompted a pilot study, which modified GES stimulation parameters using a step-up energy algorithm, to analyze the dose—response relationship between electrical dose (charge, current, total energy) and symptom relief in GES patients who failed to substantially improve with initial GES energy settings. The results of this preliminary study concluded that changes to GES stimulation parameters might be associated with symptomatic improvements and therefore appropriate energy delivered may vary between patients [4].

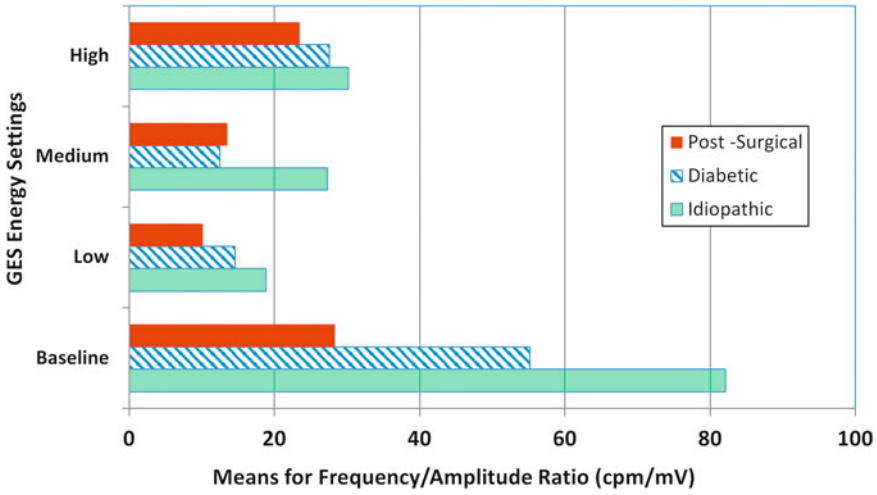

Fig. 2 Frequency/amplitude ratio changes seen at varying energy settings in differing GP etiologies

Still, this post-implantation energy algorithm remains potentially expensive as increases in energy drain the battery supply and may require frequent follow-up adjustment visits. Therefore, queries of how else one may ascertain an accurate assessment of each patient's energy requirements prompted investigations eliciting intra-operative electrogastrogram responses before and during stimulation.

An initial evaluation of intraoperative serosal EGG responses following a sequence of baseline (OFF), then standardized (ON) energy levels of low, medium, and high indicates that gastroparesis patients have abnormal baseline EGG values which immediately begin to change upon activation of GES. Approximately half of the patients in one study obtained maximal normalization in serosal frequency to amplitude ratio (FAR) with low energy [16]. Of the remaining half of patients, approximately half of these demonstrated maximal normalization at medium and the remainder at high energy levels. Figures 2 and 3 demonstrate the numbers of patients who have responded at each energy level, compared to baseline settings.

A follow-up study is presently being conducted to assess whether these observations may help predict patient prognosis, histological findings, and optimal energy range for a rapid and long-term symptom reduction [26].

7 Discussion

GES is a promising new electrophysiologic tool, but many areas of investigation remain before more widespread application of GES is accepted as a mainstay treatment of drug-refractory gastroparesis. For the understanding of Gp and it's

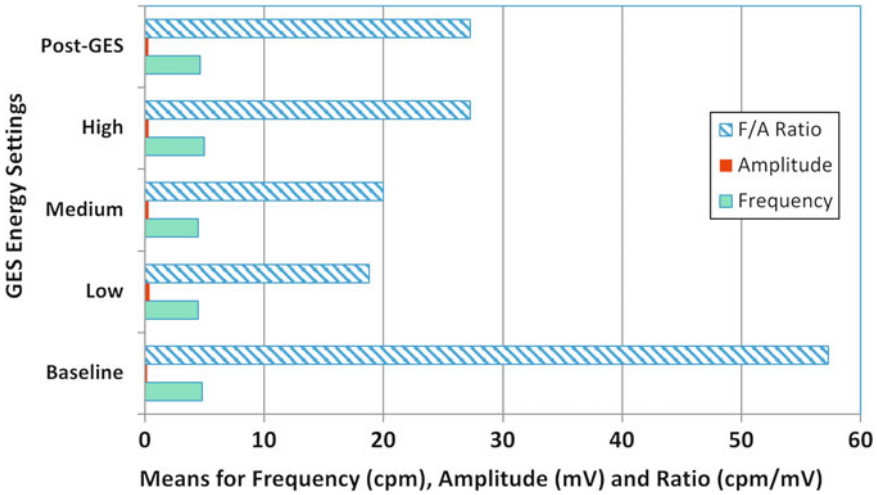

Fig. 3 Electrogastrogram variations in frequency and amplitude in response to varying energy settings

treatments to evolve, further investigations must determine the underlying pathologic neurophysiologic abnormalities manifested via symptoms associated with disordered gastric emptying and their etiologies. Presently, the use of gastric scintigraphy yields limited clinical insight in defining gastroparesis, much like ejection fraction in cardiac disorders. As it is through the electrophysiologic characterization with electrocardiogram that practitioners identify cardiac abnormalities, EGG and high-resolution mapping of the stomach may offer similar benefits in the characterization of gastroparesis. Electrical stimulation of the stomach appears a logical approach for treating what is believed to be an electrical abnormality of the stomach. However, researchers agree that electrophysiology of the stomach is more complicated than that of the heart. Future double blind, randomized, placebo controlled or sham trails are needed to scientifically determine whether GES offers equivalent findings to those found in both published non-controlled investigations and several physicians' anecdotal clinical experience as GES implantation is not without risk.

GES implantation retains standard risks associated with invasive surgery and the additional complication of possible recurrent symptoms after an initial positive results. As with most implanted devices, infections involving the stimulator would require device removal and re-implantation after infection resolution. Re-implantation also is required following battery depletion. Of note, although symptoms resume following battery depletion, new, unpublished electrophysiologic EGG findings comparing initial implantation EGG analysis to those of the battery change operation indicate greater normalization of electrophysiologic slow waves after GES therapy. Caution must be used when interpreting this finding, but this may indicate gastric histologic remodeling. As understanding of gastroparesis progresses

into a better comprehension of underlying histologic changes and their pathologic roles in electrical abnormalities manifested as Gp symptoms, proper characterization for earlier implementation of medical and electrical treatments may ameliorate Gp symptoms and ideally, alter motility abnormalities in gastroparesis.

8 Conclusion

Although gastroparesis has been investigated for nearly 200 years, the advent of gastric electrical stimulation brought about a new series of queries that have provided some insights into the underlying pathophysiology. Most importantly for physicians and patients, GES may offers some symptom relief in this notoriously difficult to treat disease, as non-controlled trials indicate. Better evaluation of individual responses to stimulation and the mechanisms affected by stimulation parameters may lead to better, reliable outcomes.

Acknowledgments The authors would like to thank Evelyn Martin, LPNII and Angela Ashley, LPN I—GES nurses. We would also like to thank the staff of the GI Division, GI Laboratory, Department of Nuclear Medicine and Department of Pathology laboratory at the University of Mississippi Medical Center for their help.

References

1. Abell TL, Van Cutsem E, Abrahamsson H et al (2002) Gastric electrical stimulation in intractable symptomatic gastroparesis. Digestion 66(4):204–212
2. Abell T, McCallum R, Hocking M et al (2003) Gastric electrical stimulation for medically refractory gastroparesis. Gastroenterology 125(2):421–428
3. Abell T, Johnson W, Kedar A et al (2011) A double-masked, randomized, placebo-controlled trial of temporary endoscopic mucosal gastric electrical stimulation for gastroparesis. Gastrointest Endoscopic 74:496–503
4. Abidi N, Starkebaum WL, Abell TL (2006) An energy algorithm improves symptoms in some patients with gastroparesis and treated with gastric electrical stimulation. Neurogastroenterol Motil 18(4):334–338. doi:10.1111/j.1365-2982.2006.00765.x
5. Anand C, Al-Juburi A, Familoni B et al (2007) Gastric electrical stimulation is safe and effective: a long-term study in patients with drug-refractory gastroparesis in three regional centers. Digestion 75(2–3):83–89
6. Chen J, Xu X, Zhang J et al (2005) Efficiency and efficacy of multi-channel gastric electrical stimulation. Neurogastroenterol Motil 17:878–882
7. Chu H, Lin Z, Zhong L et al (2011) A meta-analysis: the treatment of high-frequency gastric electrical stimulation for gastroparesis. J Gastroenterol Hepatol. doi:10.1111/j.1440-1746.2011.06999.x
8. Cutts TF, Luo J, Abell TL et al (2005) Is gastric electrical stimulation superior to standard pharmacologic therapy in improving GI symptoms, healthcare resources, and long-term healthcare benefits? Neurogastroenterol Motil 17:35–43
9. Daram S, Abell T (2011) A brief history and future directions for permanent, temporary, and endoscopic GES. In: Parkman HP, McCallum RW (eds) Gastroparesis: pathophysiology, presentation, and treatment. Springer Science+Business Media, New York

10. Dieffenbach W (1911) Electric treatment of intestinal obstruction and postoperative paralysis of the bowel. J Am Med Assoc 56(13):958–959
11. Familoni BO, Abell TL, Nemoto D et al (1997) Efficacy of electrical stimulation at frequencies higher than basal rate in canine stomach. Dig Dis Sci 42(5):892–897
12. Familoni B, Abell T, Gan Z, Voeller G (2005) Driving gastric electrical activity with stimulation. Ann Biomed Eng 33(3):355–363. doi:10.1007/s10439-005-1738-6
13. Gastroparesis Clinical Research Consortium (2011) Clinical features of idiopathic gastroparesis vary with sex, body mass, symptom onset, delay in gastric emptying, and gastroparesis severity. Gastroenterology 140(1):101–115
14. Grover M, Farrungia G, Lurken M et al (2011) Cellular changes in diabetic and idiopathic gastroparesis. Gastroenterology 140:1575–1585
15. Heberden W (1806) Commentaries on the history and causes of diseases, 3rd edn. Payne and Foss London, United Kingdom
16. Hughes JD, Griffith J, Lahr CJ et al (2011) Intraoperative electrogastrogram and longitudinal symptom scores following gastric stimulation for gastroparesis. Abstract nr 76. The international neuromodulation society 10th world congress, London, England
17. Janssen P, Oudenhove L, Bisschops R, Tack J (2011) Idiopathic gastroparesis or functional dyspepsia with delayed gastric emptying: where is the difference? Gastroenterology 140(7):2145–2146
18. Kassander P (1958) Asymptomatic gastric retention in diabetics (gastroparesis diabeticorum). Ann Intern Med 48(4):797–812
19. Kelly KA, Code CF (1971) Canine gastric pacemaker. Am J Physiol 220(1):112–118
20. Mair R, Onos K, Hembrook J (2011) Cognitive activation by central thalamic stimulation: the Yerkes-Dodson law revisited. Dose Response 9(3):313–331. doi:10.2203/dose-response.10-017.Mair
21. McCallum R, Snape W, Brody F et al (2010) Gastric electrical stimulation with enterra therapy improves symptoms from diabetic gastroparesis in a prospective study. Clin Gastroenterol Hepatol 8(11):947–954.e1
22. O'Grady G, Egbuji JU, Du P et al (2009) High-frequency gastric electrical stimulation for the treatment of gastroparesis: a meta-analysis. World J Surg 33(8):1693–1701
23. Parkman HP, Hasler WL, Fisher RS (2004) American Gastroenterological Association technical review on the diagnosis and treatment of gastroparesis. Gastroenterology 127:1592–1622
24. Pasricha P, Colvin R, Yates K et al (2011) Characteristics of patients with chronic unexplained nausea and vomiting and normal gastric emptying. Clin Gastroenterol Hepatol 9:567–576
25. Quast D, Beall A, DeBakey M (1965) Clinical evaluation of the gastrointestinal pacer. Surg Gyn Obs 120:135–137
26. Soffer E, Abell T, Lin Z et al (2009) Review article: gastric electrical stimulation for gastroparesis—physiologic foundations, technical aspects and clinical implications. Aliment Pharmacol Ther 30:681–694. doi:10.1111/j.1365-2036.2009.04082.x
27. Tougas G, Eaker EY, Abell TL (2000) Assessment of gastric emptying using a low fat meal: establishment of international control values. Am J Gastroenterol 95(6):1456–1462
28. United States Food and Drug Administration (2000) Device approvals and clearances: enterra therapy system. http://www.accessdata.fda.gov/scripts/cdrh/cfdocs/cftopic/pma/pma.cfm?num=H990014. Accessed Dec 20 2011
29. Yin J, Chen J (2006) Inhibitory effects of gastric electrical stimulation on ghrelin-induced excitatory effects on gastric motility and food intake in dogs. Scand J Gastroenterol 41(8):903–909
30. Zarate N, Farmer A, Grahame R et al (2010) Unexplained gastrointestinal symptoms and joint hypermobility: is connective tissue the missing link? Neurogastroenterol Motil 22(3):252–278

Biomagnetic Signatures of Gastrointestinal Electrical Activity

L. Alan Bradshaw, Juliana Kim, Leo Cheng and William Richards

Abstract Current flow in the cellular syncytium of the gastrointestinal tract results in measurable magnetic fields as well as the more commonly measured electrical potentials. While electrogastrography allows assessment of slow wave frequency dynamics, physical limitations introduced by abdominal volume conduction present situations in which magnetic field measurement may prove advantageous. For the gastric slow wave, spatiotemporal characteristics associated with propagation may be more easily ascertain magnetically. In the intestine, smaller signal strength coupled with the conductivity profile of the abdomen make the biomagnetic approach attractive. In this chapter, we present the historical and theoretical background of recording biomagnetic fields, explore how electrical activity in the stomach and small bowel are reflected in extracorporeal magnetic measurements and how mathematical modeling is helping to elucidate the sophisticated relationships between gastrointestinal physiology and external potentials and magnetic fields.

Abbreviations

EENG	(Electroenterogram)
EGG	(Electrogastrogram)
EMG	(Electromyogram)
GI	(Gastrointestinal)
ICA	(Independent Component Analysis)
MENG	(Magnetoenterogram)
MEG	(Magnetoencephalogram)

L. A. Bradshaw (✉) · L. Cheng
Department of Surgery, Vanderbilt University, Nashville, TN, USA
e-mail: alan.bradshaw@vanderbilt.edu

J. Kim · L. Cheng
Auckland Bioengineering Institute, The University of Auckland, Auckland, New Zealand

W. Richards
Department of Surgery, University of South Alabama, Mobile, AL, USA

L. K. Cheng et al. (eds.), *New Advances in Gastrointestinal Motility Research*,
Lecture Notes in Computational Vision and Biomechanics 10,
DOI: 10.1007/978-94-007-6561-0_9, © Springer Science+Business Media Dordrecht 2013

MGG (Magnetogastrogram)
MSR (Magnetic Shielded Room)
PCA (Principal Component Analysis)
PPD (Percentage Power Distribution)
SOBI (Second Order Blind Identification)
SQUID (RF-SQUID; DC-SQUID)

From the time of the discovery of electrical activity in biological tissue, scientists and clinicians have recognized the potential of this measure of biological function to provide noninvasive assessment of health and disease. Walter Alvarez was the first to record gastrointestinal (GI) electrical activity and noted its correlation with physiological parameters [5]. Nearly a century later, many others have studied the electrical activity of the GI system with invasive electrodes in the serosa and mucosa of the tissue as well as with less invasive body surface electrodes that record the electrogastrogram (EGG) from the stomach or electroenterogram (EENG) from the small bowel [15–19].

The electrical potentials measured by these techniques result from the flow of intra- and extra-cellular currents, which also produce magnetic fields. The ability to detect biological magnetic fields is a much newer development, dating back only about 40 years. The refinement of the electronics and technology required for sensitive magnetic field detection has led to tremendous increases in sensitivity of magnetometers, so that the magnetic detection of GI slow waves is routinely feasible. However, biomagnetometers generally tend to be much more expensive than their electrical counterparts. For researchers and clinicians, the utility of magnetic detection boils down to information content. Are there critical physiological parameters that can be measured only by magnetic detection methods or by the combination of magnetic and electric detection?

1 History and Background

1.1 Slow Waves

After Alvarez's first recording of the electrogastrogram [4], more than 50 years elapsed before its gastric origin was demonstrated conclusively [15] with only a handful of researchers working on the problem during that period (summarized in [25]). In the past 35 years, electrogastrography (EGG) research has revealed significant new information about the electrical activity of the stomach, and recently, the pace of this research has accelerated, although EGG itself appears to be declining in popularity among researchers because of its limited clinical impact [8].

The role of interstitial cells of Cajal (ICC) and their interaction with smooth muscle in generating and propagating gastrointestinal (GI) slow waves continues

to interest researchers. As explained by Beyder et al. in "New Advances in Gastrointestinal Motility Research" and Gibbons et al. in "Role of Ion Channel Mechanosensitivity in the Gut: Mechano-Electrical Feedback Exemplified by Stretch-Dependence of $Na_v1.5$" of this volume, slow waves are believed to depend on the well-coupled electrical syncytium formed by ICC and smooth muscle cells. In the stomach, slow waves appear near the proximal corpus and propagate aborally toward the pylorus. This activity seems to be omni-present with a frequency of about 3 cycles per minute in humans. Although it was formerly thought that one slow wave terminated in the pylorus as another originated in the antrum, recent data have challenged this assumption with multiple simultaneous slow waves being observed [47, 53].

In addition to the slow wave which appears to regulate motility, spiking activity superimposed on the slow wave correlates with muscle contraction [70, 28]. Although spiking activity results in a power increase in EGG signals, it has not been observed directly in the EGG in normal humans [2–6].

1.2 The Electrogastrogram

Slow waves result from current flow in the gastrointestinal musculature which gives rise to extracellular potentials. The EGG is the cutaneous summation of electric potential from underlying gastric slow waves recorded with electrodes on the body surface. EGG frequencies reflect those recorded in serosal electrodes [70, 35], but other EGG parameters like amplitude and propagation velocity do not correlate as well [35]. The electroenterogram (EENG) records the electrical activity from the intestine and is much more difficult to record because of the presence of abdominal tissue layers and the underlying intestinal activity is much weaker in amplitude. The abdomen is a volume conductor, and alternating low- and high-conductivity abdominal layers can attenuate and distort the slow wave reflected in the EGG and EENG [10].

The EGG is capable of recognizing severe gastric disease involving musculature uncoupling by evaluation of spectral power distribution [1], and the absence of postprandial increases in signal amplitude may be clinically significant [68]. However, pathological conditions that disrupt normal spatiotemporal patterns in slow wave propagation remain difficult to distinguish with EGG because of the loss of spatial resolution from abdominal volume conduction [76]. The fundamental technical limitations of the EGG include the inability to reliably detect and distinguish events such as contraction, propagation and uncoupling. Until these issues are addressed, the EGG will not enjoy widespread clinical acceptance [8]. Since the intracellular currents associated with slow waves create magnetic fields as well as electric potentials, evaluation of the slow wave magnetic field may supplement or complement the information available in the EGG.

1.3 Biomagnetism

In 1962, while a graduate student at Cambridge University, Brian Josephson postulated that a supercurrent could penetrate a physical barrier by quantum tunneling [43]. A Superconducting QUantum Interference Device (SQUID) is a superconducting loop that contains one (RF-SQUID) or two (DC-SQUID) of these barriers, called Josephson junctions. A sufficient bias current in the SQUID loop can cause a voltage to appear across the Josephson junction. External flux applied to the SQUID will induce a screening current which causes the current in the SQUID to oscillate as a function of the applied flux. The relationship between applied flux and voltage across the junction can be linearized so that the voltage detected across the junction is directly related to the applied flux. In other words, a SQUID is a magnetic flux-to-voltage converter that operates at a level of sensitivity in the quantum realm [43].

Due to the extreme sensitivity of SQUIDs to magnetic fields, they are ideal for detection of biological activity (Fig. 1). The magnetocardiogram was the first biological signal detected magnetically with conventional induction coils in the 1960s [7]. However, these signals were too noisy to support clinical interest. The implementation of a SQUID magnetometer by Cohen et al. [21] provided low-noise MCG signals that were clinically relevant. Soon after, the magnetoencephalogram (MEG) was measured [69], and since then, researchers have used SQUIDs to measure magnetic fields from a multitude of bioelectrically active sources,

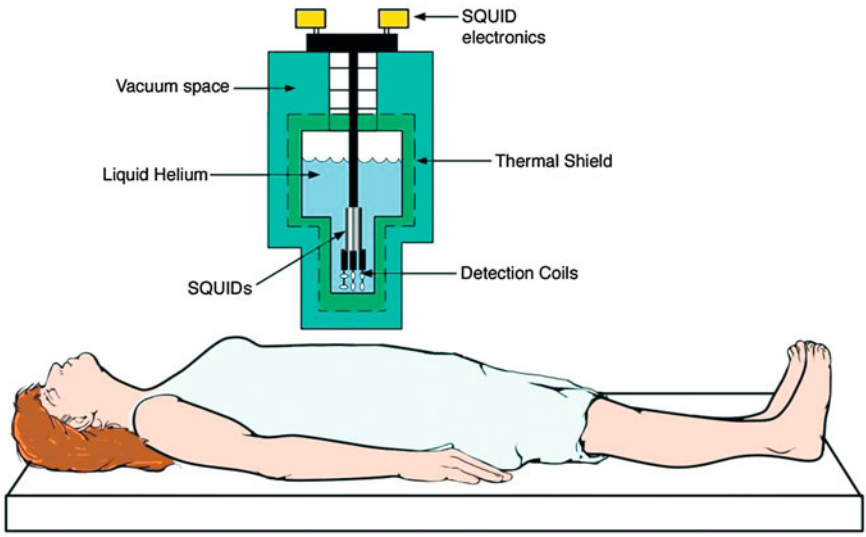

Fig. 1 To record MGG or MENG, a SQUID magnetometer is placed above the subject's abdomen. Magnetic fields incident on detection coils at the bottom of the liquid-helium filled dewar are converted to voltage signals by the SQUIDs. These signals may then be amplified, digitized and recorded

including peripheral nerves [63, 69], skeletal muscle [63], fetal heart [71], and fetal brain [67].

The magnetogastrogram (MGG) from the gastric slow wave in humans was first recorded in 1989 by DiLuzio et al. [26], and our group was the first to record the magnetoenterogram (MENG) from guinea pig small intestine in 1993 and from human subjects in 1996 [64, 65]. In those studies, we saw slow wave activity in every subject and also saw spiking activity in animal subjects.

2 The Magnetogastrogram

A number of studies have shown that the MGG records the same gastric slow wave activity detected by serosal or mucosal electromyogram (EMG) [11−72]. Figure 2 shows simultaneous recordings from a mucosal electrode in a human subject and from the SQUID magnetometer positioned above the subject's abdomen. Our group has also observed a high correlation between mucosal EMG and MGG. In animal subjects, waveform correlations of 80–90 % were commonly observed [11, 14].

2.1 MGGs and Noise

Although the MGG can be easily identified in unfiltered SQUID recordings, the use of filtering and/or noise reduction techniques greatly enhances the ability to characterize slow wave activity. The magnetic signal from the gastric slow wave has a magnitude of only a few picoTesla (pT), which is about five orders of magnitude smaller than the earth's magnetic field. Additionally, other confounding ambient signals are typically encountered, from 60 Hz power line sources to magnetic fields of metal object moving near the magnetometer.

One of the prime challenges in isolating the slow wave signal in MGG recordings is the low frequency. In the sub-1 Hz frequency range, electronic 1/f noise, also known as flicker noise, can be an issue [44], but in our experience, these noise levels are substantially lower than the gastric slow wave magnitude. Johnson noise in circuits nearby magnetic sensors as well as shot noise are potential noise sources, but most SQUID magnetometers are optimized to account for these [41, 73].

Currently, dc-SQUIDs with sufficient sensitivity for detecting pT GI activity use low-Tc (low-critical-temperature) superconductors which require liquid helium for cooling. The use of a magnetically shielded room (MSR) also assists in reducing the level of ambient magnetic noise. High-Tc superconductors could be operated with ambient magnetic noise present, and although these sensors are capable of detecting stronger biomagnetic activity such as MCG, they are presently not capable of detecting the weaker magnetic fields associated with the gastric slow wave.

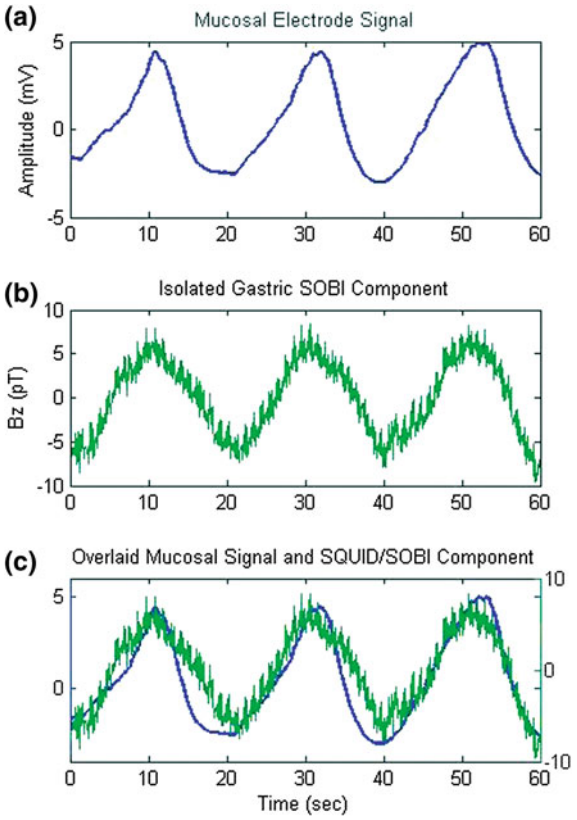

Fig. 2 **a** One-minute sample of gastric mucosal electrical recording; **b** Gastric slow wave component isolated by SOBI from a MGG recording; **c** Overlay. There is high correlation between mucosal potential recordings from the nasogastric catheter electrodes and the SQUID magnetometer

In addition to the use of an MSR, detection coils that are coupled to SQUIDs are usually configured as gradiometers. This configuration subtracts steady magnetic fields recorded in differential coils and leaves mostly intact the fields from nearby biological sources.

Finally, the use of filtering and/or signal processing techniques reduces both ambient and biological interference. Techniques such as digital filters, independent components analysis (ICA), vector projection, and most recently, second-order blind identification (SOBI) are used to separate signatures from gastric and/or intestinal sources from cardiac, respiratory and motion artifact [29–42].

2.2 Spiking Activity in MGG Signals

The MGG can record spiking activity (as described by Angeli et al. in "The Electrical Regulation of GI Motility at the Whole-Organ Level" of this volume) as well as slow waves. One of our group's earliest studies on guinea pig small intestine demonstrated that MENG could detect spiking activity [72]. It has also

been shown that PCA applied to MGG could distinguish signal components associated with spiking activity from regular slow wave components in normal human subjects [40]. Spiking increased postprandial, occurring in 61 % of analyzed segments compared with 41 % preprandial.

2.3 MGG Spatial Mapping and Vector MGG

Among the attractive features of magnetogastrography is the ability to record simultaneous signals from a large number of detectors with minimal subject preparation. In magnetoencephalography (MEG), systems with as many as 300 detectors arranged in a helmet-shaped dewar are able to record brain activity from the entire cortex [45]. SQUID systems best suited for MGG have a relatively flat dewar that can be positioned close to the subject's abdomen. The Tristan model 637 magnetometer system is employed at Vanderbilt, consisting of a flat dewar with 37 magnetic sensors. Nineteen of these sensors are arranged in a hexagonal close-packed array at the bottom of the dewar and oriented to detect magnetic field components normal to dewar surface.

Mapping the magnetic fields detected at specific sensor locations allows determination of the spatiotemporal properties of the gastric slow wave. A spatial map from an MGG recording in a healthy subject using a 61-channel SQUID system is shown in Fig. 3. The 3 cpm slow wave is evident in the upper part of the array, near the epigastrium, whereas smaller-amplitude, higher-frequency slow waves associated with intestinal activity can be seen in the lower parts of the array.

The magnetic field is a vector quantity, and sensors in orthogonal orientations can detect different components of the magnetic field vector. In addition to the 19 sensors that record normal to the dewar, the Tristan 637 also contains ten sensors at the bottom of the dewar oriented tangential to the surface that record the additional two magnetic field components, for full vector detection at five locations.

Vector MGG provides sensitivity to signal components with magnetic signatures orthogonal to conventional normal component detectors. One can project orthogonal magnetic field vector components into particular directions to optimize the recording of a particular signal or signal feature. This allows the distinction between gastric and intestinal magnetic fields in a single three-component vector recording. Further, different projections corresponding to healthy and diseased tissue can be identified. The method was also used to identify particular features of fetal cardiac signals [13]. Recording of a single magnetic field component alone results in the loss of information compared with vector recording.

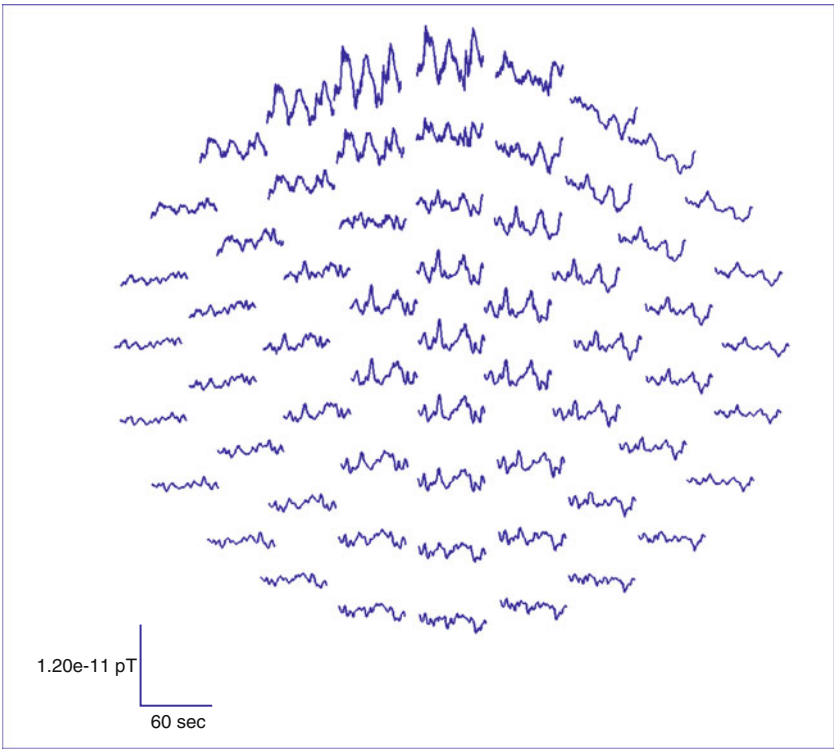

Fig. 3 Biomagnetic recording of gastrointestinal activity from a 61 channel SQUID system. Gastric slow waves at 3 cpm are seen in the upper part of the array near the epigastrium, whereas lower frequency signals from intestinal slow waves appear in the lower abdomen

2.4 MGG In Disease

MGGs from normal subjects exhibit regular 3 cpm slow waves that may be consistently detected provided a suitably low noise environment. As described by Angeli et al. in "The Electrical Regulation of GI Motility at the Whole-Organ Level" of this volume, disease states can alter slow wave activity and thus, affect MGG signals. SQUIDs have been used to measure the MGG during the abnormal situations of mechanical tissue uncoupling, electrical uncoupling following vagotomy, pharmacological uncoupling of the electrical syncytium and in patients with gastroparesis. In each case, changes in dominant signal frequency, in the percentage of power distributed (PPD) in specific ranges of frequencies, and effects on slow wave propagation are reflected in MGG.

2.4.1 Effect of Vagotomy and Mechanical Uncoupling

MGGs recorded before and after transection of the vagus nerve demonstrate no change in the dominant signal frequency; however, multiple peaks in frequency spectra are evident. PPDs show lower overall energy distributed in more tachygastric frequencies [11]. These results alone might lead to the conclusion that vagotomy causes tachygastria, but further spatiotemporal analysis of MGG data suggested that adjacent channels exhibited less coupling and consistency of signal post-vagotomy. Even though a significant increase in power distributed in bradygastric frequencies was not observed, other signal processing methods nonetheless indicate uncoupling [11].

Mechanical division of the stomach results in similar signal effects, but with some interesting differences. While no change in dominant frequency was observed there was still an overall decrease in signal power, but with power distributed preferentially in bradygastric frequency ranges [14]. No significant increase in tachygastric PPD was observed either in serosal electrodes or MGG data.

In the mechanical uncoupling experiments, our group used the surface current density (SCD) technique [41] to assess slow wave propagation in the MGG (refer to Sect. 4.1 for additional details). The SCD method calculates current density maps from the recorded magnetic field values that could be used to identify the location of the underlying sources more effectively than using magnetic field maps directly. Our recent studies have also suggested that SCD may resolve GEA propagation velocity in both simple simulations and experimental recordings [14, 73]. Figure 4. shows successive time points in the spatial maps of SCD computed from MGG data with signal energy represented as grayscale intensity. Figure 4a represents the baseline recorded before mechanical division and Fig. 4b shows the post-division signal. Regular left–right propagation (from subject's left to right), evident in the pre-division maps, is absent in post-division SCD sequences. Therefore, although frequency analysis alone might suggest bradygastria, our ability to analyze spatiotemporal variations in biomagnetic fields again suggests tissue uncoupling.

2.4.2 Gastroparesis

Patients with diabetic gastroparesis demonstrate different MGG patterns than normal control patients. As with earlier gastric studies, no significant difference in dominant gastric slow wave frequency was observed, but more power was distributed in tachygastric frequencies from MGG slow waves with patients than with controls, and a borderline significant increase was seen in bradygastric frequencies. For these data, SOBI signal classification was employed to identify propagation in the MGG. Figure 5 shows that normal controls exhibited regular left–right (subject's left to right) slow wave propagation. In patients (Fig. 5b–d), several different modes of MGG slow wave propagation were apparent. Most patients exhibited retrograde propagation patterns, but occasionally, static or

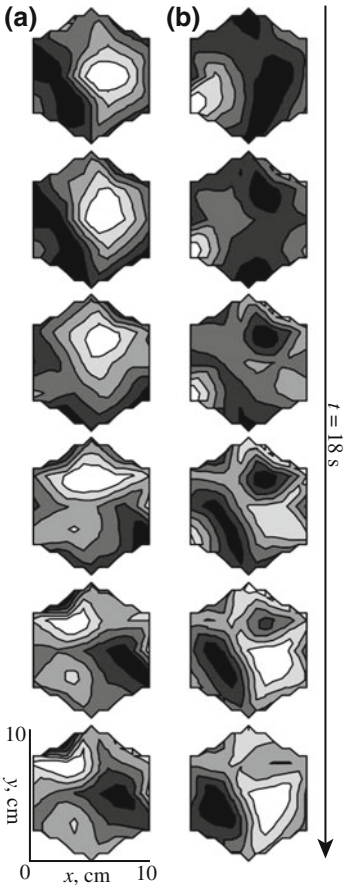

Fig. 4 An 18-s sequence of spatial grayscale maps of SCD from MGG data (**a**) *before* and (**b**) *after* mechanical division of the stomach. *Before* division, activity propagates monodirectionally from *left* to *right* across the abdomen. Similar patterns are seen in successive 20 s intervals corresponding to regular slow wave propagation. *After* division (**b**), activity is erratic and does not exhibit normal *left–right* propagation. Maxima in SCD maps can be computed to estimate propagation velocity

rotational patterns were observed. This study involved only a small number of gastroparesis patients, so additional studies are needed to ascertain the significance of different types of propagation patterns in these patients, and to determine whether these different patterns correlate with variety or severity of disease.

3 The Magnetoenterogram

Due to the volume conducting properties of the abdomen and the low amplitude of the underlying slow wave activity, the electroenterogram (EENG) is functionally unrecordable except in unusual circumstances. Abdominal tissue layers with alternating low- and high conductivity distort and attenuate the electric potential. Magnetic fields respond primarily to tissue geometries and are not as affected by conductivity differences. While EGG can accurately reflect temporal

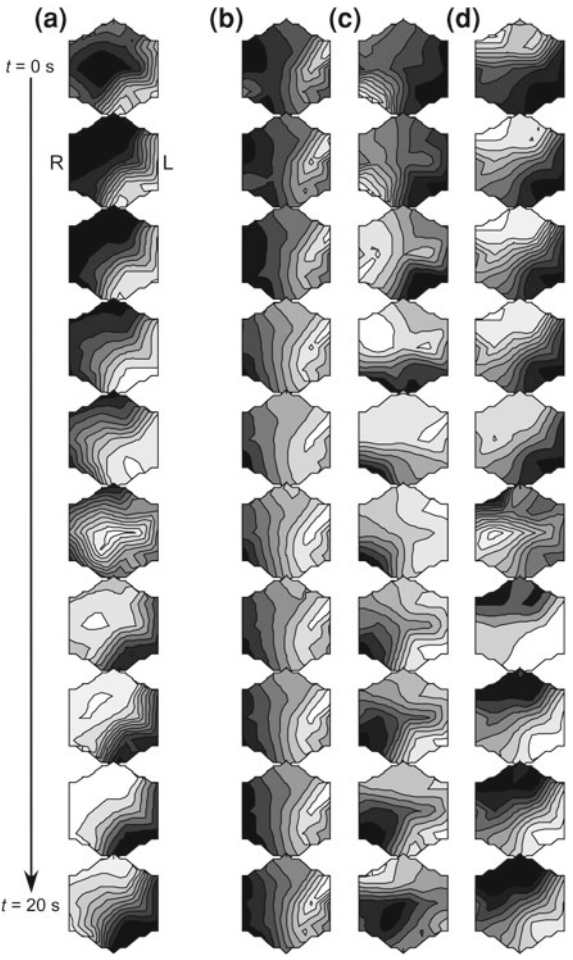

Fig. 5 SOBI propagation maps for a normal subject (**a**) and for three gastroparesis patients (**b**–**d**). Control subjects exhibit normal *left–right* slow wave propagation while the gastroparesis subjects exhibited static (**b**), rotational (**c**) and retrograde (**d**) slow wave propagation patterns

characteristics of the gastric slow wave, the presence of low-conductivity omentum combined with the lower signal power from intestinal sources reduce the signal-to-noise ratio substantially. Thus, the use of EENG has generally been limited to situations where the bowel source is electrically connected to the abdomen, although one group has had interesting results recently using Laplacian electrodes [12]. Curiously, the slow wave frequencies reported in these studies correspond to those of lower intestinal sources; this raises questions about the possible shielding of upper intestinal sources by layers of fat (omentum) that serves as an effective electrical insulator.

3.1 MENG Reflects Intestinal Serosal EMG

Simultaneous signals from the serosal EMG, EENG and transabdominal MENG in small and large animal models (rabbits, pigs) show high correlations between all three signal modalities, even to specific waveform features (see Fig. 2). In a study with rabbits, the slow wave frequencies determined from MENG had a correlation coefficient of 0.97 with serosal EMG slow wave frequencies, and EENG frequencies were similarly correlated [58]. To evaluate the effect of low-conductivity abdominal layers, a layer of surgical latex was inserted between the small bowel and the abdominal wall. Correlations between serosal EMG and MENG remained high, while EENG signals were greatly reduced in slow wave content and dominated by confounding bioelectric sources (Fig. 6).

3.2 MENG Frequency Maps Show Spatiotemporal Electrophysiology

SQUID magnetometers record all magnetic fields incident on the pickup coils at the bottom of the dewar. Although the Tristan 637 magnetometer has an 8-element noise cancellation array in hardware, we have found adaptive noise cancellation

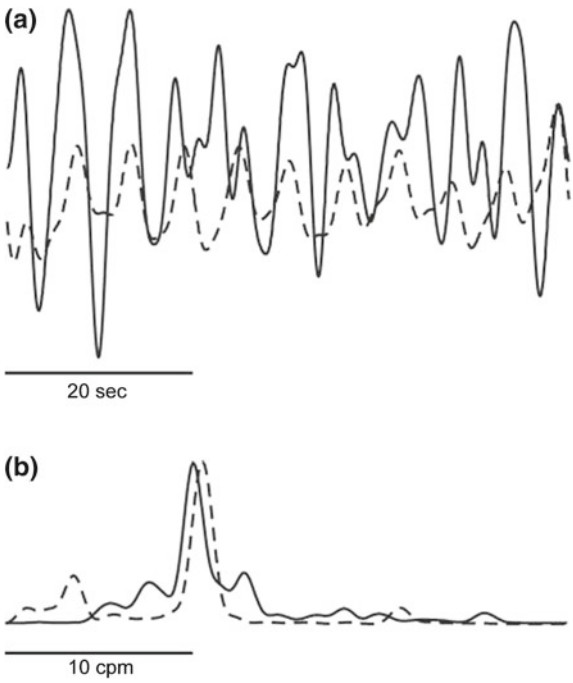

Fig. 6 Enteric slow waves recorded by MENG (*solid*) and serosal electrodes (*dashed*) show similar frequencies both in temporal waveforms (**a**) and in power spectra (**b**)

using these sensors insufficient for separating and classifying signals from distinct intestinal sources. To address noise issues, a Second Order Blind Identification (SOBI), a blind source separation technique, can be applied to the signals [29]. SOBI was more robust to separation and identification of biological and non-biological noise sources when compared with ICA. This method allows SOBI components to be identified from raw or filtered SQUID data (Fig. 7). One then either selects components to retain or to eliminate, and reconstructs the SQUID signal at each sensor location.

The multichannel capacity of the SQUID magnetometer allows investigation of the spatial properties of activity from different intestinal segments by creating isoharmonic spatial maps of the signal strength at various frequencies. Using either FFT or AR spectral analysis of each channel in the detector array, the activity in different frequency bins between 7 and 13 cpm with a bandwidth of 1 cpm is displayed. As shown in Fig. 8, activity from different parts of the intestine highlights different areas in the maps. The higher intestinal slow wave frequencies typical of proximal duodenum appear in the spatial maps between 10 and 12 cpm in the upper abdominal region, while the lower terminal ileum slow wave frequencies appear in the lower abdomen, consistent with the known bowel locations. Spatiotemporal analysis applied to these data identifies specific bowel components of interest.

We used these techniques to examine data in porcine subjects before and after enterectomy and colectomy. The results of our studies, in addition to providing conclusive evidence of the enteric and colonic origin of these signals, allowed us to map the location of different parts of the intestine using spatial maps similar to those illustrated in Fig. 8. Enteric and SOBI components, which were prominent in pre-surgical data, disappeared after organ removal (Fig. 9). Further, the frequencies we measured by SOBI agreed with internal serosal electrodes [9].

3.3 MENG Detects Mesenteric Ischemia

Mesenteric ischemia is a notoriously difficult diagnosis because there is no non-invasive radiologic, nuclear medicine imaging or biochemical test that will confirm the diagnosis once suspected on clinical grounds [30]. Most often, the diagnosis of mesenteric ischemia is made only during an invasive surgery that allows for visual inspection of the bowel. Thus, most patients have advanced disease and the surgeon finds an unsalvageable situation in which the only option is to resect necrosed bowel.

We determined that SQUIDs can detect progressive ischemia. Using porcine subjects, we caused progressive occlusion of mesenteric vessels at levels of 0, 50, 75, 90, and 100 %, and we observed the resulting serosal electric and SOBI-processed SQUID data. As Fig. 10 shows, our studies revealed that SQUIDs, identical to serosal electrodes, identified the frequency decrease associated with mesenteric ischemia at levels of 90 % occlusion [55].

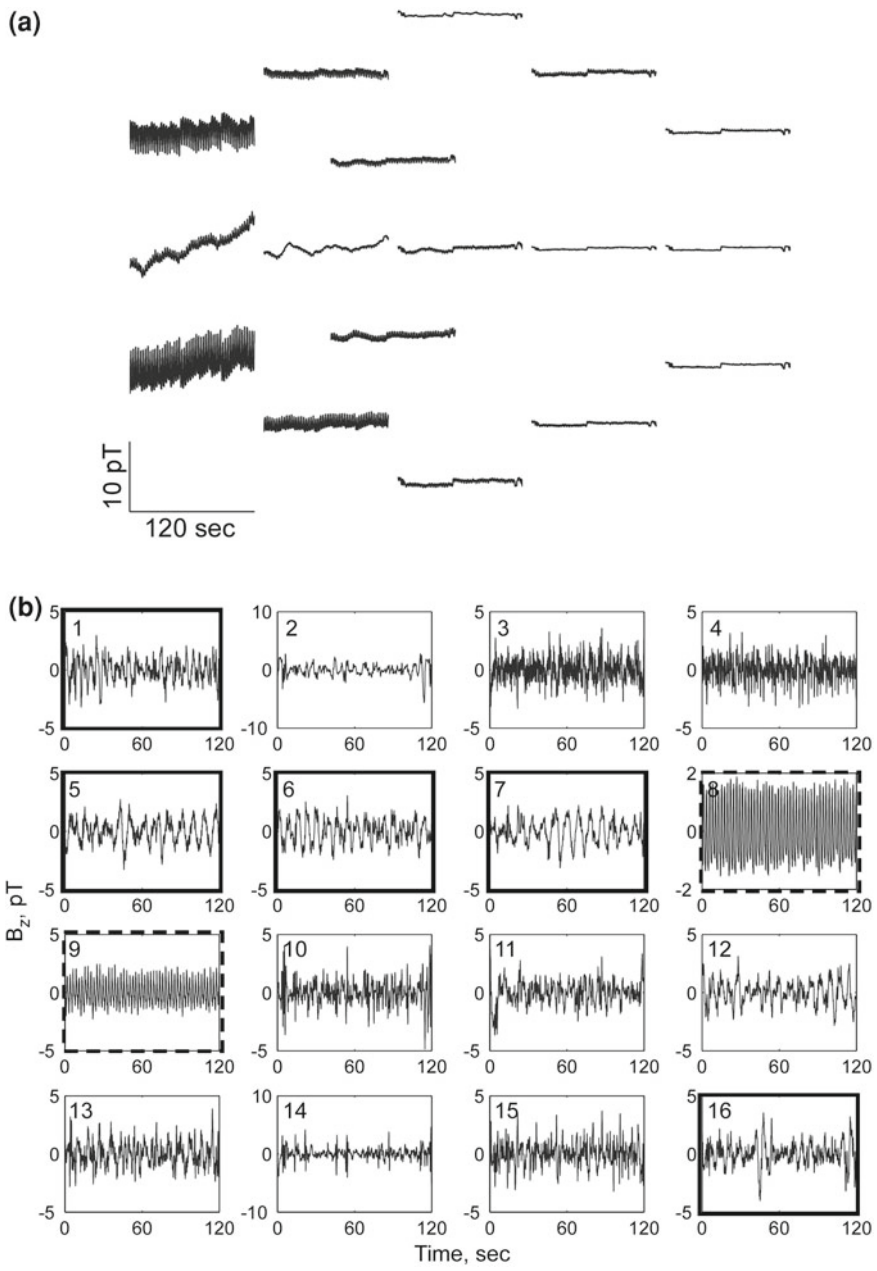

Fig. 7 **a** Raw SQUID data contains magnetic fields associated with small bowel electrical activity, but also is contaminated by respiration, cardiac, motion artifact and ambient magnetic noise. **b** SOBI applied to filtered data allowed us to identify intestinal components (signals 2, 5, 8, and 10) and respiration (signals 4 and 11). These components can then be selected for further analysis or noise components can be eliminated

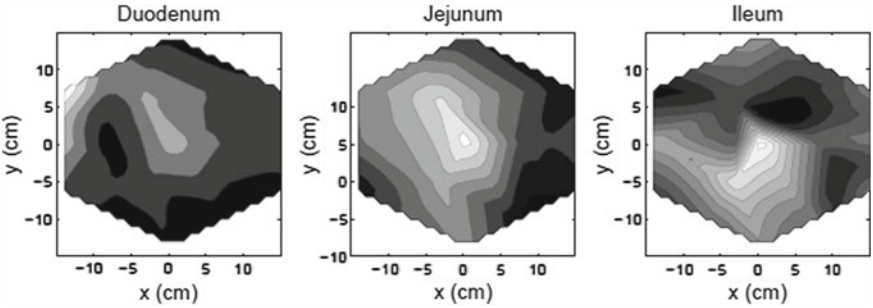

Fig. 8 Isoharmonic activity maps from reconstructed magnetoenterogram (MENG) data illustrate the relative anatomical location of duodenum, jejunum and ileum

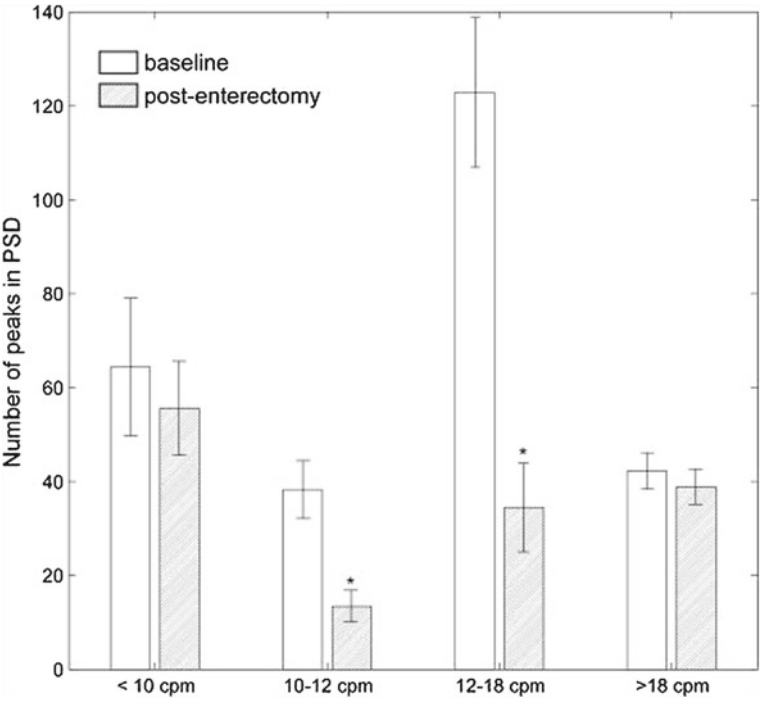

Fig. 9 SOBI-processed MENG data show that enteric frequencies between 10 and 18 cpm disappear after enterectomy while other signal components remain. The frequency range of 10–12 cpm corresponds to activity in the lower intestines (ileum) while 12–18 cpm corresponds to duodenum and jejunum activity

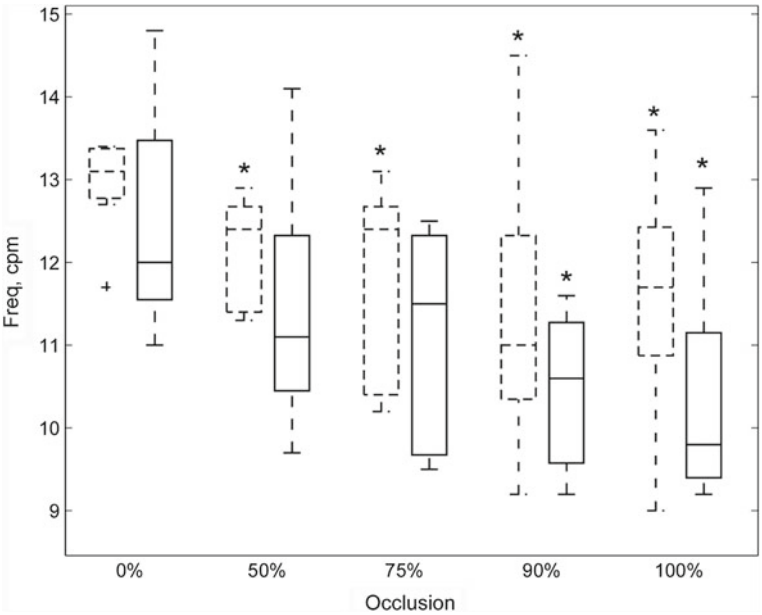

Fig. 10 SOBI shows that progressive ischemia causes lowering of the slow wave frequency as occlusion of the mesenteric artery is increased from 0 to 100 % in both SQUID (*solid*) and serosal electrodes (*dashed*). Thus, biomagnetic techniques accurately track the slow wave frequency during ischemia

3.3.1 Human Studies of Chronic Mesenteric Ischemia

Our group has conducted pre-, intra- and post-operative studies on a patient with chronic mesenteric ischemia. Intestinal slow waves were recorded using invasive serosal electrodes and correlated these with recordings from noninvasive SQUID magnetometer in pre- and post-operative studies. In the intraoperative recording, we observed normal serosal intestinal slow wave frequencies in the non-ischemic segments, and detected multiple frequencies (brady, normo- and tachyarrythmic frequencies of 7.0, 12.0, 14.3, and 19.4 cpm) from the ischemic portion of the ileum. The preoperative biomagnetic recordings also showed signals with multiple frequencies suggestive of uncoupling and intestinal ischemia similar to the intra-operative serosal recordings [32]. These preliminary data suggest that non-invasive SQUID magnetometer recordings could someday be used to detect pathologic signals of intestinal ischemia long before irreversible changes occur. Earlier diagnosis may be associated with dramatic improvements in outcomes in patients with mesenteric ischemia.

4 Mathematical Modeling for Interpreting Gastrointestinal Bioelectromagnetic Fields

EGG and MGG are attractive tools for assessing gastric myoelectrical activity because of their non-invasiveness. However, there has been a lack of clinical acceptance due in part to difficulty in accurately and reliably interpreting the recorded signals.

Using automated methods such as frequency analysis, EGG has been an elusive promise for many decades [8, 52, 75]. However, correlations between EGG and clinical abnormalities remain poorly defined. The attenuation and distortion of signals caused by different conductivity abdominal layers complicate its use in the identification of sources. The SQUID magnetometer recordings provide an alternative and complementary method for sensing the underlying GI slow wave activity due to the minimal conductivity effects on magnetic fields. However, despite showing much promise, MGG recordings also remain difficult to interpret quantitatively.

Sophisticated mathematical modeling techniques including biophysically and anatomically accurate multi-scale models similar to those described by Corrias et al. in "Modelling Tissue Electrophysiology in the GI Tract: Past, Present and Future" in this volume provide a potential pathway to aid in the interpretation of these experimental measurements. For example, given selected high-resolution slow wave recordings from a specific subject, the activity on the entire stomach can be inferred and mapped onto a realistic stomach anatomy. From this activity the theoretical surface potential fields [18] and the corresponding magnetic fields [73, 27] can be calculated as shown in Fig. 11. Such models provide an ideal data set for

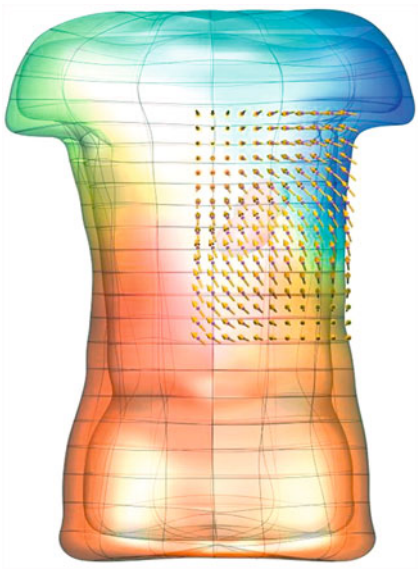

Fig. 11 Simulated magnetic fields (*arrows*) and electric potentials (*colored field*) from a realistic volume conductor using a hypothetical 176-sensor SQUID array located above the stomach

investigating the capability and accuracy for "inverse" algorithms to relate the measured electromagnetic fields back to our understanding of the behaviour of the underlying electrical activity as currently performed in the cardiac field [16, 61].

Existing methods for analysing EGG and MGG signals that are commonly used in GI research only provide a global view of the underlying activity. For example, the use of FFTs to calculate dominant frequencies is unable to differentiate between a normal 3 cpm activity, and 2 waves opposing each other both at a frequency of 3 cpm [59]. They are also unable to localize specific sites of abnormal activity and are likely to miss subtle dysrhythmic events that have been shown to exist [17].

The validation by experimental observation can inform and support the feasibility and the accuracy of the mathematical modelling. Unlike cardiology, the methods for obtaining detailed GI experimental data are still in its infancy. Obtaining signals from both stomach and skin surface simultaneously in sufficient detail, remains challenging.

4.1 Characterization of MGG Signals

The surface current density (SCD) method was first introduced by Hosaka et al. [54] to assist with the interpretation of magnetic field recordings from the heart. The SCD method calculates the surface current density (J) by taking the curl of the magnetic field as given in Eq. 1 from the recorded magnetic field values (B).

$$\mathbf{J} = \frac{1}{\mu_0} \nabla \times \mathbf{B} \tag{1}$$

where μ_0 is the magnetic permeability of free space.

The position of the maximum SCD value is believed to provide an estimate of the location of the underlying dipole sources and tracking the values at successive time instants can provide the assessment on both propagation velocity and propagation patterns. The SCD method has been applied widely in the studies of heart, nerve or brain due to the development of computing and visualization tools [38]. Recently, the use of anatomically realistic torso model and SCD methods to resolve propagation velocity of gastric electrical activity has shown promise [41, 73]. The limitation of the SCD method is its ability to only determine gastric parameters corresponding to the same plane as the sensors. Therefore, any movement in the direction normal to the sensor plane would largely be silent to this method. Another limitation is that the SCD map has only one maximum corresponding to the dominant distal source, despite the possibility of multiple slow waves being present at any point in time [53].

4.2 Characterisation of EGG Signals

The forward problem of electrogastrography relates the slow waves at the organ level to the resultant torso surface potentials. The corresponding inverse problem reconstructs the electrical information about stomach by mathematical manipulation of the measured potentials on torso surface. The potentially based inverse problem, commonly used in the field of electrocardiography, cannot be solved by simply inverting the forward model due to its ill-posed nature. A regularization technique such as the Tikihnov or Greensite-Tikhonov method [34, 20], which imposes constraints on the solution is necessary to obtain feasible stomach potentials (ϕ_S) from torso surface potentials (φ_B) as shown in Eq. 2,

$$\phi_S(y,t) = A^*_{\lambda_t}[\phi_B(x,t)] \tag{2}$$

where $A^*_{\lambda_t}$ is the regularized inverse of transfer matrix which maps stomach surface potentials to torso surface potentials. The x and y are locations on the stomach and torso respectively and t is time.

In the cardiac field, inverse methods and algorithms to reconstruct the electrical activity of heart from the body surface measurements have been a fertile research ground for many decades. Several inverse studies on heart [16, 33, 37] have successfully reconstructed activation time maps and validated the results against experimental measurements. However, to date, potential based inverse methods have not been applied in the gastric field.

Recently, potential based inverse methods have applied to gastric field and shown that realistic potential field patterns can be reconstructed from torso surface measurements [36] as shown in Fig. 12. In simulation studies, it was shown that 84 body surface electrodes were needed to accurately resolve three individual slow wave events.

4.3 Modeling Intestinal and Colonic Bioelectric and Biomagnetic Fields

The small intestine electrical activity has also been reproduced by simple computer models [46–51] and measured using EENG or MENG experimentally [19, 3, 56]. An anatomically realistic computer model was introduced for the first time in [66] and [48]. In the model, the slow wave activity was constructed using the Aliev cell model [66] and then associated magnetic and electrical fields were computed external to the body [48]. Recently published biophysically based models [49, 24] of ICC and SMC open the door to the simulations to investigate conditions such as mesenteric ischemia.

As described by Angeli et al. in "The Electrical Regulation of GI Motility at the Whole-Organ Level" and Dinning in "Colonic Manometry: What do the Squiggly Lines Really Tell Us?" of this volume, the colon is well known for the irregular

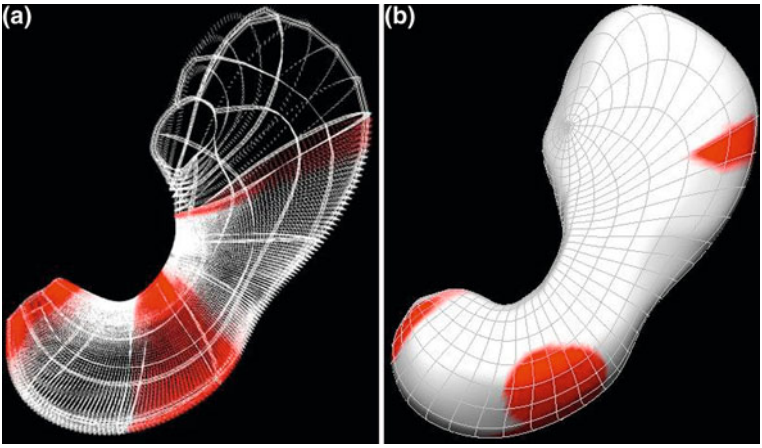

Fig. 12 Reconstruction of stomach potentials from simulated densely sampled body surface potentials. Shown are (**a**) the simulated underlying gastric slow wave activity with three slow wave events and (**b**) the reconstructed activity accurately representing the three individual slow wave events using the Greensite-Tikhonov inverse method

nature of the behavior of its electrical activity [23]. As understanding has grown of the pivotal role played by ICC in GI electrical activity, researchers have realized that colonic tissue generally is not as well populated with ICCs and electrical coupling is different in the colon compared to that in gastric and intestinal tissues. Some studies suggested that disturbed gastric motility in Irritable Bowel Syndrome (IBS) patients can be detected using EGG [39, 50] even though results have varied widely between different studies. Recently, the ability of the SQUID magnetometer to record the electrical events underlying colonic motility was first demonstrated [74]. These findings would encourage investigating the utility in assessing functional activity in the colon in the future.

5 Future Directions

The SQUID magnetometer has allowed unprecedented measurement of extremely weak biological electrical activity, and the gastrointestinal system is a ripe area of investigation. Several disease states may be characterized not only by the temporal effects of the disease on bioelectromagnetic fields, but also by the spatial and temporal mix of phenomena observed. In particular, the ability of the multichannel magnetometer to measure spatiotemporal properties of slow wave propagation in the stomach and to map intestinal frequencies could prove essential to a complete understanding of the progression of the disease.

One untapped resource in biomagnetic studies of the gastrointestinal system remains the vector nature of the field. Newer technology allowing vector

magnetometers with increased channel densities will increase the ability to determine propagation velocity more accurately and to better identify spatial location of small intestinal abnormalities. In particular, we find it interesting that we have never observed magnetically the phenomena reported recently by Lammers et al. [47] and O'Grady et al. [53] of multiple slow waves present simultaneously. These phenomena have been observed using high-resolution serosal electrode arrays, and generally, we believe that low magnetometer spatial resolution may prevent us from observing potentially weaker-strength magnetic sources when a particular slow wave may dominate any others present in the electrical syncytium, but this hypothesis needs to be tested.

The effects of ischemia and of gastric uncoupling that we have observed in our animal studies encourage us to move forward with the application of the biomagnetic technique in human patients. We have been encouraged by the ability of the SQUID to detect subtle spatiotemporal propagation changes associated with gastroparesis as well as the frequency changes associated with chronic mesenteric ischemia.

One area of tremendous interest in GI research is irritable bowel syndrome. While most research suggests that electrical activity in the colon is not as regular or predictable as that in the stomach and small bowel, our studies have shown that we can detect signals of colonic origin [74]. It is possible that some of the different types of IBS (IBS-C, IBS-D, etc.) could have distinct bioelectric or biomagnetic signatures, and we believe that experiments should be developed to ascertain whether these differences are observed.

Acknowledgments This work was funded in part by grants from the National Institutes of Health (R01 DK58197, R01 DK58697 and R01 DK64775). The authors also acknowledge the experimental assistance of the Vanderbilt Clinical Research Center and the SR Light Surgical Research Laboratory at Vanderbilt University.

References

1. Abid S, Lindberg G (2007) Electrogastrography: poor correlation with antro-duodenal manometry and doubtful clinical usefulness in adults. World J Gastroenterol 13(38):5101–5107
2. Akin A, Sun HH (1999) Time-frequency methods for detecting spike activity of stomach. Med Biol Eng Comput 37(3):381–390
3. Aliev RR, Richards W, Wikswo JP (2000) A simple nonlinear model of electrical activity in the intestine. J Theor Biol 204(1):21–28
4. Alvarez WC (1918) Differences in the behavior of segments from different parts of the intestine. Am J Physiol 45(4):342–350
5. Alvarez WC, Mahoney LJ (1922) Action Currents in Stomach and Intestine. Am J Physiol 58(3):476–493
6. Atanassova E, Daskalov I, Dotsinsky I, Christov I, Atanassova A (1995) Non-invasive electrogastrography. Part 1: Correlation between the gastric electrical activity in dogs with implanted and cutaneous electrodes. Arch Physiol Biochem 103(4):431–435
7. Baule G, McFee R (1963) Detection of the magnetic field of the heart. Am Heart J 65:95–96

8. Bortolotti M (1998) Electrogastrography: a seductive promise, only partially kept. Am J Gastroenterol 93(10):1791–1794
9. Bradshaw LA, Allos SH, Wikswo JP Jr, Richards WO (1997) Correlation and comparison of magnetic and electric detection of small intestinal electrical activity. Am J Physiol 272 (5 Pt 1):G1159–G1167
10. Bradshaw LA, Richards WO, Wikswo JP Jr (2001) Volume conductor effects on the spatial resolution of magnetic fields and electric potentials from gastrointestinal electrical activity. Med Biol Eng Comput 39(1):35–43
11. Bradshaw LA, Myers AG, Redmond A, Wikswo JP, Richards WO (2003) Biomagnetic detection of gastric electrical activity in normal and vagotomized rabbits. Neurogastroenterol Motil 15(5):475–482
12. Bradshaw LA, Myers AG, Richards WO, Drake WB Wikswo JP (2005) Vector analysis of biomagnetic fields. Med Biol Eng Comput 43(1):85–93
13. Bradshaw LA, Cheng LK, Richards WO, Pullan AJ (2009) Surface current density mapping for identification of gastric slow wave propagation. IEEE Trans Biomed Eng 56(8):2131–2139
14. Bradshaw LA, Irimia A, Sims JA, Richards WO (2009) Biomagnetic signatures of uncoupled gastric musculature. Neurogastroenterol Motil 21(7):778–e50
15. Brown BH, Smallwood RH, Duthie HL, Stoddard CJ (1975) Intestinal smooth muscle electrical potentials recorded from surface electrodes. Med Biol Eng 13(1):97–103
16. Buist ML, Cheng LK, Yassi R, Bradshaw LA, Richards WO, Pullan AJ (2004) An anatomical model of the gastric system for producing bioelectric and biomagnetic fields. Physiol Meas 25(4):849–861
17. Buist ML, Cheng LK, Sanders KM, Pullan AJ (2006) Multiscale modelling of human gastric electric activity: can the electrogastrogram detect functional electrical uncoupling? Exp Physiol 91(2):383–390
18. Chang FY (2005) Electrogastrography: basic knowledge, recording, processing and its clinical applications. J Gastroenterol Hepatol 20(4):502–516. doi:10.1111/j.1440-1746.2004.03751.x
19. Chen JD, Schirmer BD, McCallum RW (1993) Measurement of electrical activity of the human small intestine using surface electrodes. IEEE Trans Biomed Eng 40(6):598–602
20. Cheng LK, Bodley JM, Pullan AJ (2003) Comparison of potential- and activation-based formulations for the inverse problem of electrocardiology. IEEE Trans Biomed Eng 50(1):11–22. doi:10.1109/TBME.2002.807326
21. Cohen D, Edelsack EA, Zimmerman JE (1970) Magnetocardiograms taken inside a shielded room with a superconducting point. Appl Phys Letters 16(7):278–280
22. Cordova-Fraga T, Gallucci M, Bradshaw A, Berch B, Richards WO (2007) A biomagnetic assessment of colonic electrical activity in pigs. Physiol Meas 28(1):41–48
23. Corrias A, Buist ML (2007) A quantitative model of gastric smooth muscle cellular activation. Ann Biomed Eng 35(9):1595–1607
24. Corrias A, Buist ML (2008) Quantitative cellular description of gastric slow wave activity. Am J Physiol Gastrointest Liver Physiol 294(4):G989–G995
25. Davis RC, Garafolo L, Gault FP (1957) An exploration of abdominal potentials. J Comp Physiol Psychol 50(5):519–523
26. DiLuzio S, Comani S, Romani GL, Basile C, Del Gratta C, Pizzella V (1989) A biomagnetic method for studying gastro-intestinal activity. Il Nuovo Cimento 11(12):1853–1859
27. Du P, O'Grady G, Cheng LK, Pullan AJ (2010) A multiscale model of the electrophysiological basis of the human electrogastrogram. Biophys J 99(9):2784–2792
28. el-Sharkawy TY, Morgan, KG, Szurszewski JH (1978) Intracellular electrical activity of canine and human gastric smooth muscle. J Physiol 279:291–307
29. Erickson J, Obioha C, Goodale A, Bradshaw A, Richards W (2008) Noninvasive detection of small bowel electrical activity from SQUID magnetometer measurements using SOBI. Conf Proc IEEE Eng Med Biol Soc 2008:1871–1874

30. Erickson JC, Obioha C, Goodale A, Bradshaw LA, Richards WO (2009) Detection of small bowel slow-wave frequencies from noninvasive biomagnetic measurements. IEEE Trans Biomed Eng 56(9):2181–2189
31. Geldof H, van der Schee EJ, Grashuis JL (1986) Electrogastrographic characteristics of interdigestive migrating complex in humans. Am J Physiol 250(2 Pt 1):G165–G171
32. Goodale A, Obioha CB, Erickson J, Irimia A, Williams B, Bradshaw LA, Richards WO (2008) Partial mesenteric ischemia alters biomagnetic slow wave. Gastroenterology 134(4):A673
33. Greensite F, Huiskamp G (1998) An improved method for estimating epicardial potentials from the body surface. IEEE Trans Biomed Eng 45(1):98–104
34. Haberkorn W, Steinhoff U, Burghoff M, Kosch O, Morguet A, Koch H (2006) Pseudo current density maps of electrophysiological heart, nerve or brain function and their physical basis. Biomagn Res Technol 4:5
35. Hamilton JW, Bellahsene BE, Reichelderfer M, Webster JG, Bass P (1986) Human electrogastrograms. Comparison of surface and mucosal recordings. Dig Dis Sci 31(1):33–39
36. Han C, Liu Z, Zhang X, Pogwizd S, He B (2008) Noninvasive three-dimensional cardiac activation imaging from body surface potential maps: a computational and experimental study on a rabbit model. IEEE Trans Med Imaging 27(11):1622–1630. doi:10.1109/TMI.2008.929094
37. He B, Li G, Zhang X (2003) Noninvasive imaging of cardiac transmembrane potentials within three-dimensional myocardium by means of a realistic geometry anisotropic heart model. IEEE Trans Biomed Eng 50(10):1190–1202. doi:10.1109/TBME.2003.817637
38. Hosaka H, Cohen D, Cuffin BN, Horacek BM (1976) Part III: the effect of the torso boundaries on the magnetocardiogram. J Electrocardiol 9(4):418–425
39. Huizinga JD, Diamant NE, el-Sharkawy TY (1983) Electrical basis of contractions in the muscle layers of the pig colon. Am J Physiol 245(4):G482–G491
40. Irimia A, Gallucci MR, Richards WO, Bradshaw LA (2006) Separation of gastric electrical control activity from simultaneous MGG/EGG recordings using independent component analysis. Conf Proc IEEE Eng Med Biol Soc 1:3110–3113
41. Irimia A, Richards WO, Bradshaw LA (2006) Magnetogastrographic detection of gastric electrical response activity in humans. Phys Med Biol 51(5):1347–1360
42. Irimia A, Richards WO, Bradshaw LA (2009) Comparison of conventional filtering and independent component analysis for artifact reduction in simultaneous gastric EMG and magnetogastrography from porcines. IEEE Trans Biomed Eng 56(11):2611–2618
43. Jenks WG, Sadeghi SSH, Wikswo JP (1997) SQUIDs for nondestructive evaluation. J Phys D Appl Phys 30:293–323
44. Jenks WG, Thomas IM, Wikswo JP Jr (1997) SQUIDs. In: Trigg GL et al (eds) Encyclopedia of applied physics, vol 19. VCH Publishers, Deerfield Beach, pp 457–469
45. Kim JH, Bradshaw LA, Pullan AJ, Cheng LK (2010) Characterization of gastric electrical activity using magnetic field measurements: a simulation study. Ann Biomed Eng 38(1):177–186
46. Kim JH, Pullan AJ, Cheng LK (2011) Reconstruction of multiple gastric electrical wave fronts using potential based inverse methods. Conference proceedings: … annual international conference of the IEEE engineering in medicine and biology society. IEEE Engineering in Medicine and Biology Society. pp 1355–1358 doi:10.1109/IEMBS.2011.6090319
47. Lammers WJ, Ver DL, Stephen B, Smets D, Schuurkes JA (2009) Origin and propagation of the slow wave in the canine stomach: the outlines of a gastric conduction system. Am J Physiol Gastrointest Liver Physiol 296(6):G1200–G1210
48. Lin AS, Buist ML, Cheng LK, Smith NP, Pullan AJ (2006) Computational simulations of the human magneto- and electroenterogram. Ann Biomed Eng 34(8):1322–1331
49. Lin AS, Buist ML, Smith NP, Pullan AJ (2006) Modelling slow wave activity in the small intestine. J Theor Biol 242(2):356–362

50. Mazur M, Furgala A, Jablonski K, Madroszkiewicz D, Ciecko-Michalska I, Bugajski A, Thor PJ (2007) Dysfunction of the autonomic nervous system activity is responsible for gastric myoelectric disturbances in the irritable bowel syndrome patients. J Physiol Pharmacol 58(Suppl 3):131–139
51. Miftakhov RN, Abdusheva GR, Christensen J (1999) Numerical simulation of motility patterns of the small bowel. 1. formulation of a mathematical model. J Theor Biol 197(1):89–112
52. Obioha CB, Goodale A, Erickson J, Bradshaw LA, Richards WO (2008) Correlation of biomagnetic and bioelectric recordings in a patient with ischemic bowel. Gastroenterology 134(4):A674
53. O'Grady G, Du P, Cheng LK, Egbuji JU, Lammers WJ, Windsor JA, Pullan AJ (2010) Origin and propagation of human gastric slow-wave activity defined by high-resolution mapping. Am J Physiol Gastrointest Liver Physiol 299(3):G585–G592
54. O'Grady G, Egbuji JU, Du P, Lammers WJ, Cheng LK, Windsor JA, Pullan AJ (2011) High-resolution spatial analysis of slow wave initiation and conduction in porcine gastric dysrhythmia. Neurogastroenterol Motil 23(9):e345–e355
55. Oldenburg WA, Lau LL, Rodenberg TJ, Edmonds HJ, Burger CD (2004) Acute mesenteric ischemia: a clinical review. Arch Intern Med 164(10):1054–1062
56. Petrie RJ, Turnbull G, Stroink G, van Leeuwen P, Brandts BVV (1996) Single and multichannel magnetic measurements of human gastrointestinal activity. Can J Gastroenterol 10(suppl. A):S111, 48A
57. Pezzolla F, Riezzo G, Maselli MA, Giorgio I (1989) Electrical activity recorded from abdominal surface after gastrectomy or colectomy in humans. Gastroenterology 97(2):313–320
58. Prats-Boluda G, Garcia-Casado J, Martinez-de-Juan JL, Ye-Lin Y (2011) Active concentric ring electrode for non-invasive detection of intestinal myoelectric signals. Med Eng Phys 33(4):446–455
59. Pullan AJ, Cheng LK, Buist ML (2005) Mathematically modelling the electrical activity of the heart: from cell to body surface and back again. World Scientific, New Jersey
60. Qian LW, Peters LJ, Chen JD (2001) Clonidine inhibits postprandial response of antral myoelectrical activity. Dig Dis Sci 46(3):626–631
61. Ramanathan C, Ghanem RN, Jia P, Ryu K, Rudy Y (2004) Noninvasive electrocardiographic imaging for cardiac electrophysiology and arrhythmia. Nat Med 10(4):422–428. doi:10.1038/nm1011
62. Robertson-Dunn B, Linkens DA (1974) A mathematical model of the slow-wave electrical activity of the human small intestine. Med Biol Eng 12(6):750–758
63. Roth BJ (1990) Biomagnetic studies of peripheral nerves and skeletal muscle. Adv Neurol 54:101–117
64. Richards WO, Staton DJ, Golzarian J, Friedman RN, Wikswo JP (1993) Non-invasive SQUID magnetometer measurement of human gastric and small bowel. In: Deecke L, Baumgartner C, Stroink G, Williamson SJ (eds) Biomagnetism: fundamental research and clinical applications. Proceedings of the ninth international conference on biomagnetism, 9, Springer, New York
65. Richards WO, Bradshaw LA, Staton DJ, Garrard CL, Liu F, Buchanan S, Wikswo JP Jr (1996) Magnetoenterography (MENG): noninvasive measurement of bioelectric activity in human small intestine. Dig Dis Sci 41(12):2293–2301
66. Seidel SA, Bradshaw LA, Ladipo JK, Wikswo JP Jr, Richards WO (1999) Noninvasive detection of ischemic bowel. J Vasc Surg 30(2):309–319
67. Sheridan CJ, Matuz T, Draganova R, Eswaran H, Preissl H (2010) Fetal magnetoencephalography—achievements and challenges in the study of prenatal and early postnatal brain responses: a review. Infant Child Dev 19(1):80–93
68. Simonian HP, Panganamamula K, Parkman HP, Xu X, Chen JZ, Lindberg G, Xu H, Shao C, Ke MY, Lykke M, Hansen P, Barner B, Buhl H (2004) Multichannel electrogastrography (EGG) in normal subjects: a multicenter study. Dig Dis Sci 49(4):594–601

69. Smit X, Stefan de KB, Walbeehm ET, Dudok van Heel EB, van Neck JW, Hovius SE (2003) Magnetoneurography: recording biomagnetic fields for quantitative evaluation of isolated rat sciatic nerves. J Neurosci Methods 125(1–2):59–63
70. Smout AJ, van der Schee EJ, Grashuis JL (1980) What is measured in electrogastrography? Dig Dis Sci 25(3):179–187
71. Strasburger JF, Cheulkar B, Wakai RT (2008) Magnetocardiography for fetal arrhythmias. Heart Rhythm 5(7):1073–1076
72. Staton DJ, Soteriou MC, Friedman RN, Richards WO, Wikswo JP (1991) First magnetic measurements of smooth muscle in vitro using a high-resolution SQUID magnetometer. In: Proceedings of the 13th annual international conference on biomagnetism, vol 13, pp 550–551
73. Stufflebeam SM (2011) Clinical magnetoencephalography for neurosurgery. Neurosurg Clin N Am 22(2):153–167, vii–viii
74. van der Voort IR, Osmanoglou E, Seybold M, Heymann-Monnikes I, Tebbe J, Wiedenmann B, Klapp BF, Monnikes H (2003) Electrogastrography as a diagnostic tool for delayed gastric emptying in functional dyspepsia and irritable bowel syndrome. Neurogastroenterol Motil 15(5):467–473
75. Verhagen MAM, van Schelven LJ, Samsom M, Smout AJPM (1999) Pitfalls in the analysis of electrogastrographic recordings. Gastroenterology 117(2):453–460
76. Wang ZS, Elsenbruch S, Orr WC, Chen JD (2003) Detection of gastric slow wave uncoupling from multi-channel electrogastrogram: validations and applications. Neurogastroenterol Motil 15(5):457–465

Modelling Tissue Electrophysiology in the GI Tract: Past, Present and Future

Alberto Corrias, Peng Du and Martin L. Buist

Abstract Slow waves in the gastrointestinal (GI) tract constitute an important electrical signal that regulates motility. Experimental and clinical evidence indicates that abnormalities in generation and propagation of slow waves within the muscular tissues of the GI organs are of importance in the context of motility disorders. Mathematical models of tissue electrophysiology have the ability to provide a succinct description of the complex interactions involved in generation and propagation of electrical activity. Over the past few decades, a number of mathematical models of slow wave propagation have been proposed in an attempt to gain a mechanistic insight into the complex interactions that underlie GI motility disorders. Mathematical models of tissue electrophysiology in the GI tract constitute the focus of this chapter. An overview of the different approaches that have been adopted to model slow wave propagation is presented first. The mathematical background and available computational tools of the current models of GI tissue electrophysiology are discussed next. Some significant examples of simulation results are also presented. Finally, possible future directions of research in the field of modelling GI tissue electrophysiology are outlined.

1 Introduction

Electrical activity in muscular tissues provide a signal for regulation of muscle contraction. Electrical waves that are generated and propagated within the walls of the gastrointestinal (GI) tract are known as slow waves. The generation and

A. Corrias (✉) · M. L. Buist
Department of Bioengineering, National University of Singapore, Singapore, Singapore
e-mail: alberto@nus.edu.sg

P. Du
Auckland Bioengineering Institute, The University of Auckland, Auckland, New Zealand

L. K. Cheng et al. (eds.), *New Advances in Gastrointestinal Motility Research*,
Lecture Notes in Computational Vision and Biomechanics 10,
DOI: 10.1007/978-94-007-6561-0_10, © Springer Science+Business Media Dordrecht 2013

propagation of slow waves is of particular interest as abnormal electrical activity has been implicated in several maladies involving motility disorders. Over the past few decades, a number of investigators have proposed mathematical descriptions of slow wave propagation in an attempt to gain a mechanistic insight into the complex interactions involved in this process. These descriptions form the focus of this chapter.

A validated mathematical model offers a virtual medium in which hypotheses regarding the pathophysiology of certain diseases can be investigated, and the effects of treatment strategies predicted prior to their introduction to animal or human subjects. Decades of research in cardiac electrophysiology have, for example, resulted in sophisticated mathematical models that have been applied to successfully explain complex clinical questions such as the mechanisms underlying atrial and ventricular arrhythmias [57, 59] and ischemia [50]. By comparison, mathematical modelling in the gastrointestinal field is still in its infancy, partly due to the inherent complexity of the system along with our historically limited understanding of the role of the interstitial cells of Cajal (ICC) and the intracellular components that give rise to slow waves.

Nevertheless, mathematical modelling of gastrointestinal electrophysiology is gaining recognition as a significant research strategy in both basic science and clinical research [11, 19]. Multiscale GI models fall under the umbrella of the International Union of Physiological Sciences (IUPS) Physiome Project, which aims to develop computational models of the entire human body in health and disease [31]. With major developments in science and medicine occurring at the molecular, cellular, tissue, and whole-organ levels, one of the key aims envisaged by the Physiome Project is to provide a comprehensive framework for modelling the human body using mathematical and computational techniques that can incorporate the necessary physiological details.

Modelling of the GI tract has been variously termed as the Digestive Physiome or the GI-ome by different investigators, although neither term is yet in widespread usage [11]. The key challenge for this aspect of the Physiome Project is developing the ability to bridge the gaps in our current understanding of GI electrophysiology while at the same time encouraging appropriate experimental validation to consolidate our knowledge of the digestive system.

Recent advances in our understanding of the ion channels responsible for GI electrophysiology have motivated the creation of a new generation of mathematical cell models that have captured the relevant processes in biophysical detail. In particular, a Hodgkin and Huxley based approach has been adopted to model the ionic conductances in both smooth muscle cells and the interstitial cells of Cajal, allowing the simulation of GI slow waves to be related to the physiologically realistic parameters that govern the behaviour of these channels [14, 15, 23, 24].

Due to the biophysically relevant descriptions of cellular activity brought to the field by this new generation of cellular models, significant breakthroughs are also poised to occur in the area of tissue modelling. An attractive proposition is to relate slow wave propagation to the detailed underlying tissue structures within a continuum framework, as has been performed in the cardiac field. This will allow

us to better understand the normal and abnormal propagation of slow waves through complex gastrointestinal tissue structures [56, 59].

This chapter presents an overview of the mathematical models that have been proposed to describe tissue electrophysiology along the muscular walls of the GI tract. Section 2 describes some of the different approaches that have been adopted to describe GI tissue electrophysiology. Section 3 presents a comprehensive derivation of the mathematical frameworks that have been used to model tissue electrophysiology using a continuum approach. Section 4 presents an overview of the computational tools that are currently available to the community to conduct such simulations. Examples of the application of such tools to the GI tract is the topic of Sect. 5. Finally, Sect. 6 outlines the possible future directions of research in the field of modelling GI tissue electrophysiology.

2 Modelling Approaches for GI Tissue Electrophysiology

A number of different approaches have been adopted to mathematically model GI tissue electrophysiology. The resulting models can be generally classified into continuum-based models and non-continuum-based models. Details on continuum modelling can be found in Sect. 3, while a summary of the alternatives is presented here.

2.1 Coupled Relaxation Oscillator Models

A chain of coupled relaxation-oscillators was one of the earliest mathematical models of slow wave activity [41]. During the early 1970s, a network of bi-directionally coupled relaxation-oscillators was used to simulate GI slow waves [52, 53]. These relaxation-oscillator models were designed to simulate coupled slow wave propagation, which was referred to as 'frequency pulling' in the original literature [52].

The oscillatory nature of the membrane potential in the GI musculature has been known for several decades and the first attempts at modelling slow wave propagation were based on sets of ordinary differential equations (ODEs) containing polynomial equations that, once solved, gave rise to the oscillatory behaviour in the dependent variable (in this case, the amplitude of the slow waves). The theoretical framework is based on the Van der Pol equation, which was originally formulated to describe self-sustaining oscillations in which energy is fed into small oscillations and removed from large oscillations. The Van der Pol equation is given by,

$$\frac{\partial^2 x}{\partial t^2} - \alpha(1 - x^2)\frac{\partial x}{\partial t} + \omega^2 x = 0 \tag{1}$$

where t is time, x is the dependent variable (the amplitude of the oscillations), α is the damping coefficient and ω is the undamped natural frequency of the oscillations. Equation 1 can be reduced to a set of two first order differential equations. A number of investigators have adapted the Van der pol equations to simulate slow wave activity [25, 49, 52]. For example, Sarna et al. [52] derived the following equations for each oscillator,

$$\frac{dx}{dt} = \alpha(ey + fx + gx^2 + hx^3) \tag{2}$$

$$\frac{dy}{dt} = -\frac{1}{\alpha}(by + \omega x^2 + cx^2 + dx^3 - a) \tag{3}$$

where x remains as the dependent variable, y is an auxiliary state variable and all the other symbols ($(a - h)$ and ω) are model parameters with no direct physical meaning. By appropriately tuning these parameters, it was possible to reconstruct an oscillating profile that replicated slow wave activity.

In an electrically coupled tissue, such as the gastric musculature, each oscillator operates under the influence of its neighbours. The equations describing the n^{th} oscillator are given by

$$\frac{dx_n}{dt} = \alpha(ey_n + fx_n + gx_n^2 + hx_n^3 + I_n) \tag{4}$$

$$\frac{dy_n}{dt} = -\frac{1}{\alpha}(by_n + \omega x_n^2 + cx_n^2 + dx_n^3 - a) \tag{5}$$

where I_n denotes the combined input of other oscillators to the n^{th} oscillator. In the simplified example shown in Fig. 1, I_n would be given by,

$$I_n = C_{n1}x_{n-1} + C_{n2}x_{n+1} - C_{n3}x_{n+1} \tag{6}$$

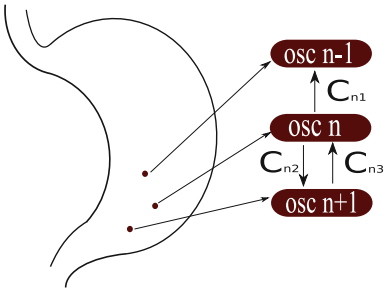

Fig. 1 Simplified diagram showing three coupled relaxation oscillator (osc $n - 1$, osc n and osc $n + 1$) arbitrarily placed in the antral region of the stomach as in the approach proposed by Sarna et al. C_{n1}, C_{n2} and C_{n3} are coupling coefficients. Note that this is a simplified example with only three oscillators for illustrative purposes only. The original publication describes thirteen oscillators arranged throughout the distal corpus and antral region of the stomach (see Fig. 2 of Sarna et al. [53])

where C_{n1}, C_{n2} and C_{n3} are the coupling coefficients.

This approach was widely used in a variety of simulated experimental setups [41, 53]. Nevertheless, several issues were raised regarding the adequacy and utility of this approach [45]. The criticisms were based on two main limitations of relaxation oscillator models. Firstly, the ability of such models to accurately replicate the waveforms that were experimentally recorded along the GI tract was put into question. Equations 2 and 3 proved unable to replicate important slow wave features such as the relatively flat inter slow wave profile and the biphasic slow wave shape (rapid upstroke followed by partial repolarisation and a plateau phase) recorded from antral preparations. Secondly, doubts were cast over the utility of relaxation oscillator models in predicting the effects of pharmacological agents. The parameters of Eqs. 2 and 3 have no direct physical meaning so it is very difficult, if not impossible, to correlate a change in one of the parameters to the effects of a particular chemical or drug and make predictions pertaining its effects on the slow wave activity. Ultimately, because of these two limitations, relaxation oscillator models became less popular and the development of biophysically-based realistic mathematical descriptions of the cellular events that lead to slow wave generation was advocated [45]. However, despite these limitations, such models were able to replicate macroscopic slow wave behaviour in the stomach and small bowel and encapsulate the entrainment of different intrinsic frequencies along the GI tract. Early work on joint experimental and modelling investigations into mechanical uncoupling and gastric electrical stimulation were also performed [51, 53]. The resulting formulations were in a compact and readily understandable form, and should be acknowledged as an important first step in the field.

2.2 Aliev's Double Cable Model

After the role of ICC in the GI tract was elucidated, Aliev et al. [1] developed a novel model of slow wave propagation that combined aspects of earlier work on relaxation oscillators with a continuum cable approach. This is the first model that explicitly models the ICC as pacemakers of slow waves. Here, the electrical behaviour of the ICC and SMC was described by a pair of equations following Fitzhugh and Nagumo [25, 40].

$$\frac{du}{dt} = ku(u-a)(1-u) - v \tag{7}$$

$$\frac{dv}{dt} = \varepsilon(\gamma(u-\beta) - v) \tag{8}$$

Here u is the normalised membrane potential, v is a recovery variable, and ε controls cell excitability. The other parameters (k, a, γ and β) are constants. Depending on the parameterisation of the equations, this system can operate in an oscillating mode (suitable for the ICC) or an excitable mode (suitable for the

SMC). These cellular descriptions were placed into two electrically coupled cable models, one for the ICC and one for the SMC, over which electrical diffusion was solved. By including an intrinsic frequency gradient in the ICC cable through the cellular excitability parameter (ε), slow wave propagation along the small intestine was simulated. The Aliev model was the first to explicitly incorporate ICC cells and use them as pacemakers. However, as with other relaxation oscillator models, the main drawback is the lack of any underlying biophysical basis for the model parameters, however, the simplicity of this approach gave rise to the first whole organ simulations in this area [48].

2.3 A Discrete Transmural Model

A one dimensional description of the gastric musculature was developed by Edwards and Hirst [22] for the study of the propagation of slow waves. The authors aimed to characterise the propagation of the electrical impulse from the ICC in the myenteric plexus towards the longitudinal SM layer and the circular SM layer. For this purpose they introduced three equivalent electrical circuits, one for the ICC-MY, one for the circular SM layer and one for the longitudinal SM layer (Fig. 2).

The equivalent circuits representing the different muscle layers were made of parallel connections between a capacitor and one or more variable resistances. The governing equations for each of the cell types was of the Hodgkin and Huxley type. The model of the circular layer [21] was based on a phenomenological

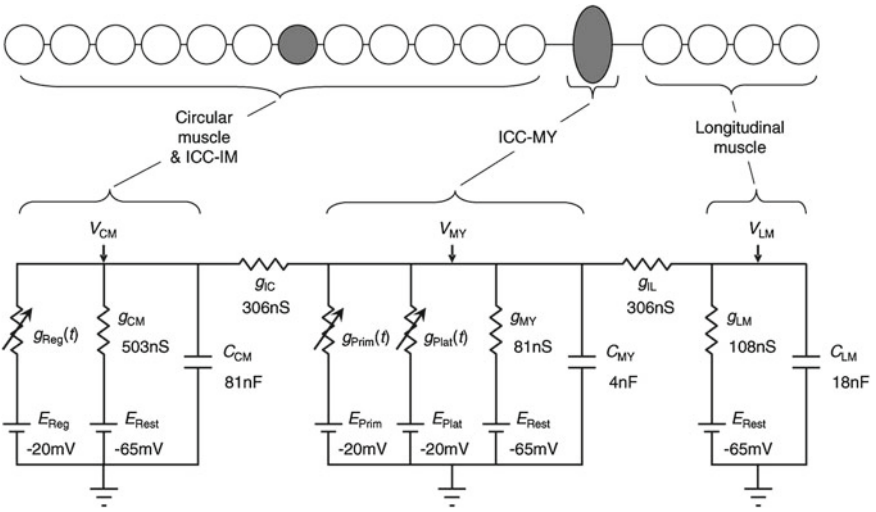

Fig. 2 Transmural model of the gastric musculature as published by Edwards and Hirst [22]. Each layer in the gastric musculature was modelled with a simple electrical circuit

description of the plateau phase of the SM slow waves (termed regenerative potentials) that was assumed by the authors to be the result of the summation of unitary potentials (small increases in membrane conductance that have been observed experimentally [3]). The rate of discharge of unitary potentials (λ) was assumed to be dependent on the concentration of a messenger, whose identity was suggested to be IP_3, according to the following Hill equation,

$$\lambda = \frac{\lambda_{max}}{1 + \left(\frac{K_d}{[messenger]}\right)^H} \tag{9}$$

where λ_{max} is the maximal discharge rate, K_d and H are the Hill half-value and steepness parameters respectively and [messenger] represents the concentration of the messenger, which was assumed to be determined by the following two-stage biochemical reaction.

$$[precursor] \underset{K_B}{\overset{mhK_F}{\rightleftharpoons}} [intermediate] \xrightarrow{K_M} [messenger] \xrightarrow{K_H} \tag{10}$$

Here m and h are Hodgkin and Huxley gating variables, K_F and K_B are the forward and backward reaction rates respectively for the intermediate species (of unspecified nature), and K_M and K_H are the reaction rates for the messenger formation and degradation respectively. The rate of discharge of unitary potential was used to compute the value of $g_{Reg}(t)$ in Fig. 2 as follows. First, $g_{Reg}(t)$ was written as the summation of N unitary conductances,

$$g_{Reg}(t) = \sum_{j=1}^{N} g_j(t) \tag{11}$$

where each $g_j(t)$ can be written, assuming a particular unitary event starting at time t_j, as

$$g_j(t) = \begin{cases} 0 & \text{if} t < t_j \\ A_j\left(e^{-(t-t_j)/0.434} - e^{-(t-t_j)/0.077}\right)^3 & \text{if} t \geq t_j \end{cases} \tag{12}$$

where the random variable A_j represents the amplitude of the unitary potential. Second, at every time step, the total number of unitary potentials, N, was related to the mean frequency of discharge of unitary potentials by,

$$\sum_{j=1}^{N} (t_j - t_{j-1}) = \frac{N}{\lambda} \tag{13}$$

Hence, at every time step, λ is calculated from the equations arising from the reaction in Eq. 10 and the intervals between forthcoming unitary potentials are modified accordingly (Eq. 13), allowing the calculation of $g_{Reg}(t)$ using Eqs. 11 and 12. The membrane potential in the CM layer (left of Fig. 2) was then calculated by,

$$C_{CM}\frac{dV_{CM}}{dt} = -(g_{Reg}(t)(V_m + 20) + g_{CM}(V_m + 65)) + I_{IC} \tag{14}$$

where I_{IC} is the current exchanged between ICC-MY and CM layers and is given by,

$$I_{IC} = g_{IC}(V_{CM} - V_{MY}) \tag{15}$$

The slow wave activity in the ICC-MY network was modelled by the equivalent circuit shown in Fig. 2 (centre). The variable conductance $g_{Prim}(t)$ was introduced to model the primary component of the slow wave and is given by,

$$g_{Prim}(t) = G_{PRIM}A * N \tag{16}$$

where G_{PRIM} is a maximal conductance value, and A and N are Hodgkin and Huxley-type voltage dependent gating variables. The other variable conductance $g_{Plat}(t)$ was introduced to simulate the plateau phase of the slow wave in the ICC. Since this phase was assumed by the authors to be the result of a summation of unitary potentials, the same formulation used for $g_{Reg}(t)$ was again employed. The governing equation for the ICC-MY layer (centre of Fig. 2) is then given by,

$$\begin{aligned} C_{MY}\frac{dV_{MY}}{dt} = & -(g_{Plat}(t)(V_m + 20) + g_{Prim}(t) \\ & + g_{MY}(V_m + 65)) - I_{IC} - I_{IL} \end{aligned} \tag{17}$$

where I_{IL} is the current exchanged between the ICC-MY and LM layers and is given by,

$$I_{IL} = g_{IL}(V_{LM} - V_{MY}) \tag{18}$$

Finally, the longitudinal muscle layer was modelled by the simple circuit shown on the right of Fig. 2. The governing equation is given by,

$$C_{LM}\frac{dV_{LM}}{dt} = -g_{LM}(V_m + 65) + I_{IL} \tag{19}$$

This model is largely phenomenological in nature as only certain aspects of the underlying physiology of the cellular components have been captured. However, the model presented by Edwards and Hirst [22] is able to accurately reproduce slow wave activity recorded from the different layers of the guinea-pig stomach.

2.4 Other Approaches

A number of other works have also appeared in the literature that attempt to describe GI tissue electrophysiology. Back in the mid 1980s, Mirizzi and Stella developed a model of the extracellular potentials in the stomach [38]. This

approach described a slow wave in terms of a charged annulus, represented by electric dipoles, moving along a cone. As the diameter of the cone decreased the charge density increased and thus the propagation velocity also increased as the wave approached the gastroduodenal junction. A computer program was written to calculate the extracellular potential field that resulted from this activity. In recent times, however, such dipole based approaches have been largely restricted to examining the far-field electric and magnetic fields that arise from GI activity.

Although not a model of slow wave propagation, the passive electrical properties of GI tissue were investigated through a system identification approach by Fu and Bardakjian [26]. The model was constructed in terms of repeated elements containing a membrane resistance, membrane capacitance, myoplasmic resistance, gap junction resistance and a gap junction capacitance, and the values of these parameters were obtained for canine GI smooth muscle. As high resolution mapping becomes more prominent in the field, such an approach may prove useful for parameterising more complex tissue models (e.g., as described by O'Grady et al. in "The Principles and Practice of Gastrointestinal High-Resolution Electrical Mapping" of this volume).

3 Continuum Modelling of GI Electrophysiology

In a model of GI tissue electrophysiology, the mathematical descriptions of the activity of each cell are incorporated into larger scale multicellular models, either as a discrete set of ICCs and/or SMCs or as a continuum representation of a volume-averaged block of tissue [47]. In both approaches, different governing equations are employed to describe the resulting slow wave activity.

In the discrete approach, each cell model acts as the basic unit of the model, such that the ICC-ICC, ICC-SMC, and SMC-SMC coupling are modelled as networks composed of connected cell models. In the early stages, cardiac modelling studies used a discrete approach to simulate propagation of cardiac electrical events in a network of coupled cells that represented a small volume of tissue (0.5 by 1.5 mm) with a large number of individual ionic and coupling conductances, and this required more than 4.5 computational hours to simulate 520 ms of propagation [39]. This level of computational load presents a problem for GI slow wave modelling, where the slow waves need to be simulated over periods of minutes. Even with the widespread use of high performance computers, it remains computationally intractable to simulate propagation of slow waves in large blocks of tissue at the discrete cell level.

For this reason, the continuum modelling approach has gained popularity in modelling tissue electrophysiology. The basic unit of a continuum model is considered in a volume-averaged sense, i.e., the conductive medium is modelled as continuous rather than being made up of discrete cells [46]. The volume-averaged treatment of the conductive medium reduces the size of the model and thereby reduces the computation time required to solve the model.

In this section, we present the various continuum modelling frameworks that have been used to model GI tissue electrophysiology. The models are presented in reverse chronological order because the simpler (and earlier) models can be derived as particular cases of the more complex (and recent) ones. Hence, we first introduce the extended bidomain framework, the most complex and most recent continuum model, in Sect. 3.1. The bidomain (Sect. 3.2), monodomain (Sect. 3.3) and cable models (Sect. 3.4) are then derived from this.

3.1 The Extended Bidomain Model

In this section we present the derivation of the equations of the extended bidomain framework [7, 16]. The extended framework is required because of the ICC and SMC relationship, i.e., they have unique intracellular spaces and share a common extracellular space in the tissue. Within each control volume into which the geometry is discretized, three domains are present: two intracellular spaces and one extracellular space as shown in Fig. 3, top left. The arrangement allows for modelling of two cell types electrically coupled with each other at each control volume. Each of the two intracellular spaces exchanges ions with the extracellular space via membrane ion channels (which will in general be different for each cell) and with each other via gap junctions. The super-scripts (1) and (2) are used to indicate the two cell types that are considered. Typically, in a GI simulations, the two cells will be ICC and SMC.

The current density in each of the intracellular domains ($\mathbf{J_i}$) and the extracellular domain ($\mathbf{J_e}$) can be modeled as the summation of an ohmic component and an externally applied stimulus $\mathbf{J_{stim}}$:

$$\mathbf{J}_\mathbf{i}^{(\mathbf{1})} = -\sigma_\mathbf{i}^{(\mathbf{1})} \nabla \phi_\mathbf{i}^{(\mathbf{1})} + \mathbf{J}_\mathbf{stim}^{(\mathbf{1})} \tag{20}$$

$$\mathbf{J}_\mathbf{i}^{(\mathbf{2})} = -\sigma_\mathbf{i}^{(\mathbf{2})} \nabla \phi_\mathbf{i}^{(\mathbf{2})} + \mathbf{J}_\mathbf{stim}^{(\mathbf{2})} \tag{21}$$

$$\mathbf{J_e} = -\sigma_\mathbf{e} \nabla \phi_\mathbf{e} + \mathbf{J}_\mathbf{stim}^{(\mathbf{e})} \tag{22}$$

where the subscripts i and e are for intracellular and extracellular spaces respectively, ϕ represents an electric potential and σ represents a conductivity tensor. The change in current density within each domain must be equal to the current flowing across the intervening membranes:

$$\nabla \cdot \mathbf{J}_\mathbf{i}^{(\mathbf{1})} = -\mathbf{A}_\mathbf{m}^{(\mathbf{1})} \mathbf{I}_\mathbf{m}^{(\mathbf{1})} - \mathbf{A}_\mathbf{m}^{(\mathbf{gap})} \mathbf{I_{gap}} \tag{23}$$

$$\nabla \cdot \mathbf{J}_\mathbf{i}^{(\mathbf{2})} = -\mathbf{A}_\mathbf{m}^{(\mathbf{2})} \mathbf{I}_\mathbf{m}^{(\mathbf{2})} + \mathbf{A}_\mathbf{m}^{(\mathbf{gap})} \mathbf{I_{gap}} \tag{24}$$

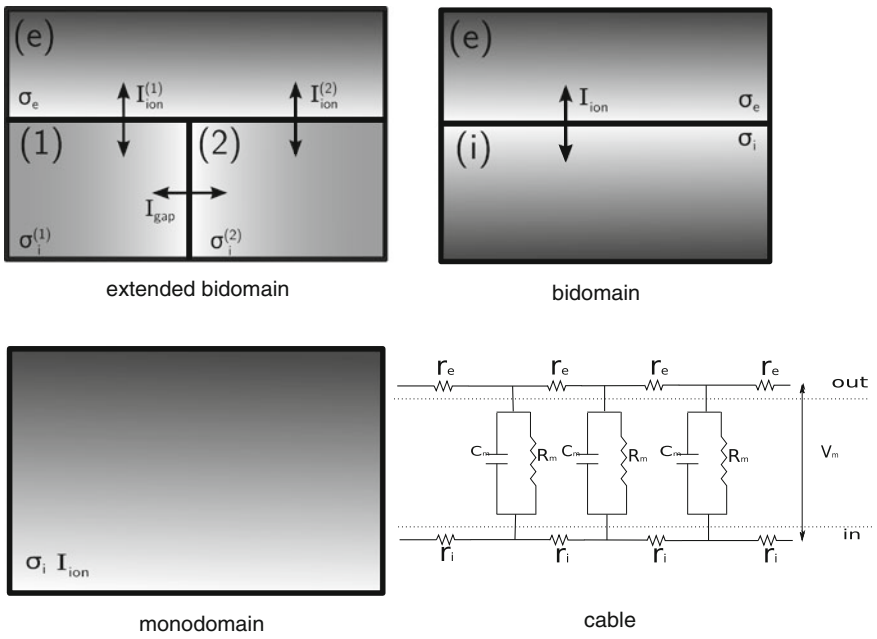

Fig. 3 Schematic representation of the continuum frameworks. *Top left*: the control volume of the extended bidomain model where *(1)* and *(2)* denotes two cells, while *(e)* indicates extracellular space; σ are the conductivities for each compartment. Each of the two cell is in communication with the extracellular space (via I_{ion}) and with each other (via I_{gap}). *Top right*: the control volume of the bidomain model where one intracellular space is in communication via I_{ion} with the extracellular space. *Bottom left*: the control volume in the monodomain model. *Bottom right*: schematic representation of the cable model

where A_m represents surface to volume ratio (in 1/cm) and the superscript *gap* refers to the gap junction separating the two intracellular spaces. Hence, $A_m^{(1)}$ and $A_m^{(2)}$ are the surface to volume ratios of the two cells while $A_m^{(gap)}$ is the surface to volume ratio of the space occupied by the gap junction. Noting that the transmembrane potential can be written as $V_m = \phi_i - \phi_e$, the two membrane currents per unit area $I_m^{(1)}$ and $I_m^{(2)}$ can be expressed as

$$I_m^{(1)} = C_m^{(1)} \left(\frac{\partial \phi_i^{(1)}}{\partial t} - \frac{\partial \phi_e}{\partial t} \right) + I_{ion}^{(1)} \tag{25}$$

$$I_m^{(2)} = C_m^{(2)} \left(\frac{\partial \phi_i^{(2)}}{\partial t} - \frac{\partial \phi_e}{\partial t} \right) + I_{ion}^{(2)} \tag{26}$$

where $I_{ion}^{(1)}$ and $I_{ion}^{(2)}$ are the total membrane ionic currents flowing between intracellular spaces of each cell and the extracellular space. Note that $I_{ion}^{(1)}$ and $I_{ion}^{(2)}$ can

be specified to be spatially heterogeneous, i.e., they can be both describing SMC in regions poor in ICC (e.g., the fundus of the stomach) or they can describe one ICC and one SMC or even two ICC in ICC-rich regions (e.g., the myenteric plexus). Combining Eqs. 20, 23 and 25 for domain (1) yields

$$-A_m^{(1)}\left(C_m^{(1)}\left(\frac{\partial\phi_i^{(1)}}{\partial t}-\frac{\partial\phi_e}{\partial t}\right)+I_{ion}^{(1)}\right)-A_m^{(gap)}I_{gap}= -\nabla\cdot\sigma_i^{(1)}\nabla\phi_i^{(1)}+\nabla\cdot\mathbf{J_{stim}^{(1)}} \tag{27}$$

and similarly, combining Eqs. 21, 24 and 26 for domain (2) yields

$$-A_m^{(2)}\left(C_m^{(2)}\left(\frac{\partial\phi_i^{(2)}}{\partial t}-\frac{\partial\phi_e}{\partial t}\right)+I_{ion}^{(2)}\right)+A_m^{(gap)}I_{gap}= -\nabla\cdot\sigma_i^{(2)}\nabla\phi_i^{(2)}+\nabla\cdot\mathbf{J_{stim}^{(2)}} \tag{28}$$

The conservation of total current applied to the extended bidomain framework prescribes that

$$\nabla\cdot\mathbf{J_i^{(1)}}+\nabla\cdot\mathbf{J_i^{(2)}}+\nabla\cdot\mathbf{J_e}=\mathbf{0} \tag{29}$$

and combining Eqs. 20, 21 and 22 with 29 yields

$$-\nabla\cdot\sigma_i^{(1)}\nabla\phi_i^{(1)}-\nabla\cdot\sigma_i^{(2)}\nabla\phi_i^{(2)}-\nabla\cdot\sigma_e\nabla\phi_e+ \nabla\cdot\mathbf{J_{stim}^{(1)}}+\nabla\cdot\mathbf{J_{stim}^{(2)}}+\nabla\cdot\mathbf{J_{stim}^{(e)}}=\mathbf{0} \tag{30}$$

Rearranging Eqs. 27, 28 and 30 and observing that $\nabla\cdot\mathbf{J_{stim}}$ is a volume stimulus current (I_{stim}), the extended bidomain equations can be written as follows:

$$\nabla\cdot\left(\sigma_i^{(1)}\nabla\phi_i^{(1)}\right)=A_m^{(1)}\left(C_m^1\left(\frac{\partial\phi_i^{(1)}}{\partial t}-\frac{\partial\phi_e}{\partial t}\right)+I_{ion}^{(1)}(\mathbf{u^{(1)}},\phi_\mathbf{i}^{(1)},\phi_\mathbf{e})\right)+\mathbf{I_{stim}^{(1)}}+\mathbf{A_m^{(gap)}I_{gap}}, \tag{31}$$

$$\nabla\cdot\left(\sigma_i^{(2)}\nabla\phi_i^{(2)}\right)=A_m^{(2)}\left(C_m^2\left(\frac{\partial\phi_i^{(2)}}{\partial t}-\frac{\partial\phi_e}{\partial t}\right)+I_{ion}^{(2)}(\mathbf{u^{(2)}},\phi_\mathbf{i}^{(2)},\phi_\mathbf{e})\right)+\mathbf{I_{stim}^{(2)}}-\mathbf{A_m^{(gap)}I_{gap}}, \tag{32}$$

$$\nabla\cdot(\sigma_e\nabla\phi_e)=-\nabla\cdot\left(\sigma_i^{(1)}\nabla\phi_i^{(1)}\right)-\nabla\cdot\left(\sigma_i^{(2)}\nabla\phi_i^{(2)}\right)+I_{stim}^{total}, \tag{33}$$

where $I_{stim}^{total}=I_{stim}^{(1)}+I_{stim}^{(2)}+I_{stim}^{(e)}$. The dependency of I_{ion} on ϕ as well as a vector of cellular state variables $\mathbf{u}$, typically representing intracellular ionic concentrations

with a regulatory effect on the ion channels or gating variables of the ion channels themselves have been included in the formulation.

$$\frac{\partial \mathbf{u^{(1)}}}{\partial t} = \mathbf{f^{(1)}}(\mathbf{u^{(1)}}, \phi_{\mathbf{i}}^{(\mathbf{1})}, \phi_{\mathbf{e}}), \frac{\partial \mathbf{u^{(2)}}}{\partial \mathbf{t}} = \mathbf{f^{(2)}}(\mathbf{u^{(2)}}, \phi_{\mathbf{i}}^{(\mathbf{2})}, \phi_{\mathbf{e}}) \tag{34}$$

Equations 31, 32 and 33 (coupled with Eq. 34) constitute the extended bidomain framework. If we assume that no current flows across the boundary surface of the domain under consideration (e.g., if simulating the whole stomach, this translates into assuming that no current flows in or out of the boundary of the organ), the boundary conditions for Eqs. 31, 32 and 33 are

$$\begin{aligned} \left(\sigma_i^{(1)} \nabla \phi_i^{(1)}\right) \cdot \mathbf{n} &= \mathbf{0} \\ \left(\sigma_i^{(2)} \nabla \phi_i^{(2)}\right) \cdot \mathbf{n} &= \mathbf{0} \\ (\sigma_i \nabla \phi_e) \cdot \mathbf{n} &= \mathbf{0} \end{aligned} \tag{35}$$

3.2 The Bidomain Model

The bidomain model is arguably the most popular model employed to simulate tissue electrophysiology. It was first proposed to model the cardiac tissue [37]. Here, the control volume is divided in two spaces, the intracellular (denoted by subscript *i*) and extracellular (denoted by subscript *e*) domains, separated by the intervening cell membrane (Fig. 3, top right). Within the gastrointestinal musculature, the intracellular domain is represented by either the ICC or SMC, and the extracellular domain represents the surrounding tissue matrix.

The full derivation of the bidomain equations is conceptually similar to the derivation in Sect. 3.1 and has been presented by many authors [28, 36, 37, 47]. Here we show the bidomain model as a particular case of the extended bidomain model. When only one intracellular domain is present, $I_{gap} = 0$ and $\phi_i^{(2)}$ is undefined. Letting the transmembrane potential $V_m = \phi_i^{(1)} - \phi_e$, Eq. 31 can be re-written as

$$\nabla \cdot (\sigma_i \nabla (V_m + \phi_e)) = A_m \left(C_m \frac{\partial V_m}{\partial t} + I_{ion}(\mathbf{u}, \mathbf{V_m}) \right) + \mathbf{I_{stim}^i} \tag{36}$$

while by adding $\nabla \cdot \sigma_i \nabla \phi_e$ to both sides of Eq. 33 and re-arranging yield

$$\nabla \cdot (\sigma_i \nabla V_m) = -\nabla \cdot ((\sigma_i + \sigma_e) \nabla \phi_e) + I_{stim}^{total}. \tag{37}$$

Given that only one intracellular domain is present, all the superscripts (1) have been eliminated for simplicity. Equations 36 and 37 constitute the bidomain

framework in its parabolic-elliptic form. Again, the boundary conditions depend on the physical problem that is being solved. If no current is assumed to flow across the surface of the boundary of the domain, then the boundary conditions can be written as

$$\begin{aligned} \left(\sigma_i \nabla (V_m + \phi_e)\right) \cdot \mathbf{n} = 0 \\ \left(\sigma_e \nabla \phi_e\right) \cdot \mathbf{n} = 0 \end{aligned} \tag{38}$$

3.3 The Monodomain Model

Under the assumption that the extracellular space is highly conductive ($\sigma_e \gg \sigma_i$) or that the extracellular and intracellular domains are equally anisotropic, the bidomain equations can be reduced to a single equation which is known as the monodomain equation (Fig. 3, bottom left).

$$\nabla \cdot (\sigma \nabla V_m) = A_m \left(C_m \frac{\partial V_m}{\partial t} + I_{ion}(\mathbf{u}, \mathbf{V_m}) \right) + I_{stim}. \tag{39}$$

The right hand side of the monodomain equation is similar to the cell membrane equation, and the left hand side of the monodomain equation describes the rate of passive conduction as a diffusion process. By ignoring the electrical conduction in the extracellular space, the monodomain equation is usually simpler to solve compared to the two equations of the bidomain framework. However, one of the key advantages of the bidomain equations over the monodomain equation is that the bidomain considers the extracellular potential (ϕ_e), which is often measured experimentally at the tissue and organ levels [33, 43].

3.4 The Cable Equation

While the monodomain equation (Eq. 39) can be solved in any number of spatial dimensions, one interesting particular case is the 1D case. Assuming a 1D cable aligned with the x axis, Eq. 39 can be written as

$$\frac{1}{r_i + r_e} \frac{\partial^2 V_m}{\partial x^2} = A_m \left(C_m \frac{\partial V_m}{\partial t} + I_{ion}(\mathbf{u}, \mathbf{V_m}) \right) + I_{stim} \tag{40}$$

where the cable conductivity σ, assumed constant along the cable, is expressed as the inverse of the cable resistivity, given by the summation of an intracellular resistivity r_i and an extracellular resistivity r_e (Fig. 3, bottom right). Equation 40

can also be derived from the Kirchhoff's current law, combined with the Ohm's law, applied to the circuits in Fig. 3, bottom right. This was the approach used by Hodgkin and Huxley [29], who first proposed the cable equation to model the propagation of an action potential along a nerve fiber.

4 Tools for GI Continuum Modelling Simulations

As mentioned earlier in Sect. 1, GI modelling can be considered to be part of the wider IUPS Physiome Project [2]. One of the specific focuses of the IUPS Physiome Project is building computational tools and model databases with the aim of establishing a comprehensive modelling infrastructure to support effective simulation, model sharing, and international collaboration in the scientific community. Here those tools that have been applied to simulating GI tissue are briefly described.

Conducting a simulation of tissue or organ level electrophysiology usually implies the solution of the partial differential equations (PDEs) arising from the continuum modelling frameworks described in Sect. 3 over a given geometry of interest. Several numerical techniques have been employed for such a purpose. These include finite difference methods (FDM), finite volume methods (FVM), and finite element methods (FEM). The FDMs solve the strong or differential form of the governing PDEs, whereas the FVM and FEM solve the weak or integral form. The FVM and FEM approaches are often more suitable for irregular and non-orthogonal computational meshes whereas the FDM approach is more suitable for regular and orthogonal meshes. One notable exception is the finite-element based finite-difference method, originally developed for cardiac electromechanics problems, which allows the finite difference method to be used on irregular meshes [8]. Although several software packages are in theory capable of solving the equations described in Sect. 3, only the two described here in Sects. 4.2 and 4.3 have, to date, been successfully applied to the GI tract.

The continuum modelling frameworks presented in Sect. 3 also usually involve the simultaneous solution of a system of ODEs that are coupled to the governing PDEs (e.g., Eq. 34). Typically these ODEs are used to represent the cellular processes that underlie the electrical activity and thus are referred to as 'cell models'. One such system of ODEs must be present at every point in the domain where a cellular contribution is required by the PDEs. Numerical solvers, the simplest of which being the Forward Euler method, can be employed to integrate the cell model at each time step. The updated values that result from such an integration step represent the new state of the underlying cell at that point in time and space, and are then used to calculate the I_{ion} terms in Eqs. 37, 39 or 31 depending on the choice of the continuum model.

4.1 The CellML Model Repository

CellML (Cell Markup Language) is an XML based language that has been designed as a standard format for storing and exchanging models of cell electrophysiology. CellML models can be solved using a number of different solving environments, e.g., COR, openCell etc. As part of this project, an online repository has been created that contains freely available implementations of the most common GI cell models along with models of many other cell types. A summary of the number of equations and parameters in a series of recently published gastrointestinal cell models from the CellML model repository are provided in the table below.

4.2 The CMISS and OpenCMISS Modelling Environments

The acronym CMISS stands for Continuum Mechanics, Image analysis, System identification and Signal processing. CMISS development began in 1980 in Auckland, New Zealand and is still ongoing (http://www.cmiss.org/). The main aim of CMISS is to create a simulation environment for biomedical engineering applications. Although the initial motivation for CMISS was centered around the heart, it has evolved rapidly to include other solution methods for many other parts of the body.

The first example of GI modelling in CMISS saw an extended version of the cable model developed by Aliev et al. [1] incorporated into an anatomically realistic human stomach geometry [6, 48]. Slow wave propagation in the human small intestine was also simulated using a similar approach [34, 35]. CMISS is not only capable of simulating tissue electrophysiology, but is also capable of simulating the body surface electrogastrograms and far-field magnetogastrograms that arise from tissue electrical activity. However, the extended bidomain equations have not been implemented in CMISS at this time.

To take full advantage of recent advances in distributed parallel computing, a significant redevelopment of the CMISS software began in 2005 as the OpenCMISS project [4]. This new initiative was also designed to leverage on the collaborative advantages of open source development. OpenCMISS has four design aims. First, the simulation environment should be consisted of a library of modules; second, the program should be generic, which allows data in different modelling applications to be expressed using the same format; third, the solution process should harness the power of parallel processing, and finally the environment should be readily accessible and understandable by researchers with a diverse range of skills and backgrounds. Although existing gastrointestinal models have not yet been incorporated into OpenCMISS, this is a priority for OpenCMISS moving forward.

4.3 The Chaste Modelling Environment

Chaste (Cancer, Heart And Soft Tissue Environment, http://www.cs.ox.ac.uk/chaste/) is a general purpose simulation package designed for the multi-scale problems that arise in biology and physiology. It is written in the C++ programming language and is available as open-source software. The tissue electrophysiology component of Chaste was originally developed for cardiac simulations at the University of Oxford with the aim of solving the monodomain (Eq. 39) and bidomain equations (Eqs. 36 and 37) across cardiac geometries using the finite element method [44].

Being built upon an MPI-based library (Petsc, http://www.mcs.anl.gov/petsc/petsc-as/index.html), Chaste is able to efficiently split the high computational demands of a tissue electrophysiology simulation over many parallel processors. Recently, a bidomain simulation of rabbit heart activity ($\sim$4 million nodes) took only 9 min for 100 ms of simulated time on 2,048 processors (http://www.cs.ox.ac.uk/chaste/performance.html).

Chaste has now been adapted such that it can simulate GI electrophysiology. Chaste was originally designed for monodomain and bidomain simulations only. However, the ability to run extended bidomain simulations (see Sect. 3.1) was recently added [16] allowing for the specification of two cells and their relevant coupling parameters at each control volume. Chaste uses a built-in and automated translation tool (Pycml, [12]) to translate a cell model (specified by its CellML implementation) into suitable C++ files [13] in order to be able to compute cellular activity. Hence, including GI specific cell models into Chaste simply involved directing Chaste to the CellML files containing the GI cell models (Table 1). Upon the inclusion of appropriate tissue conductivities, monodomain, bidomain and extended bidomain simulations can be run using Chaste on anything from a single processor to a distributed computing cluster.

Table 1 Gastrointestinal mathematical cell model comparison

	ODEs	Parameters	Simulation time (ms)
Youm et al., 2006 [58]	14	53	621
Faville et al., 2009 [23]	78	630	5140
Corrias et al., 2008 [15]	22	116	387
Corrias et al., 2007 [14]	14	43	307

A 60 s simulation period of slow wave activity was simulated using the Cellular Open Resource (COR) software. The simulations were solved using the Newton-Raphson method on an Intel(R) Core(TM)2 Duo 2.60 GHz CPU

5 Examples of Continuum Modelling Simulations

After introducing the relevant mathematical background (Sect. 3) and computational tools (Sect. 4), here a selection of GI tissue electrophysiology simulations are presented to highlight what can be achievable with these technologies.

5.1 A Bidomain Model of Detailed ICC Networks

The structural integrity of the ICC network in the GI tract is an important factor for normal slow wave entrainment and GI motility. Simulations of GI slow waves at the tissue level involving a large physical network of ICC and SMC have generally adopted an idealised layered setup [10, 11]. In contrast, here a series of 2D images of the Kit-positive ICC structures were obtained from mice as previously described in the experimental study by Tharayil et al. [55]. The myenteric plexus ICC (ICC-MY) networks were obtained from a depth-averaged image data taken from a wild-type (WT) mouse. The depth-averaging was possible due to the relative thinness of the ICC-MY plexus in the transmural direction, and because the majority of the network geometry lay in-plane.

The ICC network geometries were obtained from the 2D images of the WT sample at the original in-plane resolutions. Each pixel in the image was represented by a grid point in the 2D model. A total of 262,144 grid points were generated for every image. The grid points were categorised as either a continuum ICC point (green in Fig. 4) or a non-ICC tissue point (black in Fig. 4). The

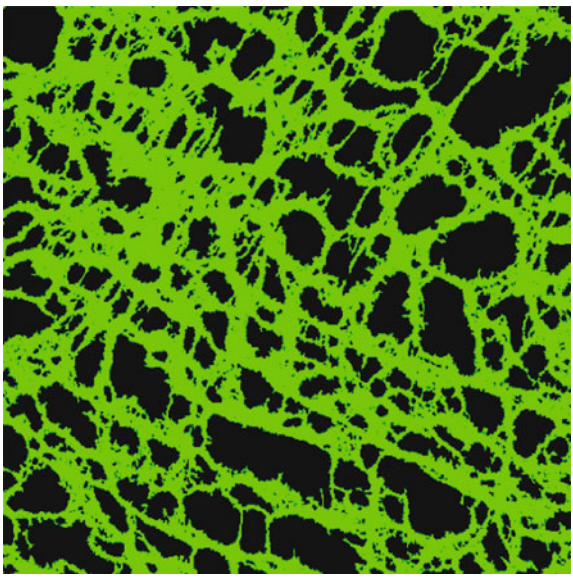

Fig. 4 A reconstructed image of the myenteric plexus ICC (ICC-MY) in a wild-type (WT) mouse intestine. The imaging process involved the whole mount preparations of the muscularis propria from the jejunum of four week old mice. The width of the image is approximately 300 μm. ICC were labelled using antibody specific agents. Images of the labelled structures were collected by a laser scanning confocal microscope

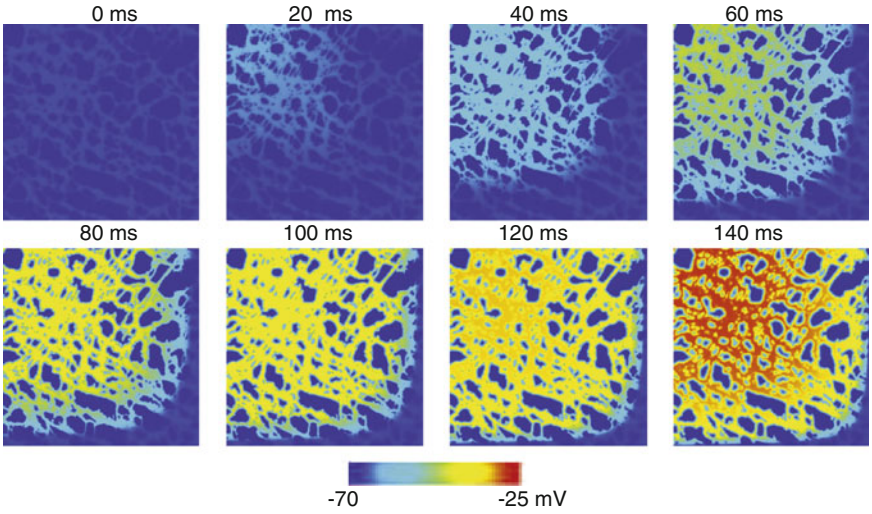

Fig. 5 Simulated slow propagation in the 2D model containing a normal ICC network structure using CMISS. Results were obtained by solving Eqs. 36 and 37 over the domain shown in Fig. 4. The *blue colour* represents the resting membrane potential and the *red colour* represents depolarised activity. The first image in the *top row* shows the V_m at time $t = 0$ ms and each subsequent image, from *left to right*, then down to the next row, is 20 ms apart. The propagation velocity was ~ 1.6 mm s^{-1}, while the main direction of depolarisation occurred from the *top left corner* towards to the *bottom right corner* of the tissue domain

bidomain model was solved to simulate propagation of slow waves along the resulting ICC network. The non-ICC tissue nodes were set to be membrane potential independent through prescribing $I_{ion} = 0$. The purpose of this was to eliminate any active responses from the background tissues while preserving their passive properties.

The ICC network in the 2D model was assigned a linear gradient of intrinsic frequencies from 3.0 to 2.9 cpm. The intrinsic frequency gradient was intentionally very small due to the limited physical dimensions of the tissue domain. Frequencies close to the intrinsic frequency of gastric slow waves were applied to the intestinal tissue geometries for two practical reasons. First, the selected ICC model was originally designed to reproduce gastric slow waves and it was most stable between 1 and 5 cpm. Second, the simulations focused only on the activation phase (the first 400 *ms*) of slow wave activity, whereas the duration of the slow wave is on the order of seconds. Therefore, the absolute value of the intrinsic slow wave frequencies was not an important factor for the simulation outcomes. The highest intrinsic frequencies were assigned to ICC in the top left corner of the 2D model, where the density of ICC was qualitatively the highest (Fig. 4).

Upon closer inspection of the activation wave fronts, it can be seen that the 2D model demonstrated a relatively uniform propagating slow wave, due to the relatively uniform distribution of the intact ICC network (Fig. 5). It has been

predicted that there is a degree of surplus capacity in ICC networks, such that ICC loss up to a threshold level may be inconsequential to transit, with impairments only manifesting if ICC loss is greater than a certain threshold [55]. Future modelling studies within the framework established here could focus on predicting the level of ICC loss that may lead to functional consequences for motility and transit in the gut.

5.2 The Extended Bidomain Model

The extended bidomain model (Sect. 3.1) was recently proposed [7] as a more accurate way of describing GI tissue as two or more different cell types can be incorporated at each point in the solution domain. Here we present a simulation that gives a direct comparison between the extended bidomain model and an equivalent traditional bidomain model.

As ICC and SMC are ubiquitously present throughout GI tissues, a comprehensive GI tissue model is obliged to include both cell types. The traditional bidomain framework (Sect. 3.2) allows only one intracellular space within each control volume (i.e., one cell type). One way of overcoming this limitation is to lump an ICC and a SMC into a single control volume while solving for the diffusion only between the ICC [18]. However, gap junctions have been identified not only between ICCs, but between ICCs and SMCs, and also between adjacent SMCs [17, 27]. Therefore, the approach of lumping an ICC and a SMC into one cell neglects the diffusion that is known to occur via gap junctions between neighbouring SMCs. The extended bidomain framework was designed to incorporate two cell types at each control volume and thus facilitates the SMC-SMC diffusion that is missing from the traditional bidomain model [7, 16].

Figure 6 shows the effects of omitting diffusion via gap junction between neighbouring SMC. Here a simplified 2D geometry was considered. Chaste (Sect. 4.3) was used to perform the simulations. In the traditional bidomain case, a lumped $ICC + SMC$ cell model was present with no connections between SMC. On the other hand, in the case of the extended bidomain, the ICC were modelled as cell (1) and the SMC were modelled as cell (2) (see Fig. 3) allowing for the additional electrical connection between SMCs (Fig. 6, top right). The values of tissue conductivities (σ) and gap junction conductance (G_{gap}) were prescribed to be the same in the two sets of simulations. Results (Fig. 6, lower panel) showed that neglecting the connections between SMCs (lumped $ICC + SMC$ case) caused noticeable differences in the ICC voltage profile and even more significant differences in the plateau potentials in the SMC.

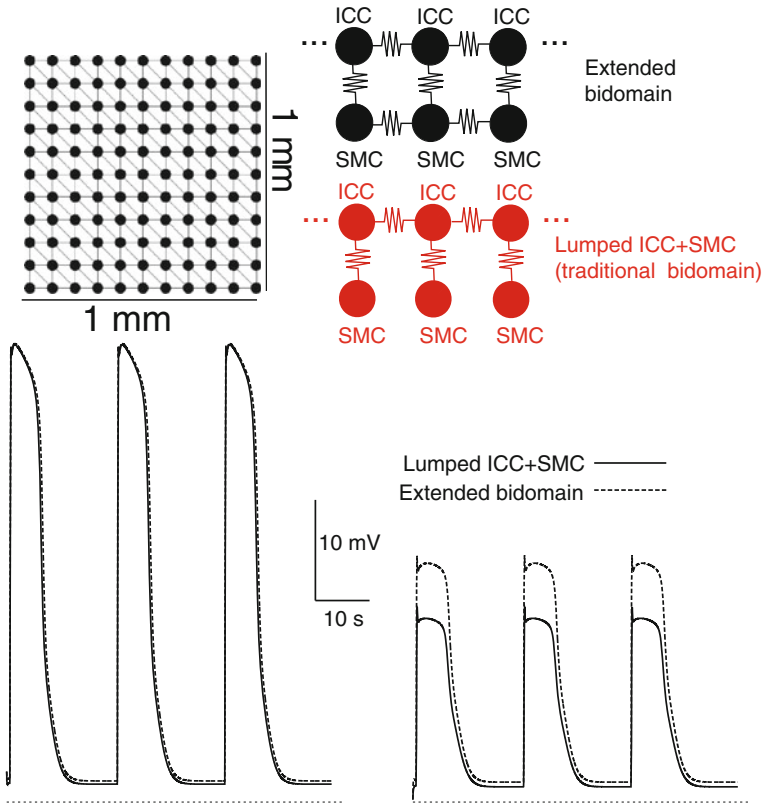

Fig. 6 Comparison between the extended bidomain framework and the traditional bidomain framework with lumped *ICC + SMC*. Simulations were run on a two-dimensional square sheet with a side of 1 mm (*upper panel*). In the lumped *ICC + SMC* situation, no connection is present between neighbouring SMC. The lower panel shows nodal time traces (from a node in the center of the square) for ICC (*left*) and SMC (*right*) voltage. Time and voltage bars in the lower panel apply to all traces. The *dotted blue line* indicates −70 mV

5.3 Whole Organ Modelling

The application of the continuum modelling frameworks presented in Sect. 3 to whole organ simulations depends upon an appropriate geometric description of the anatomy of the organ under consideration. One approach that has been adopted to create an anatomically-realistic geometry of a GI organ is to fit a derivative continuous finite element mesh to a cloud of data points that describes the surface of an organ of interest, e.g., the stomach. The surface geometry of the organ can be created from the data cloud by an iterative linear fitting technique, and a volumetric mesh of the organ wall can be subsequently constructed. The wall of the organ can be further refined to define the layered structure of the tissue model as

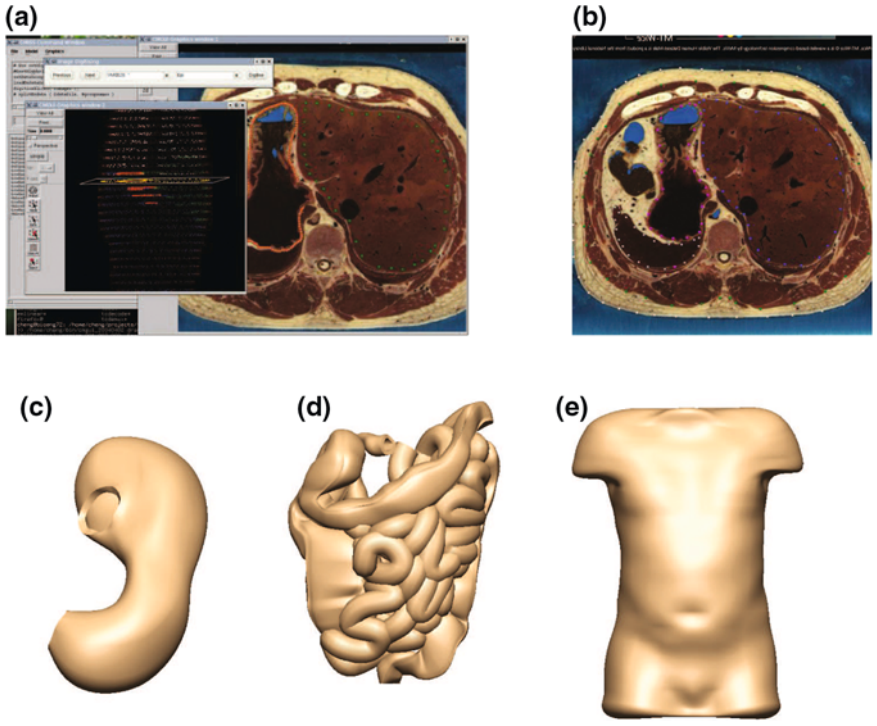

Fig. 7 Digitisation of gastrointestinal models. **a** Digitisation of the stomach using the CMGUI software. **b** A slice from the visible human project was used. **c** A stomach geometric model. **d** An intestine (small intestine and colon) geometric model. **e** A torso geometric model

required. Using this approach, the anatomical details of GI organs have been digitised from photographic images from the Visible Human Project [54] (Fig. 7) [11, 48].

Slow wave activation over whole-organ geometries has been modelled using the continuum approach [11, 19]. Until relatively recently, however, the phenomenological Fitzhugh-Nagumo cell models, such as the one proposed by Aliev et al. [1], were the only cell models that had been integrated into a whole-organ model [10]. The resulting simulations have generally shown a reasonable approximation of sequential activation of gastric or intestinal slow waves across the many layers of the organ models. For example, normal gastric slow waves have been simulated in a human stomach model, with outcomes successfully matching the conduction velocity and entrained frequency observed from sparse-electrode experiments [20]. Recent studies have also investigated the effects of functional uncoupling of slow waves, where the stomach model contained more than one entrainment frequencies [5]. By altering the excitability profile of ICCs in the antrum, a condition which allowed decoupled slow wave generation at the cellular level was imposed on the organ model within the multiscale framework.

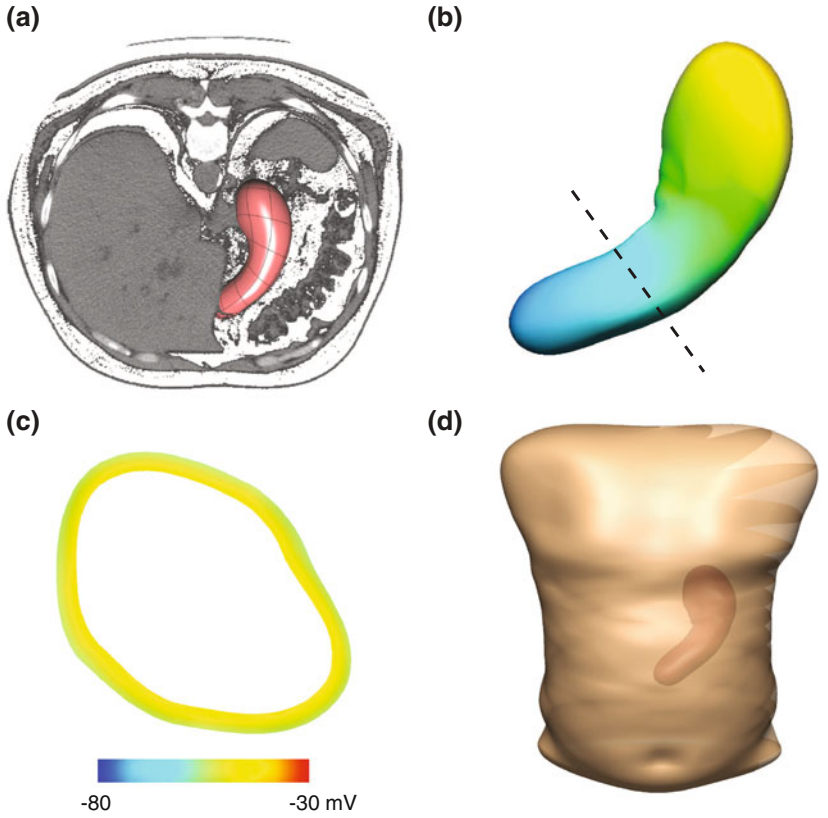

Fig. 8 Construction of a subject-specific virtual anatomical stomach model and torso model. **a** An axial view of the virtual stomach model embedded in the CT images taken of the patient prior to surgery. **b** The virtual stomach model that was constructed from the CT images. **c** A 10 mV membrane potential gradient was imposed across the gastric wall (site of shown cross-section of the stomach indicated by the *dashed-line* in **b**). **d** The virtual torso in which the stomach model was embedded to match the approximate orientation in the CT images

Here, slow wave activity in a whole-organ is demonstrated in a subject-specific virtual anatomical model of the stomach. First, a patient specific model was generated from a preoperative CT taken from a human patient (Fig. 8a). This particular subject was chosen as the reference model because a complete description of gastric slow wave times were obtained by intra-operative HR mapping and this patient was representative of typical normal activity [43]. The 3D outline of the stomach was manually digitised from the CT images. A derivative continuous finite element mesh was fitted to the digital outline of the stomach, from which the anatomical model was constructed [10]. The surface of the initial stomach mesh was then projected towards the centre-line of the mesh to obtain a muscle layer thickness of 2.66 mm [30]. The final anatomical model of the stomach is as shown in Fig. 8b.

A gradient of resting membrane potentials was also set in the whole-organ model (−30 to −43 mV in the fundus; −30 to −43 mV in the corpus; −58 to −67 mV in the antrum). A 1.04× variation in the resting potentials was included between the greater curvature and the lesser curvature of the stomach, and a gradient of −10 mV was also assigned across the stomach wall (Fig. 8c).

Simulated gastric slow waves in the whole organ model are illustrated in Fig. 9. The frequency of simulated slow waves at the organ level was the same as at the cellular level (i.e., 3.0 cpm). It took approximately 60 s of simulated time (i.e., one complete propagation cycle) for the activity to reach a steady state. The initial 60 s of simulated slow waves was therefore omitted from the analysis. The origin of the gastric slow wave was consistently situated at the appropriate pacemaker region on the greater curvature of the proximal corpus (e.g., depolarised events (coloured red) visible at $t = 4$ and 24 s). The initial propagation from the pacemaker region formed a wide wavefront in a band by approximately $t = 4$ s, which then propagated in the antegrade direction towards the pylorus. By 24 s, the onset of the second slow wave cycle was visible in the pacemaker region of the virtual stomach model, with the first cycle of activity having reached the mid corpus. By 44 s, the onset of the third slow wave cycle was visible in the pacemaker region, while the active edge of the first cycle of slow wave activity had entered the antral region. A maximum of four simultaneous wavefronts were visible (e.g., at 60 s), while the minimum number of simultaneous wavefronts was three. The global average of the

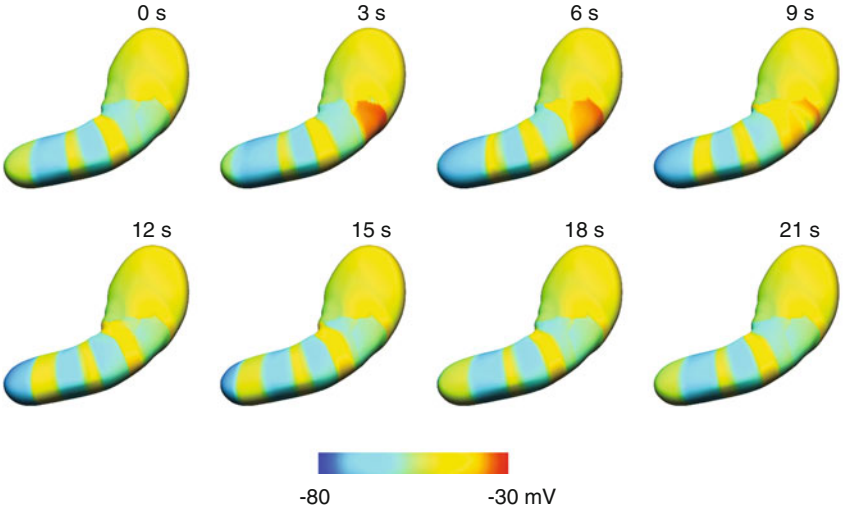

Fig. 9 Simulated slow waves in a virtual stomach model based on generic activation times of slow waves from human experiments [43]. A total of 21 s of propagation is shown. The *red colour* represents depolarised activity and the *blue colour* represents the resting membrane potentials. The simulation demonstrates that gastric slow waves originate from a pacemaker region (located in the upper corpus on the greater curvature), propagates into the corpus, and then continues into the antrum. There are also multiple and simultaneous wavefronts in the stomach

propagation velocity was $\sim$6.4 mm s^{-1}, with substantial regional variations ($\sim$7.7 mm s^{-1} in the pacemaker region, $\sim$2.8 mm s^{-1} in the corpus, and $\sim$5.9 mm s^{-1} in the antrum). The width of the slow wave depolarisation (coloured yellow in Fig. 9) was approximately 16 mm in the corpus and approximately 37 mm in the distal antrum. The slower local corpus velocity resulted in accrual of multiple narrow wavefront bands, with a wavefront separation displacement of approximately 50 mm. All of these modelled slow wave propagation dynamics were in accordance with experimental data [43].

6 Conclusions and Future Directions

Advances in molecular biology and related fields have meant that more and more information is being uncovered about GI electrophysiology, its control mechanisms, and its relationship with motility at the cellular and subcellular levels. Although significant insights can be gathered by examining the cellular level effects of an abnormality, the multi-cellular tissue level system is remarkably adaptable. The electrotonic load, along with modulation by the enteric and central nervous systems, help to smooth out cellular heterogeneities and result in an electrically robust tissue construct. Therefore, one of the key roles of tissue level modelling is to identify which cellular and subcellular maladies can affect tissue and subsequently organ function.

As illustrated in Sects. 3 and 5, the continuum modeling approach is currently the most widely used for describing the events at multiple scales that lead to propagation of electrical activity across GI tissues. Historically, due to limitations in computational power, there has often been a trade-off between the complexity of the cell model used and the scale of the continuum model. This is evident by the fact that earlier GI models often employed cell models with relatively few parameters. Recent advancements in computational power and the use of parallel computing for large 3D models of GI organs (Sect. 4) are increasingly facilitating researchers to simulate slow wave propagation across entire organs starting from accurate cellular descriptions (Table 1).

In parallel with the potential benefits of biophysically detailed tissue models, there are also significant challenges. With the development of new conceptual frameworks, such as the extended bidomain model, we have the tools necessary to solve tissue level problems but it is the parametrization of such models that remains an open question. The GI tract is a truly three dimensional layered structure that includes multiple cell types. The electrical coupling coefficients between the layers, within each layer, in each direction, between cells of the same type, and between cells of different types have yet to be properly quantified. It is also known that significant regional heterogeneities exist, even within the same organ. While the conceptual models, and indeed their implementations, have the facilities to incorporate these heterogeneities, without quantification there remains

too large a number of free parameters. One potential source of parameters are the recent high resolution extracellular recordings of O'Grady et al. [43]. These can at least aid in ensuring that the chosen set of model parameters can reproduce local macroscopic behaviour. It is our hope that in the near future data from arrays of plunge electrodes, as have been used in the cardiac field, may be available to give quantitative 3D information on electrical coupling and propagation.

The majority of the work presented in this chapter have focussed on gastric slow wave activity. One reason is that there are relatively limited knowledge and simulations about intestinal and colonic slow waves. While the slow wave activity in other areas of the GI tract share many similarities with the stomach, there remain many important fundamental differences, which should be addressed when modelling slow wave activity in those other GI organs.

An accurate, multi-scale 3D description of the electrical propagation in GI tissues is seen as critical for at least two major future directions of research. The first one aims at coupling models of mechanical contraction to the underlying electrophysiology described in this chapter. While several electromechanical models of contractions of the whole heart have been proposed [9, 42], none exists for any organ along the GI tract. The lack of an integrated electromechanical description of the GI tract is hindering a full understanding of several GI motility disorders, particularly so when considering recent characterizations of mechano-sensitive ion channels in the GI tract [32].

Another interesting line of research that may stem from an accurate 3D electrophysiological characterization of GI tissues is that of inverse modelling (as described by Bradshaw et al. in "Biomagnetic Signatures of Gastrointestinal Electrical Activity" of this volume). This class of problems aims at relating electrical (or magnetic) recordings obtained at the body surface to the underlying organ activity. Any attempt of interpreting far-field signals using a mathematical model has the detailed knowledge of the underlying phenomenon as a pre-requisite. In the GI tract, this translates into having a precise 3D model of slow wave activation and propagation across the various tissues.

The progresses in modelling GI electrophysiology at tissue level described in this chapter will therefore be important in providing a better understanding of the pathophysiology of GI motility disorders both from a basic science standpoint and in a clinical setting.

References

1. Aliev RR, Richards W, Wikswo JP (2000) A simple nonlinear model of electrical activity in the intestine. J Theor Biol 204(1):21–28
2. Bassingthwaighte J, Hunter P, Noble D (2009) The Cardiac Physiome: perspectives for the future. Exp Physiol 94(5):597–605
3. Beckett EA, Bayguinov YR, Sanders KM, Ward SM, Hirst GD (2004) Properties of unitary potentials generated by intramuscular interstitial cells of Cajal in the murine and guinea-pig gastric fundus. J Physiol 559(1):259–69

4. Bradley C, Bowery A, Britten R, Budelmann V, Camara O, Christie R, Cookson A, Frangi AF, Gamage TB, Heidlauf T, Krittian S, Ladd D, Little C, Mithraratne K, Nash M, Nickerson D, Nielsen P, Nordbø O, Omholt S, Pashaei A, Paterson D, Rajagopal V, Reeve A, Röhrle O, Safaei S, Sebastian R, Steghöfer M, Wu T, Yu T, Zhang H, Hunter P (2011) Opencmiss: a multi-physics & multi-scale computational infrastructure for the vph/physiome project. Prog Biophys Mol Biol 107(1):32–47
5. Buist ML, Cheng LK, Sanders KM, Pullan AJ (2006) Multiscale modelling of human gastric electric activity: can the electrogastrogram detect functional electrical uncoupling? Exp Physiol 91(2):383–90
6. Buist ML, Cheng LK, Yassi R, Bradshaw LA, Richards WO, Pullan AJ (2004) An Anatomical Model of the Gastric System for Producing Bioelectric and Biomagnetic Fields. Physiol Meas 25:849–864
7. Buist ML, Poh YC (2010) An extended bidomain framework incorporating multiple cell types. Biophys J 99(1):13–8
8. Buist ML, Sands GB, Hunter PJ, Pullan AJ (2003) A deformable finite element derived finite difference method for cardiac activation problems. Ann Biomed Eng 31(5):577–588
9. Campbell SG, McCulloch AD (2011) Multi-scale computational models of familial hypertrophic cardiomyopathy: genotype to phenotype. J Roy Soc (Interface) 8(64): 1550–1561
10. Cheng LK, Komuro R, Austin TM, Buist ML, Pullan AJ (2007) Anatomically realistic multiscale models of normal and abnormal gastrointestinal electrical activity. World J Gastroenterol 13(9):1378–83
11. Cheng LK, O'Grady G, Du P, Egbuji J, Windsor JA, Pullan AJ (2010) Gastrointestinal system. Wiley Interdiscip Rev Syst Biol Med 2(1):65–79
12. Cooper JP (2009) Automatic validation and optimisation of biological models. PhD thesis, University of Oxford, http://ora.ouls.ox.ac.uk/objects/uuid:24b96d62-b47c-458d-9dff-79b27dbdc9f2
13. Cooper JP, Corrias A, Gavaghan D, Noble D (2011) Considerations for the use of cellular electrophysiology models within cardiac tissue simulations. Progress in Biophysics and Molecular Biology 107(1):74–80
14. Corrias A, Buist ML (2007) A quantitative model of gastric smooth muscle cellular activation. Ann Biomed Eng 35(9):1595–607
15. Corrias A, Buist ML (2008) Quantitative cellular description of gastric slow wave activity. Am J Physiol Gastrointest Liver Physiol 294(4):989–95
16. Corrias A, Pathmanathan P, Gavaghan D, Buist ML (2011) Modelling tissue electrophysiology with multiple cell types: applications of the extended bidomain framework. Integrative Biology 4(2):192–201
17. Daniel EE (2004) Communication between interstitial cells of Cajal and gastrointestinal muscle. Neurogastroenterol Motil 16(Suppl 1):118–22
18. Du P, O'Grady G, Cheng LK, Pullan AJ (2010) A multi-scale model of the electrophysiological basis of the human electrogastrogram. Biophys J 99(9):2784–92
19. Du P, O'Grady G, Davidson G, Cheng LK, Pullan AJ (2010) Multi-scale modelling of gastrointestinal electrophysiology and experimental validation. Crit Rev Biomed Eng 38(3):225–54
20. Du P, O'Grady G, Windsor J, Cheng LK, Pullan AJ (2009) A tissue framework for simulating the effects of gastric electrical stimulation and in-vivo validation. IEEE Trans Biomed Eng 56(12):2755–61
21. Edwards FR, Hirst GD (2003) Mathematical description of regenerative potentials recorded from circular smooth muscle of guinea pig antrum. Am J Physiol Gastrointest Liver Physiol 285(4):G661–70
22. Edwards FR, Hirst GD (2006) An electrical analysis of slow wave propagation in the guinea-pig gastric antrum. J Physiol, 571(Pt1):179–89

23. Faville RA, Pullan AJ, Sanders KM, Koh SD, Lloyd CM, Smith NP (2009) Biophysically based mathematical modeling of interstitial cells of Cajal slow wave activity generated from a discrete unitary potential basis. Biophys J 96(12):4834–52
24. Faville RA, Pullan AJ, Sanders KM, Smith NP (2008) A biophysically based mathematical model of unitary potential activity in interstitial cells of Cajal. Biophys J 95(1):88–104
25. Fitzhugh R (1962) Computation of impulse initiation and saltatory conduction in a myelinated nerve fiber. Biophys J 2:11–12
26. Fu P, Bardakjian BL (1991) System identification of electrically coupled smooth muscle cells: the passive electrical properties. IEEE Trans Biomed Eng 38(11):1130–1140
27. Hanani M, Farrugia G, Komuro T (2005) Intercellular coupling of interstitial cells of cajal in the digestive tract. Int Rev Cytol 242:249–82
28. Henriquez CS (1993) Simulating the electrical behavior of cardiac tissue using the bidomain model. Crit Rev Biomed Eng 21(1):1–77
29. Hodgkin AL, Huxley AF (1952) A quantitative description of membrane current and its application to conduction and excitation in nerve. J Physiol 117(4):500–44
30. Huh CH, Bhutani MS, Farfan EB, Bolch WE (2003) Individual variations in mucosa and total wall thickness in the stomach and rectum assessed via endoscopic ultrasound. Physiol Meas 24:N15–22
31. Hunter PJ, Borg TK (2003) Integration from proteins to organs: the Physiome Project. Nat Rev Mol Cell Biol 4:237–243
32. Kraichely RE, Farrugia G (2007) Mechanosensitive ion channels in interstitial cells of Cajal and smooth muscle of the gastrointestinal tract. Neurogastroenterol Motil 19(4):245–52
33. Lammers WJ, Stephen B, Arafat K, Manefield GW (1996) High resolution electrical mapping in the gastrointestinal system: initial results. Neurogastroenterol Motil 8(3):207–16
34. Lin AS, Buist ML, Cheng LK, Smith NP, Pullan AJ (2006) Computational simulations of the human magneto- and electroenterogram. Ann Biomed Eng 34(8):1322–31
35. Lin AS, Buist ML, Smith NP, Pullan AJ (2006) Modelling slow wave activity in the small intestine. J Theor Biol 242:356–62
36. R. MacLeod and M. L. Buist. The Forward Problem of Electrocardiography, chapter Comprehensive Electrocardiology, pages 247–288. Springer, second edition, 2010.
37. Miller WT, Geselowitz DB (1983) A bidomain model for anisotropic cardiac muscle. Ann Biomed Eng 11(3–4):191–206
38. Mirizzi N, Stella R, Scafoglieri U (1985) A model of extracellular waveshape of the gastric electrical activity. Med Biol Eng Comp 23:33–37
39. Muller-Borer BJ, Erdman DJ, Buchanan JW (1994) Electrical coupling and impulse propagation in anatomically modeled ventricular tissue. IEEE Trans Biomed Eng 41(5):445–54
40. Nagumo J, Arimoto S, Yoshizawa S (1962) An active pulse transmission line simulating nerve axon. Proc IRE 50:2061–2070
41. Nelsen TS, Becker JC (1968) Simulation of the electrical and mechanical gradient of the small intestine. Am J Physiol 214:749–57
42. Nordsletten DA, Niederer SA, Nash MP, Hunter PJ, Smith NP (2011) Coupling multi-physics models to cardiac mechanics. Progr Biophys Mol Biol 104(1–3):77–88
43. O'Grady G, Du P, Cheng LK, Egbuji JU, Lammers WJEP, Windsor JA, Pullan AJ (2010) Origin and propagation of human gastric slow-wave activity defined by high-resolution mapping. Am J Physiol Gastrointest Liver Physiol 21(3):G585–92
44. Pitt-Francis J, Pathmanathan P, Bernabeu MO, Bordas R, Cooper J, Fletcher AG, Mirams GR, Murray P, Osborne JM, Walter A, Chapman SJ, Garny A, van Leeuwen IMM, Maini PK, Rodriguez B, Waters SL, Whiteley JP, Byrne HM, Gavaghan DJ (2009) Chaste: a test-driven approach to software development for biological modelling. Computer Physics Communications 180(12):2452–2471
45. Publicover NG, Sanders KM (1989) Are relaxation oscillators an appropriate model of gastrointestinal electrical activity? Am J Physiol 256(2 pt 1):G265–74

46. Pullan AJ, Buist ML, Cheng LK (2005) Mathematically modelling the electrical activity of the heart: from cell to body surface and back again. World scientific publishing Co Pte Ltd, Singapore
47. Pullan AJ, Buist ML, Sands GB, Cheng LK, Smith NP (2003) Cardiac electrical activity-from heart to body surface and back again. J Electrocardiol 36(Suppl):63–7
48. Pullan AJ, Cheng LK, Yassi R, Buist ML (2004) Modelling gastrointestinal bioelectric activity. Prog Biophys Mol Biol, 85:523–50
49. Richards FA (1969) Simulation of the phenomenon of concealed conduction. Comput Biomed Res 2(4):362–72
50. Rodriguez B, Trayanova N, Noble D (2006) Modeling Cardiac Ischemia. Annals of the New York Academy of Sciences 1080(1):395–414
51. Sarna SK, Daniel EE (1973) Electrical stimulation of gastric electrical control activity. Am J Physiol 225(1):125–131
52. Sarna SK, Daniel EE, Kingma YJ (1971) Simulation of slow-wave electrical activity of small intestine. Am J Physiol 221:166–175
53. Sarna SK, Daniel EE, Kingma YJ (1972) Effects of partial cuts on gastric electrical control activity and its computer model. Am J Physiol 223(2):332–40
54. Spitzer V, Ackerman MJ, Scherzinger AL, Whitlock D (1996) The visible human male: a technical report. J Am Med Inform Assoc 3:118–30
55. Tharayil VS, Wouters MM, Stanich JE, Roeder JL, Lei S, Beyder A, Gomez-Pinilla PJ, Gershon MD, Maroteaux L, Gibbons SJ, Farrugia G (2010) Lack of serotonin 5-HT2B receptor alters proliferation and network volume of interstitial cells of Cajal in vivo. Neurogastroenterol Motil, 22(4):462–9
56. Trew ML, Caldwell BJ, Sands GB, Hooks DA, Tai DC, Austin TM, LeGrice IJ, Pullan AJ, Smaill BH (2006) Cardiac electrophysiology and tissue structure: bridging the scale gap with a joint measurement and modelling paradigm. Exp Physiol 91(2):355–70
57. Xie F, Qu Z, Yang J, Baher A, Weiss JN, Garfinkel A (2004) A simulation study of the effects of cardiac anatomy in ventricular fibrillation. J Clin Invest 133(5):686–93
58. Youm JB, Kim N, Han J, Kim E, Joo H, Leem CH, Goto G, Noma A, Earm YE (2006) A mathematical model of pacemaker activity recorded from mouse small intestine. Philos Transact A Math Phys Eng Sci 364(1842):1135–54
59. Zhao J, Trew ML, Legrice IJ, Smaill BH, Pullan AJ (2009) A tissue-specific model of reentry in the right atrial appendage. J Cardiovasc Electrophysiol 20(6):675–84

Colonic Manometry: What Do the Squiggly Lines Really Tell Us?

Phil G. Dinning

Abstract Colonic motility consists of a range of motor patterns that ensure net flow rates appropriate for the break down of food, absorption of water and nutrients and excretion of waste. Abnormalities in these motor patterns remain a leading hypothesis to explain the cause of functional colonic disorders such as constipation. However, whilst manometric catheters are used as one of the primary tools to record colonic motor patterns, we are as yet unable to define motor patterns that clearly separate patients from controls. Indeed in many instances while some changes in the patterns of manometric squiggly lines can be identified, it remains a matter of intuition and speculation as to how these changes may relate to a patient's symptoms. In this chapter, motor patterns recorded by colonic manometry will be compared to description of colonic wall motion and luminal transit. In doing so the chapter will attempt to detail what manometry is really telling us about colonic function. In addition the future direction and current advances in colonic manometry will also be discussed.

1 Introduction

Functional colonic disorders convey significant financial and societal burdens. One of the most common of these disorders is constipation, with an estimated 15 % of adults and 9 % of children reporting symptoms [23]. The direct and indirect costs of constipation are substantial. In the USA alone, an estimated $US1.7 billion/year is spent on adults [43] with a further $US3.9 billion/year on children [69]. Despite the expenditure a third of all patients will fail to gain relief of their symptoms [19, 78]. In 1908 the English gastroenterologist Arthur Hertz published a paper on the treatment

P. G. Dinning (✉)
Departments of Gastroenterology and Surgery, Flinders Medical Centre,
Flinders University, Bedford Park, South Australia 5042, Australia
e-mail: Phil.Dinning@flinders.edu.au

L. K. Cheng et al. (eds.), *New Advances in Gastrointestinal Motility Research*,
Lecture Notes in Computational Vision and Biomechanics 10,
DOI: 10.1007/978-94-007-6561-0_11, © Springer Science+Business Media Dordrecht 2013

of constipation [49] and his opening sentence was "*The treatment of chronic constipation is always experimental. One method is tried after another until by chance, that suited to the individual case is discovered*" [49]. Over 100 years later many gastroenterologists and colorectal surgeons could write a similar sentence, when faced with a patient with idiopathic slow transit constipation.

The gastrointestinal tract can be regarded as a viscoelastic body with active muscular components. Controlled propulsion and mixing of content along the digestive tract is achieved by a rich repertoire of motor patterns that ensure net flow rates appropriate for the break down of food, absorption of nutrients and excretion of waste. These movements are due to coordinated contractions and relaxations of the internal circular smooth muscle layer and the external longitudinal smooth muscle. These smooth muscle layers are controlled by both myogenic (initiated by non-neural pacemaker cells) and neurogenic mechanism (initiated by enteric neurons), which interact to generate diverse motor behaviour of the intestine. When problems occur with these fundamental controlling mechanisms functional gastrointestinal disorders are likely to develop. Over many decades, the disciplines of physiology and neuroscience have developed techniques to study the motility of the gut. One of these, used to measure the in-vivo contractions of the colon, is colonic manometry. This has provided valuable insight into the normal physiology of the colon and also the pathophysiology that exists in constipation. However, the clinical worth of colonic manometry, particularly in adults, remains unproven. In many instances while some changes in the patterns of squiggly lines can be identified, it remains a matter of intuition and speculation as to how these changes may relate to a patient's symptoms.

This chapter will provide an overview of findings from colonic manometry studies and the advances that have been made. It also will relate the motility patterns, detected by manometry, to data obtained from historic and recent measures of actual colonic transit. In doing so, an attempt will be made to establish whether or not colonic manometry is capable of detailing the motility of the colon. In short it will provide insight into what the colonic manometric trace is actually telling us.

2 Nomenclature

Studies of colonic manometry have used a wide range of terminologies to describe the recorded motor patterns. These include pressure waves, propagating contractions, propagating sequences, propagating pressure waves, high amplitude propagating contractions, high amplitude propagating sequences, and giant migrating contractions. As there is no standardised terminology in this chapter, the generic term "pressure event" will be used to encompass motor pattern detected by colonic manometry. For pressure events that are deemed to be propagating the generic term "*propagating event*" will be used. When specifics regarding the amplitude of the *propagating events* are required, the terms "*high amplitude*

propagating events" or "*low amplitude propagating events*" will be used. Commonly used abbreviations will be avoided.

When referring to transit studies or propagating events the polarity (direction of movement or travel) is important. Again a range of different terminology is used. Here "*antegrade*" will refer to the anal or aborad direction and "*retrograde*" will refer to the oral or orad direction. In many historic papers detailing colonic transit the terminology of peristalsis (anal) or antiperistalsis (oral) is used, here these will also be referred to as antegrade or retrograde, respectively.

3 Colonic Manometry

There have been several recent reviews that have detailed colonic manometry methodology and the findings derived from these studies [30, 34, 35], a brief overview of the more significant findings are provided below.

Since the introduction of intraluminal pressure recording by Legros and Onimus in 1869 [66], intraluminal manometry has been recognised as a useful experimental technique to record gastrointestinal motility. In the human colon the initial manometric devices consisted of air filled balloons connected to pressure transducers [47, 83, 89]. These initial studies were conducted under non-physiological conditions, with the manometric catheters placed through colostomies and the colonic activity was stimulated with laxatives or balloon distension. In the late 1980s water perfused manometric catheters with multiple recording sites were introduced into the colon colonoscopically [11, 73]. The catheters spanned the transverse, descending and sigmoid colon and heralded a new era in in-vivo colonic research. Over the subsequent two decades these manometric studies have attempted to define the normal physiology of the colon in healthy controls and the pathophysiology in patients with functional colonic disorders.

From the first of the 24 h colonic manometry recordings [11] it became apparent that the colon consisted of a large quantity of spontaneous motor activity that was present for most of the recording time. These motor pattern have been classified by Bassotti et al. [10] into either; (i) segmental activity, which consisted of single pressure events or bursts of rhythmic/arrhythmic pressure events; or (ii) propagated activity which consisted of low-amplitude propagated events or high-amplitude propagated events.

For most studies of colonic manometry, it has been the presence or the absence of the high amplitude propagating events that has differentiated the colonic motility between patients and controls. For example in healthy controls the frequency of high amplitude propagating events is reported to be between 6–20/24 h and this frequency has been shown to be either absent or diminished in patients with severe constipation (Fig. 1). In health there is also a postprandial increase in the frequency of these events [11, 3, 40], and this meal response has been shown to be absent or diminished in constipated patients [40, 12, 13, 16, 25, 26, 27, 53, 61, 68, 79] (Fig. 1).

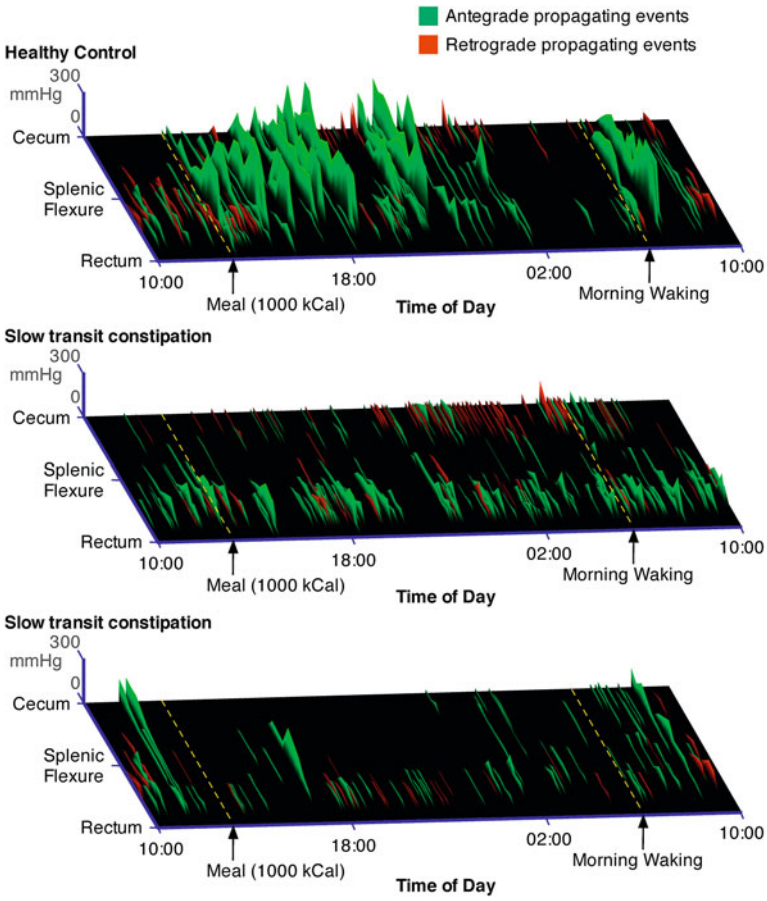

Fig. 1 Twenty four spatiotemporal maps of propagating events recorded throughout the colon in a healthy control (*top*) and two patients with slow transit constipation (*middle* and *bottom*). In each map the ridges represents individual antegrade or retrograde propagating events. The antegrade propagating events originate at the orad end of the ridge, and retrograde events originate at the anal end of the ridge. The proximal margin of each antegrade and retrograde ridge indicates the precise site and time of the origin of that propagating event. The axial length of the ridge indicates the extent of propagation. The high amplitude propagating events are clearly evident in the healthy control (*top*) as is a colonic response to a meal and morning waking. These responses are not as evident in the patients. However in the second of the patients (*bottom* map) 6 propagating events were recorded with component pressure waves exceeding 100 mmHg. These can classified as high amplitude propagating events, indicating the overlap in motor patterns that can exists between patients and controls

However, these findings are not consistent amongst all studies. Both adults [29] and children [61] with delayed colonic transit are capable of generating a daily frequency of high amplitude propagating events that falls within the normal range (Fig. 1). Whilst in a short duration study (3 h) of descending colonic motility no

significant difference was found between the frequency of high amplitude propagating events between healthy controls and patients with constipation [74].

The fact that constipated patients can generate pressure events associated with normal colonic motility is a significant problem when trying to use colonic manometry to either diagnose or guide treatment for constipation. Indeed as recently as 2008, a consensus paper published by the American Neurogastroenterology and Motility Society concluded that: "*There are no published quantitative data of phasic contractility that unequivocally differentiate normal colonic function from colonic inertia*" [17].

Furthermore, there is a long held, but unproven belief that colonic manometry does not "*record contractions that fail to occlude the lumen up to the diameter of the recording tube*" [85]. As the colonic manometry catheters are relatively thin (3–5 mm) in relation to the maximal distended diameter of the colon ($\approx$50 mm) it has been assumed that colonic manometry may miss the majority subtle wall movements and pressure events. This idea has been championed by a study utilizing a barostat device, which indicated that when the colon exceeds a diameter of 5.6 cm, manometry may miss up to 70 % of contractile events [92].

It needs to be recognized that the "5.6 cm" diameter quoted in that study was derived by isobaric distension of the colon using the barostat balloon, and it is therefore highly unlikely to represent the natural working diameter of the colon. Nevertheless, the fact remains that there is doubt surrounding the recording capabilities of colonic manometry. To assess what colonic manometry is capable of recording, the following sections examine manometry data in light of the findings and observation made from studies of colonic transit.

4 Colonic Transit

In 1895, Wilhelm Conrad Röntgen discovered x-radiation (Rontgen Ray or x-rays) [90], and with their discovery researchers were able to study the movement of content through the digestive tract. The first published account of colonic transit defined by x-rays in humans was in 1907 by Arthur Hertz [48] and by 1912 he was publishing accounts of the speed of transit through the human colon [50]. To this day radio-opaque markers are still used to make up the bulk of colonic transit studies conducted throughout the world [34]. However, with ethical constraints introduced into the field once the dangers of radiation exposure were known, modern x-ray transit studies only provide a snap shot of colonic motility. It is only through the historic publication involving x-ray of the human colon that a detailed concept of colonic movement and wall motion can be determined. More modern techniques such as radionuclide scintigraphy and the recently emerging Magnetic Tracking System have also significantly helped to build a picture of motility throughout the colon. The methodology and pros and cons of these techniques have been discussed in detail elsewhere [28, 33].

5 Associating Luminal Transit with Pressure Events

5.1 Retrograde Flow and Retrograde Propagating Events

In 1902 the first real proponent to utilise x-ray to describe colonic motility was Walter Cannon [18]. His seminal work defined the temporal relationships that exist between muscle contractions of the cat colon with movement of colonic content. In his work he not only described antegrade movement but he also described retrograde movement in the transverse and ascending colon. While this retrograde flow in cats had been previously described in 1890 by Carl Jacobj [24], such flow in the human colon was originally thought not to exist. In 1913 Arthur Hertz published a paper on the human ileocolonic junction in which he wrote "*Our X-ray investigations have, however, shown that antiperistalsis does not occur in man under normal conditions*" [51]. This belief was held at least until 1925 where Arthur Hurst wrote "*But we know that under normal conditions there is no antiperistalsis in the proximal part of the colon* [58]. However, by 1933 the opinions on retrograde events had begun to change with Fred Kruse describing their importance in the proximal colon, in his paper on functional disorders of the colon [64].

With the development and use of radio-opaque disks, evidence of retrograde flow became evident. In 1965 Halls reported that radio-opaque disks ingested 12 h before obtaining an x-ray were lying distal to the ones ingested 24 h earlier [46]. More recently the real-time monitoring of an ingested magnet with the Magnet Tracking System [54] has shown that "*retrograde displacement was clearly demonstrated as part of the colonic motility pattern in every colonic segment*".

In 1989 a combined study of colonic scintigraphy and manometry indicated that recordable pressure events were associated with the movement of the isotopic tracer [72]. In that study a manometric catheter with only three recording ports spaced at 15 cm was used. As such only one sensor was located in the transverse, descending and sigmoid colon. The study described the direction of movement of the tracer as being determined by the levels of motor activity in adjacent sites; always moving from regions of high activity to low activity [72]. Moreno-Osset et al. also claimed that 80 % antegrade distal colonic movement of radioisotope refluxed back (retrograde movement) into the transverse colon. However, they were unable to associate this with specific motor events.

In 2000 Cook et al. published a study of combined colonic scintigraphy and manometry, utilising a catheter with 12 recording sites spaced at 10 cm intervals. The study identified retrograde propagating events, primarily in the proximal colon, and 10 % were associated with retrograde flow [22]. Cook et al. also observed that antegrade propagating events were either non-propulsive or inefficient in their propulsion.

To help interpret the finding from Cook et al. [22], we can look to animal studies. In 2001 Bedrich and Ehrlien published a highly detailed and rarely cited study of combined x-ray and manometry in the sheep colon [14]. They were able to record movement through the colon in real-time and correlate this movement

with the intraluminal pressure. The following observation was made in relation to the movement of content associated with pressure events "*Because the constrictions did not occlude the lumen, digesta simultaneously flowed backwards through the central orifice of the circular constriction. When the waves faded out, a jetlike backflow occurred*". The study also confirmed that all of the antegrade and retrograde propagating events swept digesta in front of the waves [14].

Bedrich and Ehrlien's study is likely to help explain the lack of propulsion reported by Cook et al. [22]. The scintigraphic images in Cook's study were taken every 15 s and therefore they would have missed the reflux of isotope, leaving the investigators with an impression that nothing moved on many occasions. In subsequent studies of combined colonic scintigraphy and manometry, the vast majority all of the identified retrograde propagating events were associated with retrograde flow [36, 37]. The increased correlation between flow and motor patterns was attributed to two factors; (1) improved techniques of analysing scintigraphic images [32]; and (2) a increased spatial resolution between recording sites on the manometric catheter. Retrograde propagating events tend to travel shorter distances along the colon [3, 22] when compared to antegrade ones. Therefore, the closer the recording sites are spaced the more likely to capture retrograde events (*also see* Sect. 7).

Summary: These data would suggest that when retrograde propagating events are identified in the human colon they are propulsive of content. Their role in the physiology of the colon is likely to be the retardation of antegrade flow as well as helping to mix colonic content. It can also be concluded that retrograde flow in the form of reflux occurs during and immediately following antegrade propagating events. This helps in holding content in the colon for sufficient time to allow absorption of water and electrolytes and explains why transit through the colon is so much slower than other regions of the gastrointestinal tract.

5.2 Antegrade Flow

In 1907 Prof Arthur Hertz published the description of an event that he witnessed in the human colon in which digesta was moved rapidly from one section to another [48]. This became known as the colonic *"mass movement"* and over the following years several other investigators reported similar observations [89, 1, 55, 56, 84]. The description of a mass movement remains one of the most recognisable motility features of the colon to this day [48].

The early radiological observations concluded that the "mass movement" was the normal movement in the colon and that it only occurred 3–4 times a day and for the remainder of the time the colon remained inactive. Indeed the radiologist Guido Holzknecht claimed that in a thousand observations he had seen the colon move only twice [54]. With the development of x-ray cinematography, these claims began to be refuted. In 1911 Gottwald Scharz published a paper stating that

the colon is rarely inactive and instead consists of many slow peristaltic movements throughout the day [56].

When colonic manometry was combined with x-ray observation, the studies helped to confirm that artificially induced "mass movements" was temporally associated with regular sequence of pressure events that travelled along the colon behind the moving bolus of content [47, 83, 89]. Subsequent analysis of 24-hour colonic water perfused manometry studies identified spontaneous high amplitude propagating events that were labelled as the manometric equivalent of the mass movement [11]. By combining scintigraphic recordings with colonic manometry, Cook et al. showed that these spontaneous high amplitude propagating events were temporally associated with incomplete luminal propulsion [22].

While the combined manometry/scintigraphy or radiology studies have helped to provide evidence of the propulsive nature of high amplitude propagating event, the early descriptive radiographic studies in human colon combined with data collated from animal studies can help to indirectly determine the propulsive nature of pressure events in the absence of any measure of transit. In 1909 when Guido Holzknechtg described his rarely seen colonic movement he wrote, "*the haustral segmentation evident in the ascending and transverse colon, disappeared as the colonic content shifted to the descending colon. Once the movement was complete the haustral indentations soon reappeared*" [56]. Such description reflects the coordinated interactions that exist between the longitudinal and circular muscles layers of the colon. The disappearance of the haustra, indicates a relaxation of the longitudinal muscle layers and movement of content suggests a propagated contraction of the circular muscle. Over the next 60 years, these detailed descriptions were repeated by several investigators [13, 52, 55, 57]. In addition the same phenomena has been described by Bedrich in the sheep colon in-vivo [48], Ehrlein in the rabbit proximal colon in-vivo [58] and by Lentle in the rabbit proximal colon in-vitro [67].

When these descriptors are viewed in light of the colonic manometry recording, the phenomena can be easily seen (Fig. 2). In Fig. 2 low amplitude and high amplitude pressure events can be seen. The low amplitude events disappear in the zone immediately prior to the high amplitude propagating events. This zone has been described as a region of "descending inhibition" [85] and marks the point where the flow, described in the studies above, occurs. After the high amplitude propagating event has passed, the low amplitude activity returns. In radiographic descriptions this activity is described as return of the haustral indentations [56].

The formation of the haustra has been associated with mixing [6] and the subtle movements of colonic content [84]. These findings are supported by the Magnet Tracking System in which the authors describe a one third of the movements made by the ingested magnet as "slow" (<10 cm/min) displacements [89]. Studies have also show that these low amplitude propagating pressure events are associated with subtle movement of colonic content [37]. Collectively these data confirm previous speculation [10, 9] that the low amplitude propagating and nonpropagating events are associated with segmentation and perhaps the actual formation of haustra.

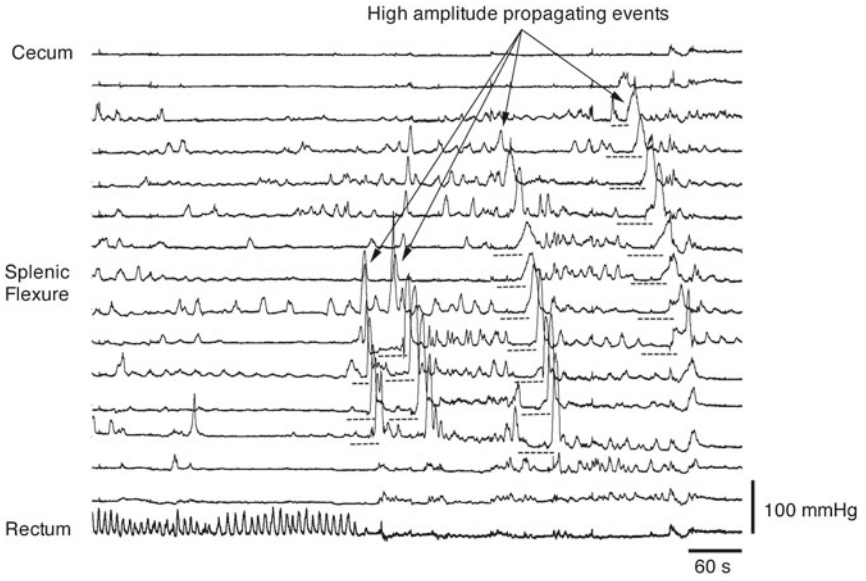

Fig. 2 A sequence of four high amplitude propagating events recorded in a healthy female. Note that prior to each of the high amplitude events a region of inhibition is evident (*hatch grey line*). After the high amplitude propagating event has passed the low amplitude activity recommences. This trace represents the manometric equivalent of the description of luminal transit and wall motion made in both human and animal studies. Note also that each subsequent high amplitude event does not commence where the previous event finished. Instead in commences at more proximal location of the bowel. This pattern of propagation matches similar events described by Ritchie [84] in his radiographic observation of colonic transit

Finally it is important to note that in all studies measuring both transit and colonic manometry in the human colon, there were numerous subtle transit events that were not associated with identifiable propagating pressure events.

Summary: the pressure events that are detected by colonic manometry bear a remarkable resemblance to actual movements of the colon wall described through historic radiographic studies of the human colon [89, 1, 56, 84, 5] and the highly descriptive animal studies [14, 42, 67]. As combined colonic scintigraphy/manometry studies have also associated these pressure events with actual movement of content [22, 36, 37] it could be concluded that while colonic manometry may not detect every ripple of the human colon it is likely to detect the motor patterns that are responsible for the majority of significant movements. In addition, while the high amplitude propagating events have drawn most of the attention over the years of prolonged colonic manometry recordings a true assessment of "normal" colonic motility needs to take on board all detectable colonic events.

5.3 Spatiotemporal Organisation of Propagating Events

Over the past 3 years our motility group has been reporting on the spatiotemporal organisation of the propagating pressure events throughout the colon [40, 39]. In analysing the pancolonic manometric data recorded from healthy controls we began to notice that each sequential propagating event started in a different location of the colon to the previous one and the extent of propagation of each new propagating event overlapped the extent of propagation of the previous one (Fig. 2). The reporting of this phenomena is similar to that reported by Richie in 1970 through viewing radiographic images of colonic transit [84]. In that paper Richie et al. wrote "*If the wave of contraction stops, it does not appear to be able to re-establish its progression at the same point, though its propulsive activity may be taken over by another peristaltic movement starting afresh from farther up the bowel*".

Summary: pan-colonic manometry appears to detect the spatiotemporal organisation of propagating events observed in colonic transit studies.

5.4 Meal Response

The colonic meal response is another of the well described events that has been noted in both manometric and transit studies. In the papers published by Hertz in 1913 [51, 52] the ileal and colonic response to a meal was described. In particular he noted active peristalsis in the terminal ileum, which emptied into the colon. A mass movement in the colon soon followed. Ritchie et al. [82] in 1968 also reported that after a meal the 'haustral shunting' decreased while 'segmental propulsion' increased. After a meal Moreno-Osset et al. [72] reported a large movement of tracer into the transverse, descending and sigmoid colon. In that study, movement was associated with a significant increase in colonic pressure events. Many manometric studies in health have reported altered motility in the colon after a meal. This is manifested as either an increase in high amplitude propagating events and/or an increase in the general motility of the colon (Fig. 1) [40, 12, 13, 16, 25, 26, 27, 53, 61, 68, 79].

Summary: In response a high calorie meal colonic transit studies report an increase in the propulsion of luminal content and manometric studies report an increase in the frequency of high amplitude propagating events.

5.5 Defecation

The end result of colonic motility is the excretion of stool. From the early days of radiological investigation of colonic motility it became apparent that defecation

was more than just an anorectal event. In 1907 Hertz reported that during defecation "*the contents of the caecum and ascending colon move bodily into the transverse colon, whilst everything beyond the splenic flexure was carried through the pelvic colon and rectum and evacuated*" [48]. These early radiological observations were supported in the 1960s by Halls [46], whilst in the 1995 Lubowski et al. utilising colonic scintigraphy, demonstrated that during defecation the entire colon could be emptied [70].

In 1992 Kamm et al. [60] demonstrated pan-colonic propagating events were associated with chemically induced defecation in patients with idiopathic constipation. In 2000 Bampton et al. [4] demonstrated that both high and low amplitude propagating events were closely associated with spontaneous defecation in healthy controls. In addition Bampton's study showed that there was a stereotypic pattern of propagating events prior to stool expulsion. The first of these would originate in the descending colon and each subsequent propagating event would originate in a more proximal location, such that the final propagating event (usually a high amplitude one) would often originate in the ascending colon. Such patterns of motility, fit the radiological observation of Hertz [48] described above, and would favour the expelling of content from the distal colon whilst also moving content from the proximal colon to a more distal regions.

Summary: The manometric pressure events recorded in the colon prior to defecation match the radiological observations of actual wall motion of the colon prior to defecation.

6 Using Colonic Manometry to Define Functional Disorders and Guide Treatment

6.1 Defining Subtypes

The term constipation means different things to different people. Typically it is associated with various combinations of the following symptoms; (i) infrequent passing of stool; (ii) straining; (iii) feelings of incomplete evacuation; (iv) the need to digitally evacuate stool; (v) passing hard stool. Clinically, constipation can be viewed in broad but often overlapping categories; (1) those with slow colonic transit; (2) those with normal transit constipation; and (3) those with rectal evacuation disorders [15, 44].

The need to define patients on these broad definitions is of clinical importance because it can help to guide treatment and improve a patient's chance of a successful outcome [20, 59, 62, 63, 65, 80]. However, for a substantial number of patients, current treatments do not work [19, 78]. Improving treatment success rates will only stem from a clearer understanding of the causes of the problem. This is one of the primary reasons for using colonic manometry. Unfortunately, particularly in adults, the technique has been unable to identify suitable biomarkers

that help subtype constipation or guide treatment. Indeed in adults, there has only been a handful of studies that have attempted to use manometry in constipated patients to determine if biosignatures can be identified [53, 74, 8, 81].

The first of these studies was unable to identify any pressure events that separated constipated patients with or without delayed transit [8]. The second, in a study of descending colonic motility, concluded that manometry could not be used to discriminate between subgroups of patients with either slow colonic transit or rectal evacuation disorder [74]. The third study attempted to use the colon manometry studies in an attempt to differentiate 40 adult patients with slow transit constipation [53]. While this study managed to separate the patients into 4 groups, based on the presence or absence of high amplitude propagating events, the colonic response to a high calorie meal or the increased presence of pressure events in the sigmoid colon, the clinical impact of the findings remained undetermined. The final and most recent of these studies, recorded manometry (and barostat) from the descending and sigmoid colon of constipated patients with; (i) slow transit constipation; (ii) an evacuation disorder; or (iii) normal transit constipation. Based on manometry alone they were not able to identify distinctive motor patterns that separated the three groups [81]. The study did show that between 40–53 % of patients in the different groups demonstrated reduced fasting and/or postprandial colonic tone and/or compliance. Of course the converse of this is that 47–60 % of the patients did not show these characteristics [81].

6.2 Guiding Treatment

When discussing the treatment of colonic disorders based upon colonic manometry data it is important to note that there is a difference in the acceptance of the acquired data between the paediatric and adult clinical practices. In children, colonic manometry studies are far more likely to guide treatment options. Indeed it is reported that colonic manometry may be the only test that can differentiate an intrinsic colonic neuromuscular disorder from a behavioural cause of constipation in children [30]. The manometric findings of colonic manometry studies in children has been covered in two recent reviews [30, 35]. This chapter will focus upon the data recorded in adults.

In adults only 2 studies have attempted to use colonic manometry to guide treatment. In 1992 Bassotti et al. [7] reported on just 3 patients with severe constipation. He demonstrated that these patients had a reduced frequency of high amplitude propagating events, a reduction in "motility" throughout the colon, a poor colonic meal response and no response to edrophonium chloride stimulation [7]. These patients had failed all standard treatment and based on the results from the colonic manometry it was deemed that the colon would continue to be insensitive to treatment measures or spontaneous improvement, therefore surgical removal of the colon was recommended. Two of the patients underwent a total colectomy and one a hemicolectomy. The outcome of these procedures was not

well described with "fairly good results at follow-up" reported and no long-term data provided.

In 2004 Rao et al. [79] published a study in which he performed 24 h colonic manometry in 21 patients with slow transit constipation. They investigated the colonic response to ingestion of a meal and morning waking, and recorded the frequency of high amplitude propagating events. Based on the presence, absence or perceived reductions in two or more of these factors, patients were classified as having normal colonic motility, a myopathy or a neuropathy. The myopathy was based on a "reduced response" to 2 or more factors while an absence of two or more factors was deemed a neuropathy. For those patients with a suspected neuropathy, colectomies were offered (performed in 7/10). While those with a myopathy were offered a regime of biofeedback and laxatives. Again the study lacked a detailed description of clinical outcomes with "improved" bowel symptoms reported for the colectomies, whilst those with suspected myopathy reported a "modest improvement" at 1 year. This study has continued with the recent publication in which 80 patients with slow transit constipation have been evaluated [87].

The definitions of a colonic myopathy or neuropathy used in Rao's 2004 [79] study requires further comment. On the basis of in-vitro investigation the colonic smooth muscle activity is controlled by two main parallel interacting mechanisms [85, 21, 57]. The first of these is the muscular apparatus, which consists of the activity generated from the smooth muscle and nets of pacemaker cells called the interstitial cells of Cajal (ICC). Collectively these generate rhythmic oscillations of muscle membrane potential. When these reach a mechanical threshold a phasic contraction results. The neural apparatus is superimposed on this activity, and consists of complex neural circuits within the enteric nervous system and this apparatus determines different motor patterns described in the sections above.

The colonic response to a meal or morning waking is likely to be mediated by the central nervous system, therefore when no colonic response is detected this may well provide evidence of a neurogenic disorder. However, it does not follow that a diminished response reflects a myogenic disorder, indeed based out our current understanding of how colonic contractile activity is generated, a diminished response simply provides evidence of a potential neuropathy.

Manometric evidence of a genuine disorder of the muscular apparatus is difficult to assess. In pediatric manometry studies such a disorder is defined as a complete absence of pressure events [1]. Such a definition has merit and given the fact that there is evidence to suggest a decrease in the numbers of ICCs in the colon of patients with slow-transit constipation [71, 93] a lack of phasic activity may well represent evidence of a abnormality within the muscular apparatus.

However, in adults there are several pieces of evidence that argue against such a hypothesis; (1) most adult studies utilizing colonic manometry show ample evidence of spontaneous phasic activity [40]; (2) studies of colonic manometry in patients with constipation (including slow transit constipation) have shown that electrical [31] and chemical stimulants [60] can induce colonic propagating events; and (3) A recent in-vitro study has shown that the patterns of motor activity

recorded from the entire colon removed for patients with slow transit constipation do not differ from the motility patterns recorded in resected "healthy" colonic tissue in regions proximal or distal to a colonic carcinoma. Collectively these observations suggest that the intrinsic pacemaker mechanisms underlying the generation of propagating events is present at some level in constipated patients but the extrinsic neural input is in some way attenuated. Thus the failed or attenuated colonic response to physiological stimuli is more likely to reflect varying degrees of a neuropathy.

Realistically until there is a proven manometric-histopathological correlation definitions of manometrically defined myogenic or neurogenic disorders will always remain largely speculative. In children, no morphological changes reflecting possible myogenic or neurogenic disorders in muscle tissue were correlated with particular features of colonic manometric recordings [91]. Therefore at present attributing myogenic or neurogenic tags to manometric findings is largely unsupported.

7 Future Directions

Given that manometry appears to be capable of detecting the majority of significant propulsive events described in measures of colonic transit, why is it that in the adult population we struggle to use it as a beneficial clinical tool? Indeed, despite the many years of research, colonic manometry is viewed largely for use in research only [88]. To add clinical significance, it is likely that the entire procedure needs to be overhauled. In reality colonic manometry and the analyses of data have essentially remained unchanged since 1988. In contrast clinicians around the world use pharyngeal/oesophageal manometry to not only subtype swallowing disorders but predict treatment outcome [75, 76]. There are several reasons for this. The oesophagus is short and easily accessible and has relatively controlled motility—a patient can be told when to swallow. The motor responses of interest are immediate and short lived (<20 s), meaning that a diagnostic study can be performed in under 30 min and analysed rapidly by eye according to well validated and relatively easily recognised pressure "signatures".

However, oesophageal manometry has seen some major technical advances over the past decade. One of the most crucial has been the development of high-resolution manometry [28]. The ability to miniaturize transducers and incorporate then into flexible tubing has seen solid-state catheters become the standard choice for oesophageal manometry. The catheters contain up to 36 sensors, spaced at 1 cm intervals, and this provides a detailed profile of pressures along the entire studied region.

Another of the technical advances is the creation of visual and analytical software. For oesophageal manometry interpolation between pressure points allows for the creation of spatiotemporal colour maps of pressure profiles that allow the uninitiated to quickly grasp the concepts of normal or abnormal pressure

patterns [45]. This has allowed the technology to be adapted outside the research setting. More recently the development of automated software for the analysis of the data collated from combined pharyngeal manometry and impedance has been used to accurately predict the likelihood of aspiration in patients with swallowing disorders [75]. Determining a patient's likelihood of aspiration can have a significant impact upon their quality of life and reduce health care cost by keeping the patient out of hospital.

Until recently high resolution catheters of sufficient length to record pressures throughout the entire colon simply had not existed. However, over the past few years fibre-optic manometry catheters have begun to change this [28, 2, 38, 41, 77]. These catheters allow for a dramatic increase in sensors (up to 144 at 1 cm intervals) without compromising the flexibility of the device or the outer diameter (<3 mm). The significance of this development is apparent when viewed in light of the data obtained from colonic studies. Analysing subsets of data from high-resolution recordings we have been able to show that catheters with recording sites spaced at >7 cm miss or mislabelled up to 90 % of retrograde and 40 % of antegrade propagating pressure events (Fig. 3) [2, 38, 41, 77]. The data obtained from traditional catheters with widely spaced sensors can lead to an effect analogous to aliasing in signal processing. For colonic manometry, this process refers to the confusion that results when a signal is sampled at sensor spacing greater than that of the propagating activity itself. In practice, colonic manometry data may have been measuring manometric signals at spacing up to twice that of many of the propagated events we are trying to record. Therefore a proportion of the existing data may have little or no correlation to what is truly occurring.

Along with the improved spatial resolution of recording sites along manometry catheters, a re-evaluation of the analysis of colonic manometry data is needed. The simplistic summing up of the number of high amplitude pressure events or reporting on the area under the pressure curve are clearly not sufficient to be able to separate all patients from healthy controls [17]. Except in extreme cases it is unlikely that there is any specific motor pattern that can separate patients groups or indeed patients from controls. It is more likely that the analysis should take on board factors such as the spatiotemporal relationships that exist between all pressure events recorded throughout the entire colon [40, 39]. The healthy colon appears to have a high degree of coordination between sequential propagating events and patients with constipation may lack this coordination [40, 39]. Indeed as far back as 1933 such suggestions have been made [64]. After viewing fluoroscopic images Fred Kruse was of the opinion that "*it is the incoordination of the muscular motor function, rather than its paralysis, that is at the basis of all constipation, except the definitely mechanical obstructive type*" [64].

The analysis should also move beyond the idea that a lack of high amplitude pressure events is the most obvious measure of a potential neurogenic disorder. Inhibitory neural input also affects the colonic manometry and in many of our patients with constipation we have shown an increased frequency of low amplitude antegrade and/or retrograde propagating events, especially at night when quiescence is the norm [40, 29] (Figs. 1, 4). The lack of inhibition of these motor

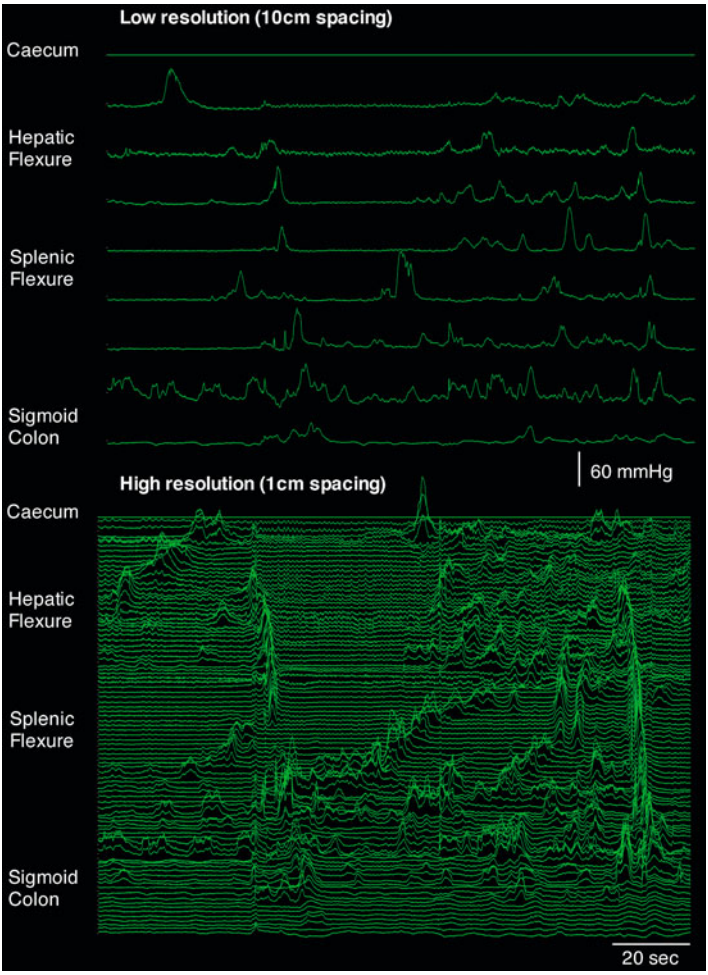

Fig. 3 Colonic manometry in a healthy female. A low resolution (10 cm spaced recording sites) image is displayed at the top of the figure. At the bottom of the figure is a high-resolution (1 cm spaced recording sites) image of the same data. Note that while a large number of pressure events are detected with the low resolution manometry the ability to determine the polarity of propagation (antegrade or retrograde) is difficult. In particular in the high resolution image a number of short extent retrograde propagating events are evident and these can not be seen in the low resolution image

patterns should also be viewed as a sign of a potential neurogenic disorder and would add to the general opinion of 'incoordination' described above.

In all fields of medical science (or science in general) progress is required to improve our understanding of normality and abnormality. The field of colonic manometry is no different and such progress is needed if we are to begin to truly define abnormalities in a patient population, and then use these data to help guide treatment.

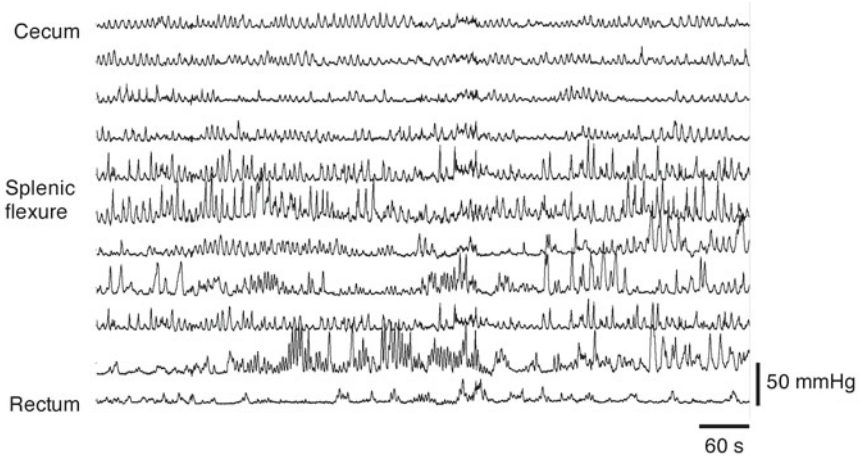

Fig. 4 Low amplitude pressure events recorded in a patient with slow transit constipation. This activity was evident for hours at time. The apparent lack of inhibition of such activity could be viewed as a neuropathy

References

1. Alvarez WC (1948) An introduction to gastroenterology, 4th edn. Paul B Hoeber Inc., New York
2. Arkwright JW, Underhill ID, Maunder SA, Blenman NG, Szczesniak MM, Wiklendt L, Lubowski DZ, Cook IJ, Dinning PG (2009) Design of a high-sensor count fibre optic manometry catheter for in vivo colonic diagnostics. Opt Express 17(25):22423–22431
3. Bampton PA, Dinning PG, Kennedy ML, Lubowski DZ, Cook IJ (2001) Prolonged multi-point recording of colonic manometry in the unprepared human colon: providing insight into potentially relevant pressure wave parameters. Am J Gastroenterol 96(6):1838–1848
4. Bampton PA, Dinning PG, Kennedy ML, Lubowski DZ, de Carle DJ, Cook IJ (2000) Spatial and temporal organization of pressure patterns throughout the unprepared colon during spontaneous defecation. Am J Gastroenterol 95(4):1027–1035
5. Barclay AE (1912) Note on the movements of the large intestine. Br J Roentgenol 16:422–424
6. Barclay AE (1935) Direct X-ray cinematography with a preliminary note on the nature of the non-propulsive movements of the large intestine. Br J Radiol 8:652–658
7. Bassotti G, Betti C, Pelli MA, Morelli A (1992) Extensive investigation on colonic motility with pharmacological testing is useful for selecting surgical options in patients with inertia colica. Am J Gastroenterol 87(1):143–147
8. Bassotti G, Chiarioni G, Vantini I, Betti C, Fusaro C, Pelli MA, Morelli A (1994) Anorectal manometric abnormalities and colonic propulsive impairment in patients with severe chronic idiopathic constipation. Dig Dis Sci 39(7):1558–1564
9. Bassotti G, Clementi M, Antonelli E, Pelli MA, Tonini M (2001) Low-amplitude propagated contractile waves: a relevant propulsive mechanism of human colon. Dig Liv Dis 33(1):36–40
10. Bassotti G, de Roberto G, Castellani D, Sediari L, Morelli A (2005) Normal aspects of colorectal motility and abnormalities in slow transit constipation. World J Gastroenterol 11(18):2691–2696

11. Bassotti G, Gaburri M (1988) Manometric investigation of high-amplitude propagated contractile activity of the human colon. Am J Physiol Gastrointest Liver Physiol 255:G660–664
12. Bassotti G, Imbimbo BP, Betti C, Dozzini G, Morelli A (1992) Impaired colonic motor response to eating in patients with slow transit constipation. Am J Gastroenterol 87:504–508
13. Bazzocchi G, Ellis J, Villanueva-Meyer J, Fain JW, Jing J, Mena I, Snape WJ (1990) Postprandial colonic transit and motor activity in chronic constipation. Gastroenterology 96:686–693
14. Bedrich M, Ehrlein H (2001) Motor function of the large intestine and flow of digesta in sheep. Small Rumin Res 42:141–155
15. Bharucha AE (2007) Constipation. Best Pract Res Clin Gastroenterol 21(4):709–731
16. Brown AJ, Horgan AF, Anderson JH, McKee RF, Finlay IG (1999) Colonic motility is abnormal before surgery for rectal prolapse. Br J Surg 86(2):263–266
17. Camilleri M, Bharucha AE, di Lorenzo C, Hasler WL, Prather CM, Rao SS, Wald A (2008) American neurogastroenterology and motility society consensus statement on intraluminal measurement of gastrointestinal and colonic motility in clinical practice. Neurogastroenterol Motil 20(12):1269–1282
18. Cannon WB (1902) The movements of the intestines studied by means of the Rontgen rays. Am J Physiol 6:251–277
19. Chiarelli P, Brown W, McElduff P (2000) Constipation in Australian women: prevalence and associated factors. Int Urogynecol J 11(2):71–78
20. Chiarioni G, Salandini L, Whitehead WE (2005) Biofeedback benefits only patients with outlet dysfunction, not patients with isolated slow transit constipation. Gastroenterology 129(1):86–97
21. Cook IJ, Brookes SJ, Dinning PG (2010) Sensory and motor function of the colon. In: Feldman M, Friedman LS, Brandt LJ (eds) Sleisenger and Fordtran's gastrointestinal and liver disease, vol 2, 9th edn. Saunders, Philadelphia, pp 1660–1674
22. Cook IJ, Furukawa Y, Panagopoulos V, Collins PJ, Dent J (2000) Relationships between spatial patterns of colonic pressure and individual movements of content. Am J Physiol Gastrointest Liver Physiol 278:G329–G341
23. Cook IJ, Talley NJ, Benninga MA, Rao SS, Scott SM (2009) Chronic constipation: overview and challenges. Neurgastroenterol Motil 21(s2):1–8
24. Davenport HW (2011) Gastrointestinal physiology, 1895–1975: motility. Compr Physiol 1–101
25. De Schryver AM, Samsom M, Smout AI (2003) Effects of a meal and bisacodyl on colonic motility in healthy volunteers and patients with slow-transit constipation. Dig Dis Sci 48(7):1206–1212
26. Di Lorenzo C, Flores AF, Reddy SN, Hyman PE (1992) Use of colonic manometry to differentiate causes of intractable constipation in children. J Pediatr 120(5):690–695
27. Di Lorenzo C, Flores AF, Reddy SN, Snape WJ, Bazzochi G, Hyman PE (1993) Colonic manometry in children with chronic intestinal pseudo-obstruction. Gut 34(1):803–807
28. Dinning PG, Arkwright JW, Gregersen H, O'Grady G, Scott SM (2010) Technical advances in monitoring human motility patterns. Neurgastroenterol Motil 22(4):366–380
29. Dinning PG, Bampton PA, Andre J, Kennedy ML, Lubowski DZ, King DW, Cook IJ (2004) Abnormal predefecatory colonic motor patterns define constipation in obstructed defecation. Gastroenterology 127:49–56
30. Dinning PG, Di Lorenzo C (2011) Colonic dysmotility in constipation. Best Prac Res Clin Gastrolenterol 25(1):89–101
31. Dinning PG, Fuentealba SE, Kennedy ML, Lubowski DZ, Cook IJ (2007) Sacral nerve stimulation induces pan-colonic propagating pressure waves and increases defecation frequency in patients with slow-transit constipation. Colorectal Dis 9(2):123–132
32. Dinning PG, McKay E, Cook IJ (2006) Validation of a semi-automated scintigraphic technique for detecting episodic, real time, colonic flow. Neurogastroenterol Motil 18:547–555

33. Dinning PG, Scott SM (2011) Novel diagnostics and therapy of colonic motor disorders. Curr Opin Pharmacol 11:624–629
34. Dinning PG, Smith TK, Scott SM (2009) Pathophysiology of colonic causes of chronic constipation. Neurogastroenterol Motil 21(s2):20–30
35. Dinning PG, Southwell BR, Benninga MA, Scott SM (2010) Paediatric and adult colonic manometry: A tool to help unravel the pathophysiology of constipation. World J Gastroenterol 16(41):5162–5172
36. Dinning PG, Szczesniak MM, Cook IJ (2008) Determinants of postprandial flow across the human ileocecal junction: a combined manometric and scintigraphic study. Neurogastroenterol Motil 20:1017–1021
37. Dinning PG, Szczesniak MM, Cook IJ (2008) Proximal colonic propagating pressure waves sequences and their relationship with movements of content in the proximal human colon. Neurogastroenterol Motil 20:512–520
38. Dinning PG, Szczesniak MM, Cook IJ (2008) Twenty-four hour spatiotemporal mapping of colonic propagating sequences provides pathophysiological insight into constipation. Neurogastroenterol Motil 20:1017–1021
39. Dinning PG, Szczesniak MM, Cook IJ (2009) Spatio-temporal analysis reveals aberrant linkage among sequential propagating pressure wave sequences in patients with symptomatically defined obstructed defecation. Neurgastroenterol Motil 21(9):945–e975
40. Dinning PG, Zarate N, Hunt LM, Fuentealba SE, Mohammed SD, Szczesniak MM, Lubowski DZ, Preston SL, Fairclough PD, Lunniss PJ, Scott SM, Cook IJ (2010) Pancolonic spatiotemporal mapping reveals regional deficiencies in, and disorganization of colonic propagating pressure waves in severe constipation. Neurgastroenterol Motil 22:e340–e349
41. Dinning PG, Hunt L, Arkwright JW, Patton V, Szczesniak MM, Wiklendt L, Davidson JB, Lubowski DZ, Cook IJ (2012) Pancolonic motor response to subsensory and suprasensory sacral nerve stimulation in patients with slow-transit constipation. Br J Surg 99:1002–1010
42. Ehrlein HJ, Reich H, Schwinger M (1983) Colonic motility and transit of digesta during hard and soft faeces formation in rabbits. J Physiol 338:75–86
43. Everhart JE, Ruhl CE (2009) Burden of digestive diseases in the united states Part I: overall and upper gastrointestinal diseases. Gastroenterology 136:376–386
44. American College of Gastroenterology Chronic Constipation Task Force (2005) An evidence-based approach to the management of chronic constipation in North America. Am J Gastroenterol 100(Suppl 1):S1–4
45. Grubel C, Hiscock R, Hebbard G (2008) Value of spatiotemporal representation of manometric data. Clin Gastroenterol Hepatol 6(5):525–530
46. Halls J (1965) Bowel content shift during normal defaecation [summary]. Proc R Soc Med 58:859–860
47. Hardcastle JD, Mann CV (1968) Study of large bowel peristalsis. Gut 9:512–520
48. Hertz AF (1907) The passage of food along the human alimentary canal. Guy's Hosp Rep 61:389–427
49. Hertz AF (1908) The pathology and treatment of chronic constipation. Proc R Soc Med 1(Med Sect):119–149
50. Hertz AF (1912) An Address on investigations of the motor functions of the alimentary canal by means of the x rays: delivered before the Brighton division of the British medical association on Nov. 22, 1911. Br Med J 1(2666):225–229
51. Hertz AF (1913) The ileo-caecal sphincter. J Physiol 47(1–2):54–56
52. Hertz AF, Newton A (1913) The normal movements of the colon in man. J Physiol 47(1–2):57–65
53. Herve S, Savoye G, Behbahani A, Leroi AM, Denis P, Ducrotte P (2004) Results of 24-h manometric recording of colonic motor activity with endoluminal instillation of bisacodyl in patients with severe chronic slow transit constipation. Neurogastroenterol Motil 16(4): 397–402
54. Hiroz P, Schlageter V, Givel JC, Kucera P (2009) Colonic movements in healthy subjects as monitored by a magnet tracking system. Neurgastroenterol Motil 21(8):838–857

55. Holdstock DJ, Misiewicz JJ, Smith T, Rowlands EN (1970) Propulsion (mass movements) in the human colon and its relationship to meals and somatic activity. Gut 11(2):91–99
56. Holzknechtg G (1909) Die normale Persistatlik des Kolon. Muench Med Wochenschr 47:2401–2403
57. Huizinga JD, Martz S, Gil V, Wang XY, Jimenez M, Parsons S (2011) Two independent networks of interstitial cells of cajal work cooperatively with the enteric nervous system to create colonic motor patterns. Front Neurosci 5:93
58. Hurst AF (1925) An address on the sphincters of the alimentary canal and their clinical significance: delivered before the Manchester medical society (October 8th, 1924). Br Med J 1(3343):145–151
59. Kamm MA, Hawley PR, Lennard-Jones JE (1988) Outcome of colectomy for severe idiopathic constipation. Gut 29:969–973
60. Kamm MA, van der Sijp JRM, Lennard-Jones JE (1992) Observations on the characteristics of stimulated defaecation in severe idiopathic constipation. Int J Colorect Dis 7:197–201
61. King S, Catto-Smith AG, Stanton MP, Sutcliffe J, Simpson D, Cook IJ, Dinning PG, Hutson JM, Southwell BR (2008) 24-Hour colonic manometry in pediatric slow transit constipation shows significant reductions in antegrade propagation. Am J Gastroenterol 103(8):2083–2091
62. Knowles CH, Dinning PG, Pescatori M, Rintala R, Rosen H (2009) Surgical management of constipation. Neurgastroenterol Motil 21(s2):62–71
63. Knowles CH, Scott M, Lunniss PJ (1999) Outcome of colectomy for slow transit constipation. Ann Surg 230(5):627–638
64. Kruse FH (1933) Functional disorders of the colon: the spastic colon, the irritable colon, and mucous colitis. Cal West Med 39(2):97–103
65. Kuijpers HC (1990) Application of the colorectal laboratory in diagnosis and treatment of functional constipation. Dis Colon Rectum 33(1):35–39
66. Legros C, Onimus ENJ (1869) Mouvements de l'intestin. J Anat Physiol (Paris) 6:37–65
67. Lentle RG, Janssen PW, Hume ID (2009) The roles of filtration and expression in the processing of digesta with high solid phase content. Comp Biochem Physiol A Mol Integr Physiol 154(1):1–9
68. Leroi AM, Lalaude O, Antonietti M, Touchais JY, Ducrotte P, Menard JF, Denis P (2000) Prolonged stationary colonic motility recording in seven patients with severe constipation secondary to antidepressants. Neurogastroenterol Motil 12(2):149–154
69. Liem O, Harman J, Benninga M, Kelleher K, Mousa H, Di C (2009) Lorenzo health utilization and cost impact of childhood constipation in the United States. J Pediatr 154(2):258–262
70. Lubowski DZ, Meagher AP, Smart RC, Butler SP (1995) Scintigraphic assessment of colonic function during defaecation. Int J Colorect Dis 10:91–93
71. Lyford GL, He CL, Soffer E, Hull TL, Strong SA, Senagore AJ, Burgart LJ, Young-Fadok T, Szurszewski JH, Farrugia G (2002) Pan-colonic decrease in interstitial cells of Cajal in patients with slow transit constipation. Gut 51(4):496–501
72. Moreno-Osset E, Bazzocchi G, Lo S, Trombley E, Ristow E, Reddy SN, Villanueva-Meyer J, Fain J, Jing J, Mena I, Snape WJ (1989) Association between postprandial changes in colonic intraluminal pressure and transit. Gastroenterology 96:1265–1273
73. Narducci F, Bassotti G, Gaburri M, Morelli A (1987) Twenty four hour manometric recording of colonic motor activity in healthy man. Gut 28:17–25
74. O'Brien M, Camilleri M, vonderOhe M, Phillips S, Pemberton J, Prather C, Wiste J, Hanson R (1996) Motility and tone of the left colon in constipation: a role in clinical practice? Am J Gastroenterol 91(12):2532–2538
75. Omari T, Dejaeger E, Van Beckevoort D, Goeleven A, Davidson GP, Dent J, Tack J, Rommel N (2011) A method to objectively assess swallow function in adults with suspected aspiration. Gastroenterology 140(5):1454–1463
76. Pandolfino JE, Ghosh SK, Rice J, Clarke JO, Kwiatek MA, Kahrilas PJ (2008) Classifying esophageal motility by pressure topography characteristics: a study of 400 patients and 75 controls. Am J Gastroenterol 103(1):27–37

77. Patton V, Arkwright JW, Lubowski DZ, Dinning PG (2013) Sacral nerve stimulation alters distal colonic motility in patients with faecal incontinence. Br J Surg. doi:10.1002/bjs.9114. [Epub ahead of print]
78. Rantis PC Jr, Vernava AM 3rd, Daniel GL, Longo WE (1997) Chronic constipation-is the work-up worth the cost? Dis Colon Rectum 40(3):280–286
79. Rao SS, Sadeghi P, Beaty J, Kavlock R (2004) Ambulatory 24-hour colonic manometry in slow-transit constipation. Am J Gastroenterol 99(12):2405–2416
80. Rao SSC, Seaton K, Miller M, Brown K, Nygaard I, Stumbo P, Zimmerman B, Schulze K (2007) Randomized controlled trial of biofeedback, sham feedback, and standard therapy for dyssynergic defecation. Clin Gastroenterol Hepatol 5(3):331–338
81. Ravi K, Bharucha AE, Camilleri M, Rhoten D, Bakken T, Zinsmeister AR (2010) Phenotypic variation of colonic motor functions in chronic constipation. Gastroenterology 138(1):89–97
82. Ritchie JA (1968) Colonic motor activity and bowel function. I. Normal movement of contents. Gut 9(4):442–456
83. Ritchie JA, Ardran GM, Truelove SC (1962) Motor activity of the sigmoid colon of humans. A combined study by intraluminal pressure recording and cineradiography. Gastroenterology 43:642–668
84. Ritchie JA, Truelove SC, Ardan GM, Tuckey MS (1971) Propulsion and retropulsion of normal colonic contents. Am J Dig Dis 16(8):697–704
85. Sarna SK (2010) Colonic motility: from bench side to bedside. colloquium series on integrated systems physiology: from molecule to function to disease, 2011/04/01 edn. Morgan and Claypool Life Sciences, New York
86. Scharz G (1911) Zur Physiologie und Pathologie der menschlichen Dickdarmbewegungen. Muench Med Wochenschr 58:1489–1494
87. Singh S, Heady S, Valestin J, Rao SS (2011) Clinical utility of ambulatory colonic manometry in adults with slow transit constipation: can underlying pathophysiology guide therapy? Gastroenterology 140 5(Suppl 1):S-52
88. Smout AJPM (2006) Recent developments in gastrointestinal motility. Scand J Gastroenterol Suppl 41(5):25–31
89. Torsoli A, Ramorino ML, Ammaturo MV, Capurso L, Paoluzi P, Anzini F (1971) Mass movements and intracolonic pressures. Am J Dig Dis 16(8):693–696
90. Underwood EA (1946) Wilhelm Conrad Rontgen (1845-1923) and the early development of radiology. Can Med Assoc J 54:61–67
91. van den Berg MM, Di Lorenzo C, Mousa HM, Benninga MA, Boeckxstaens GE, Luquette M (2009) Morphological changes of the enteric nervous system, interstitial cells of cajal, and smooth muscle in children with colonic motility disorders. J Pediatr Gastroenterol Nutr 48(1):22–29
92. von der Ohe MR, Hanson RB, Camilleri M (1994) Comparison of simultaneous recordings of human colonic contractions by manometry and a barostat. Neurogastroenterol Motil 6:213–222
93. Wedel T, Spiegler J, Soellner S, Roblick UJ, Schiedeck TH, Bruch HP, Krammer HJ (2002) Enteric nerves and interstitial cells of Cajal are altered in patients with slow-transit constipation and megacolon. Gastroenterology 123(5):1459–1467

Spatiotemporal Mapping Techniques for Quantifying Gut Motility

Patrick W. M. Janssen and Roger G. Lentle

Abstract We review current methods for the spatiotemporal (ST) mapping of phasic and tonic contractile activity in the various components of the intestinal tract. Basic mapping techniques extract the movement of gut organ boundaries from a sequence of images and condense this information into 2D maps. More complex techniques determine the extent to which locations on the gut organ are lengthening or shortening in a particular direction and also present this data in a 2D map. The latter either track the position of applied markers or use cross-correlation of consecutive images to quantify the movement of serosal patterns. In situations where the above techniques have difficulties, intensity mapping can be useful for identifying motility patterns but is less quantitative. Finally, we discuss ancillary methods for deriving further information from ST maps and practical considerations for applying the mapping techniques.

1 Introduction

The role of gut motility in the process of digestion has long been of interest to physiologists (Erasistratus 304–250 BC [40]). The process of extraction of nutrients from solid and liquid foods is complex and involves physical as well as chemical processes [11]. More specifically, segments of the vertebrate gut triturate, filter, mix, propel and absorb nutrient components of the diet. The principal action facilitating the physical processes within the lumen is the phasic and/or tonic contraction of visceral smooth muscle [35]. Suitably vectored by morphology, the contraction of circularly-, longitudinally- and obliquely-disposed sheets of smooth muscle cells act to shear and propel digesta, and to develop sufficient flow between the elements of

P. W. M. Janssen (✉) · R. G. Lentle
Institute of Food, Nutrition and Human Health, Massey University,
Private Bag 11222 Palmerston North, New Zealand
e-mail: P. Janssen@massey.ac.nz

L. K. Cheng et al. (eds.), *New Advances in Gastrointestinal Motility Research*,
Lecture Notes in Computational Vision and Biomechanics 10,
DOI: 10.1007/978-94-007-6561-0_12, © Springer Science+Business Media Dordrecht 2013

solid phase to enable digestive secretions to be conveyed to their surfaces and to convey any dissolved or digested nutrients to the gut mucosa [32].

An understanding of the physical processes of digestion is fundamental to the development of interventions that promote or retard digestive efficiency. A number of studies have underscored the importance of physical processing during digestion [29], and in particular, the significant effects of agents that influence the apparent viscosity of digesta (e.g., guar gum) on the rates of absorption of nutrients such as glucose [12]. These findings, along with an upsurge of interest in *in-silico* [9, 48] and mechanical models [23, 36, 37] for assessing the effects of the physical form and formulation of foods on the digestion and assimilation of nutrients, have stimulated interest in quantifying local contractile processes and their effects on mixing within the lumen of the gut.

Electrophysiologists have undoubtedly made a significant contribution to our understanding of gut motility, particularly in regard to the genesis, regulation, frequency and velocity of propagation of the electrical impulses that underlie contractile events (see "The Principles and Practice of Gastrointestinal High-Resolution Electrical Mapping" by O'Grady et al. in this volume). However, electrophysiological data alone do not provide a reliable means by which movement of the gut wall or the resultant change in volume may be directly quantified. These latter parameters are necessary both to provide a basis for the construction of realistic models of flow dynamics within various segments of the gut and to enable the influence of the rheological properties of digesta on the form of phasic contractile events to be assessed. The importance of methods that relate underlying electrophysiological phenomena to phasic and tonic contractile outcomes is reflected in recent work, enabling propagating contractions to be visualised with calcium fluorophores as they propagate across the walls of the gut [39].

Early workers drew [10], filmed [2, 51] and X-rayed [7, 10] the contractile behaviour of various segments of the gut in an effort to characterise the physical characteristics of these processes and to assess whether their effect on lumen contents in particular could generate sufficient turbulence to distribute nutrients homogenously across the lumen as well as propelling digesta through the lumen [34, 35]. The detailed analysis of propulsive contractile events was advanced in the advent of the Trendelenburg preparation [52, 53] in which a reproducible pattern of contraction could be triggered when living segments of intestine are distended with perfusing fluid. Apart from affording a means of exploring the electrophysiological events that accompany contractile activity, these preparations have allowed the physical form of intestinal contractions and their action on the lumen contents to be directly assessed [6, 36, 46]. Studies of the residence time distribution (RTD) of fluid traversing ex-vivo segments of the ileum of the brushtail possum indicated that flow regime, and modes of mixing and mass transfer vary with location along the gut and with the rheology of the contained digesta [21]. In particular, turbulence and intensive mixing is possible at more proximal sites where the luminal contents that are of lower viscosity, while digesta at more distal sites is more viscous and mass transfer must depend on vortical flow in which the gut contents move in closed or spiralling streamlines.

The quantitative evaluation of the local characteristics of gastrointestinal contractions have been greatly facilitated following the development of computational image processing [20, 44]. This led to the development of ST mapping techniques [3] that allowed both diametric and longitudinal movements [15] to be studied simultaneously and to be related to the local development of force [8]. In quantifying intestinal motility, we are principally interested in characteristics of the image that relate either directly or indirectly to tonic and phasic contractions. The use of 2D ST techniques where a matrix of carbon dots are applied to the surface of an ex-vivo segment of intestine has led to the discovery that phasic contractile processes are surprisingly diverse both in space and time [25]. ST mapping techniques have proven to be useful not only in studying the effects of these contractions on flow and mixing of the lumen contents but also in studying the patterns of contractile processes activated by networks of ICCs and elements of the enteric nervous system, in circular and longitudinal smooth muscle. While subtle asymmetries in these patterns may induce local mixing in regions of the lumen that are close to the wall [28], the displacement or accommodation of typically viscous and pseudoplastic digesta in a segment of gut must ultimately result from the overall diametric and longitudinal components of contraction. These contractile movements may vary locally with asymmetry in the thickness of longitudinal and circular muscle layers, e.g., between the mesenteric and antimesenteric surfaces of the small intestine, and between the species of experimental animal [33]. In this respect, the diametric and longitudinal ST mapping techniques, with which this review is principally concerned, are those that can provide accurate assessment of relevant parameters notably the local amplitude, frequency, speed and direction of propagation of phasic contractions as well as the profiles of their leading and trailing edges.

ST mapping of contractile movement capitalises on the fixed position of the video camera or other imaging system in relation to the sample so that variations in the positions of elements within the image can be tracked frame by frame through time. This allows the rate of movement of a defined single point or an entire edge to be determined. Although not dealt with in this chapter, ST maps can also be generated for any time-varying parameter that can be simultaneously measured at multiple locations, such as florescent intensity from voltage sensitive dyes [45] driven by Ca^{2+} transactions during slow wave activity in smooth muscle [39] or luminal pressure as measured by a fibre-optic catheter with a series of Bragg grating elements (as described by Dinning in "Colonic Manometry: What Do the Squiggly Lines Really Tell Us?" of this volume) [13].

2 ST Mapping Using the Boundaries of Gut Segments

These ST mapping techniques represent a measurement derived from the boundaries of a gut segment as a function of time and a spatial parameter. For instance, in a diameter map (D map) the derived diameter measurement is represented as a

function of the length along the gut segment and its variation over time. The first step in generating such maps is the identification of the gut segment boundaries in each image. The most straightforward method is to convert the greyscale image to a binary image by thresholding (Fig. 1). For ex-vivo preparations, this can be facilitated by placing a black card behind the organ bath to accentuate the contrast between the light organ and dark background. There are a range of methods available for automatically selecting the threshold level [44] but using the minimum value of the smoothed intensity histogram appears to be adequate in most situations. For situations in which there is less contrast between organ and background, there is scope to incorporate edge detection algorithms that utilise some form of differential filter, e.g., Sobel operator [44]. This can be useful in studying segments of gut that have subsidiary compartments such as the rumen as it allows the boundaries of the subsidiary compartment under study to be distinguished from the tissues of others that are in view.

The boundary of the gut segment can be traced on the thresholded image using a simple algorithm to search for pixels with both black and white neighbours. In the final step, some form of measurement is derived from the moving boundary depending on the morphology of the particular gut segment.

2.1 Diametric Constriction of Tubiform Segment; D Maps

The simplest configuration is a tubiform segment of gut mounted in the organ tank so that its long axis is oriented horizontally across the images. After thresholding an original image, the upper and lower boundaries of the segment are located. The algorithm then steps along successive pixel columns of the image and calculates the distance in pixels between the boundaries, which can be taken as the diameter of the segment at that position. Each diameter estimate is translated into a single map pixel shaded from dark (i.e., distension) to light (i.e., constriction) in proportion to the chosen scaling factors. Each row of pixels of the D map is compiled from successive diameter estimates along the long axis of the segment from a single image. Rows derived from successive images are stacked sequentially in the vertical dimension of the map, i.e., with run time increasing downwards from the top of the map.

Provided they are of sufficient clarity, such D maps provide insight into the characteristics of diametric constriction. Within the zone of constriction of a peristaltic event travelling along the length of a tubular segment of gut, D maps will largely reflect the behaviour of circular muscle. However in other sites, notably in advance of the zone of constriction, they may also reflect relaxation of longitudinal smooth muscle, the resulting change in wall compliance promoting or inhibiting diametric outpouching of the wall due to pressure from displaced lumen contents.

A peristaltic constriction that is propagating along the long axis of a segment of gut will appear as an angled band of lighter shade on the D map (Fig. 2). The angle of the band to the horizontal plane of the map will reflect the speed and direction

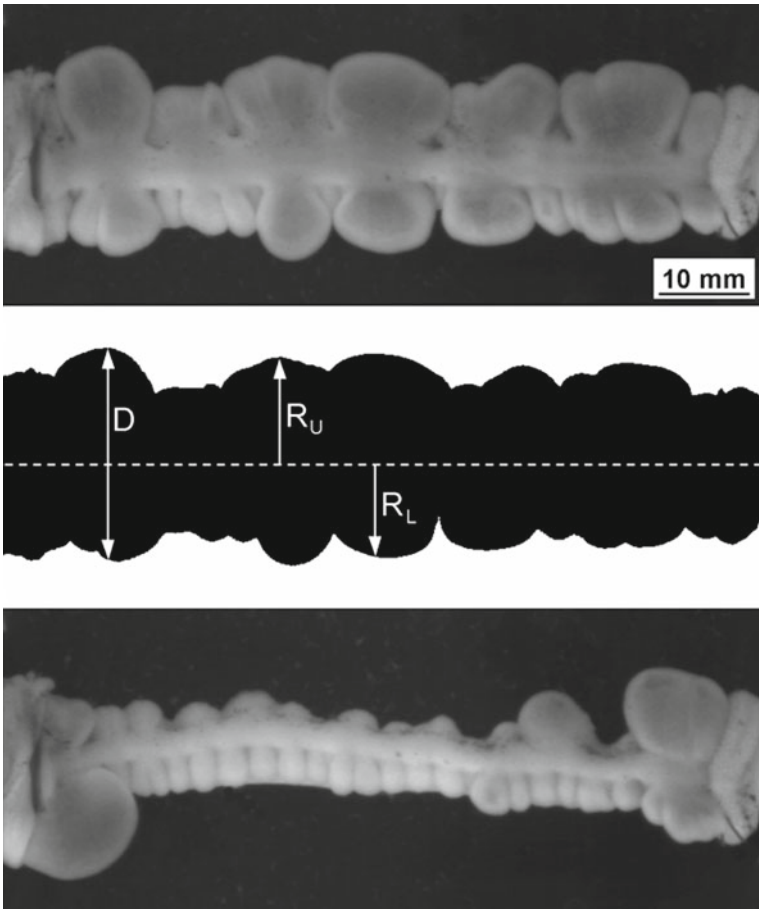

Fig. 1 Original rabbit colon (*upper*) and thresholded (*middle*) image with the derived measurements used in D maps and R maps (see Sect. 2.2) indicated. The lower image shows the same specimen during a mass peristaltic event (see Fig. 9) [30]

(orad or aborad) of travel of the contraction. The width of the band in the horizontal direction reflects the length of the intestine that is undergoing constriction while the vertical width indicates the duration of constriction. A regular sequence of contractions will appear as a series of lighter bands stacked vertically and their frequency of occurrence can be determined by counting the number of bands that traverse a vertical reference line of defined length (time), which corresponds to a particular location along the length of the intestine.

High fidelity D maps generally have sufficient resolution to enable subsidiary components that contribute to each peristaltic event to be detected. For instance, the D maps of small intestinal contractions contain subsidiary stripes of alternate lighter and darker hue within the broad band formed by the peristaltic constriction [1, 28, 38]. The speeds with which these stripes propagate (i.e., their angle to the

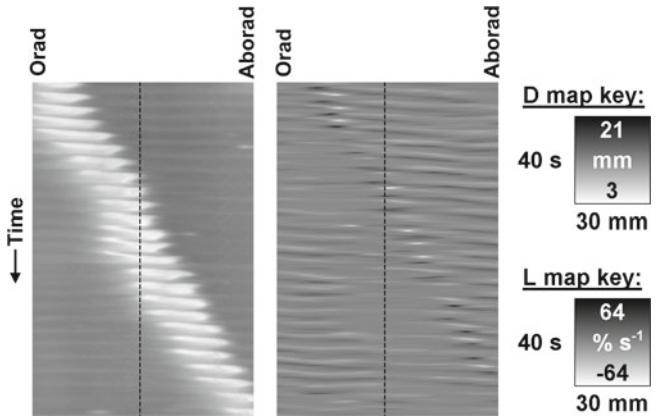

Fig. 2 Synchronous D map (*left*) and longitudinal strain rate map (L map) (*right*) showing a peristaltic event in the ex-vivo possum ileum. The D map shows smaller diameters as a lighter shade. On the L map (see Sect. 3.2), a *darker shade* indicates a relaxing (+ve) strain rate in the longitudinal direction and a lighter shade a contracting (−ve) strain rate. Profiles along the *vertical dashed* reference *lines* are shown in Fig. 3 [28]

horizontal) differ from the speed with which the whole peristaltic contraction propagates along the length of the segment (Fig. 2). Generally, the stripes propagate more rapidly within the zone of constriction than does the peristaltic contraction itself (i.e., their angle is closer to the horizontal), and hence, they are termed fast phasic components [28, 38]. The frequencies with which these stripes occur can be determined directly in the time domain by counting the number of stripes that traverse a vertical reference line on the D map (Fig. 3). Alternatively, fast Fourier transforms of data along this reference line can be used to reveal subtle differences in frequency [38] and the effects of specific agents, such as nitroarginine and tetrodotoxin, on these fast subsidiary frequencies can be quantitatively explored [42]. The latter procedure can allow components with specific frequencies that are known to be myogenic or neuronally mediated to be indentified and filtered from the D map [38]. However, caution is required in concluding that all the component frequencies in such a fast Fourier transform are associated with a propagating contraction as ongoing baseline fast phasic contractions may continue in the absence of a peristaltic event (Fig. 3) [28].

Darker areas associated with the lighter zones of peristaltic constriction on the ST map can provide information regarding the movement of contents. In particular, a darkened zone resulting from relative distension of the lumen often occurs in advance of the propagating diametric constriction of peristalsis (lighter area) (Fig. 2). The horizontal extent of such a darkened area on the D map reflects the length of the intestine that is occupied by displaced digesta at a given time, and hence, may reflect the apparent viscosity of the contents, i.e., the ease with which they can be expelled and flow ahead of the constricting segment and the extent of any zone of relaxation that travels in advance of the zone of peristaltic constriction.

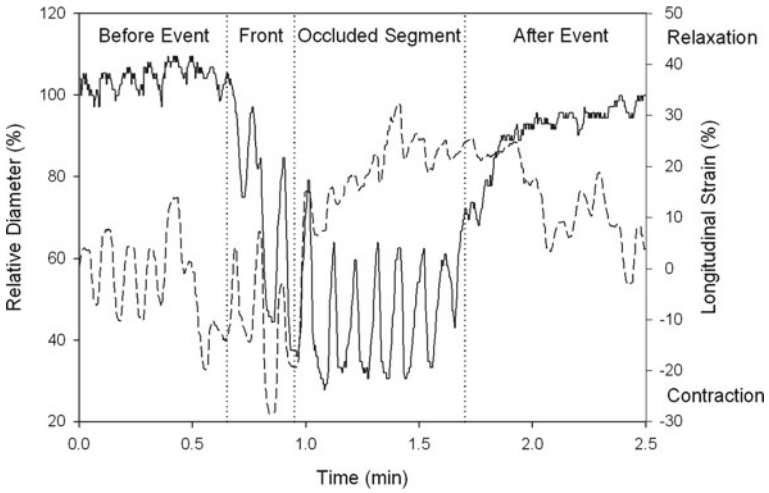

Fig. 3 The relationship between diametric (*solid*) and longitudinal (*dashed*) strains during a peristaltic contraction. Values were taken from the reference lines drawn on the maps in Fig. 2. The relative diameter of the intestine was calculated by dividing the actual diameter by the mean diameter and the longitudinal strain by integrating the strain rate. Note that the ileum within the occluded segment is lengthened relative to before and after the peristalsis, but that the higher frequency components within the occluded segment are in phase in the radial and longitudinal directions [28]

If the array of longitudinal velocity values (see Sect. 3.2) is integrated with respect to time it enables the derivation of displacement maps that follow the longitudinal position of fixed points on the gut segment. While such maps are of little physiological interest, they can be used to systematically correct a D map so that a column of the D map corresponds to a fixed point on the segment surface rather than a certain distance along the segment.

2.2 Asymmetric Radial Constriction of a Tubiform Segment; R Maps

In situations where the upper and lower boundaries of a segment of gut are likely to be moving independently of each other, e.g., the separate intertaenial domains of a triply haustrated colon [30], the construction of radius maps (R map) to separately record the behaviour of each will allow assessment of the extent to which they are coordinated. In a similar manner to that used for D maps, each image is thresholded, and the upper and lower boundaries of the gut segment are traced on the thresholded image. A demarcation line is then positioned midway along the long axis of the gut component so as to separate it into upper and lower halves, the position of this separating line being programmed to be invariant

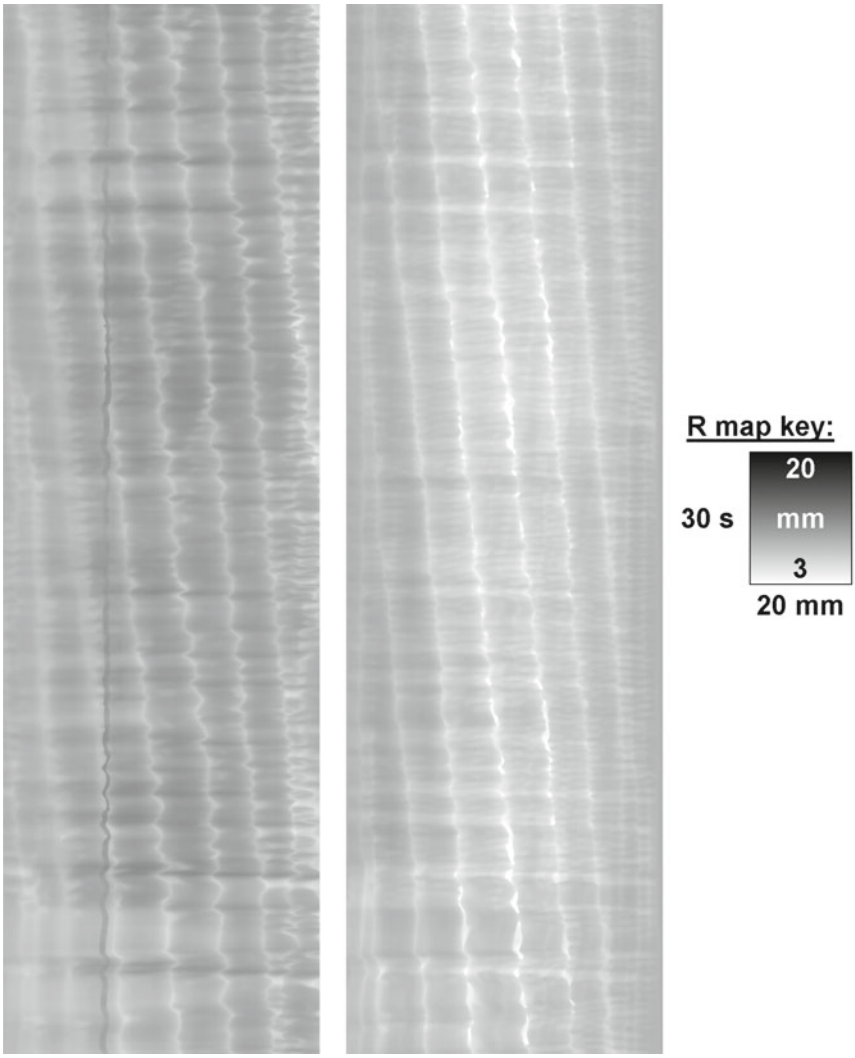

Fig. 4 R maps of corresponding intertaenial domains during a period of haustral progression when the proximal colon of the rabbit is perfused with 1 % guar gum solution. The steeply *sloped light lines* representing the haustral boundaries are moving slowly in an aboral direction [30]

between frames. The algorithm is adjusted to determine the number of pixels in each subsidiary column above and below the line (Fig. 1). The upper and lower R maps are each compiled in a similar manner to D maps with the long axis of the gut segment displayed in the horizontal direction and with scans derived from successive images stacked sequentially in the vertical dimension (Fig. 4).

2.3 Other Gut Morphologies

For sacculate gut segments, the curved geometry requires a different approach with regard to the spatial coordinates. For instance, the greater curvature of the guinea-pig stomach has been approximated by two arcs separated by a straight section [5] while that of the rat can be described adequately by a single arc [31]. In the latter, movements of the stomach wall were related to a single pivot point chosen to lie at the centre of the radius of the greater curvature of the stomach (Fig. 5). The distances from the pivot point to the greater and to the lesser curvature (R_G and R_L respectively) were determined at angle increments of 2°. Raw ST maps were compiled with the cumulative angle of deviation from the pivot point in the horizontal direction and with successive scans stacked sequentially in the vertical direction. The intensity of each map pixel corresponded to the distance of R_G or R_L from the pivot point, a shorter length represented by a lighter pixel shade and a longer by a darker shade.

The scaling of the raw maps was subsequently converted to enable the various parameters of motility to be quantified (Fig. 6). This included converting the horizontal dimension from an angle to the cumulative linear distance from the pyloric sphincter along the greater or the lesser curvature. The intensity of map pixels was adjusted to represent displacement from the average location. A map of antral diameter was derived by plotting the difference between the distances from the pivot point to the line of lesser curvature (R_L) from that to the line of the greater curvature (R_G).

The scaling of ST maps so that the horizontal dimension represents the cumulative linear distance from the pylorus is a necessary precaution to prevent a contraction with a reasonably constant speed of propagation appearing curved (i.e., variable) on the ST map. It should be noted that in some preparations of the rat

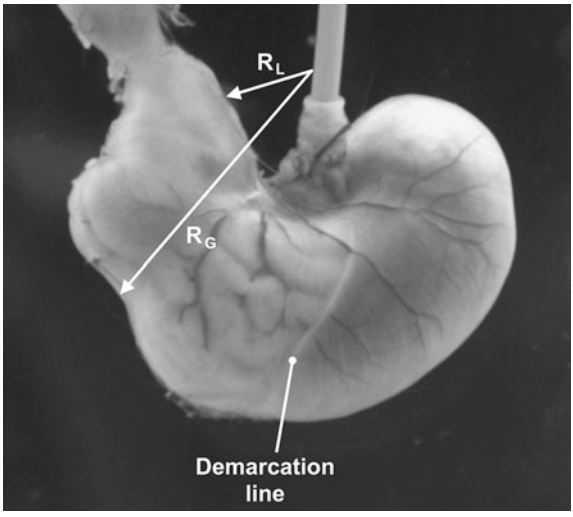

Fig. 5 Image of rat stomach showing dimensions used in mapping and the dorsoventral demarcation line between corpus and fundus. The *arrow* on the greater curvature is located on an antrocorporal contraction wave

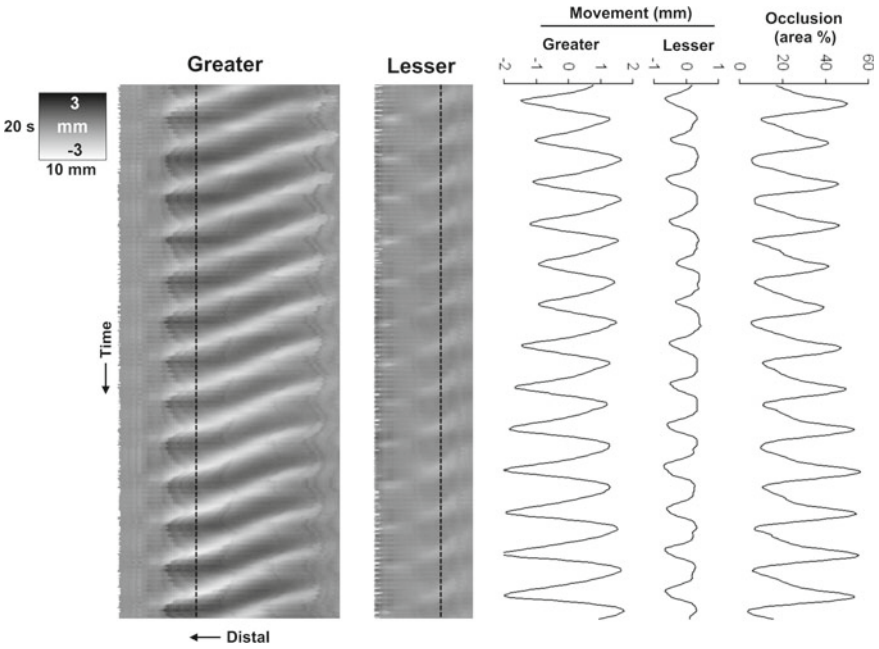

Fig. 6 Spatiotemporal maps of the greater and lesser curvatures of an ex-vivo rat stomach that was perfused with 1.5 % guar gum solution. The *line plots* on the right correspond to amplitudes and occlusion calculated at the position shown by the vertical reference lines on the maps. Note that the spatial dimension is inverted in this example [31]

stomach the lines of antrocorporal contraction were of a bilinear form, the slope of the distal part of the line being more horizontal than the proximal part, indicating that the speed of propagation in the pyloric antrum was significantly faster than that in the corpus [31]. As the lines were bilinear rather than curved, it implied that this was a result of the neuroanatomical configuration as would be expected if contractions are conducted by different components of the ICC network in the corpus and antrum, i.e., ICC-IM versus ICC-AP [24].

3 ST Mapping Using Surface Features

Although mapping gut segment boundaries has been very useful in assessing the contraction patterns of the circular muscle layer, it provides little information about the longitudinal layer [26]. This shortcoming led researchers to place surface markers at regular intervals along a preparation and use changes in the distances between successive markers to estimate longitudinal shortening or lengthening [15, 36]. Recently, more convenient techniques have been developed based on cross-correlation, originally to calculate the strain rate of longitudinal muscles in

tubiform gut segments [28] but later the technique was generalised to deal with strain rate in any direction [19].

The cross-correlation technique avoids the laborious task of applying markers and does not require the location and direction of the contractions of interest to be specified a priori. This is of particular use when dealing with complex morphologies such as the juncture on ileum, caecum and colon [19]. However, the cross-correlation mapping technique has difficulty evaluating tonal changes such as the slow increase in caecal length associated with receptive relaxation [28]. This is due to the algorithm determining long term change by summating the many small changes that occur between sequential images over that time, a process that tends to accumulate errors over long periods of time. Applying surface markers has the advantage in this situation as the markers should remain in the same positions relative to the preparation throughout the experiment.

3.1 ST Mapping Using Applied Markers

The application of high contrast markers to the surface of a preparation allows the automated tracking of the absolute position of discrete locations on the preparation using comparatively low quality images. Some of the markers employed include India ink [36], silk knots [15], dots of soot [25] and 100 μm flecks of glitter [17]. The markers can be disposed either linearly [36] to assess contraction in a single muscle layer or in a 2D array [25] to assess circular and longitudinal layers.

The tracking can be achieved by a simple search for the pixel of minimum intensity beginning from the marker's position in the previous image. The distance in a particular direction between markers can be calculated and after using interpolation to find intermediate values, the distances converted to greyscale in order to construct an ST map in a process analogous to that used for D maps [15]. To allow maps from different preparations to be compared, it is desirable to scale or normalise the distances by dividing by the average or maximum distance between each pair of markers during the image sequence [17].

3.2 Strain Rate Mapping Using Cross-Correlation

3.2.1 Cross-Correlation of Sequential Images

Where the quality of the images is sufficient to allow resolution of a series reference points on fine vascular arcades visible over the entire serosal surface of the ileum it is possible to determine relative longitudinal displacement during contractile events by cross-correlation between successive frames [28]. In segments that do not bear such distinctive natural reference points, a sprinkling of fine carbon particles that adhere to the serosal surface in a random pattern may provide

a similar basis for assessing displacement. In either case, the movement of a reference point is typically detected in a 21 × 21 pixel square surrounding it, although the size of the square can be adjusted to suit image quality. The cross-correlation function between the image pattern within that square and that within a displaced square in the subsequent frame is given by:

$$C(x,y) = \sum_{i=-10}^{+10} \sum_{j=-10}^{+10} \left(\left(p(i,j) - \boldsymbol{\mu}_p \right) - \left(Q(i + x, j + y) - \boldsymbol{\mu}_Q \right) \right)^2 \qquad (1)$$

where C(x,y) is the cross-correlation function corresponding to a displacement of x and y pixels between the current and subsequent frames. P and Q are individual pixel intensities from the current and subsequent frames respectively, while μ_P and μ_Q are mean pixel intensities for the 21 × 21 pixel squares in these frames. A simpler expression of the cross-correlation function based on the sum of the absolute difference in pixel intensities has also been used [18] but our experience is that this is not a critical factor.

The cross-correlation function is evaluated over a range of integer x and y values that are selected to cover the maximum displacements observed between frames, typically −15 to +15 pixels. The minimum of this function represents the movement in pixels of a point at the centre of the square between the successive frames, and hence, the local velocity as the frames were captured at regular time intervals [20]. Earlier work simply searched for the pixel displacement with the lowest function value [18, 28]. We have subsequently refined the technique to determine the minimum by fitting a 2D cubic spline to the cross-correlation data and calculating the minimum value on the fitted spline to give the displacement vector as real numbers, i.e., as fractions of a pixel.

3.2.2 Longitudinal Strain Rate; L Maps

For a tubiform segment mounted in the organ tank so that its long axis is oriented horizontally across the images, the horizontal component of the local velocity represents movement in the longitudinal direction and is used for further calculation while the vertical component can be discarded. The above cross-correlation procedure is repeated at multiple reference points that are evenly spaced, typically 10 pixels apart, along the length of the intestine generating an array of longitudinal velocity values each with a sign indicating the direction of movement.

A 3 × 3 or 5 × 3 median filter can be applied to the array of longitudinal velocity values to remove spurious values. Each row of the filtered array is numerically differentiated with respect to the position along the length of the gut component yielding the longitudinal strain rate. The preferred technique is to fit a penalised spline to the row of velocity values (Fig. 7). These splines have two user-specified parameters: the number of spline knots; and a roughness penalty, which controls the level of smoothing applied [43]. Once a spline is fit, it is straightforward to obtain interpolated values of the differential of the spline, which

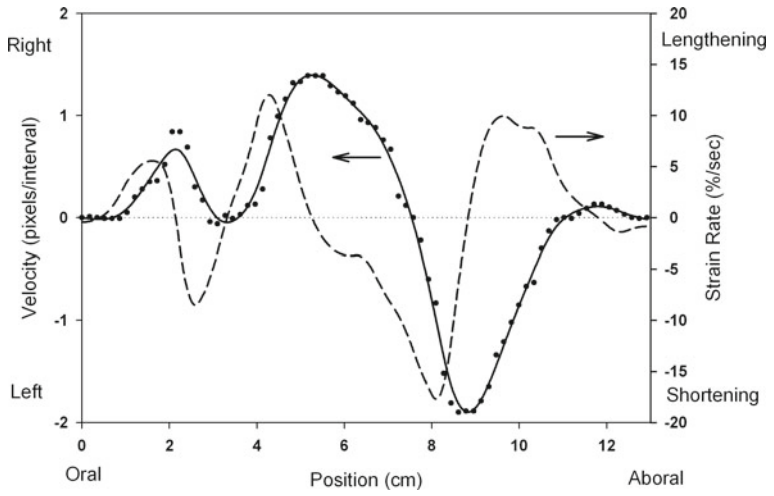

Fig. 7 Showing the procedure for generating one row of a longitudinal strain rate map (L map). Cross-correlation of two consecutive images was used to determine the displacement per sampling interval (i.e., longitudinal velocity) at 76 reference points (*dots*) along the preparation. A penalised spline (*solid line*) was fitted to the velocity data using 30 knots and a 0.2 roughness penalty. The spline was differentiated with respect to position (*dashed line*) to obtain the strain rate and the latter was evaluated along the preparation to provide one row of the L map. In this example, a segment of the ileum of the brushtail possum was fixed at both ends and two longitudinal contractile events were occurring (i.e., at approximately 3–8 cm). *Arrows* indicate appropriate y axis

correspond to the strain rate distribution along the gut segment at that time. Each interpolated strain rate value yields one map pixel with its intensity scaled to indicate regions of longitudinal muscle undergoing shortening (lighter shade) or lengthening (darker shade), i.e., muscle motility. Repeating the spline fitting and differentiation procedure for every row in the velocity array yields a map of longitudinal strain rate (L map). If the interpolation is performed at distances corresponding to the width of a pixel in the original images, it will result in a strain rate map with the same horizontal scaling as the D or R maps of the same preparation for easy comparison. To interpret strain rate maps, it should be noted that if the ends of the gut segment are fixed, a contraction in one location requires extension at other locations along the length of the segment (Fig. 7).

High definition L maps of intestinal strain rate generally show longitudinal contraction to be distributed over small lengthwise segments. Hence, comparison of strain rates in adjacent segments of the wall of the intestine that spans a contractile event has allowed increased insight into its structure. High definition L maps of peristalsis in an ex-vivo preparation of possum ileum show an area of ongoing longitudinal contraction in the region lying immediately in advance of the diametrically contracting segment (Fig. 2), which is thought to aid in promoting mixing along the wall [28].

L maps allow the direction and speed with which changes in strain propagate along a length of intestine to be determined but it is important to note that these changes can result either from circular or longitudinal contractile activity. Thus local strain rate can become negative indicating shortening in the longitudinal dimension either directly from contraction of longitudinal smooth muscle or indirectly from reduction in the volume of a segment by circular muscle contraction concomitantly reducing both diametric and longitudinal distension of the wall (Fig. 3). While segmentative activity is thought to result largely from contraction of circular smooth muscle [49] ST maps of contractile activity in the proximal duodenum show there is concomitant variation in longitudinal strain [25].

In the same way that upper and lower R maps can be used to compare radial movements of mesenteric and antimesenteric borders of the intestine, L maps may be constructed with their line of cross-correlation reference points lying nearer either to the mesenteric or to the antimesenteric border. Comparison of the L maps obtained from these different regions allows differences in the extent of longitudinal movement across the radial dimension to be assessed and the degree of asymmetry of movement to be evaluated [33].

3.2.3 Generalised Strain Rate Maps

The cross-correlation technique derives the displacement of reference points in two dimensions but only one of these is utilised in the L map technique described above. However, a generalised strain map that utilises the 2D data is useful for more complex morphologies such as the rabbit caecum and its associated junctions (Fig. 8) [19]. In this variation, the movements of points equally spaced along a user-specified line of interest (LOI) are determined by considering a 21 × 21 pixel square surrounding each point. In the generalised case, the components of

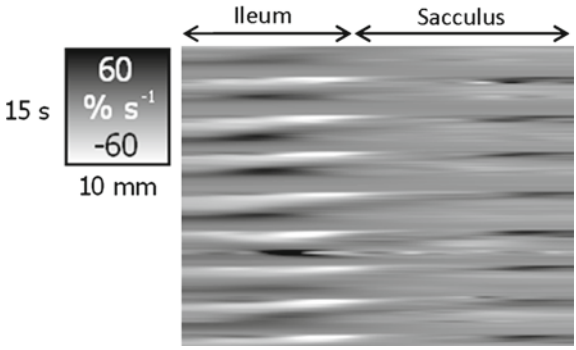

Fig. 8 Generalised strain rate map of the distal ileum and sacculus rotundus of the rabbit generated from a LOI placed axially along the preparation. Propagating ileal contractions appear to be synchronous with an instantaneous lengthening of the adjacent sacculus rotundus. This pattern suggests that the ileal contraction is displacing digesta into the sacculus rotundus [19]

movement in the direction of the LOI are used to generate the array of velocities. The remaining procedure is the same as that used for generating L maps.

4 Intensity Maps

The use of D and L maps depends on the identification of movements in the edges or boundaries of the gut wall or of lengthwise movements of distinctive and repeatedly recognisable features or structures on its surface. When a section of a preparation moves in the direction of the camera's line of sight, these techniques are inapplicable. However, the contraction can often be seen in a sequence of images because the movement changes the angle of the preparation surface, and hence, the intensity of light reflected towards the camera. The rows of an intensity map simply correspond to the pixel intensities along a user-specified LOI for sequential images. An intensity map does not provide any information about the amplitude of contractions but can be used to estimate their frequency and propagation velocity [4, 19]. The intensity map methodology can be used to track the movement of any localised quantitative variable across the surface of an intestinal component including the migration of cellular florescence associated with contractile activity [39] and the migration of electrophysiological phenomena [25, 49].

It should be noted that the method can be prone to inaccuracies when reflected light is being used and where the variable that is being mapped transits a 3D structure. Thus, where a segment of gut is illuminated by light from a fixed direction, ongoing displacement of the wall may cause the direction in which light is subsequently reflected from its surface to the camera to change, i.e., light may initially be reflected from the apex of the travelling region of distension and subsequently from the side of the distension. In such a situation, the rate of progression of the brightest region in the intensity map will not provide a true estimate of the rate of propagation of the distended area. Therefore, it is advisable to validate the values obtained from intensity maps by checking against estimates obtained by other means.

5 Deriving Further Information

5.1 Derived Maps

A number of parameters can be derived from ST maps of contraction patterns, e.g., the speed and direction of propagation, the duration of constriction and the frequency of occurrence (see Sect. 2.1). The calculation of these parameters can be automated and then applied to one of the base ST maps described earlier to derive new maps such as frequency and velocity maps [16]. Another technique for

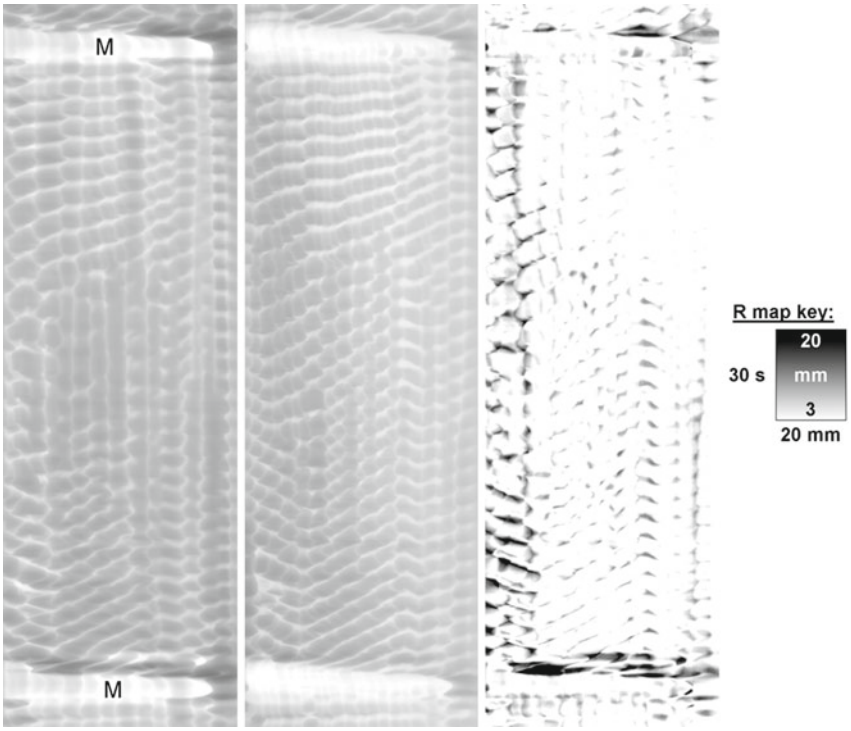

Fig. 9 Corresponding R maps (*left* and *centre*) showing organisation of ripple contractions in the absence of haustration in the upper and lower halves of an ex-vivo preparation of the proximal colon of the rabbit during an interval between successive mass peristaltic events (M, see Fig. 1). The heavier white lines that are of shallower gradient are the boundaries of ripple contractions that are moving predominantly orad with locally varying rates. The fainter near-vertical lines are folds, which appeared to be due to a fixed anatomical element rather than a motility pattern. Also shown (*right*) is a map of the absolute differences between the two R maps. This highlights differences in coordination between the intertaenial domains in the two halves (regions of greater difference appear *darker*). Note that the timing and directions of propagation of ripple contractions are generally coordinated across the two intertaenial domains but that there are local regions of incoordination [30]

accentuating areas of high phasic activity is to apply the absolute operator to a strain rate map and then smooth the result to remove the phasic contraction frequency [33].

In essence, ST maps themselves are 2D images and many conventional image processing operations can be applied to them: high, low and band pass filters; mathematical operations with scalars or other images; autocorrelation; and 2D Fourier transforms [20, 44]. For instance, one simple method of assessing the difference between two images is by subtracting one image from the other, a technique that has been used to highlight the limited coordination of the ripple contractions between two of the intertaenial domains of a haustrated colon (Fig. 9).

Another common task is the removal of regular fine horizontal lines from maps such as those due to the rhythmic displacement of the stomach generated by pendular contractions of the attached proximal end of the duodenum [31]. This can be removed by applying a moving average filter to each column of the map with the size of the filter window set to the wavelength of the duodenal contractions (1.6 s for the rat). The moving average filter is straightforward to implement and has a convenient frequency response, i.e., it completely removes all the harmonics of the frequency that has a wavelength corresponding to the moving average window size.

5.2 Autocorrelation

The cross-correlation of an image with itself (i.e., autocorrelation) is a useful technique for identifying and quantifying repeating features within an image [44]. The operation has the effect of averaging the individual repeating features and removing noise. The central point of the autocorrelation image represents the correlation of points with themselves, and hence, is the lightest, i.e., has the higher value. Another lighter point at a particular angle and distance from the centre of the autocorrelation image would indicate a high correlation value between the points in the original image and the points that overlie them after the entire image has been displaced in the same direction by the same distance.

Autocorrelated ST maps can sometimes improve the identification of propagating contractions in regions where activity is of low amplitude [22]. For instance, this can allow hydraulic distension of a region induced by regular contractions in other regions of the segment to be more readily distinguished from the effects of propagating contractions. Hence, the patterns generated by (instantaneous) hydraulic distension appear as parallel horizontal lines on the autocorrelogram whereas those formed by (more slowly) propagating phasic contractions show as parallel angled lines, the speed of their propagation being inversely proportional to their slope.

5.3 Evaluating Mixing Within a Gut Segment

An important goal in understanding the physical processing of digesta is to establish the link between the motility of a gut segment and the nature of the mixing occurring within. One approach is to conduct ST mapping synchronously with measurements of the concentration of a dye marker as it passes through the segment [21]. Data from D maps can be further processed to quantify variations in the volume of the segment over time, which can then be used to assess changes in the velocity of the luminal contents as they flow backwards and forward within the segment. This information can be combined with that provided by the residence

time profiles of a dye marker and with the rheological characteristics of the perfusate to determine the mixing regime within the lumen.

It remains to evaluate mixing outcomes. To this end groups are currently augmenting established computational methods for simulating luminal flow (see "Computational Modeling of Gastrointestinal Fluid Dynamics" by Ferrua et al. in this volume) by incorporating real time data obtained from ST mapping with relevant rheological data to achieve this aim. We plan to validate this method by comparing dye marker RTD profiles predicted by the computation with those from concurrent physiological experimentation.

6 Practical Considerations

6.1 Experimental Conditions

As with most techniques ST mapping is not without its pitfalls. It is important at the outset to state that movements of the gut wall in-vivo or in an ex-vivo preparation reflect the resultant of the opposing forces applied by the smooth muscle cells in the wall and the resistance of the lumen contents to displacement. Hence, any study that seeks to quantify movements in a segment of gut for subsequent use in computer simulations that attempt to recapitulate the normal contractile events must take care that the physical characteristics of digesta mirror those normally found in-vivo. In some cases, notably the stomach, these characteristics may vary over time and such variation must be simulated if the results are to be biologically meaningful. It is noteworthy that a great many physiological experiments have been conducted in which watery fluid are used to perfuse the lumen. Such experiments run the risk of allowing the smooth muscles to act in a manner that is outside their normal range of operation, e.g., by allowing greater amplitude of peristaltic contraction and lumen occlusion than would be encountered in-vivo [27].

6.2 Image Quality and Acquisition Frequency

One approach to image acquisition is to record an experiment on video tape and subsequently scan it into a computer [15]. This method is convenient and has a comparatively high scan rate (e.g., 25 frames/s) but the image storing algorithms associated with video recording and storage will compromise the quality of the images. While the images obtained may be adequate for mapping gut segment boundaries they will generally be unsuitable for strain rate mapping using the cross-correlation technique. The latter is better achieved by using monochrome cameras connected directly to a computer and saving the high resolution images in a lossless format such as TIFF or PNG.

It is important to develop ST mapping procedures with due regard to the time scale of the events that they are intended to analyse. In ex-vivo preparations, phasic contractions are generally easier to map than changes in tone as they take place rapidly with respect to the life of the preparation. Changes in intestinal tone generally occur more slowly, and hence, the gradual increase or decrease in the volume of a gut segment may extend over a period of 30 min and be evident as a gradual change in the mean grey scale value of a D map over the duration of the recording.

The minimum rate of image acquisition must take into account the frequency of the fastest movement in the type of preparation that is to be used. For example, if it is desired to distinguish fast phasic contractions from instantaneous hydraulic effects on a D map then image acquisition and subsequent analysis must be conducted on a sufficiently fast time scale to ensure that the slope of the relevant line on the D map that results from a rapidly propagated phasic contraction can be distinguished from the horizontal line generated by an instantaneous dilatation. In theory, the sampling interval should be less than half the shortest wavelength of interest [50]. Our experience is that frame rates of 5–8 frames/s are a good compromise between temporal resolution and computational overhead.

Similar considerations pertain to spatial resolution in ST maps, i.e., the spacing between applied markers or cross-correlation reference points. A fine level of spatial resolution is required to prevent aliasing, an artefact in which different signals become indistinguishable when sampled. This can be seen in some early longitudinal maps that were based on widely-spaced applied markers [15]. In the latter, there is some doubt as to whether the phasic contractions are moving orad or aborad at a slower speed.

6.3 Effects of the Geometry of the Preparation

Spatiotemporally-based calculations of parameters such as speed of propagation that are based on the analyses of 2D images of a 3D surface will underestimate the movement as they can only measure partial components of what is a 3D propagation, i.e., those that are perpendicular to the camera's line of sight. For instance, in strain rate maps of tubiform segments of gut where contractions appear to travel transversely across the long axis of the segment of intestine in the video image, the velocity of their propagation will increase towards the centre and decrease towards the boundaries of the segment as its surface is in fact convex toward the camera. This indicates the importance of questioning the assumption that the propagation of contractile events should be related to a simple linear axis and of considering the physiology of the gut segment under examination before deciding the relevant axis on which to track movement.

Although it is sometimes assumed that the contractile behaviour of a tubular gut segment will be similar regardless of any rotation, the pattern of propagation may not be symmetrically distributed around the circumference of the tube and the

contractile characteristics will vary accordingly. For example, asymmetry is reported between the mesenteric and antimesenteric borders of the lumen of the guinea-pig ileum [47] and rat duodenum [33].

Finally, it is important to note that ST maps that rely on surface markers to determine changes in radial and longitudinal dimensions of a tissue surface, e.g., diametric and longitudinal contractions in a gut segment, may emphasise the contribution of longitudinal with respect to circular muscle activity. Morphological or artificial markers on the surface of the intestine are located directly over the surface of the longitudinal muscle, and hence, may be expected to respond with high fidelity. However, their responses to movements of circular muscle may be weaker as this muscle layer is deeper and connected to the surface by a series of viscoelastic linkages [25]. In the latter case, the use of D maps is to be preferred.

7 Future Directions

In principle, there is no reason why the reference points of the cross-correlation technique need to lie along a LOI. When analysing the motility of an organ like the stomach, it may be advantageous to use a grid of reference points, which should allow the derivation of motility maps with two spatial dimensions comparable to the electrophysiological maps generated using electrode arrays [24]. From a practical perspective, the obvious difficulty is the need to accommodate an extra spatial dimension, which can be accomplished by using colour maps rather than greyscale.

Currently, the bulk of ST mapping has been conducted in ex-vivo preparations and we are aware of only one group that has conducted ST mapping in-vivo [6, 14]. The advantage of using ex-vivo preparations lies in the reduction of extraneous motions that may compromise ST mapping by cyclic or irregular displacement of the segment that is being mapped, e.g., a ST map obtained from an ex-vivo preparation of the stomach will be free of movement artefacts induced by pulsation of the underlying aorta and by respiratory excursions of the diaphragm. However, the cross-correlation mapping technique should be comparatively robust against movement artefacts as it is based on the relative movement between adjacent reference points along the LOI and would be a good starting point.

In conclusion, ST maps of gut wall movement offer promise in gaining greater understanding of the link between electrophysiological and contractile processes, the patterns of forces that are applied to digesta and the degree of general or local mixing that they engender. It has recently become apparent that electrophysiological studies with concurrent fine scale resolution ST mapping of contractile movement may be required to resolve the ongoing debate regarding the origin of extracellular electrophysiological activity [41]. Finally, the method has attracted the interest of medical researchers as the identification of fine patterns of contraction in the quiescent bowel may permit prompt distinction of ischemic from healthy bowel at laparotomy.

References

1. Abdu F, Hicks GA, Hennig G, Allen JP, Grundy D (2002) Somatostatin sst(2) receptors inhibit peristalsis in the rat and mouse jejunum. Am J Physiol 282:G624–G633
2. Alvarez WC, Zimmermann A (1927) The absence of inhibition ahead of peristaltic rushes. Am J Physiol 83:52–59
3. Benard T, Bouchoucha M, Dupres M, Cugnenc PH (1997) In vitro analysis of rat intestinal wall movements at rest and during propagated contraction: a new method. Am J Physiol 273:776–784
4. Bercik P, Bouley L, Dutoit P, Blum AL, Kucera P (2000) Quantitative analysis of intestinal motor patterns: spatiotemporal organization of non-neural pacemaker sites in the rat ileum. Gastroenterology 119:386–394
5. Berthoud HR, Hennig G, Campbell M, Volaufova J, Costa M (2002) Video-based spatiotemporal maps for analysis of gastric motility in vitro: effects of vagal stimulation in guinea-pigs. Neurogastroenterol Mot 14:677–688
6. Bogeski G, Shafton AD, Kitchener PD, Ferens DM, Furness JB (2005) A quantitative approach to recording peristaltic activity from segments of rat small intestine in vivo. Neurogastroenterol Mot 17:262–272
7. Bowditch H (1897) Movements of the alimentary canal. Science 5:901–902
8. Brookes SJH, Chen BN, Costa M, Humphreys CMS (1999) Initiation of peristalsis by circumferential stretch of flat sheets of guinea-pig ileum. J Physiol 516:525–538
9. Brown B, Ng K, Kwong K, Duthie H, Whittaker G, Franks C (1971) Computer analysis and simulation of human gastroduodenal electrical activity. Med Biol Eng Comput 9:305–314
10. Cannon WB (1898) The movements of the stomach studied by means of the Röntgen rays. Am J Physiol 1:359–382
11. Cannon WB (1911) The mechanical factors of digestion. Edward Arnold, London
12. Dikeman CL, Fahey GC (2006) Viscosity as related to dietary fiber: a review. Crit Rev Food Sci Nutr 46:649–663
13. Dinning PG, Arkwright JW, Costa M, Wiklendt L, Hennig G, Brookes SJH, Spencer NJ (2011) Temporal relationships between wall motion, intraluminal pressure, and flow in the isolated rabbit small intestine. Am J Physiol 300:G577–G585
14. Ferens DM, Chang EC, Bogeski G, Shafton AD, Kitchener PD, Furness JB (2005) Motor patterns and propulsion in the rat intestine in vivo recorded by spatio-temporal maps. Neurogastroenterol Mot 17:714–720
15. Hennig GW, Costa M, Chen BN, Brookes SJH (1999) Quantitative analysis of peristalsis in the guinea-pig small intestine using spatio-temporal maps. J Physiol 517:575–590
16. Hennig GW, Gregory S, Brookes SJH, Costa M (2010) Non-peristaltic patterns of motor activity in the guinea-pig proximal colon. Neurogastroenterol Mot 22:e207–e217
17. Hennig GW, Spencer NJ, Jokela-Willis S, Bayguinov PO, Lee H, Ritchie LA, Ward SM, Smith TK, Sanders KM (2010) ICC-MY coordinate smooth muscle electrical and mechanical activity in the murine small intestine. Neurogastroenterol Mot 22:e138–e151
18. Huizinga JD, Lammers WJEP, Mikkelsen HB, Zhu Y, Wang XY (2010) Toward a concept of stretch coupling in smooth muscle: a thesis by Lars Thuneberg on contractile activity in neonatal interstitial cells of Cajal. Anat Rec 293:1543–1552
19. Hulls C, Lentle RG, de Loubens C, Janssen PWM, Chambers P, Stafford KJ (2012) Spatiotemporal mapping of ex vivo motility in the caecum of the rabbit. J Comp Physiol B182:287–297
20. Jähne B (2004) Practical handbook on image processing for scientific and technical applications, 2nd edn. CRC Press, Boca Raton
21. Janssen PWM, Lentle RG, Asvarujanon P, Chambers P, Stafford KJ, Hemar Y (2007) Characterisation of flow and mixing regimes within the ileum of the brushtail possum using residence time distribution analysis with simultaneous spatio-temporal mapping. J Physiol 582:1239–1248

22. Janssen PWM, Lentle RG, Hulls C, Ravindran V, Amerah AM (2009) Spatiotemporal mapping of the motility of the isolated chicken caecum. J Comp Physiol B179:593–604
23. Kong F, Singh RP (2010) A human gastric simulator (HGS) to study food digestion in human stomach. J Food Sci 75:E627–E635
24. Lammers W, Ver Donck L, Stephen B, Smets D, Schuurkes JAJ (2009) Origin and propagation of the slow wave in the canine stomach: the outlines of a gastric conduction system. Am J Physiol 296:1200–1210
25. Lammers WJE, Dhanasekaran S, Slack JR, Stephen B (2001) Two-dimensional high-resolution motility mapping in the isolated feline duodenum: methodology and initial results. Neurogastroenterol Mot 13:309–323
26. Lammers WJEP, Cheng LK (2008) Simulation and analysis of spatio-temporal maps of gastrointestinal motility. BioMed Eng OnLine 7:2
27. Larson M, Schulze K (2002) Appearance of peristaltic reflex in isolated guinea pig ileum in response to boluses of air, water, oil, and cellulose. Dig Dis Sci 47:2644–2650
28. Lentle RG, Janssen PWM, Asvarujanon P, Chambers P, Stafford KJ, Hemar Y (2007) High definition mapping of circular and longitudinal motility in the terminal ileum of the brushtail possum *trichosurus vulpecula* with watery and viscous perfusates. J Comp Physiol B177:543–556
29. Lentle RG, Janssen PWM (2008) Physical characteristics of digesta and their influence on flow and mixing in the mammalian intestine: a review. J Comp Physiol B178:673–690
30. Lentle RG, Janssen PWM, Asvarujanon P, Chambers P, Stafford KJ, Hemar Y (2008) High definition spatiotemporal mapping of contractile activity in the isolated proximal colon of the rabbit. J Comp Physiol B178:257–268
31. Lentle RG, Janssen PWM, Goh K, Chambers P, Hulls C (2010) Quantification of the effects of the volume and viscosity of gastric contents on antral and fundic activity in the rat stomach maintained ex vivo. Dig Dis Sci 55:3349–3360
32. Lentle RG, Janssen PWM (2011) The physical processes of digestion. Springer, New York
33. Lentle RG, De Loubens C, Hulls C, Janssen PWM, Golding MD, Chambers JD (2012) A comparison of the organization of longitudinal and circular contractions during pendular and segmental activity in the duodenum of the rat and guinea pig. Neurogastroenterol Mot 24(7):686–695, e298
34. Macagno EO, Christensen JM (1980) Fluid mechanics of the duodenum. Annu Rev Fluid Mech 12:139–158
35. Macagno EO, Christensen JM (1981) Fluid mechanics of gastrointestinal flow. In: Johnson LR (ed) Physiology of the gastrointestinal tract. Raven, New York, pp 335–358
36. Melville J, Macagno E, Christensen J (1975) Longitudinal contractions in the duodenum: their fluid-mechanical function. Am J Physiol 228:1887–1892
37. Mendoza L, Lejia L, Garay L, Ramos EG (1997) Physical model of the stomach motor activity. In: Engineering in Medicine and Biology Society. Proceedings of the 19th annual international conference of the IEEE, pp 2201–2204
38. Neal KB, Parry LJ, Bornstein JC (2009) Strain specific genetics, anatomy and function of enteric neural serotonergic pathways in inbred mice. J Physiol 587:567–586
39. Park KJ, Hennig GW, Lee HT, Spencer NJ, Ward SM, Smith TK, Sanders KM (2006) Spatial and temporal mapping of pacemaker activity in interstitial cells of Cajal in mouse ileum in situ. Am J Physiol 290:1411–1427
40. Prioreschi P (1996) A history of medicine: greek medicine. Horatius Press, Omaha
41. Rhee PL, Lee JY, Son HJ, Kim JJ, Rhee JC, Kim S, Koh SD, Hwang SJ, Sanders KM, Ward SM (2011) Analysis of pacemaker activity in the human stomach. J Physiol 598(Pt 24):6105–6118. doi:10.1113/jphysiol.2011.217497
42. Roberts RR, Ellis M, Gwynne RM, Bergner AJ, Lewis MD, Beckett EA, Bornstein JC, Young HM (2010) The first intestinal motility patterns in fetal mice are not mediated by neurons or interstitial cells of Cajal. J Physiol 588:1153–1169
43. Ruppert D, Wand MP, Carroll RJ (2003) Semiparametric regression. Cambridge University Press, Cambridge

44. Russ JC (2006) The image processing handbook, 5th edn. CRC Press, Boca Raton
45. Schemann M, Michel K, Peters S, Bischoff SC, Neunlist M (2002) Cutting-edge technology. III. Imaging and the gastrointestinal tract: mapping the human enteric nervous system. Am J Physiol 282:919–925
46. Schulze-Delrieu K (1992) Clearance patterns of the isolated guinea pig duodenum. Gastroenterology 102:849–856
47. Schulze-Delrieu K (1999) Visual parameters define the phase and the load of contractions in isolated guinea pig ileum. Am J Physiol 276:G1417–G1424
48. Schulze K (2006) Imaging and modelling of digestion in the stomach and the duodenum. Neurogastroenterol Mot 18:172–183
49. Seerden TC, Lammers W, De Winter BY, De Man JG, Pelckmans PA (2005) Spatiotemporal electrical and motility mapping of distension-induced propagating oscillations in the murine small intestine. Am J Physiol 289:G1043–G1951
50. Shannon CE (1949) Communication in the presence of noise. Proc IRE 37:10–21
51. Tasaka K, Farrar JT (1969) Mechanics of small intestinal muscle function in the dog. Am J Physiol 217:1224–1229
52. Trendelenburg P (1917) Physiologische und pharmakologische versuche über die dünndarmperistaltik. Naunyn-Schmiedeberg's Arch Pharmacol 81:55–129
53. Trendelenburg P (2006) Physiological and pharmacological investigations of small intestinal peristalsis. Naunyn-Schmiedeberg's Arch Pharmacol 373:101–133

Computational Modeling of Gastrointestinal Fluid Dynamics

Maria J. Ferrua and R. Paul Singh

Abstract Knowledge of the fluid dynamic behavior of gastrointestinal (GI) contents during digestion is essential to further understand and model the bioavailability of nutrients and pharmaceuticals in health and disease. The dynamics that develop within the GI tract are the result of a complex and self-regulated interplay between the physical properties of the intraluminal contents and the motor responses of the GI wall. Recent advances in the characterization of GI motility patterns have facilitated the use of engineering simulation tools to investigate the mechanisms driving different GI functions. In this chapter, current research aimed at using computational fluid dynamic (CFD) techniques to predict the flow and mixing behavior of gastric and small intestinal contents during digestion will be reviewed. The unique capability and potential applications of this new approach to advance research in the food and health sectors will be discussed.

1 Introduction

During digestion the ingested meal is transformed and absorbed by a complex interaction of chemical and mechanical effects, triggered and regulated by the secretionary and motor responses of the gastrointestinal (GI) tract. Mechanical forces and fluid motions generated by muscle contractions of the GI wall promote the physical breakdown and transport of the ingested meal along the tract, while a series of digestive juices secreted along the tract also promote the enzymatic

M. J. Ferrua (✉)
Riddet Institute, Massey University, Palmerston North, New Zealand
e-mail: M.Ferrua@massey.ac.nz

R. P. Singh
Department of Biological and Agricultural Engineering and Department of Food Science and Technology, University of California, Davis, CA 95616, U.S.A

L. K. Cheng et al. (eds.), *New Advances in Gastrointestinal Motility Research*, Lecture Notes in Computational Vision and Biomechanics 10,
DOI: 10.1007/978-94-007-6561-0_13, © Springer Science+Business Media Dordrecht 2013

splitting of the food macromolecules into simpler and more easily absorbed forms. As expected, these two mechanisms are not independent of each other. By weakening the structure of the food, chemical effects will also enhance the mechanical breakdown of the meal; while by efficiently mixing and churning GI contents, mechanical effects will also promote and enhance the enzymatic splitting and easy absorption of food macronutrients.

For more than 50 years, extensive research has been carried out to understand and characterize food digestion. Since the late 1950s, several research groups have shown the marked effect that dietary fibers have on the metabolism of carbohydrates and lipids. As a result, understanding the mechanisms of these actions has become an important area of research [13]. Different in-vivo studies have shown that the composition and structure of the diet affect a number of processes during digestion, including not only the motor and secretionary response of the GI tract, but also the distribution, mixing and transport of the digesta along the system [4, 7, 12, 52, 53, 64]. Despite the diverse and complex interaction of the physiological and physical mechanisms that control these processes, it is generally accepted that the properties of the diet will ultimately affect the metabolism of nutrients and bioactive compounds by influencing the physical and rheological properties of the digesta along the GI tract and, as a consequence, its dynamic behavior during digestion [14, 19, 22, 41, 43, 51, 75].

As evidenced from the preceding discussion, to fully understand and model food digestion it is essential to first understand the fluid-mechanical forces driving the distribution and transport of the meal at all sites of the GI tract [42, 63]. This need has also been identified as critical for the development of novel delivery systems aimed at improving the bioavailability and controlled release of bioactive compounds within the GI tract. In particular, the in-vivo efficacy of these systems has been found to depend on the way in which the properties of the diet affect their gastric distribution during digestion [20, 21, 71].

As discussed by Angeli et al. in "The Electrical Regulation of GI Motility at the Whole-Organ Level", by Dinning in "Colonic Manometry: What do the Squiggly Lines Really Tell Us?", and by Janssen and Lentle in"Spatiotemporal Mapping Techniques for Quantifying Gut Motility" of this volume, the use of advanced mapping techniques, as well as real-time imaging tools [55, 66] have enabled the in-vivo analysis of different GI functions. However, the capability of these techniques to analyze and quantify the fluid dynamic behavior of the GI contents is still limited [63]. As an alternative approach, since peristalsis is one the major mechanisms for the transport of GI contents, analytical solutions of peristaltic flows have been used to characterize the fluid dynamics of food digesta. Jimenez-Lozano and Sen [34] used this approach to show the complex flow behavior (i.e., transitions between backward, trapping and augmented flows) that develop even in the case of a simple planar or axisymmetric peristaltic flow of an incompressible Newtonian fluid. However, while this approach has been extensively used in many classical fluid-dynamic studies, it is constrained by a series of approximations that do not necessarily reflect the geometry and functionality of the GI tract [50, 62, 67, 81]. In particular, it is limited to only low Reynolds numbers peristaltic flows, that

develop within infinite planar or axisymmetric conduits, by the periodic, sinusoidal and long wave deformations of their walls. In particular, the limited scope of this approach to characterize the flow behavior within the finite and curved passages that occur along the GI tract has been recently highlighted in literature [1, 44].

The use of computational fluid dynamic (CFD) techniques has been recently identified as a unique and promising tool to characterize and model the fluid dynamic mechanisms driving digestion [63]. For decades, mathematical and numerical methods such as CFD have been successfully used as an evaluation tool in many engineering industries, particularly aerospace and automotive. However, recent advances in the mathematical modeling of complex multiphysics phenomena, and the increasing availability of high-performing computing, have triggered the use of CFD as a design and development tool in a growing number of industrial and commercial sectors (ranging from sport and leisure to chemical and electronic). By predicting the environmental and physical phenomena occurring during a real application, numerical simulations can provide a unique understanding of the key problems that need to be addressed at early stages of the product development process. In addition, by facilitating the evaluation of a broad range of alternative designs without the need of expensive prototypes, numerical simulations can also promote the efficient development of novel and innovative designs. Within the biomedical sector, engineering simulation tools have been used to assist with the development and design of a wide range of products (from prosthetics and artificial organs to medical and diagnostic equipment), and to investigate the function of different parts and organs of the human body in health and disease (including the transmission of loads in the human spine, the effect of vascular stiffness on pulmonary hypertensive hemodynamics, the blood flow in cerebral aneurisms, the airflow in human noses and the flow in healthy and diseased lungs).

The possibility of numerically analyzing the dynamics of food digesta systems under different physiological conditions offers new opportunities to better understand the role of GI motility on the function of the GI tract in health and disease. While feasible, this approach faces several challenges. In addition to a series of numerical and modeling issues (associated with the complex geometry, motility and physics of the digestive process), this approach also requires a good in-vivo understanding of the interplay that occurs between the properties of the digesta and the motor response of the GI wall. It is well established that the sole presence and properties of the digesta generate the chemical and mechanical stimulus that regulate, through a series of endocrine, paracrine and neural pathways, the biomechanical functions of the GI wall. However, due to a number of practical and ethical issues, a good quantitative characterization of this complex interaction of factors is still limited [2, 41–43].

In the following, a brief review of our current understanding of the physical properties of food digesta and the motility functions of the stomach and small intestine will be first provided. After that, current and novel research aimed at using CFD as a tool to investigate the dynamics of GI contents (in particular within the stomach and small intestine) will be discussed.

2 Physiological Conditions Driving GI Fluid Dynamics

As mentioned in the introduction, a good characterization of the physical properties of the digesta and the associated GI motility are essential to accurately model the physiological conditions driving the flow behavior and transport of the meal along the GI tract.

2.1 Physical Properties of Food Digesta

As food travels along the GI tract, its physical properties undergo significant changes. In the oral cavity, food structures are mechanically broken down into smaller pieces and mixed with saliva to form a lubricated food bolus suitable for its transport through the oesophagus into the stomach. Once in the stomach, the food is further fragmented by a complex interaction of mechanical and chemical effects. Muscle contractions of the stomach wall promote the mechanical breakdown of the food bolus and its efficient mixing with gastric juices. As a result of gastric digestion, the bolus is converted into a semi-liquid mass (called chyme) of partially digested food, water, hydrochloric acid, mucus and enzymes suitable for further digestion in the small intestine. The motor response of the intestinal wall facilitates the final digestion and absorption of nutrients by mixing the chyme with a series of digestive secretions, controlling its transport along the intestine, and ensuring its repeated contact with the absorptive surface of the mucosa. As a result of its transit along the small intestine, the digesta becomes increasingly less fluid. Once in the large intestine, most of the remaining water and minerals will be absorbed, and a compact mixture of residual indigestible matter and sloughed-off mucosal cells will be obtained.

By modulating the motor activity of the GI wall and determining the way in which intraluminal contents flow and/or deform under stress, the physical properties of the digesta (in particular its rheology) are expected to have a critical role in the dynamics and transport of the meal along the GI tract.

2.1.1 Rheology of GI Contents

During the last two decades, research has been conducted to better understand how the rheology of GI contents at different sites of the GI tract is affected by the initial composition and structure of the diet. However, the difficulty in measuring the rheology of particulate suspensions, the complex and progressive changes experienced by the digesta along the GI tract, and the ethical and practical issues involved in in-vivo trials, have so far prevented a fundamental understanding of its flow properties [13, 41].

Ellis et al. [18] have shown the direct and non-linear effect of dietary fibers on the viscosity of jejuna digesta of pigs. Pig diets supplemented with 20 g guar gum/kg diet led to 51 and 28-fold increases in viscosity of the digesta after 30–60 min of meal intake, respectively. While a supplement of 40 g guar gum/kg diet led to 45 and 93-fold increases at the same corresponding times. Dikeman et al. [15] experimentally characterized the pseudoplastic behavior of the ileal digesta of dogs and showed the complex interaction of effects through which the properties of the diet might affect the rheology of food digesta. In particular, they found that differences triggered by the composition and structure of the diet on the secretionary responses of the GI tract might be as important as the initial rheology of the diet. They also found that the presence of gelling agents in the diet does not appear to impact the viscosity of terminal ileum digesta, but indicated a possible relationship between its viscosity and the amount of dry matter remaining in it. The effects of solid particles on the rheological behavior of the digesta have been analyzed by different research groups. Takahashi and Sakata [74] reported that the sole presence of fine dietary particles is enough to impart a non-Newtonian behavior to pig cecal contents. Their rheology was characterized by an apparent Bingham plastic behavior, whose yield stress was significantly increased by the concentration of large particles. Lentle et al. [39] found that the intestinal digesta of brushtail possums exhibited a shear-thinning flow behavior. Its apparent viscosity increased during its transit along the intestine, and this increment could be positively related to its dry matter content. In addition, the authors also investigated its viscoelastic properties and found that the elastic modulus was greater than the viscous modulus, even in the small intestine. They associated this rheological behavior with that of weak gels, and found that fluid was extruded from all intestinal digesta on compression at physiological pressures. In a subsequent study, Lentle et al. [40] analyzed the rheology of the proximal and distal colonic digesta of the possum, and found that its viscoelastic behavior fitted the Burger's model of creep compliance. The physical properties of the digesta were found to change with sustained shear stress (a phenomenon that they associated with the extrusion of liquids from it) and a significant viscoelastic recovery of the digesta plug was observed following the cessation of the stress. Based on these results, the authors suggested that the motor response of the intestine may actually promote the digestion and the absorption of nutrients by an alternate extrusion and reabsorption of intraluminal fluids form the digesta plug, instead of by the typical dynamics of peristaltic flows.

2.2 Geometry and Motor Response of the Stomach and Small Intestine During Digestion

The driving force promoting the dynamics and transport of the meal along the GI tract is determined by the motor activity of the GI wall in response to the presence and properties of the digesta. Therefore, any CFD analysis of the dynamics of food

digesta along the GI tract will first require a fundamental understanding and modeling of the geometrical and mechanical deformations undergone by the GI wall during digestion.

Recent advances in medical imaging techniques, such as real time MRI [55, 66] and the use of spatio-temporal mapping techniques (as described by Dinning in "Colonic Manometry: What do the Squiggly Lines Really Tell Us?" of this volume) have allowed a better insight and understanding of GI motility. However, a good and detailed characterization of the motor functions of the GI wall, as well as their interplay with the physical properties of the digesta, remain to be developed [42].

2.2.1 Stomach Geometry and Functionality During Digestion

The human stomach is a J-shaped hollow organ, which unlike any other organ of the GI tract undergoes significant volume variations to receive and retain the ingested meal. Its geometry varies significantly among individuals and it is continuously influenced by a large number of factors, such as the position of the body, the condition of the surrounding organs, the amount, composition and type of meal, and the digestive time [45, 63]. As a general description, the characteristic dimensions of an average human stomach after a typical meal are summarized in Table 1 [17, 27, 35, 36, 63].

Within seconds after the ingestion of a meal, a reduction in gastric tone and an increase in compliance of the proximal gastric wall enable the stomach to receive the ingested meal without a significant increase in gastric pressure [10]. This "receptive relaxation" is then maintained by a second response known as "adaptive relaxation", which actually modulates gastric tone in response to the specific properties of the meal [32]. These two responses (commonly known as "gastric accommodation") allow the stomach to act as a reservoir and are also suspected to affect the distribution and emptying of gastric contents [65]. Although the gastric accommodation for different macronutrients and body positions have been characterized using non-intrusive MRI and single photon emission computed tomography (SPECT) studies, this information has only been reported in terms of changes in the stomach volume [28, 38, 65, 73, 80]. To the best of our knowledge, no accurate characterization of this particular motor response has been published yet.

Table 1 Characteristic dimensions of an average-sized human stomach

Characteristic dimension	Average-sized stomach[a]
Greater curvature length (cm)	26–31
Widest section wide (cm)	8–10
Pyloric ring diameter (cm)	0.5–1.5
Volume capacity (L)	~0.94

[a] From Einhorn [17], Geliebter et al. [27], Keet [35], Schulze [63]

Table 2 Experimental characterization of the dynamics of the antral contraction waves (ACWs) after 20–30 min of meal ingestion

Characteristic dimension	ACW dynamics[a]
Frequency (1/min)	2.6–3.2
Velocity (cm/s)	0.22–0.33
Width (cm)	1.2–1.8
Maximum occlusion (%)	60–90
End location—distance from pylorus (cm)	~1.2

[a] From Pal et al. [60], Steingoetter et al. [72], Kwiatek et al. [38], Treier et al. [78], Pal et al. [61]

In addition to "gastric accommodation", the stomach motility during the postprandial state is also characterized by a series of regular-peristaltic antral contractions waves (ACWs). These ACWs originate as shallow indentations at the site of the gastric pacemaker, which deepen as they propagate towards the pylorus [58, 60]. Several research groups have suggested that the main purpose of these contractions is to generate the mechanical forces and fluid motions that promote the physicochemical disintegration of food structures during gastric digestion, and there is a current debate regarding whether they also contribute to the gastric emptying of nutrient liquids, as their propagation has been highly correlated to the valvular activity of the pyloric sphincter. [9, 30, 31, 38, 54, 66, 72]. Unlike gastric accommodation, the dynamics of these ACWs have been successfully characterized by using advanced MRI techniques. The frequency, velocity, occlusion and width of the waves have been quantified by several research groups, as summarized in Table 2 [38, 60, 61, 72, 78].

2.2.2 Small Intestine Geometry and Motility During Digestion

The small intestine is a long, narrow and hollow tube that extends from the stomach to the colon. It has an approximate length of 6 m and its diameter ranges from 4 cm at its junction with the stomach to 2 cm at its end at the ileocecal valve [56, 70]. The main functional segments of the small intestine are the duodenum, the jejunum, and the ileum. The duodenum is only 23–28 cm long, but has an essential role in the food digestion process. It receives and mixes the partially digested food coming from the stomach with bile salts secreted by the liver, pancreatic juices secreted by the pancreas, and digestive juices secreted by its own wall. The jejunum and ileum segments account for the rest of the small intestine, and it is within these regions where the nutrients are absorbed into the blood stream. Although there is no absolute point at which the jejunum ends and the ileum begins, it is assumed that the jejunum accounts for the upper 40 % of the small intestine below the duodenum.

By promoting the mixing and transport of intestinal contents, the movement of the intestinal wall is critical to facilitate the digestion and absorption of the food during the postprandial period [49]. The motor response of the intestine is the result

of spontaneous and independent contractions of the two layers of smooth muscle that constitute the muscularis coat of the wall [48]. Despite its complex dynamics, intestinal motility has been generally described in terms of two main contractive patterns, commonly referred as segmental and peristaltic contractions [3].

Segmental contractions are localized, circumferential contractions that involve a segment of only 1 or 2 cm of the intestine wall [29]. These contractions are expected to divide, separate and churn intestinal contents, ensuring a thorough mixing of the food with the digestive juices and a repeated contact of nutrients with the absorptive surface of the intestine. As the chyme moves from the duodenum to the ileum, the number of segmental contractions is expected to decrease [70]. Christensen et al. [11] investigated the spatial and temporal correlations of these contractions in the duodenum after the ingestion of a glass of skim milk. They found that, while contractions appeared to be spatially uncorrelated, successive contractions along the duodenum occur at frequency of one every 5 s. They also found that 70 % of the contractions occurring at one particular location can be considered as isolated events, being separated by at least 10 s of rest. Two successive contractions of the same segment of the duodenum only occurred 20 % of the time, and more than that became increasingly less probable.

Peristaltic contractions are reflex responses initiated when the intestinal wall is stretched by the presence of the digesta. These contractions are primarily responsible for the transport of intraluminal contents towards the colon [26]. They can be characterized as an advancing ring (or wave) that travels at a velocity of 0.5–2.0 cm s^{-1} over a short segment of 3–5 cm [29, 79].

3 Computational Modeling of Gastrointestinal Fluid Dynamics

3.1 Modeling the Flow Through the Gastro Esophageal Junction

Gastro esophageal junction (GOJ) dysfunction is suspected to be the main cause of gastro-oesophageal reflux disease, a condition that affects up to 20 % of the population of Western countries and accounts for around 5 % of a primary-care physician's workload [46]. McMahon et al. [57] used CFD techniques to analyze the flow patterns that develop in the GOJ during a reflux event and to better understand its function as a valvular mechanism to prevent gastric contents from flowing back into the oesophagus. The geometry and pressure difference at both sides of the GOJ during a reflux event were determined in-vivo by using a functional lumen imaging probe (FLIP). Based on this information a simplified 2D model of the GOJ geometry was created, and a negative pressure difference of 10 cm H_2O between the upper and lower boundaries defined. The upwards and steady fluid flow of a water-like fluid across the GOJ under these particular

conditions was numerically predicted. The fluid flow reached a maximum velocity of almost 2 m s^{-1} at the narrowest section of the GOJ (1.46 mm in diameter), and was characterized by the formation of a jet that bent towards the left side of the oesophagus. The authors correlated these results with reflux events evidenced to occur as the GOJ sphincter relaxes in absence of a swallow, and highlighted the promising use of CFD to analyze the nature and complexity of the GOJ function in health and disease. They also stressed the need for models capable of replicating the 3D geometry and motility of the GOJ to improve the accuracy of the results. In addition, it is noteworthy that alike FLIP, HR esophageal manometry can be used as valuable source of information to set the in-vivo conditions to which the flow will be exposed during a reflex event.

3.2 Modeling Gastric Flows During Digestion

Understanding the dynamics of gastric contents during digestion is becoming an area of increasing research, due to their role on food disintegration and subsequent bioavailability of nutrients and bioactive compounds. To the best of our knowledge, the first numerical analysis of how gastric motility affects the behavior of gastric contents during digestion was performed by Pal et al. [60]. In this study, a simplified 2D model of the stomach geometry and motility during digestion was developed based on in-vivo MRI data. The ACWs were modeled as 1.8 cm wide waves, initiated every 20 s at 14.4 cm from the pylorus. They travelled down at a speed of 2.5 mm/s and gradually increased their amplitude until becoming totally occlusive at the pylorus. The pylorus sphincter closed whenever an advancing wave was 2 cm from it, and remained as such until the wave disappeared. Gastric emptying was modeled based on a linear decrease in the stomach volume of 35 % during 15 min. The flow behavior that develops within the stomach was predicted using a "lattice Boltzmann" algorithm. To investigate the effect of different physiological conditions on behavior of the gastric flow, the amplitude and width of the ACWs, the rate of gastric emptying, and the opening period of the pylorus sphincter were respectively modified. The baseline dynamics of the gastric flow was characterized by the formation of two main flow patterns within the antrum region: a strong retropulsive jet-like motion at the location of the most occluding ACW, and slow recirculations (eddies) in between successive waves. As the ACW propagated distally and became more occlusive, the retropulsive jet and eddies structures strengthened reaching velocities of up to 7.4 mm s^{-1} and 2 mm s^{-1}, respectively. Retropulsive velocities were found to be only sensitive to the occlusion of the wave (the higher the occlusion, the stronger the retropulsion), while the eddies' strength was also sensitive to the width of the wave (the narrower the wave, the stronger the eddies). Neither the rate of gastric emptying, nor the opening pattern of the pylorus, produced any significant effect on development and characteristics of these two main flow structures. A well-defined 'zone of mixing' within the antrum region was also predicted. The retropulsive structure separated

fluid particles longitudinally, while the slow eddies transported them laterally towards the gastric wall. This mixing dynamics was again only affected by the geometrical characteristics of the ACWs, being enhanced by more occluding and narrower waves. The model also predicted the development of a series of peristaltic pressure waves within the distal antrum. The periodic pattern of these pressure waves was in good agreement with in-vivo data, but their magnitudes were two orders of magnitude smaller [31]. Despite this disagreement, this work made a significant and pioneering contribution to the study of gastric functions. It is arguably the first study where CFD tools were used in combination with advanced MRI techniques to develop a new level of understanding of the effect of gastric motility on the dynamics of gastric flows.

Pal et al. [61] then used the baseline model previously developed to analyze the effect of gastric motility on the emptying pattern of a liquid meal (10 % liquid glucose). To do this, the trajectories of 6200 fluid particles (initially distributed uniformly within the stomach) were traced during the first 10 min of digestion. In this period, the rate of gastric emptying was modeled to comply with a linear decrease in the stomach volume of 23 %. The fluid particles leaving the stomach over this period of time were identified and their initial location tracked.

As illustrated in Fig. 1, the results obtained challenged the classical description of a plug emptying from the distal antrum (pattern that was only predicted in the case of gastric flows only driven by fundic contractions, without any ACW activity). Under standard conditions of gastric motility, the stomach was emptied along a narrow and long path close to its lesser curvature, allowing fluid particles from the fundus to be directly drawn into the duodenum without experiencing much mixing. This emptying pattern was found to be slightly affected by the width and occlusion ratio of the ACWs: the narrower and more occlusive the waves, the closer the path to the lesser curvature of the stomach and the deeper it extended into the fundus region. As stated by the authors, these results might have critical implications in the design of oral delivery systems for nutrients and drugs. Systems designed to release their contents on these narrow paths of gastric emptying will draw high concentrations of the bioactive compound directly into the duodenum, while those designed to release their contents off these paths will give them the chance to mix well within the stomach and slowly enter the duodenum at lower concentrations.

Singh [68] used the geometrical dimensions and motility reported by Pal et al. [60] to create a 3D model of a 500 mL human stomach. The model was used to characterize the dynamics of a water-like fluid during digestion, and the affect of the propagation speed and occlusive profile of the ACWs on it. Similar to the work of Pal et al. [60], this study also indicated the formation of a strong retropulsive jet in the pyloric region, as well as flow recirculations between successive ACWs. However, the maximum retropulsive and eddy velocities predicted in this study were significantly higher (19.7 mm s^{-1} and 7.5 mm s^{-1}, respectively). The strength of these two flow patterns were affected by the speed and occlusion of the ACWs. An increase of 10 % in the wave speed increased the maximum velocity and length of the retropulsive jet (by 6.5 and 11.3 %, respectively), as well as the

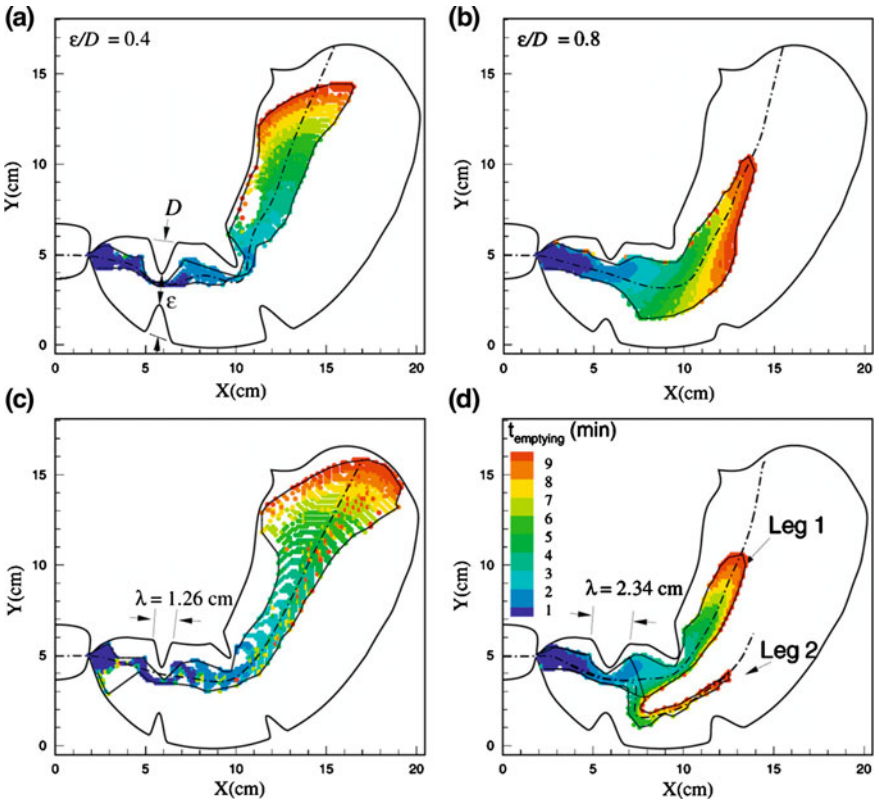

Fig. 1 Initial location of fluid particles emptied during 10 min of gastric digestion under different variations of the ACW geometry. Baseline geometry: ε/D = 0.6, λ = 1.8 cm. From Pal et al. [61]

size of eddies. While a decrease of about 30 % in the occlusion pattern of the wave led to a 70 % decrease in the maximum retropulsive velocity developed within the model. The author also analyzed the effect of the density and viscosity of the fluid on the dynamics developed within the model. The results indicated that while the density of the fluid may not have any significant impact on the gastric flow, its viscosity does. In particular, an increase of the viscosity from 1 to 50 cP decreased the length of the retropulsive jet by 80 % [69].

Kozu et al. [37] numerically investigated how the viscosity of gastric fluids affects the flow behavior within the distal stomach and the mixing dynamics of a digestive enzyme secreted from the wall. A simplified 2D model of the distal part of the stomach was created (Fig. 2a). The pyloric region was represented by a 10 cm long conical frustum whose upper and smaller base (1 cm in diameter) represented the pylorus sphincter. The lower base (3 cm in diameter) was prolonged into a 10 cm long cylinder that represented the antrum. The dynamics of the ACWs were modeled based on the in-vivo data informed by Pal et al. [60]. The

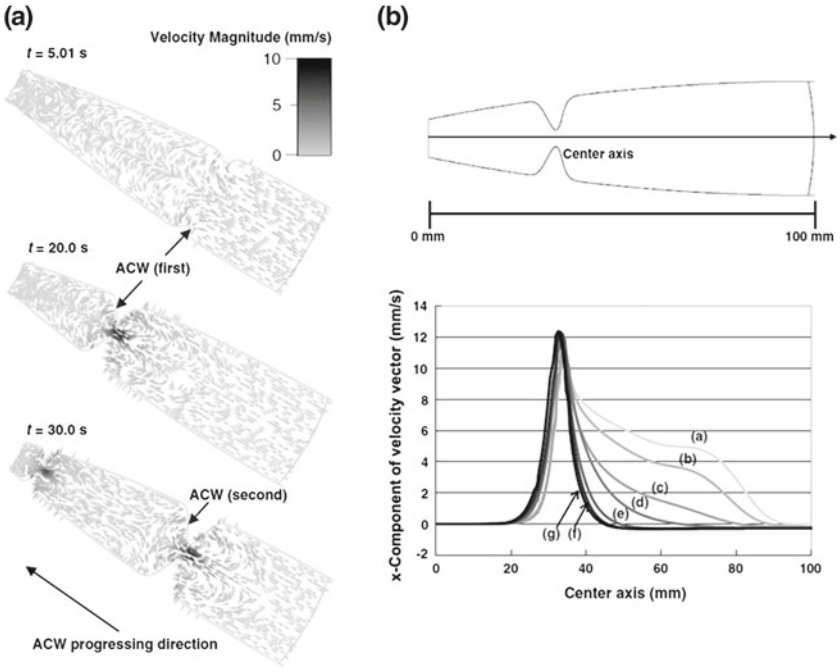

Fig. 2 Flow behavior of different Newtonian fluids within a 2D model of the distal stomach. **a** Velocity field of a fluid with a density of 1.0 g.cm^{-3} and a viscosity of 3.8 cP **b** Velocity profile along the center axis for fluids with different viscosity (a: 0.7cP, b: 1.0cP, c: 1.9cP, d: 3.8cP, e: 12.3cP, f: 147cP, g: 4760cP). From Kozu et al. [37]

gastric secretion of pepsin was represented by assuming a constant concentration of the enzyme (50 μM) at the wall. The flow behaviors of a series of Newtonian fluids with viscosities ranging from 0.7 to 4700 cP were analyzed using a CFD software package (ESI Group). The convective and diffusive transport of the enzyme within each of these flow systems was then analyzed. Similar to the work of Pal et al. [60], this study also suggested that gastric flows can be generally characterized by the formation of retropulsive and eddies structures close to the ACWs (Fig. 2). Similar to the work of Singh [68], this study also suggested that while an increase in the viscosity of the fluid did not affect the maximum velocity developed within the system (with values ranging from 11 to 12 mm s^{-1}), retropulsive motions immediately behind the wave peak decreased remarkably (Fig. 2b). The transport of pepsin within the model was governed by convective effects. Regardless of the fluid viscosity, the flow field induced by the ACWs promoted an efficient mixing of pepsin within the model. However, the migration rate and mixing dynamics was significantly affected by the viscosity (Fig. 3).

Ferrua and Singh [23] used CFD to develop a 3D model of the stomach geometry and motility during digestion. As shown in Fig. 4, the stomach was modelled as a "J"-shaped organ, and its dimensions reproduced the average size of

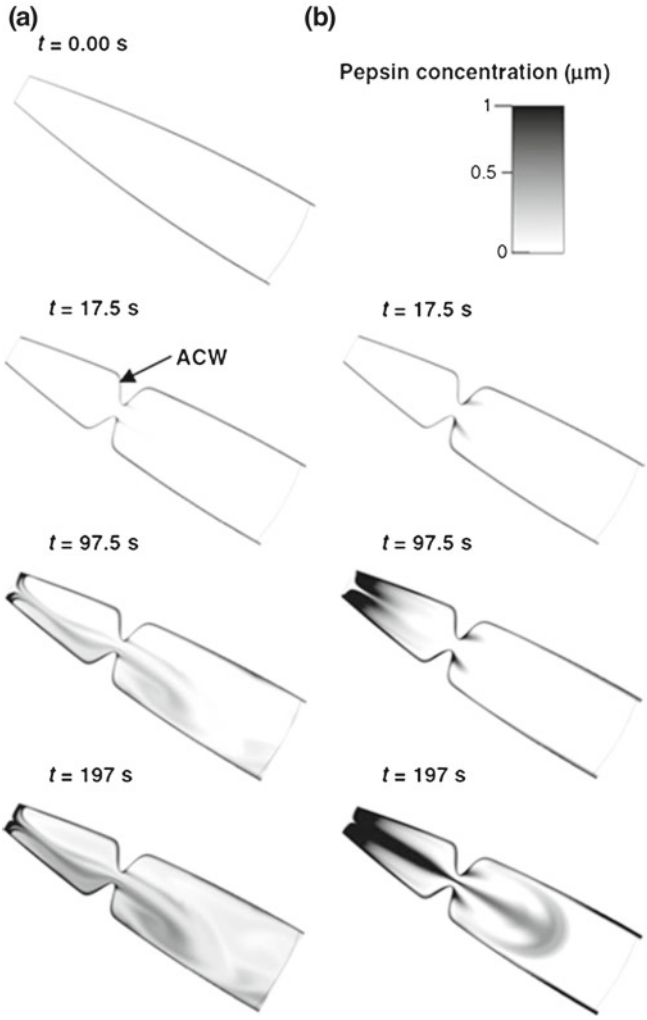

Fig. 3 2D transport of pepsin within Newtonian gastric fluids of different viscosity. **a** 0.7 cP, **b** 3.8 cP. From Kozu et al. [37]

a human stomach after a typical meal (as reported in Table 1). The dynamics of the ACWs were modeled based on the in-vivo characterization informed by Pal et al. [60]. In addition, since the stomach was modeled as a closed system, a series of tonic contractions of the proximal wall were defined to compensate for the variation in the stomach capacity induced by the ACW activity.

This model was then used to numerically analyze the dynamics of gastric fluids with different rheological properties [23, 24]. The laminar behavior of two Newtonian fluids (which can be exemplified by water and honey) and a non-Newtonian shear thinning fluid (such as tomato juice) were analyzed. The

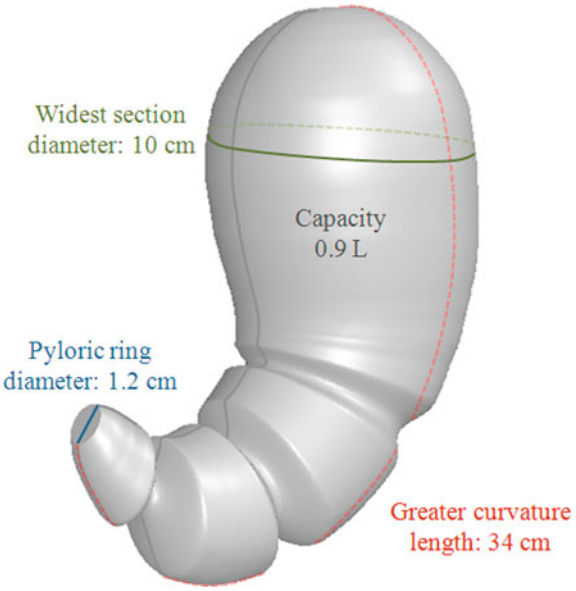

Fig. 4 3D model of a human stomach. From Ferrua and Singh [25]

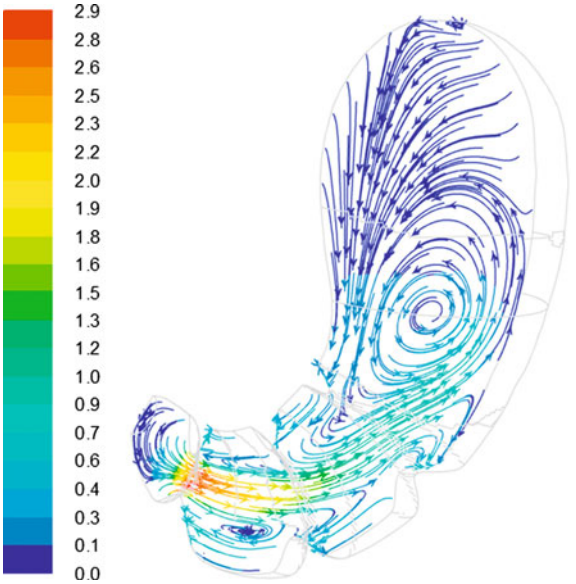

Fig. 5 Instantaneous streamlines of a water-like fluid flow within the 3D model developed by Ferrua and Singh [23], colored by velocity magnitude (cm s^{-1})

predicted results showed the complex and highly 3D flow behavior developed during digestion (Fig. 5). Although the strongest fluid motions were always predicted within the antropyloric region, a slow but constant recirculation of gastric fluids occurred between the top and bottom regions of the stomach. (Fig. 5).

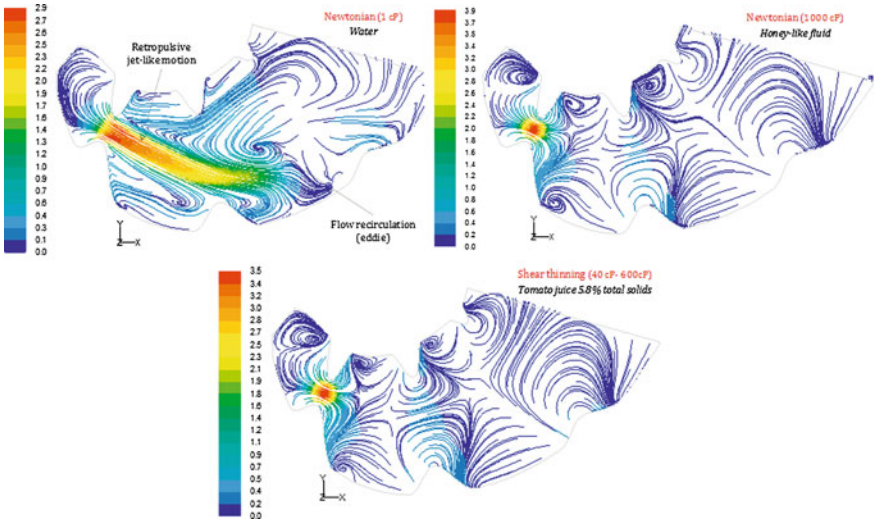

Fig. 6 Instantaneous streamlines colored by velocity magnitude (cm s^{-1}) within the middle plane of the stomach model. From Ferrua et al. [25]

As also suggested by Kozu et al. [37] and Singh [68], the flow field behavior within the antropyloric region was significantly affected by the rheological properties of the fluid (Fig. 6). In the case of the water-like fluid, the flow field was in good agreement with the classical description of gastric motions (i.e., characterized by strong retropulsive jet-like motions and eddies structures extended throughout the entire region). However, by increasing the viscosity of the fluid or changing its Newtonian properties, the formation of the retropulsive jet was significantly compromised and eddy structures became confined to regions closer to the deformed wall. It was observed that despite these detrimental effects, an increased viscosity led to higher velocities and vorticity values at the peak of the terminal and highly occluded ACW (increasing from 7.6 to 12 cm s^{-1}, and from 10 to 20 s^{-1}, respectively). However, it is noteworthy that in this model (as well as in the preceding ones) the motility pattern of the gastric wall remained the same despite the different rheological properties of the digesta. Due to this assumption, the effect of viscosity on the magnitudes of the velocity, shear, vorticity and even pressure fields can be easily misleading.

The maximum velocities predicted in this work were in good agreement with peak velocities measured in-vivo (which ranged between 2 and 8 cm s^{-1} for different types of liquid meals [5]. However, these velocities, as well as the pressure fields predicted in this work, were one order of magnitude higher than the ones predicted by Pal et al. [60, 61] and Kozu et al. [37]. The authors attributed this difference to the use of a model that actually captures the three dimensional characteristics of the gastric function. To prove the relevance and importance of reproducing the 3D features of the stomach to accurately capture the dynamics of gastric flows, Ferrua et al. [25] performed a comparison between the flow fields

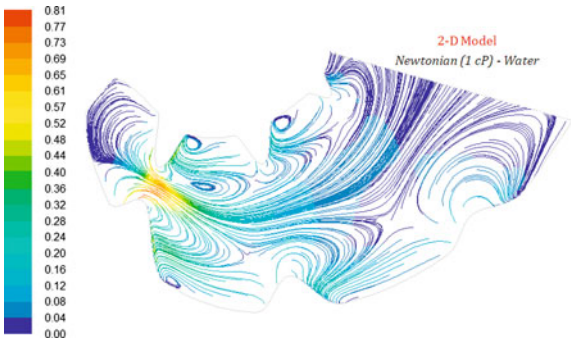

Fig. 7 Instantaneous streamlines (colored by velocity magnitude, cm s^{-1}) predicted within a simplified 2D model. From Ferrua et al. [24]

predicted by the 3D model previously discussed and a simplified 2D version of it (Fig. 7).

Ferrua and Singh [25] used the 3D model to numerically investigate how the viscosity of gastric fluids affects the intragastric distribution of a series of discrete particles of food. The amount and size distribution of the particles released inside the model were based on the mass and size distribution of raw carrot particles present in the bolus immediately before swallowing [33]. Particles with diameters of 0.4–4 mm were released at the site of the oesophago-gastric junction with a speed of 0.2 m s^{-1} [57]. The trajectory of the particles was tracked within the two Newtonian fluid flows previously analyzed by the authors.

In the case As expected, the higher the viscosity of the fluid, the longer the time that the particles remained suspended and dragged by the gastric flow of a water-like fluid the particles settled down over the greater curvature of the stomach model within seconds after being released, where they remain trapped as the simulation progressed (Fig. 8). Although successive ACWs propeled the particles forward, the increasing occlusion of the wave and the sigmoid shape of the terminal antrum forced them back into the dependent portion of the stomach (even after experimenting a 60 % reduction in their original size, Fig. 9). These results were in good agreement with in-vivo data previously reported in literature [8], and highlight how despite the rapid and strong fluid motions that develop in the case of a low viscous fluid, buoyancy effects can keep particles only slightly denser than the fluid trapped in the sinus region (regardless of their size). Based on this result, the authors pointed out the relevance of investigating how structural changes experienced by food particles during digestion may affect their dynamics and emptying within the stomach by modifying not only the size of the particles but also their density (Fig. 9).

In the case of a highly viscous fluid flow (such as honey), the intragastric distribution of the particles was controlled by viscous effects. The particles released in the stomach at 0.2 m s^{-1} were rapidly slowed down by the practically stationary flow that developed at the level of the oesophago-gastric junction (Fig. 8). Despite the absence of rapid and strong fluid motions, this highly viscous flow was able to easily suspend particles, regardless of their density and size. This particular result might explain why an increase in the viscosity of a meal was

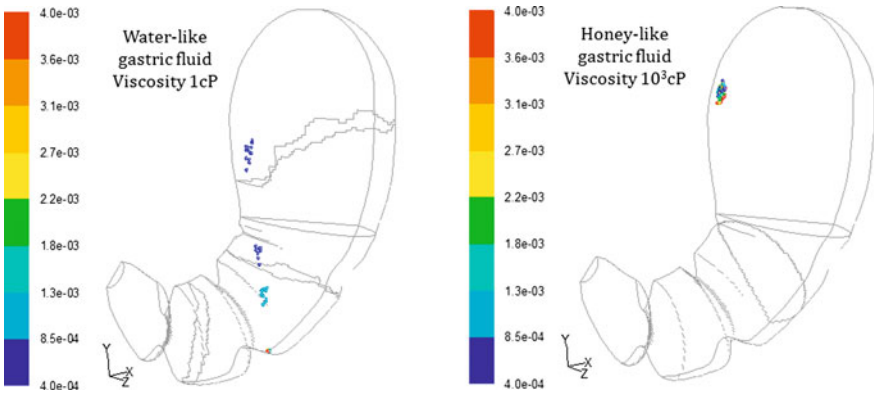

Fig. 8 Effect of gastric fluid viscosity on the distribution of carrot particles (colored by diameter, m) after 6 s of being released into the stomach

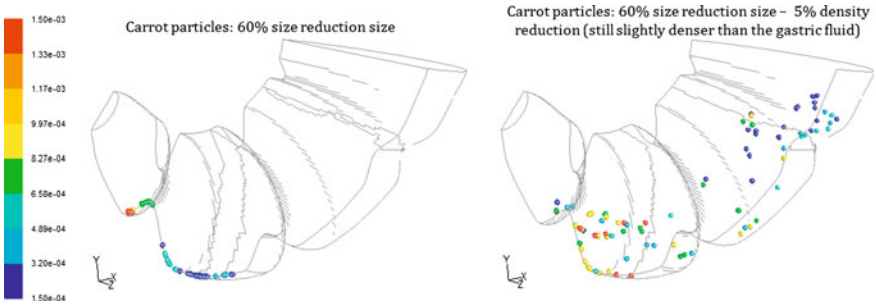

Fig. 9 Effect of size reduction and density change in the distribution of carrot particles (colored by diameter, m) within a water-like fluid flow

found to facilitate the gastric emptying of solid beads from human stomachs [52]. From an overall point of view this work suggested that, at least at the beginning of the process, the dynamics and disintegration of discrete particles of food may not be driven by the formation of strong fluid motions, but by a complex interaction of factors (including the viscosity of the fluid, the size and relative density of the particles, and the geometrical configuration of the terminal antrum).

3.3 Modelling the Flow Through the Antroduodenal Junction

By regulating the rate of gastric emptying and the mixing of gastric chyme with digestive secretions in the first part of the duodenum, the morphology and valvular activity of the pylorus are thought to play an important role in food digestion.

However, the underlying mechanisms modulating these functions are still poorly understood.

Dillard et al. [16] used CFD to analyze how different anatomical and physiological conditions of the antroduodenal junction affect the dynamics and mixing of gastric effluents in the duodenum. To achieve this goal, the region of interest (comprising the distal antrum, pylorus and superior duodenum of a cat gut) was modelled as a simplified 2D channel.

In the first part of this work, a relaxed configuration of the pylorus was considered and modeled by a localized narrowing of the channel of about 40 %. The flow field that developed when a steady flow was forced through the relaxed pylorus was characterized by two main flow structures that do not mix with each other: recirculative eddies immediately behind the occluding region of the pylorus, and an advective flow motion along the core of the duodenum. As illustrated by the authors, while gastric effluents were forced and stretched by the rapid and ordered advective motion they were not efficiently mixed. To investigate the effect of a pulsative motion of gastric emptying, a temporal variation on the flow rate forced through the relaxed pylorus was imposed. As a result of this pulsative flow, a significant improvement in the mixing of gastric effluents was observed. Acceleration and decelerations of the inlet flow promoted the disruption of the previous flow patterns. As the inlet velocity increased, eddies grew further into the luminal core, becoming detached from the wall and carried away as the inlet velocity decelerates. This periodic formation and shedding of vortex structures was found to provide a key mechanism for the efficient mixing of gastric effluents.

In addition, the authors also investigated how the valvular activity of the pylorus in coordination with the propagation of the ACWs affect the mixing of gastric effluents in the duodenum. It is well documented that the pyloric orifice closes as the ACWs approach it [2]. To investigate this effect, the boundary representing the pyloric orifice in the model moved from a fully open position to a total closure while the velocity pulse was imposed at the inlet. A sinusoidal reopening of the pylorus was modeled during a quiescent phase following the velocity pulse. The results obtained illustrated how the valvular activity of the pyloric orifice can significantly enhance the mixing of gastric effluents. By increasing the axial momentum of the core flow and the size and number of recirculating motions, the valvular activity of the pylorus further stretched and rolled gastric effluents within the entire domain.

The authors also investigated the effect of the anatomical structure of the pylorus orifice, by considering the “notched” configuration produced by the increased tonicity of both pyloric muscle loops. The results suggested that the asymmetrical properties of pylorus are a critical contributor to the efficiency of mixing in the proximal duodenum. As fluid is accelerated through the pylorus, gastric effluents are drawn downstream and away from the centreline of the duodenum to collide with the wall of the channel, and then deflected away towards the lower wall enhancing their residence time and mixing.

Finally, the authors also analyzed the effect of the chyme viscosity on the dynamics of mixing. They found that, if the viscosity of the chyme is such that

leads to a Reynolds number lower than 10 (i.e., 30 times larger than the viscosity of the saline solution previously modeled), viscous stresses control the dynamics of the flow and prevent any significant mixing of the contents (even in the case of a pulsative flow through a closing and "notched" pylorus).

3.4 Modeling the Intestinal Flow During Digestion

The small intestine plays a critical role in the digestion process of the meal. It not only has a primary role in the enzymatic breakdown of food macronutrients, but also on the final absorption of the nutrients into the blood stream. It is generally accepted that the segmental and peristaltic contractions of the intestine facilitates these processes by thoroughly mixing the food with digestive secretions, while promoting its transport and repeated contact with the absorptive surface along the intestine. However, despite their relevance, the fluid dynamic behavior of intestinal contents is still not fully understood.

Tharakan's doctoral thesis [77] focused on understanding the mechanisms by which the physical properties of the digesta and motor activity of the small intestine affect the digestion and absorption of nutrients. As part of this work, an in-vitro model that mimicked the geometry and contractive activity of the intestinal wall was developed. By using this model, Tharakan et al. [76] found that (unlike peristaltic contractions) the segmental motion of the intestinal wall can significantly improve the delivery of nutrients to the absorptive surface, while an increased viscosity of the digesta can significantly reduce it. The authors hypothesized that these results can be explained by the way in which the segmental motions and the viscosity of the digesta affect the convective mixing within the intestine and the renewal of nutrients along the surface. Unfortunately, the complex geometry and dynamics of the deforming wall prevented the experimental characterization of the dynamics of the flow at the site of the segmental contractions. Instead, in order to prove their hypothesis, Tharakan [77] followed a CFD approach. The CFD model was validated against the experimental flow field that develops in between successive contractions, and showed the marked effect that fluid viscosity has on the average velocity and shear rates that developed within the system. Although this work did not focus on the use of CFD as a design tool, it certainly pointed out the unique capability of CFD to provide an accurate and rapid insight into the mechanisms driving the molecular delivery of nutrients and bioactive molecules to the absorptive wall of the intestine.

Lim [47] also used CFD tools to investigate the possibility of using the manometric techniques described by Dinning in "Colonic Manometry: What do the Squiggly Lines Really Tell Us?" of this volume as a diagnostic tool for intestinal motility disorders. Intestinal motility disorders (such as chronic intestinal pseudo-obstruction) can be extremely debilitating and account for at least 36 % of all visits to gastroenterologists [59]. However, their diagnosis is often complicated by the number and complexity of the mechanisms involved. In this work, a simplified

2D channel was developed to represent an isolated (30 cm long) segment of the rabbit small intestine. While the dynamic activity of the segmental motions was not considered in this study, the deformations imposed by them were modelled by using a bell-shaped Gaussian function. The amplitude and width of the contractions were parameterized in terms of the relaxed radius of the intestine (3 mm). The flow behavior and pressure drop across successive contractions were numerically analyzed under different physiological conditions, by assuming a flow rate of 4 mL min^{-1} of a Newtonian water-like fluid through the channel. The results showed that the pressure differences that developed within the intestine depended in a complex and non-linear fashion on a series of different parameters, such as fluid viscosity, intestinal radius and the relative occlusion imposed by the contraction. In particular, it was found that while the pressure drop across a contraction increased with the occlusion ratio, its value remained independent of the location and number of contractions simulated within the intestine. Similarly, while the pressure drop across any given contraction depended on the diameter of the relaxed intestine in a non-linear fashion, a linear relationship could be drawn by using dimensional analysis with respect to the oclusion ratio of the wave and the diameter of the intestine. Although much more work needs to be done to model these relationships, these results highlight the possibility of linking pressure recordings with intestinal activity.

4 Future Challenges

As illustrated in this chapter, the use of CFD techniques offers new opportunities to better understand and model the mechanisms driving human digestion. Despite been largely constrained by simplified descriptions of the geometry, function and physics of the GI tract and its contents during digestion, initial models have demonstrated the ability of this approach to provide a improved understanding of the fluid dynamic conditions mediating the GI function under different physiological conditions. However, more work is needed to further advance the physiological relevance of these models and their contribution to the food and health sectors.

The increased availability of high performance computing and numerical packages for the simulation of complex multiphysics phenomena will certainly support the development of more realistic and accurate models of the GI tract within the near future. By then, the ability of these models to predict the in-vivo dynamics of GI contents will be largely determined by our understanding and characterization of the complex synergy of physicochemical and physiological processes underlying human digestion. In particular, it will become essential to develop a better understanding of the physicochemical properties of GI contents at different sites of the digestive tract, and their impact on the in-vivo function of the GI wall during the process. While there is still no efficient way to in-vivo characterize the physicochemical properties of GI contacts, recent advances in spatiotemporal mapping techniques and medical imaging technologies have

proved useful, offering unique methods to visualize and further characterize the motor and secretionary functions of the GI wall for a number of different diets.

The ability of numerical models to further advance GI research within the food and health sectors is promising. However, as previously discussed, the future and successful development of this approach depends on a series of complex and multidisciplinary challenges that can only be addressed by a combined effort across disciplines (including mathematics, medicine, science and engineering).

References

1. Ali N, Sajid M, Abbasa Z, Javed T (2010) Non-Newtonian fluid flow induced by peristaltic waves in a curved channel. Eur J of Mech B/Fluids 29:387–394
2. Barret KE, Raybould HE (2010) The gastric phase of the integrated response to a meal. In: Koeppen BM, Stanton BA (eds) Berne and Levy physiology, 6th edn. MOSBY Elsevier, Philadelphia
3. Barret KE, Raybould HE (2010) The small intestinal phase of the integrated response to a meal. In: Koeppen BM, Stanton BA (eds) Berne and Levy physiology, 6th edn. MOSBY Elsevier, Philadelphia
4. Blackburn NA, Holgate AM, Read NW (1984) Does guar gum improve post-prandial hyperglycaemia in humans by reducing small intestinal contact area? Brit J Nutr 52:197–204
5. Boulby P, Moore R, Gowland P, Spiller RC (1999) Fat delays emptying but increases forward and backward antral flow as assessed by flow-sensitive magnetic resonance imaging. Neurogastroenterol Motil 11:27–36
6. Brennen CE (2005) Fundamentals of multiphase flow. Cambridge University Press, New York
7. Brown NJ, Worlding J, Rumsey RDE, Read NW (1988) The effect of guar gum on the distribution of a radiolabelled meal in the gastrointestinal tract of the rat. Brit J Nutr 88:223–231
8. Brown BP, Schulze-Delrieu K, Schrier JE, Abu-Yousef MM (1993) The configuration of the human gastroduodenal junction in the separate of emptying of liquid and solids. Gastroenterology 105:433–440
9. Camilleri M, Malagelada JR, Brown ML, Becker G, Zinsmeister AR (1985) Relation between antral motility and gastric emptying of solids and liquids in humans. Am J Physiol 249:G580–G585
10. Cannon W, Lieb C (1911) The receptive relaxation of the stomach. Am J Physiol 29:267–273
11. Christensen J, Glover JR, Macagno E0, Singerman RB, Weisbrodt NW (1971). Statistics of contractions at a point in the human duodenum. Am J Physiol 221:1818–1823
12. Coupe AJ, Davis SS, Wilding IR (1991) Variation in gastrointestinal transit of pharmaceutical dosage forms in healthy subjects. Pharm Res 8:360–364
13. Dikeman CL, Fahey GC Jr (2006) Viscosity as related to dietary fiber: a review. Crit Rev Food Sci Nutr 46(8):649–663
14. Dikeman CL, Murphy MR, Fahey GC Jr (2006) Dietary fibers affect viscosity of solutions and simulated human gastric and small intestinal digesta. J Nutr 136:913–919
15. Dikeman CL, Murphy MR, Fahey GC Jr (2007) Diet type affects viscosity of ileal digesta of dogs and simulated gastric and small intestinal digesta. J Anim Physiol Anim Nutr 91:139–147
16. Dillard S, Krishnan S, Udaykumar HS (2007) Mechanics of flow and mixing at antroduodenal junction. World J Gastroenterol 13(9):1365–1371

17. Einhorn M (1898) Diseases of the stomach: a text-book for practitioners and students. W. Wood and Company, New York. http://www.archive.org/details/diseasesstomach01einhgoog
18. Ellis PR, Roberts FG, Low AG, Morgan LM (1995) The effect of high-molecular-weight guar gum on net apparent glucose absorption and net apparent insulin and gastric inhibitory polypeptide production in the growing pig: relationship to rheological changes in jejunal digesta. Brit J Nutr 74:539–556
19. Ellis PR, Rayment P, Wang Q (1996) A physico-chemical perspective of plant polysaccharides in relation to glucose absorption, insulin secretion and the entero-insular axis. P Nutr Soc 55:881–898
20. Faas H, Schwizer W, Feinle C, Lengsfeld H, de Smidt C, Boesiger P, Fried M, Rades T (2001) Monitoring the intragastric distribution of a colloidal drug carrier model by magnetic resonance imaging. Pharm Res 18(4):460–466
21. Faas H, Steingoetter A, Feinle C, Rades T, Lengsfeld H, Boesiger P, Fried M, Schwizer W (2002) Effects of meal consistency and ingested fluid volume on the intragastric distribution of a drug model in humans-a magnetic resonance imaging study. Aliment Pharmacol Ther 16:217–224
22. Feinle C, Grundy D, Read NW (1997) Effects of duodenal nutrients on sensory and motor responses of the human stomach to distension. Am J Physiol 273:G721–G726
23. Ferrua MJ, Singh RP (2010) Modeling the fluid dynamics in a human stomach to gain insight of food digestion. J Food Sci 75(7):R151–R162
24. Ferrua MJ, Kong F, Singh RP (2011) Computational modeling of gastric digestion and the role of food material properties. Trends Food Sci Tech 22(9):480–491
25. Ferrua MJ, Singh RP (2011) Understanding the fluid dynamics of gastric digestion using computational modeling. Proc Food Sci 1: 1465–1472.
26. Ganong W (2005) Review of medical physiology, 22nd edn. McGraw-Hill, New York
27. Geliebter A, Mellon PM, McCray RS, Gallagher DR, Gage D, Hashim SA (1992) Gastric capacity, gastric emptying, and test-meal intake in normal and bulimic women. Am J Clin Nutr 56:656–661
28. Goetze O, Steingoetter A, Menne D, van der Voort IR, Kwiatek MA, Boesiger P et al (2007) The effect of macronutrients on gastric volume responses and gastric emptying in humans: a magnetic resonance imaging study. Am J Physiol Gastrointest Liver Physiol 292:G11–G17
29. Guyton AC, Hall JE (2005) Textbook of medical physiology, 11th edn. Elsevier, Edinburgh
30. Hausken T, Gilja OH, Ødegaard S, Berstad A (1998) Flow across the human pylorus soon after ingestion of food, studied with duplex sonography. Effect of glyceryl trinitrate. Scand J Gastroenterol 33:484–490
31. Indireshkumar K, Brasseur JG, Faas H, Hebbard GS, Kunz P, Dent J et al (2000) Relative contributions of pressure pump and peristaltic pump to gastric emptying. Am J Physiol Gastrointest Liver Physiol 278:G604–G616
32. Jahnberg T, Martinson J, Hulten L, Fasth S (1975) Dynamic gastric response to expansion before and after vagotomy. Scand J Gastroenterol 10:593–598
33. Jalabert-Malbos M-L, Mishellany-Dutour A, Woda A, Peyron M-A (2007) Particle size distribution in the food bolus after mastication of natural foods. Food Qual Prefer 18:803–812
34. Jiménez-Lozano J, Sen M (2010) Streamline topologies of two-dimensional peristaltic flow and their bifurcations. Chem Eng Process 49:704–715
35. Keet AD (1993) Infantile hypertrophic pyloric stenosis. In: The pyloric sphincteric cylinder in health and disease. Springer, Berlin, New York. ISBN 3-540-55814-4
36. Kim D-Y, Camilleri M, Murray JA, Stephens DA, Levine JA, Burton DD (2001) Is there a role for gastric accommodation and satiety in Asymptomatic Obese People? Obes Res 9(11):655–661
37. Kozu H, Kobayashi I, Nakajima M, Uemura K, Sato S, Ichikawa S (2010) Analysis of flow phenomena in gastric contents induced by human gastric peristalsis using CFD. Food Biophys 5:330–336

38. Kwiatek MA, Steingoetter A, Pal A, Menne D, Brasseur JG, Hebbard GS et al (2006) Quantification of distal antran contractile motility in healthy human stomach with magnetic resonance imaging. J Magn Reson Imaging 24:1101–1109
39. Lentle RG, Hemar Y, Hall CE, Stafford KJ (2005) Periodic fluid extrusion and models of digesta mixing in the intestine of a herbivore, the common brushtail possum (Trichosurus vulpecula). J Comp Physiol B 175(5):337–347
40. Lentle RG, Hemar Y, Hall CE (2006) Viscoelastic behaviour aids extrusion from and reabsorption of the liquid phase into the digesta plug: creep rheometry of hindgut digesta in the common brushtail possum Trichosurus vulpecula. J Comp Physiol B 176(5):469–475
41. Lentle RG, Janssen PWM (2008) Physical characteristics of digesta and their influence on flow and mixing in the mammalian intestine: a review. J Comp Physiol B 178:673–690
42. Lentle RG, Janssen PWM (2010) Manipulating digestion with foods designed to change the physical characteristics of digesta. Crit Rev Food Sci Nutr 50:130–145
43. Lentle RG, Janssen PWM, Goh K, Chambers P, Hulls C (2010) Quantification of the effects of the volume and viscosity of gastric contents on antral and fundic activity in the rat stomach maintained ex vivo. Dig Dis Sci 55:3349–3360
44. Li M, Brasseur JG (1993) Non-steady peristaltic transport in finite-length tubes. J Fluid Mech 248:129–151
45. Liao D, Gregersen H, Hausken T, Gilja OH, Mundt M, Kassab G (2004) Analysis of surface geometry of the human stomach using real-time 3-D ultrasonography in vivo. Neurogastroenterol Motil 16(3):315–324
46. Liker H, Hungin P, Wiklund I (2005) Managing gastroesophageal reflux disease in primary care: the patient perspective. J Am Board Fam Pract 18:393–400
47. Lim J (2010) Modelling fluid flow in the small intestine. Final year project report. Department of Engineering Science, The University of Auckland, Auckland
48. Macagno EO, Christensen J (1980) Fluid-Mechanics of the Duodenum. Annu Rev Fluid Mech 12:139–158
49. Macagno EO, Christensen J, Lee CL (1982) Modeling the effect of wall movement on absorption in the intestine. Am J Physiol 243:541–550
50. Manton MJ (1975) Long-wavelength peristaltic pumping at low Reynolds number. J Fluid Mech 68:681–693
51. Marciani L, Gowland PA, Spiller RC, Manoj P, Moore RJ, Young P, Al-Sahab S, Bush D, Wright J, Fillery-Travis AJ (2000) Gastric response to increased meal viscosity assessed by echo-planar magnetic resonance imaging in humans. J Nutr 130:122–127
52. Marciani L, Gowland PA, Fillery-Travis A, Manoj P, Wright J, Smith A, Young P, Moore R, Spiller RC (2001) Assesment of antral grinding of a model solid meal with echo-planar imaging. Am J Physiol Gastrointest Liver Physiol 280:G844–G849
53. Marciani L, Gowland PA, Spiller RC (2001) Effect of meal viscosity and nutrients on satiety, intragastric dilution and emptying assessed by MRI. Am J Physiol Gastrointest Liver Physiol 280:G1227–G1233
54. Marciani L, Young P, Wright J, Moore R, Coleman N, Gowland PA et al (2001) Antral motility measurements by magnetic resonance imaging. Neurogastroenterol Motil 13(5):511–518
55. Marciani L (2011) Assessment of gastrointestinal motor functions by MRI: a comprehensive review. Neurogastroenterol Motil 23:399–407
56. Martini FH (2006) Fundamentals of anatomy & physiology, 7th edn. Pearson/Benjamin Cummings, San Francisco CA
57. McMahon BP, Odie KD, Moloney KW, Gregersen H (2007) Computation of flow through the oesophagogastric junction. World J Gastroentero 13(9):1360–1364
58. O'Grady G, Du P, Cheng LK, Egbuji JU, Lammers WJEP, Windsor JA et al (2010) Origin and propagation of human gastric slow-wave activity defined by high-resolution mapping. Am J Physiol Gastrointest Liver Physiol 299(3):G585–G592
59. Parkman HP, Doma S (2006) Importance of gastrointestinal motility disorders. Pract Gastroenterol 9:23–40

60. Pal A, Indireshkumar K, Schwizer W, Abrahamsson B, Fried M, Brasseur JG (2004) Gastric flow and mixing studied using computer simulation. Proc R Soc Lond B 271:2587–2594
61. Pal A, Brasseur JG, Abrahamsson B (2007) A stomach road or "Magenstrasse" for gastric emptying. J Biomech 40:1202–1210
62. Pozrikidis C (1987) A study of peristaltic flow. J Fluid Mech 180:515–527
63. Schulze K (2006) Imaging and modeling of digestion in the stomach and the duodenum. Neurogastroenterol Motil 18(3):172–183
64. Schwartz SE, Levine RA, Weinstock RS, Petokas S, Mills CA, Thomas FD (1988) Sustained pectin ingestion: effect on gastric emptying and glucose tolerance in non-insulin dependent diabetic patients. Am J Clin Nutr 48:1411–1413
65. Schwizer W, Steingotter A, Fox M, Zur T, Thumshirn M, Boesiger P et al (2002) Non-invasive measurement of gastric accommodation in humans. Gut 51(Suppl 1):i59–i62
66. Schwizer W, Steingoetter A, Fox M (2006) Magnetic resonance imaging for the assessment of gastrointestinal function. Scand J Gastroenterol 41:1245–1260
67. Shapiro AH, Jaffrin MY, Weinberg SL (1969) Peristaltic pumping with long wavelengths at low Reynolds number. J Fluid Mech 37:799–825
68. Singh SK (2007) Fluid flow and disintegration of Food in human stomach. Doctoral Thesis, University of California, Davis
69. Singh SK, Singh RP (2011) Gastric digestion of foods: Mathematical modeling of flow field in a human stomach. In: Aguilera JM, Barbosa-Canovas GV, Simpson R, Welti-Chenas J, Bermudez-Aguirre D (eds) Food engineering interfaces. Springer, New York
70. Smith ME, Morton DE (2001) The digestive system. Churchill Livingstone, Edinburgh
71. Steingoetter A, Weishaupt D, Kunz P, Mäder K, Lengsfeld H, Thumshirn M, Boesiger P, Fried M, Schwizer W (2003) Magnetic resonance imaging for the in vivo evaluation of gastric-retentive tablets. Pharm Res 20(12):2001–2007
72. Steingoetter A, Kwiatek MA, Pal A, Hebbard G, Thumshirn M, Fried et al. (2005) MRI to assess the contribution of gastric peristaltic activity and tone to the rate of liquid gastric emptying in health. Proc Int Soc Magn Reson Med 13:426
73. Steingoetter A, Fox M, Treier R, Weishaupt D, Marincek B, Boesiger P et al (2006) Effects of posture on the physiology of gastric emptying: a magnetic resonance imaging study. Scand J Gastroenterol 41:1155–1164
74. Takahashi T, Sakata T (2002) Large particles increase viscosity and yield stress of pig cecal contents without changing basic viscoelastic properties. J Nutr 132:1026–1030
75. Takahashi T, Karita S, Ogawa N, Goto M (2005) Crystalline cellulose reduces plasma glucose concentrations and stimulates water absorption by increasing the digesta viscosity in rats. J Nutr 135:2405–2410
76. Tharakan A, Rayment P, Fryer PJ, Norton IT (2007) Modelling of physical and chemical processes in the small intestine. Proc Eur Congr Chem Eng (ECCE-6), Copenhagen, Denmark, 16–20 Sep
77. Tharakan A (2008) Modelling of physical and chemical processes in the small intestine. Doctoral thesis, University of Birmingham, England
78. Treier R, Steingoetter A, Weishaupt D, Goetze O, Boesiger P, Fried M et al (2006) Gastric motor function and emptying in the right decubitus and seated body position as assessed bymagnetic resonance imaging. J Magn Reson Imaging 23:331–338
79. Trendelenburg P (2006) Physiological and pharmacological investigations of small intestinal peristalsis (Translation of the article "Physiologische und pharmakologische Versuche über die Dünndarmperistaltik". Arch Exp Pathol Pharmakol 81:55–129, 1917). Naunyn Schmiedebergs Arch Pharmacol 373(2):101–133
80. van den Elzen BDJ, Bennink RJ, Wieringa RE, Tytgat GNJ, Boeckxstaens GEE (2003) Fundic accommodation assessed by SPECT scanning: comparison with the gastric barostat. Gut 52(11):1548–1554
81. Zien TF, Ostrach S (1970) A long wave approximation to peristaltic motion. J Biomech 3:63–75